ABSTRACT

Title of Document: WIRING THE RIBOSOME: FUNCTIONS OF RIBOSOMAL PROTEINS L3 AND L10, AND 5S rRNA

Alexey Petrov, Ph.D., 2006

Directed By: Associate Professor Dr Jonathan D. Dinman, Department of Cell Biology and Molecular Genetics

The ribosome is a megadalton complex that performs protein synthesis with tremendous speed and accuracy. Atomic resolution ribosome structures have been resolved within the last five years. These have provided the 3-dimensional locations of all ribosomal components, and have revealed structures of the active centers. However, the precise mechanisms of the various functions performed by the ribosome are still unknown. This work is an attempt to understand some of the functional relationships between different active centers of the ribosome (or the "wiring" of the ribosome), and mechanisms by which such communication occurs. Here we present an analysis of three ribosomal components: ribosomal proteins L3 and L10, and 5S rRNA. Studies of L3 suggest that accommodation of aminoacyl-tRNAs (aa-tRNA) may be the mechanism that induces the "active" conformation of the peptidyl transferase center. We have proposed a mechanism in which rRNA movement associated with aa-tRNA accommodation facilitates conformational changes in the

peptidyl transferase center (PTC) through the formation of a network of hydrogen bond interactions. A saturation mutagenesis analysis of 5S rRNA disproves the previous notion that 5S rRNA is a resilient molecule. An analysis of naturally occurring 5S rRNA variants suggests that this molecule may participate in posttranscriptional regulation of gene expression via the nonsense-mediated mRNA decay (NMD) pathway. Lastly, a random mutagenesis analysis of ribosomal protein L10 has resulted in the creation of a powerful toolbox that will be used for elucidation of ribosome export/maturation pathways. Future structure/functional analyses of these mutants may also help to reveal roles of helices 38 and 89 of 25S rRNA.

WIRING THE RIBOSOME: FUNCTIONS OF RIBOSOMAL PROTEINS L3 AND L10, AND 5S rRNA

By

Alexey Petrov

Dissertation submitted to the Faculty of the Graduate School of the
University of Maryland, College Park, in partial fulfillment
of the requirements for the degree of
Doctor of Philosophy
2006

Advisory Committee:
Associate Professor Jonathan D. Dinman, Ph.D., Chair
Associate Professor Jason Kahn Ph.D.
Professor Anne Simon Ph.D.
Associate Professor Richard C. Stewart Ph.D.
Assistant Professor Gerald Wilson Ph.D.

Dedication

Acknowledgements

I would like to thank my adviser Dr. Jonathan D. Dinman, who provided guidance and years of support. I would like to thank all members of Dinman laboratory for their help, advice and discussion.

I also would like to thank our collaborator Sergey Kiparisov, q member of the O. Dontsova laboratory, who performed chemical protection analysis of 5S rRNA strains.

Table of Contents

List of Tables

List of Figures

List of Acronyms

ASL	Anticodon stem loop
CMCT	1-cyclohexyl-3-(2-morpholinoethyl) carbodiimide metho-p-toluene
CFU	Colony forming unit
DLR	Dual luciferase reporter
DMS	Dimethyl sulfate
DTE	1,4-dithioerythritol
EDTA	Ethylenediaminetetraacetic acid
GAC	GTPase associated center
HIV	Human Immunodeficiency Virus
HPLC	High Performance Liquid Chromatography
IBV	Infectious Bronchitis Virus
IUB	International Union of Biochemistry
IUPAC	International Union of Pure and Applied Chemistry
NMD	Nonsense mediated decay
NS	Nonsense suppression
OD	Optical density at specified wavelength
ORF	Open Reading Frame

OU	Optical unit
PMSF	Phenylmethylsulfonyl fluoride
PT	Peptidyl transfer
PTC	Peptidyl transferase center
PRF	Programmed Ribosomal Frameshifting
RDRP	RNA dependent RNA polymerase
RPL	Protein of the large ribosomal subunit
RPS	Protein of the small ribosomal subunit
SARS	Severe Acute Respiratory Syndrome
SRL	Sarcin-ricin loop

Chapter 1. Literature review

Introduction

The ribosome is the largest RNA-protein complex in the cell. It translates the information contained in mRNAs into polypeptide chains, thus linking the worlds of nucleic acids and proteins. In the late 1990's, the combined efforts of several groups resulted in the elucidation of ribosomal structure at the atomic level [1,2]. The three dimensional (3-D) structure revealed the contacts and relative positions of most of the ribosomal components. Together with previously accumulated biochemical data, those studies gave birth to multiple hypotheses regarding the roles of individual ribosomal components, most of which failed subsequent empirical testing. Currently the exact mechanisms through which the ribosome performs its functions are still unclear. This work describes our attempts to understand the roles of individual ribosomal components in translation.

Initiation

Translation consists of three phases: initiation, elongation, and termination. Initiation is the first step of the cycle. During initiation, mRNA forms a complex with ribosome, which then recognizes and selects the appropriate start codon and begins translation in the correct reading frame.

The majority of eukaryotic mRNAs have 5' 7mG caps and poly A tails, structural features recognized by cellular translational factors that are required for efficient translation initiation [3,4]. Initiation can be divided into consecutive steps: 43S pre-initiation complex assembly, mRNA recognition, 48S initiation complex

formation, 5'→3' scanning, initiation codon recognition, and 60S subunit joining (Figure 1.1) [5]. The first step is formation of the 43S pre-initiation complex. The ternary complex formed by eIF2, GTP and Met-tRNA^{Met} binds to the free 40S ribosomal subunit; where it then recruits eIF1, eIF1A, eIF3 and eIF5. The binding of eIF3 finalizes assembly of pre-initiation complex and renders it competent for mRNA interaction. The 43S complex gets recruited to mRNA by initiation factor 4F (eIF4F), to form the 48S initiation complex [5,6]. eIF4F is a hetero-tetramer, composed of the eIF4A, eIF4B, eIF4E and eIF4G subunits [7]. eIF4E binds the mRNA cap structure and recruits eIF4G. As a scaffolding protein, eIF4G has three particularly important sets of interactions. First, eIF4G interacts with poly A binding protein (PABP), circularizing the mRNA and bringing translation regulatory sequences located in the 3' UTR close to the initiation complex [8,9]. Second, eIF4G interacts with eIF3, which in turn recruits the 60S ribosomal subunit to mRNA. Third, it recruits eIF4A and eIF4B, which have ATP dependent RNA helicase activities [10,11]. After formation of the 48S initiation complex, eIF1 and eIF1A act synergistically to enable scanning in the 5' to 3' direction [12]. Scanning is ATP dependent and continues to the initiation codon [13]. The exact way in which the proper AUG codon is recognized is unknown. It has been proposed that basepairing between the anticodon stem loop of tRNA^{Met} and the AUG codon triggers GTP hydrolysis by eIF5 and eIF2. The hydrolysis of GTP leads to the displacement of eIF2:GDP and the rest of the initiation factors, allowing 60S subunit joining. This results in formation of an elongation competent 80S ribosome with the initiation tRNA placed in the P site [14].

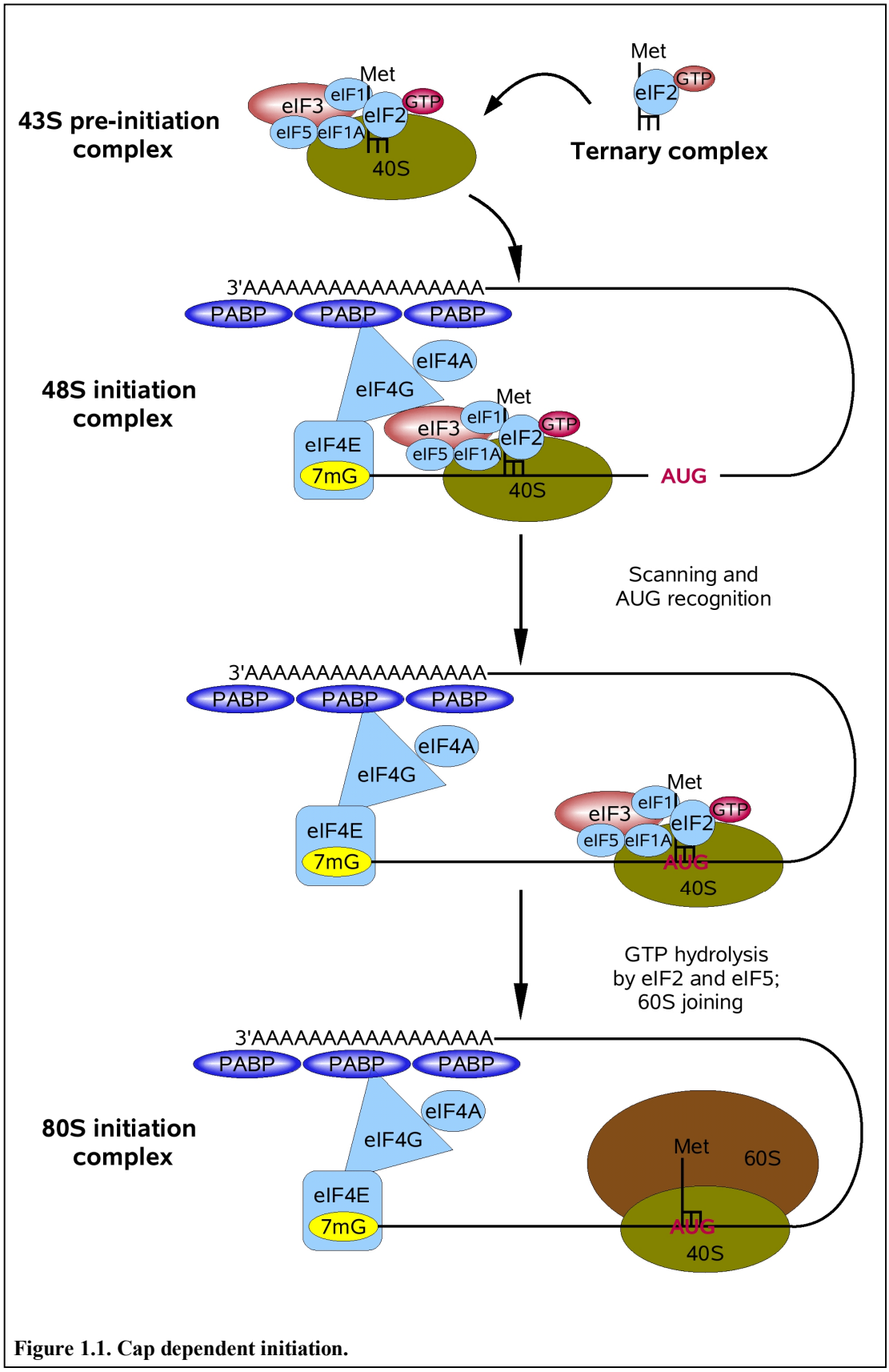

Figure 1.1. Cap dependent initiation.

There are also multiple examples of cap independent initiation in viruses and higher organisms. It includes substitution of the cap by a specific mRNA binding protein, or initiation at Internal Ribosome Entry Sites (IRES'es). The mechanisms of the cap independent initiation are diverse and each differs from one another. Structural determinants in mRNAs that define efficient initiation, sets of required canonical translation factors, and use of non canonical cellular or viral factors for initiation. The size of IRES'es can vary from tens to hundreds of nucleotides, and the set of required factors may vary from none (*e.g.* for the Cricket Paralysis Virus IRES [15,16]) to use both canonical factors and non-canonical initiation proteins (e.g. the Hepatitis C Virus IRES [17,18]). It appears that there are no obvious correlations between different IRESes in conditions required for initiation, and they differ on case-to-case basis.

The elongation cycle

The elongation cycle contains three major steps: aminoacyl-tRNA (aa-tRNA) selection, peptidyl transfer, and translocation. First, the ternary complex of EF-Tu:GTP:aminoacyl-tRNA (eEF-1:GTP:aminoacyl-tRNA in eukaryotes) brings correct tRNAs into the A-site of the ribosome. Next, aminoacyl-tRNA binding is followed by thermodynamically spontaneous formation of the peptide bond and transfer of the peptidyl moiety to the A-site tRNA [19]. Finally, elongation factor EF-G (eEF-2 in eukaryotes) catalyzes translocation. Translocation involves replacement of the deacylated tRNA by the peptidyl-tRNA in the P-site of the ribosome, and movement of the deacylated tRNA into the E-site (Figure 1.2) [20].

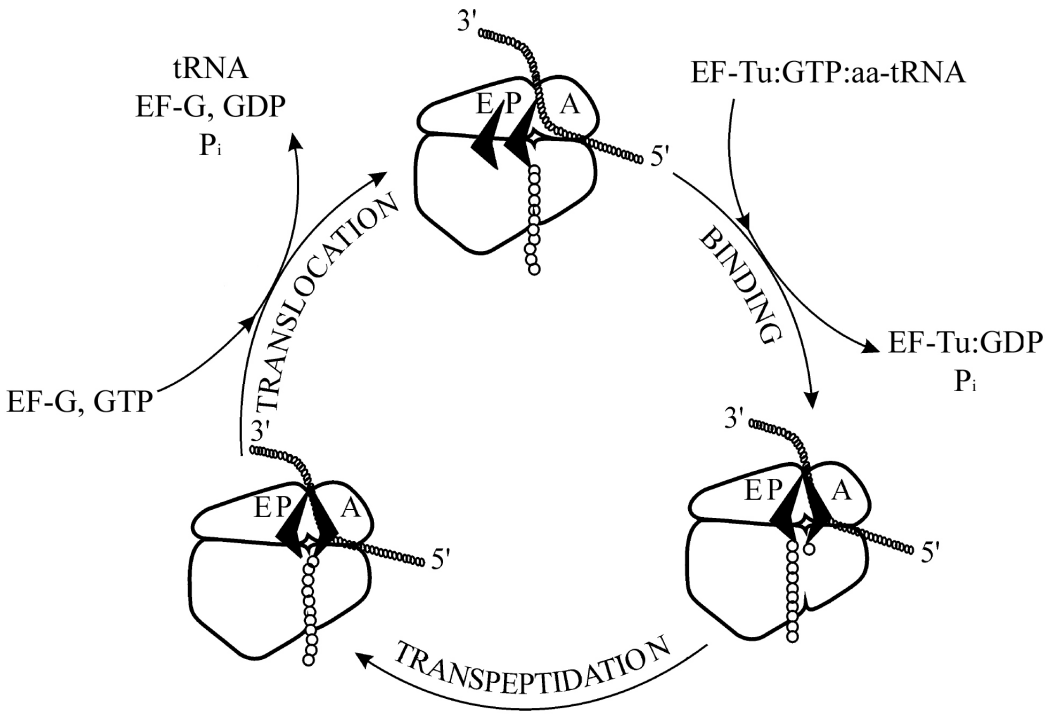

Figure 1.2. The allosteric model of the elongation cycle.

The elongation cycle includes three major steps: aminoacyl-tRNA selection, peptidyl transfer and translocation. First step is selection of the correct A-site tRNA as part of the ternary complex of composed of EF-Tu:GTP:aminoacyl-tRNA. Binding of the aminoacyl-tRNA to the A-site triggers release of the E-site tRNA from the E-site. Aminoacyl-tRNA binding is followed by spontaneous formation of the peptide bond and transfer of the peptidyl moiety to the A-site tRNA. Finally, elongation factor EF-G catalyzes translocation, which involves movement of the peptidyl tRNA from the A-site to the P-site of the ribosome, shift of the deacylated tRNA from the P-site to the E-site. Modified from Spirin A.S. [19].

Aminoacyl-tRNA selection

Selection of the correct aminoacyl-tRNA is the first step of the elongation cycle. Numerous studies of translational fidelity and kinetics of aminoacyl-tRNA selection have been distilled into the "kinetic proofreading" model of A-site tRNA selection [21,22]. This model postulates that aminoacyl-tRNA discrimination by the ribosome takes place in two major steps: initial selection before, and proofreading after GTP hydrolysis. It includes six intermediate steps: (1) initial binding, (2) codon recognition, (3) EF-Tu (eEF-1 in eukaryotes) conformation change and GTPase activation, (4) GTP hydrolysis by EF-Tu and phosphate release, (5) dissociation of EF-Tu from the ribosome, and (6) either accommodation of the aminoacyl-tRNA into the A/A site or its rejection and dissociation from the ribosome (Figure 1.3) [23].

Initial binding is a rapid and non-specific step that places the aminoacyl-tRNA into the A/T site on 80S subunit. At this stage, the anticodon end of the aminoacyl-tRNA is located in the decoding center, and the acceptor end of the aa-tRNA does not interact with the ribosome and occupies the so called T-site [24,25] [i]. Subsequent formation of codon - anticodon base pairs between tRNA and mRNA stabilizes the ribosome - cognate tRNA complex [26-28], while non- and near- cognate tRNAs that fail to form codon - anticodon helices rapidly dissociate from the ribosome [26-28]. Thus codon recognition is the first selective step of the aa-tRNA selection. The crystallographic studies of *T. thermophilus* ribosomes illustrated that base pair

[i] T-site is not really a site, because the acceptor end of the aa-tRNA does not interact with the active centers of the ribosome. However it establishes contacts with the surface side of the ribosome. Also, in contrary to the other ribosomal sites, tRNA could not bind to the T-site only. This term rather should be used to describe the tRNA conformation in the ribosome:eEF-1:aa-tRNA complex

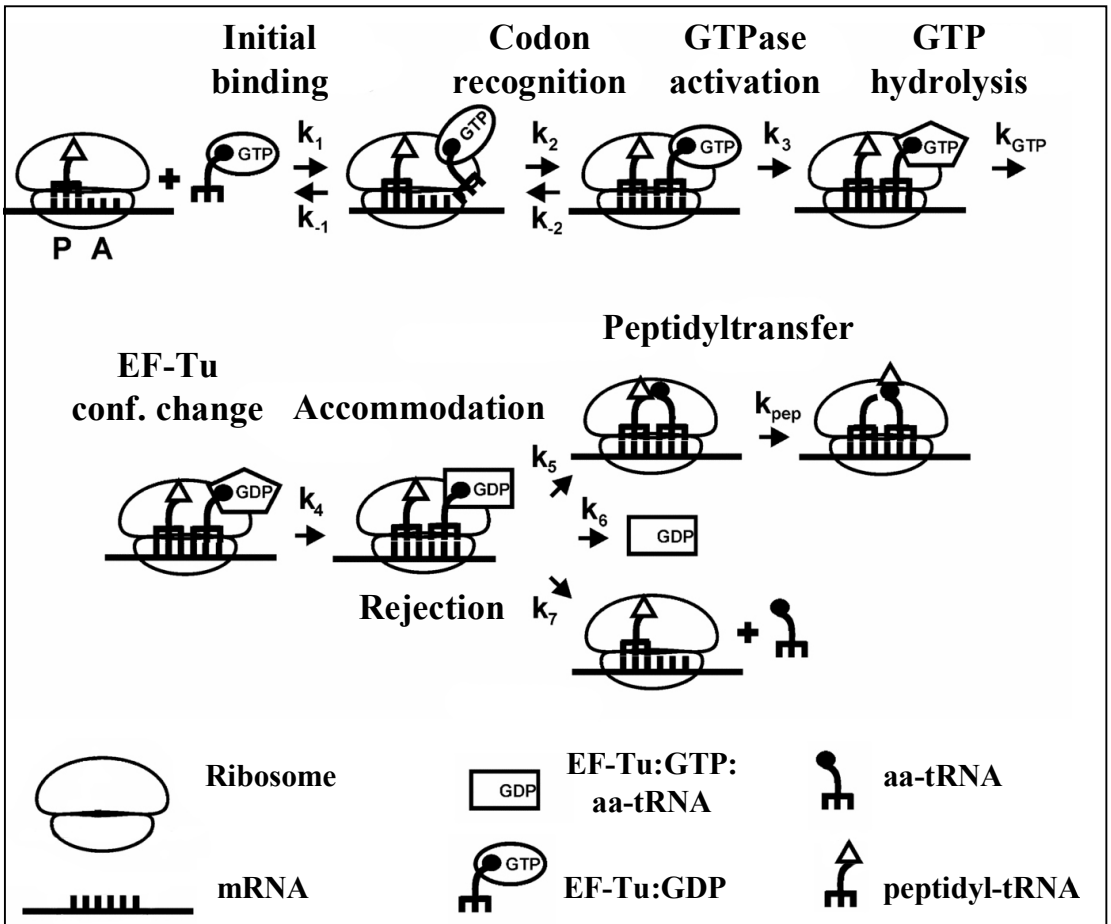

Figure 1.3. Kinetic proofreading model of aminoacyl-tRNA selection.

Kinetically resolved steps are indicated by rate constants $k_1 - k_7$, k_{-1}, k_{-2} and the two chemical steps that are rate-limited by the preceding step are designated k_{GTP} and k_{pep}. The selection of proper aminoacyl-tRNA includes two phases: initial selection and proofreading. GTPase activation and reverse reaction of codon recognition are selective steps in the initial phase. Accommodation is the second selective stage. Adopted from Wintermeyer W., *et al* [29].

formation is monitored through a complex network of interactions with 16S rRNA [30]. The universally conserved A1493 (in helix 44[ii], base numbering according *T. thermophilus*) binds in the minor groove of the first codon-anticodon base pair (counting from the 5' to the 3' end of mRNA). The second base pair is monitored through interactions between A1492, G530 and the minor groove of the second pair. In the third pair, C1054 (in *T. thermophilus,* h34) stacks against the first base of the anticodon. The third base of the mRNA codon directly interacts with G530, through a magnesium ion with C518, and amino acid residue P48 (in *T. thermophilus*) of protein S12 (S13 in *S. cerevisiae*, Figure 1.4). Formation of this network of interactions promotes conformational changes in h34 and h44 of 16S rRNA, as well as in the aminoacyl-tRNA. These conformational changes then triggers structural changes in the large subunit and EF-Tu [31]. Thus, activation of EF-Tu is induced by formation of the codon-anticodon helix, which is followed by rapid GTP hydrolysis. Kinetic studies suggest that rates of GTP hydrolysis are the same for cognate and non-cognate tRNAs and they are strongly induced by preceding conformational changes [28,31,32]. Upon GTP hydrolysis and phosphate release, EF-Tu adopts the GDP bound conformation [33,34] and rapidly dissociates from the tRNA and the ribosome [35]. The kinetic parameters of dissociation are similar for cognate and near cognate tRNAs and do not limit subsequent steps [36]. EF-Tu release is followed by accommodation. Accommodation includes movement of the 3' end of the aa-tRNA into the peptidyl transferase center (PTC) [37], formation of specific interactions between the 3'-CCA end of aminoacyl-tRNA and residues in the inner core of

[ii] Starting from here RNA helices are designated by the letter "h" followed by the helix number.

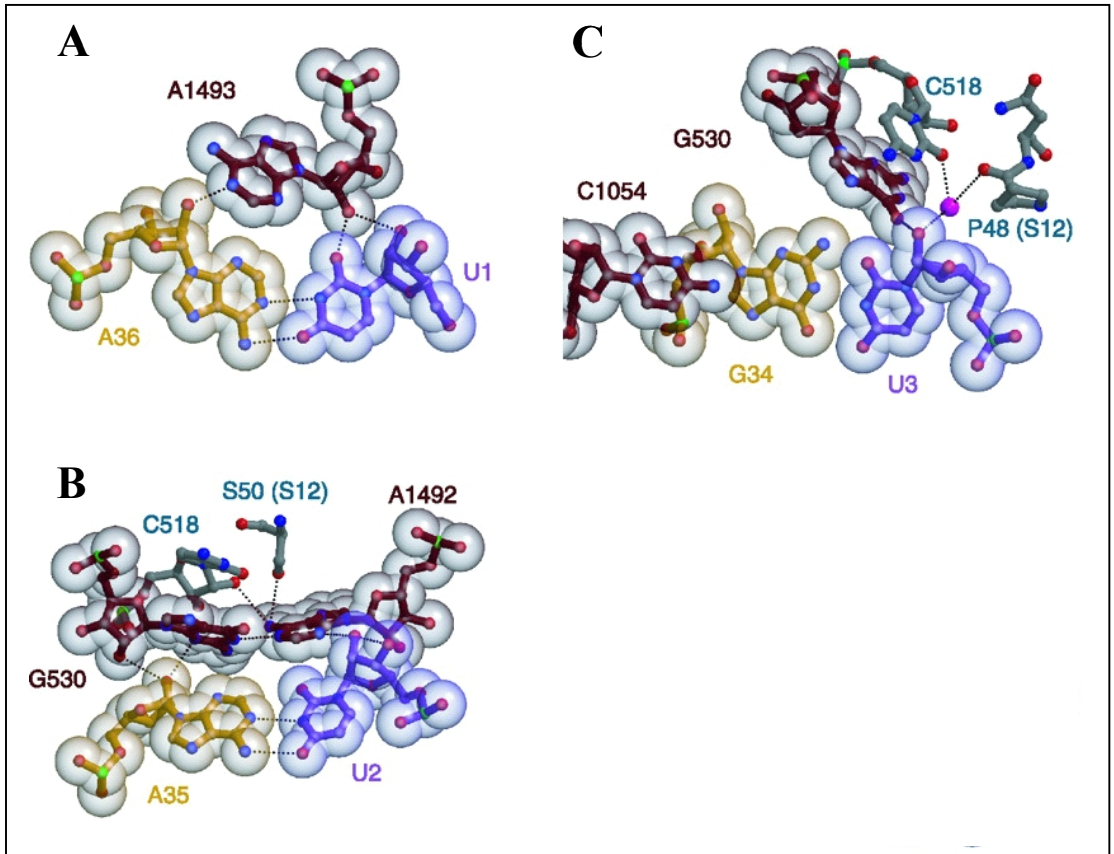

Figure 1.4. Codon recognition at the decoding center.

The tightness of the interactions is shown by the semitransparent van der Waals surface. A. In the first position, A1493 binds in the minor groove of the A36-U1 base pair. B. In the second position, G530 and A1492 (both brown) act in concert to monitor the A35-U2 base pair. C. The third G34-U3 base pair is monitored by C1054, G530 and C518. C1054 stacks against G34 of the anticodon stem loop (ASL). U3 interacts with G530, and indirectly through an Mg^{2+} ion (magenta) with C518 and residue Pro48 (*E. coli* Pro44) from protein S12 (gray). Adopted from Ogle J.M., *et al* [30].

peptidyl transferase center (A-loop [*aka* h38] and h92 of 23S rRNA) [38], and finally, adoption of the active conformation by the PTC [39,40]. Alternatively, at this step tRNA can be rejected and dissociate from the ribosome. The rate of accommodation is approximately 70 times lower and the rate of rejection is at least 20 times higher for the near-cognate tRNA compared to the cognate tRNA [21,23]. Thus, accommodation represents the second selective step in aminoacyl-tRNA discrimination.

Accommodation

The process of accommodation has been computationally simulated [37]. Prior to accommodation, the aa-tRNA occupies the A/T state. At this stage, the anticodon end of tRNA occupies the decoding center, and the acceptor end is kinked out in the D-loop region and is relatively free of interactions with ribosome. The aminoacyl-tRNA acceptor end establishes contacts with the GTPase associated center, (*E. coli* A1060, *S. cerevisiae* A1235, in h40), the tip of h89 (*E. coli* U2473, *S. cerevisiae* U2841), and the sarcin-ricin loop (*E. coli* A2660 and G2661; *S. cerevisiae* A3026 and G3027). At early stages of accommodation, the acceptor end slides smoothly along h89 and h90 until it pauses at the first of two "gates". This gate is formed by two nucleotides that lay at the base of h89 (*E. coli* U2492, *S. cerevisiae* U2860) and in the A-loop (h92, *E. coli* C2556, *S. cerevisiae* C2924). These two bases sterically interfere with progression of the 3'-CCA end into the peptidyl transferase center. Both the acceptor end of the tRNA and the A-loop of 23S rRNA flex to allow transition through this gate. Immediately after passage through the first gate, the 3'-CCA end clashes with U2573 (h92, *E. coli*, *S. cerevisiae* U2841), pausing for a second time. This is the second gate. At the final stage, the acceptor end moves through this gate

(*E. coli* C2556 and U2573; *S. cerevisiae* C2924 and U2941) and establishes interactions with residues in the inner core of the peptidyl-transferase center. Notably, h89, h90, and h92 together with ribosomal protein L16 (*S. cerevisiae* L10) guide the aa-tRNA during accommodation and constantly monitor its position. Thus, these residues may be involved aa-tRNA selection, and may participate in conformational changes that required for downstream reactions of the elongation cycle.

This computational simulation provides an explanation for the proofreading mechanism during accommodation. Before accommodation, the aminoacyl-tRNA adopts a distorted conformation. First, the kink in the flexible "variable loop" at the anticodon end is associated with formation of codon-anticodon helix [41]. Second, the major kink in the D-loop region of tRNA displaces the acceptor end of the molecule (Figure 1.5) [25], which puts the acceptor end outside of the A-site. Accommodation relaxes the aminoacyl-tRNA and allows it to adopt a conformation that more closely resembles its solution state. Thus the initial conformation of the aa-tRNA would likely affect the trajectory of the 3'-CAA end, and the ability of the acceptor end to pass through two gates. Near- and non-cognate aminoacyl-tRNAs fail to promote the conformational changes associated with codon recognition [21,42]. Thus during accommodation of these tRNAs the amino acceptor end may move along a different trajectory, which may affect ability of the tRNA to pass through accommodation gates thus resulting in aa-tRNA rejection [37].

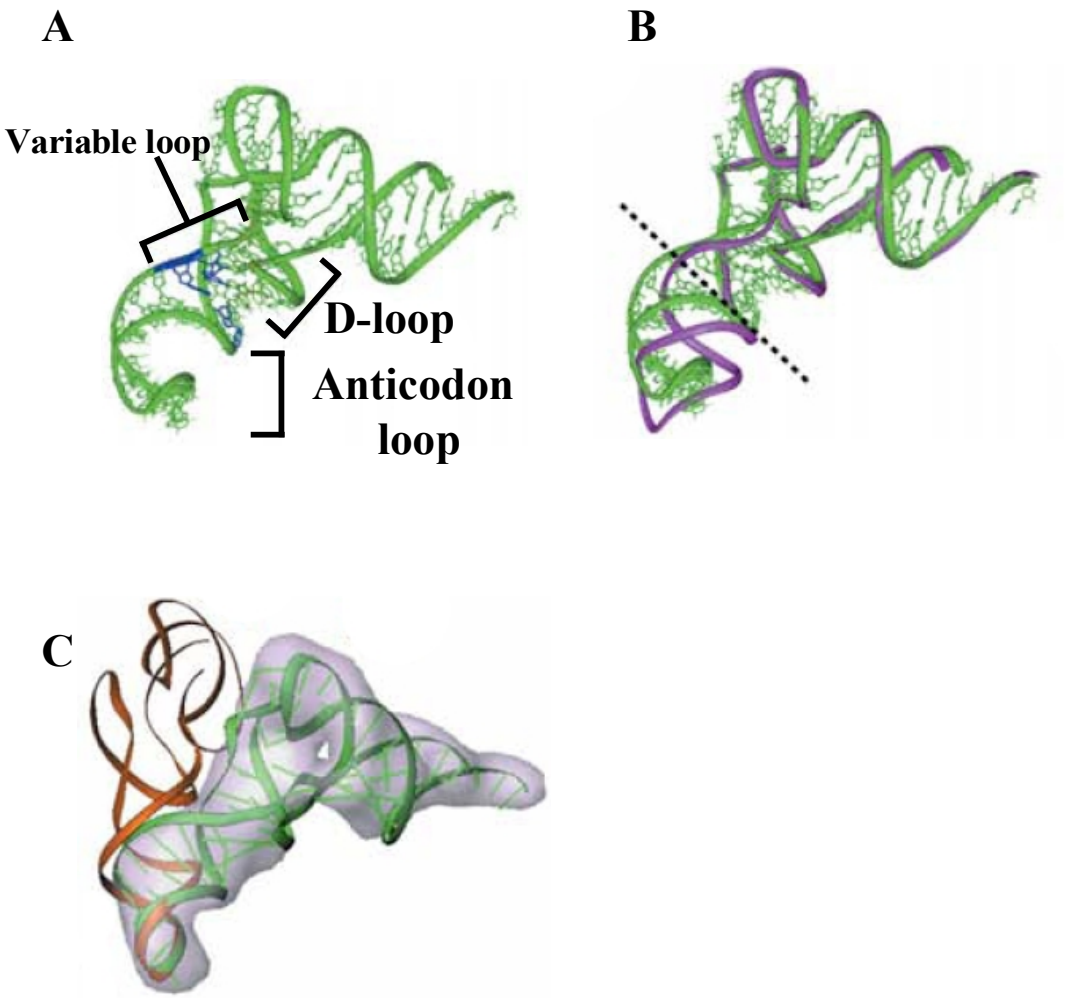

Figure 1.5. Conformational changes associated with accommodation and codon recognition.

A. tRNA conformation in the EF-Tu ternary complex. B. tRNA after codon recognition is shown in purple. Codon recognition triggers conformational changes in the variable loop and promotes the kink of the anticodon arm, designated by the dashed line. C. Superimposition of the tRNA structure before (shown in green) and after accommodation (shown in orange). During accommodation tRNA relaxes and adopts a conformation which mostly resembles the conformation of free tRNA. Modified from Valle M., *et al* [41].

Peptidyl transfer

Accommodation of aminoacyl-tRNA is followed by peptidyl transfer. This catalytic activity is mediated entirely by the 23S rRNA, thus the ribosome is a ribozyme. The 3-D structure of the ribosome demonstrated that the peptidyl transferase center is entirely composed of the 23S rRNA [43,44], and no proteins or conserved metal ions come within 18Å of the active site [45]. Recent structural studies suggest an induced fit mechanism of peptidyl transferase activation [39]. Binding of the A-site substrate induces structural rearrangements in the PTC, specifically affecting the bases in the loop between h89-90 and h90-93. In this conformation, the ester bond between the P-site tRNA and the peptide chain becomes accessible for nucleophilic attack by the primary amino group of the A-site substrate (Figure 1.6). Despite advances in crystallography and biochemical characterization of the peptidyl transfer, the precise mechanism of the peptidyl transfer is still unknown. Multiple hypotheses have proposed acid-base [46], substrate assisted [47,48] and proximity mechanisms [49,50]. Many different functional groups have been implicated as actively participating in catalysis. These include: the primary amino group of A2451 (in *E.coli, S.cerevisiae* A2841) [40], the 2'-OH of the A2451 ribose [51], the N3 ring nitrogen of A2451, and 2'-OH of A76 of peptidyl-tRNA [47,52].

Translocation

Following formation of the peptide bond, the tRNA:mRNA complex must be translocated in the 3' direction by precisely three nucleotides. Consequent to translocation, the peptidyl-tRNA replaces the deacylated tRNA in the P-site, and the

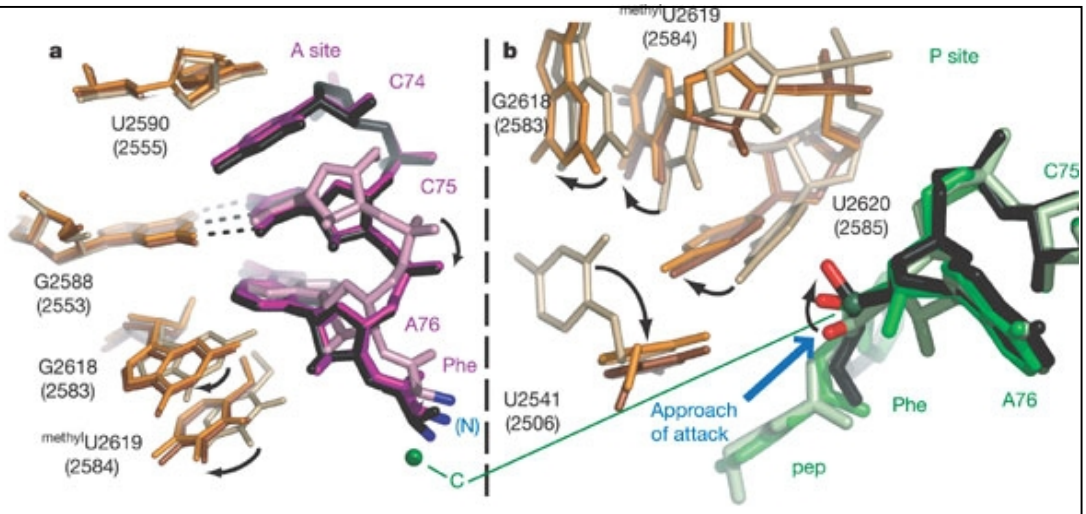

Figure 1.6. Induced fit conformational changes in PTC

Structures of the ribosome in uniduced, induced conformations, and in the complex with the transition state analog (TSA). A. A-site. B. P-site. The rRNA in uniduced conformation is shown in gray and in the induced conformation it is shown in orange. A-site substrate for uninduced conformation is shown in pink and for induced conformation in purple. The P-site substrate in uninduced conformation is shown in green and in induced conformation in light green. The transition state analog (TSA) which is thought to mimic transition intermediate during peptidyl transfer is shown in black. The rRNA of the ribosome in the complex with TCA is shown in dark brown. The proposed movements of the RNA bases are indicated by arrows. Modified from Pape T., *et al* [26].

deacylated tRNA moves into the E-site. Efficient translocation requires EF-G and GTP hydrolysis. However the requirement for EF-G:GTP can be waived, albeit the non-enzymatic translocation is ~100 fold slower . The exact mechanism of translocation is also unknown. There are currently a few hypotheses describing the movement of the tRNAs during translocation. An initial "three site model" described translocation as a single simultaneous movement of the peptidyl-tRNA from the A-site into the P- site, and deacylated tRNA into the E-site without the any intermediate steps. The "allosteric three site model" extends this hypothesis. It proposes that: 1) before translocation the E-site is unoccupied; 2) translocation involves movement of the deacylated tRNA into the vacant E-site; and 3) binding of the incoming aminoacyl-tRNA to the A-site promotes dissociation of the deacylated tRNA from the E-site, thus preparing it for the next round of translocation [20,53,54]. Alternatively, the hybrid states model implies that spontaneous movement of both acceptor ends occurs after peptidyl transfer. This movement shifts the acceptor end of the A-site tRNA into the P-site and acceptor end of the P-site tRNA into E-site, thus placing the peptidyl-tRNA into the hybrid A/P site and the deacylated tRNA into the P/E site. EF-G completes translocation and promotes movement of the tRNAs into the P/P and A/A sites (Figure 1.7) [55]. Chemical footprinting [55,56] and fluorescence experiments [57] support the existence of hybrid states, and cryo-EM reconstruction at high magnesium concentration tentatively demonstrated tRNA in the hybrid position [58]. In contrast, toeprinting experiments, biochemical assays, computational simulations, and the bulk of the structural data [41,59] have not been able to confirm the existence of this intermediate step.

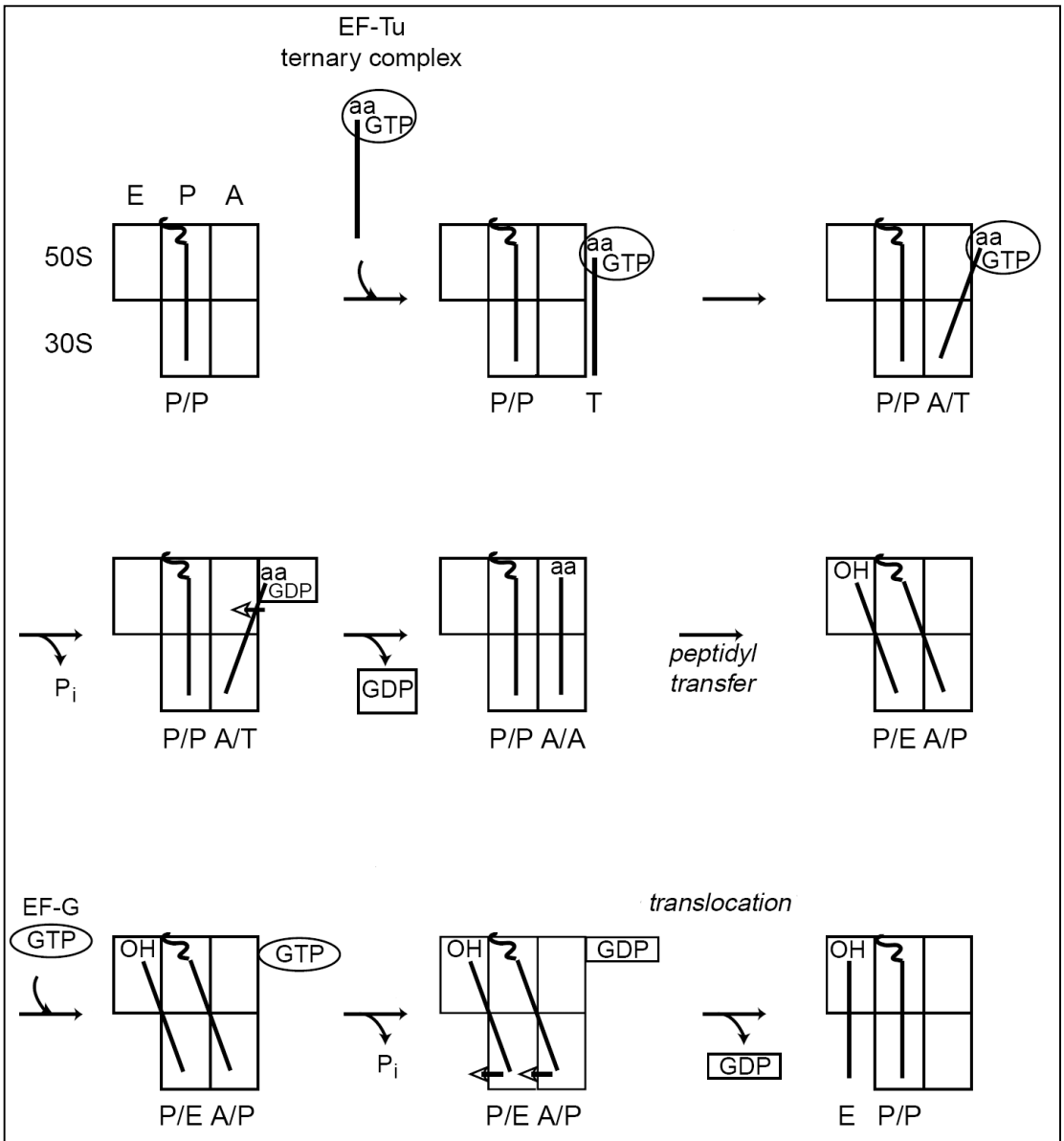

Figure 1.7. The hybrid states elongation model.

Spontaneous movement of the acceptor ends of the peptidyl and deacylated tRNAs occurs after peptidyl transfer. This movement places peptidyl-tRNA into the hybrid A/P site and deacylated tRNA into the P/E site. EF-G finalizes translocation and promotes movement of the tRNAs into P/P and A/A sites. Modified from Puglisi J.D., *et al* [60].

The molecular mechanism of translocation is unclear. The resemblance of overall shape between the ternary complex of EF-Tu:GTP:aa-tRNA and EF-G:GTP ("molecular mimicry", Figure 1.8) suggests that these factors may function in a similar manner. The structural resemblance between the anticodon stem loop of tRNA in EF-Tu:GTP:aa-tRNA suggests that during translocation the EF-G extension finger may fit into the A-site on the small subunit thus displacing the peptidyl-tRNA from the A-site and leveraging it into the P-site [61]. This position of the EF-G finger was observed in cryo-EM structures of EF-G:ribosome complexes, suggesting that displacement of the A-site tRNA by EF-G may be the driving force of translocation [62].

Termination

Termination is the final stage of translation process. It includes the hydrolysis of the ester bond between the P-site tRNA and polypeptide chain and release of the newly synthesized protein from the ribosome. Termination is triggered by the presence of a stop codon in the A-site of the ribosome and promoted by the release factors (Figure 1.9). There are two classes of release factors, denoted class I and class II [63]. Class I release factors decode the stop codon in the A-site of the ribosome and promote ester bond hydrolysis by the large subunit of the ribosome [64,65]. Class II release factors stimulate activity of the class I factors and tune their specificity. Prokaryotes have two class I release factors, RF1 and RF2, and one class II factor, RF3. RF1 recognizes UAA and UAG, and RF2 recognizes UAA and UGA codons [66]. The RF3 can stimulate both factors to recognize all three stop codons and is also required for subsequent dissociation of class I factors from the ribosome [67,68].

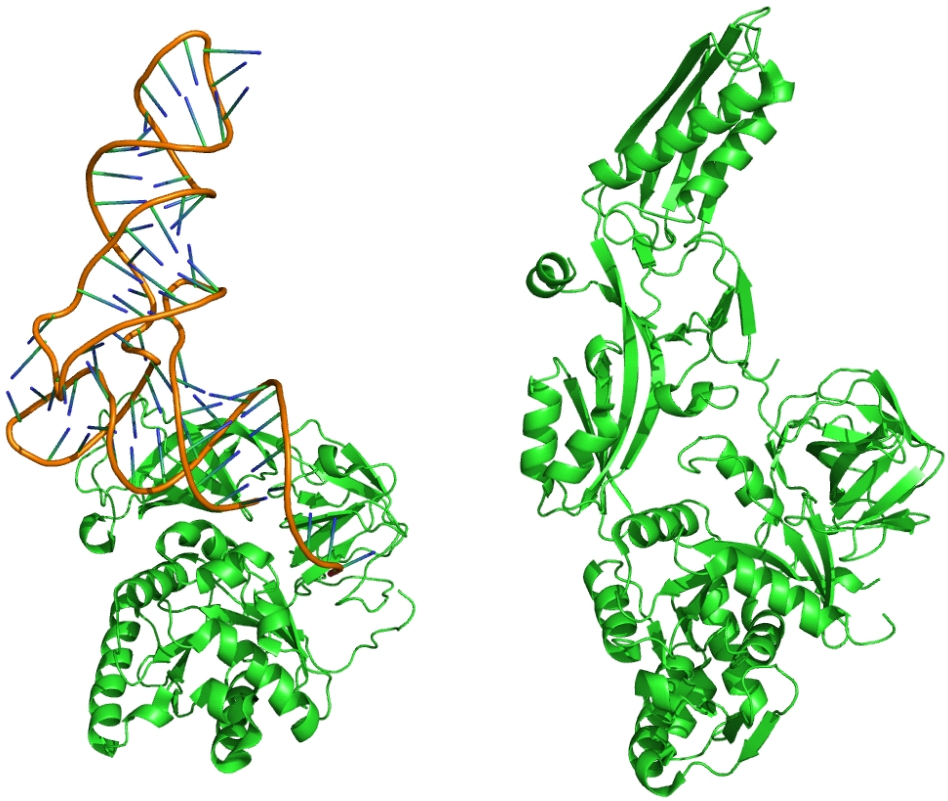

Figure 1.8. Ternary structures of EF-Tu and EF-G.

EF-G in the GTP bound form resembles the ternary complex of EF-Tu:GTP:aa-tRNA. The structure of EF-Tu:GTP:Phe-tRNA^{Phe} is from Kristensen O., *et al* [69] and the structure of EF-G is from Hansso S., *et al* [70].

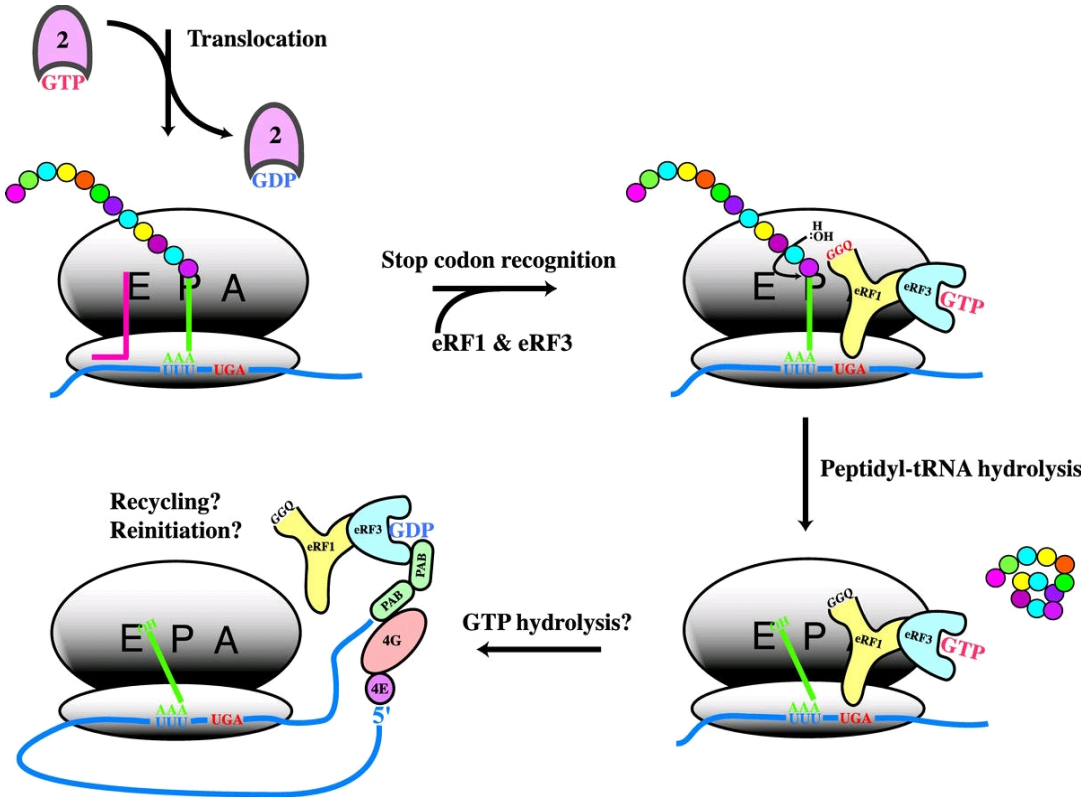

Figure 1.9. Translation termination in eukaryotes

Termination is triggered by the presence of the stop codon in the A-site of the ribosome. The stop codon recognition by the eRF1 or eRF1:eRF3:GTP complex promotes ester bond hydrolysis followed by the GTP hydrolysis by eRF3 and dissociation of the factors from the ribosome. From Kapp L.P. and Lorsch J.R. [63].

Eukaryotes have only one class I factor (eRF1) which is responsible for recognition of all three stop codons [71]. In contrast to elongation factors which are conserved among different kingdoms, there are no similarities in either primary or in ternary structures between free class I prokaryotic factors and eRF1 [72,73]. Thus, either the mechanism of termination is not conserved, or these proteins diverged beyond the simple similarity recognition. In fact, while the ternary structures of the free translation factors are dissimilar, the structure of eRF1 in complex with ribosome resembles the shape of free RF1, thus suggesting the possibility of divergent evolution [74,75]. Eukaryotes also have the single class II factor eRF3. RF3 and eRF3 do not posses any similarity at the level of primary structure, except in the GTP binding motif. Also in contrast to prokaryotes, eRF3 forms a cytosolic complex with eRF1, while no such complex has been observed in prokaryotes [76,77]. Since the conservation of the termination mechanism through evolution is unclear we decided to focus on the termination in eukaryotes to prevent further confusion.

In eukaryotes, termination includes three stages. First, the presence of a stop codon in the A-site is decoded by eRF1 or the eRF1:eRF3:GTP complex. This complex triggers hydrolysis of the ester bond. It is thought that this is followed by eRF3 mediated GTP hydrolysis and dissociation of these factors from the ribosome (Figure 1.9). The exact mechanism of termination is unclear. The resemblance of the overall shape of the class I factors and ternary complex of the EF-Tu:GTP:aa-tRNA promoted a molecular mimicry hypothesis [78]. In this concept, the overall resemblance between the ternary complex and the release factors is thought to allow termination factors to interact with the ribosome and function in the way similar to the ternary complex - ribosome interactions. In conjunction with this hypothesis, mutagenesis

studies identified the presence of the protein "anticodon" in RF1 and RF2. The three amino acid sequences PAT and SPF determine selectivity of RF1 and RF2 correspondingly to the specific stop codon [79,80]. However genetic studies of eRF1 did not reveal such a discriminatory motif; rather the entire domain that interacts with mRNA is responsible for mRNA recognition (Figure 1.10) [81,82].

Stop codon recognition is followed by ester bond hydrolysis. Genetic studies identified the universally conserved GGQ motif, which is required for activation of peptidyl-tRNA hydrolysis. However the role of the GGQ motif in hydrolysis is unclear. It was proposed that binding of release factor to the ribosome rearranges its ternary structure and places the GGQ motif in the peptidyl transferase center [74,83]. Two possible mechanisms were suggested. First, the glutamine residue may be involved in coordination of the water molecule, thus promoting nucleophilic attack by the water molecule [72]. However, mutagenesis studies demonstrated that mutations in this position did not affect the ability of eRF1 to promote ester bond hydrolysis [84], while two adjacent glycine residues are essential for this function [85]. Alternatively, hydrolysis may be catalyzed by the peptidyl transferase center of the ribosome, while termination factors trigger the conformational changes in the PTC but do not actively participate in catalysis [85]. The recently proposed induced fit hypothesis suggests a possible mechanism of ester bond hydrolysis. As was previously discussed (Chapter 1. Peptidyl transfer), binding of the EF-Tu:GTP:aa-tRNA to the A-site of the ribosome triggers conformational changes in the PTC (Figure 1.6). These structural rearrangements deprotect the ester bond of the peptidyl-

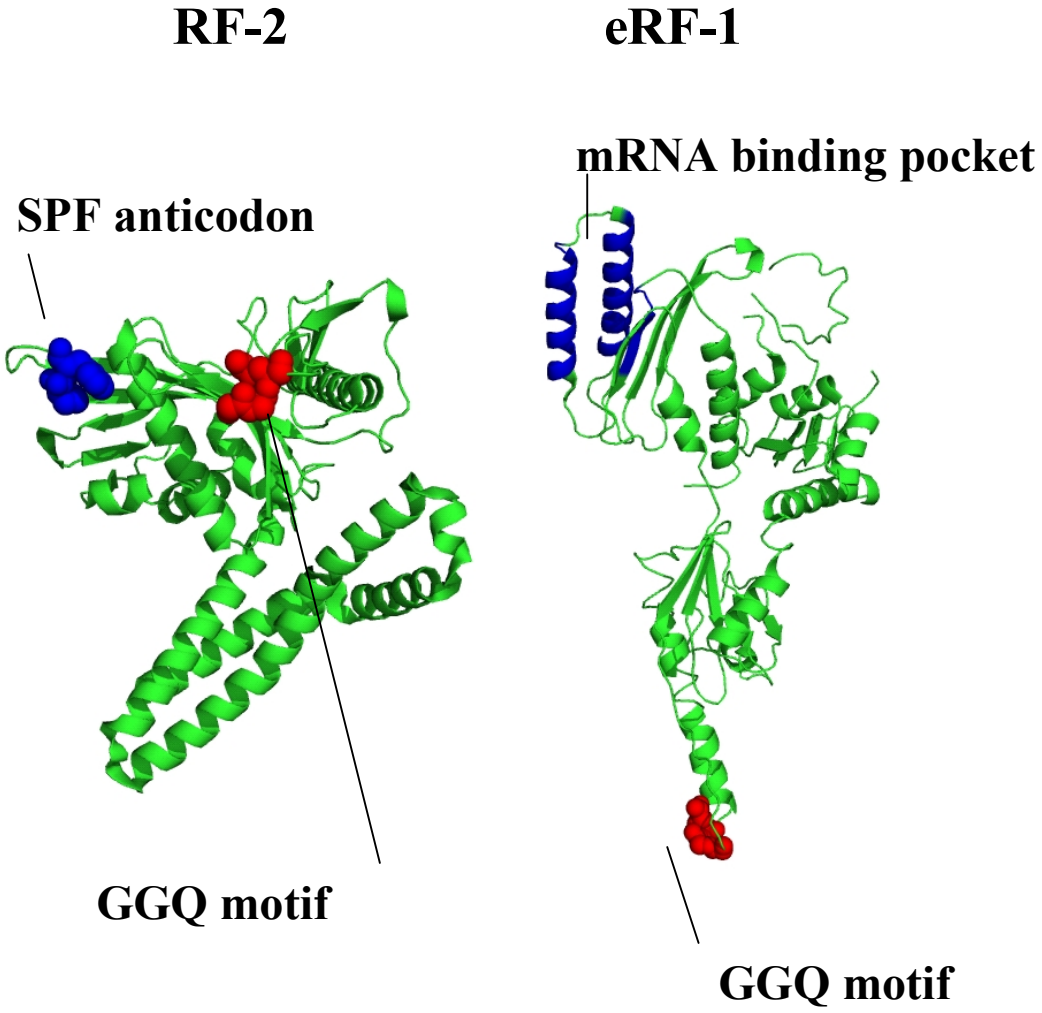

Figure 1.10. Ternary structures of class I release factors.

The *E. coli* RF-2 (from Vestergaard B., *et al* [73]) and of *H. sapiens* eRF-1 (from Song H., *et al* [72]) do not share similarities in primary nor ternary structures. The mRNA interacting regions are shown in blue and peptidyl transferase activating regions are shown in red.

tRNA from nucleophilic attack by the primary amino group of the aa-tRNA [39]. It was suggested that termination factors might trigger the same kind of movement in the PTC, which in absence of aa-tRNA would result in hydrolysis of the ester bond by water. In support of this model, fitting of theoretical water molecules in the 3-D ribosomal structure demonstrated that in the uninduced state the ester bond is protected from water mediated nucleophilic attack by the A2486 and U2620 bases (in *H. marismortui*, *S. cerevisiae* A2819 and U2953). Movement of U2620 during the adoption of the active conformation would allow a water molecule to enter into the PTC, thus permitting the hydrolysis of the ester bond (Figure 1.11) [39]. In accordance with this hypothesis the GGQ motif would be involved in PTC activation rather than directly participating in catalysis.

eRF3 mediated GTP hydrolysis follows cleavage of the ester bond and promotes dissociation of the release factors from the ribosome. The exact mechanism of GTPase activation and role of GTP hydrolysis during eukaryotic termination is unknown. The mechanism of function of eRF3 is likely to be distinct from RF3. In prokaryotes, RF3 binds the ribosome in the GDP bound form. Subsequent cleavage of the ester bond promotes GTP exchange, which triggers dissociation of the class I factors from the ribosome [67]. It is thought that following GTP hydrolysis by RF3 is required for subsequent RF3 dissociation from the ribosome [67,86]. In contrast to eukaryotes, eRF3 does not require a class I factor for GTP exchange and binds to the ribosome in its GTP bound form. It was proposed that GTP hydrolysis by eRF3 may trigger dissociation of the factors from the ribosome in a manner similar to that of

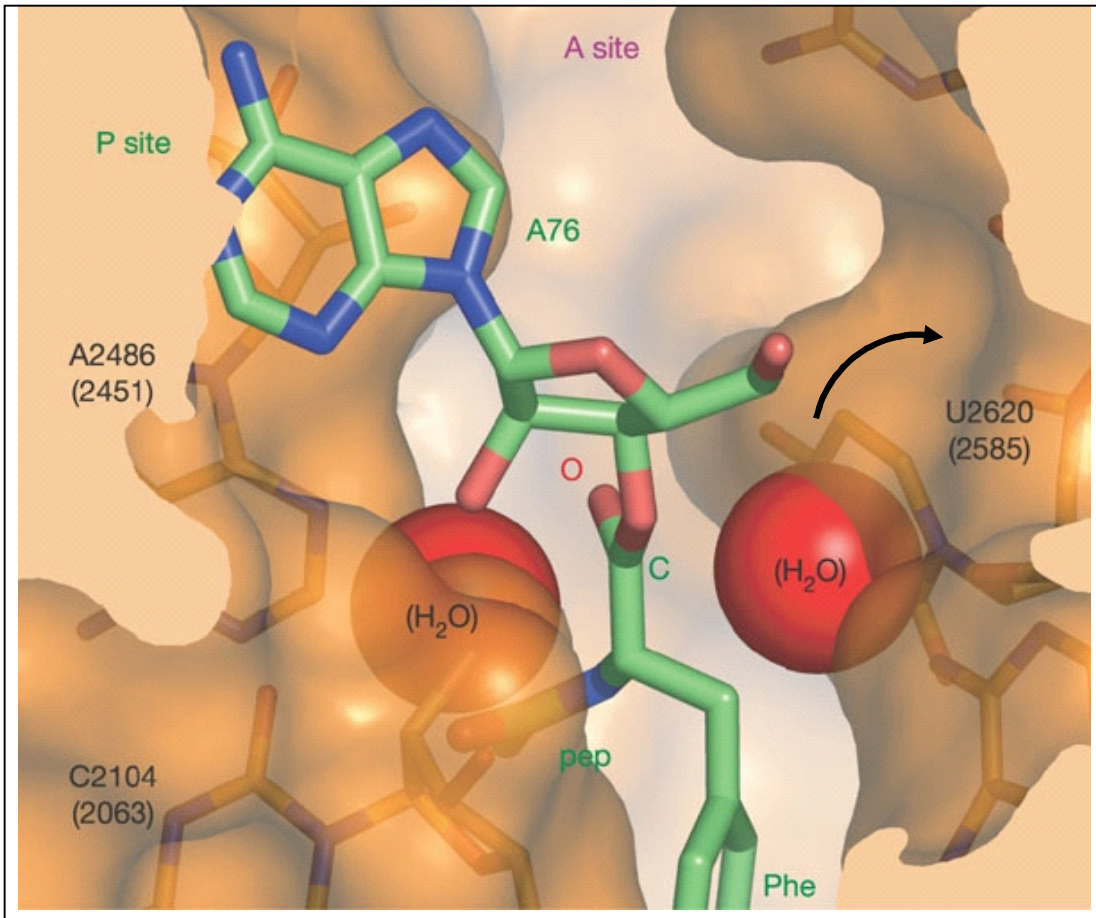

Figure 1.11. Proposed mechanism of ester bond hydrolysis between the peptidyl-tRNA and new polypeptide chain.

The ribosome in uninduced conformation (depicted above) sterically excludes water from the PTC. The proposed movement of U2620 (in *H. marismortui*, indicated by the black arrow) upon adoption of the induced conformation would allow a water molecule to enter into the peptidyl transferase center in absence of the A-site substrate. Release factors may function in a similar manner as the A-site tRNA and promote such movement, which in the absence of the aa-tRNA in the A-site would result in hydrolysis of the bond between peptidyl-tRNA and polypeptide chain. From Schmeing T.M., *et al* [39].

RF3 [86]. It is possible that eRF3 is result of regressive evolution of RF3. The requirement of nucleotide exchange for class I factor release may have been lost during evolution, while GTP hydrolysis is still required for release of class II factors from the ribosome. Thus, the functions of the prokaryotic and eukaryotic class II factors could be at least partially similar.

Translational recoding

During the elongation cycle, the ribosome moves along the mRNA decoding nucleotide triplets, eventually terminating at the stop codon. However, multiple examples of translational "recoding events" that disrupt frame maintenance are known to occur. Examples include long "hops" of 50 nucleotides or more, slips of a few bases in either direction, and "shunts" around large mRNA structures [87,88].

Nonsense codon suppression

Nonsense suppression is one such recoding event. There are two different types of the nonsense suppression: programmed and non-programmed. Programmed stop codon suppression occurs in response to downstream *cis*- signals in mRNA and *trans*-acting factors. This is a conserved mechanism for selenocysteine incorporation in all three kingdoms of life (except higher plants and fungi), and for pyrrolysine incorporation in bacteria. Incorporation of these amino acids happens with nearly 100% efficiency [89-91]. Non-programmed nonsense codon suppression (later referenced as nonsense suppression) occurs as result of stop codon decoding by natural suppressor tRNAs [92], and its efficiency depends on the intrinsic ability of the ribosomes to distinguish between the EF-Tu:GTP:aa-tRNA ternary complex and termination factors. Various suppressor tRNAs are known for different organisms.

For example, *E. coli*, $tRNA^{Gln}$ suppresses all three stop codons [93,94]. In *Tetrahymena thermophila* $tRNA^{Gln}_{UmUC}$ [iii], $tRNA^{Gln}_{UmUC}$ and $tRNA^{Gln}_{UmUA}$ can also decode all three stop codons[95,96], and in *Methanococcus jannaschii* stop codons encoded by $tRNA^{Tyr}$ [97]. In *S. cerevisiae* $tRNA^{Gln}_{CUG}$ is able to decode the UUA and UUG codons, and $tRNA^{Gln}_{UUG}$ can decode UUG [98,99]. Notably, non-programmed nonsense suppression can be influenced by the surrounding mRNA context [92,100]. The significance and mechanism of this effect is currently unknown. However it is thought that in general, non-programmed nonsense suppression occurs as result of the non specific incorporation of the amino acid at a termination codon. Genetic studies have determined a large number of mutations in tRNAs, eEF-1, termination factors and ribosomal proteins that affect nonsense suppression, thus reinforcing a notion that this kind of nonsense suppression depends on the ability of the ribosome to properly decode stop codon [101]. Through out our studies we have utilized nonspecific nonsense suppression as the tool to assess translational fidelity.

Programmed -1 Ribosomal Frameshifting

Programmed -1 Ribosomal Frameshifting (-1PRF) is another translational recoding event, and it is widely used by viruses and transposable elements to regulate expression of structural and enzymatic proteins. -1PRF signals have been identified and characterized from the Severe Acute Respiratory Syndrome virus (SARS-CoV) [102], Human Immunodeficiency Virus (HIV-1) [103], Infectious Bronchitis Virus (IBV) [104], the L-A virus [105] and many others. More recent studies have demonstrated that

[iii] Here superscript designates amino acid specificity of the tRNA and subscript designates an anticodon oif this tRNA.

-1PRF is not unique to viruses, and that functional -1 frameshift signals are present in the yeast [106], mouse [107-109], and human genomes [107,110].

-1PRF is directed by two *cis* acting mRNA signals: a heptameric nucleotide slippery site *N NNW WWH*[iv] (the incoming 0-frame is indicated by spaces) immediately followed by an mRNA pseudoknot or strong stem loop (Figure 1.12). During -1PRF, translating ribosomes stall at the pseudoknot, pause over the slippery site, and slip by 1 base in the 5' direction. Eventually, the ribosomal helicase resolves the pseudoknot and translation resumes in the -1 frame [88]. The "simultaneous slippage model" was the first proposed mechanism of -1PRF [103]. In this model, the ribosome stalls over the slippery site and the A- and P-site tRNAs simultaneously slip one base in the 3' direction and then re-pair in the new frame (Figure 1.13). The original model did not define when -1PRF happens. However since the mRNA moves by 3 nucleotides during the each translocation step of the elongation cycle, it was assumed that -1PRF is a "distorted" translocation step and that slippage occurs co-translocationally. However, genetic and pharmacological evidence show that alteration of eEF-2 function has no effect on -1PRF [111-113], suggesting that post peptidyl transfer ribosomes cannot slip. In addition, protein sequencing of the frameshift products demonstrated incorporation of amino acids corresponding both to the 0 and -1 frames at the second codon of slippery site, which suggests that the identity of the amino acid at the A-site can be monitored (or aa-tRNA is selected) after tRNA slippage [114]. The peptidyl transfer presents

[iv] All sequences in this thesis are given in the standard IUB/IUPAC amino acid and nucleic acid codes. Where W is A or T (U in RNA), and H is A, C or T (U in RNA).

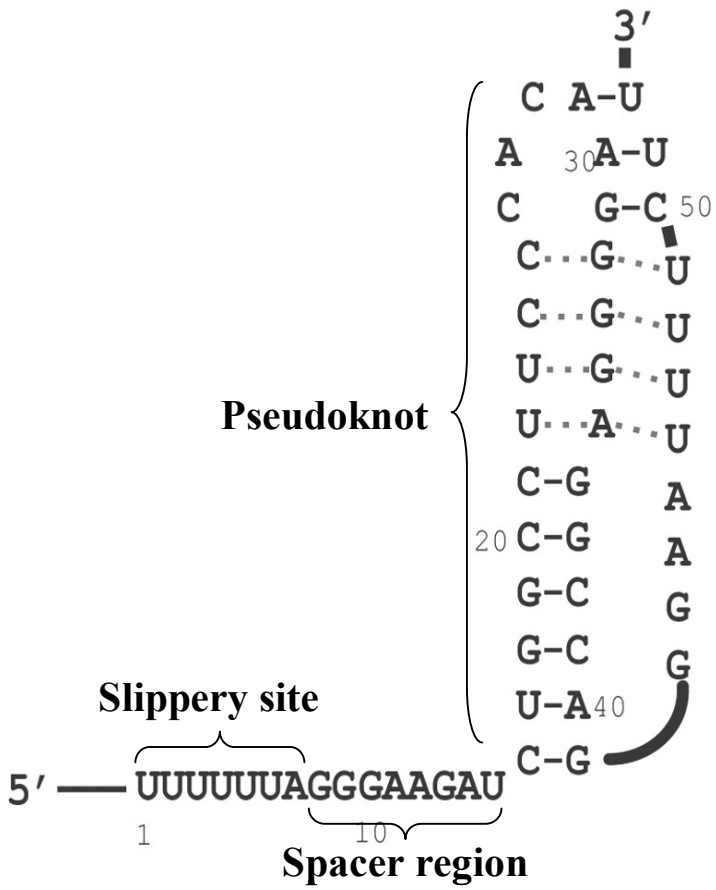

Figure 1.12. -1PRF signal of HIV-1 virus

The heptameric slippery site is separated from the pseudoknot by an eight nucleotide spacer. Adopted from Dinman J.D., *et al* [115].

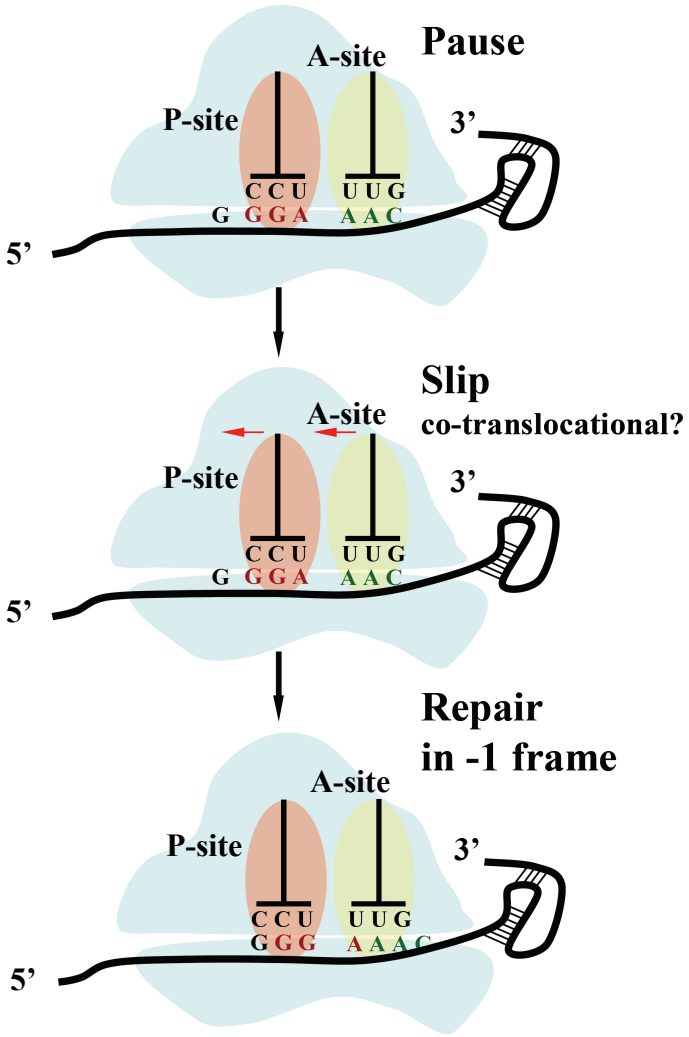

Figure 1.13. Simultaneous slippage model.

An mRNA pseudoknot induces elongating ribosomes to pause with their A- and P-site tRNAs positioned over the heptameric N NNW WWH (G GGA AAC) slippery site (the 0-frame is indicated by spaces). The nature of the slippery site is such that if the ribosome shifts by 1 base in the 5' direction (red arrows), the non-wobble bases of both the A- and P-site tRNAs can re-pair with the new –1 frame codons. After slippage, the mRNA pseudoknot is eventually denatured, and elongation continues in new reading frame.

the point of no return in aminoacyl-tRNA selection, thus -1PRF is unlikely to occur after peptidyl transfer and therefore co-translocationally. To accommodate these findings, an "integrated model" has been proposed. This model is essentially the same as "simultaneous slippage model" but defines the timing of slippage. It suggests that -1PRF takes place prior to peptidyl transfer, probably during the aminoacyl-tRNA selection step [116].

One of the main questions in the field is how mRNA pseudoknots promote efficient levels of –1PRF. Multiple studies demonstrated that a mRNA pseudoknot is essential for promoting efficient -1PRF. Disruption of the pseudoknot results in abolishing -1PRF [105,117]. Substitution of the pseudoknot with a stem loop of similar size and stability also abrogated frameshifting [104]. Notably, the -1PRF signal from HIV-1 initially identified as a stemloop was shown to form a pseudoknot, thus probably making the pseudoknot a ubiquitous requirement for efficient -1PRF and suggesting that the pseudoknot contains structural features that may be required for -1PRF.

The "9Å solution" was proposed to explain how pseudoknots might trigger -1PRF. A major consideration of this model of –1PRF is that a pseudoknot has two regions with opposite 5' - 3' directionality. This, it makes the pseudoknot topologically more difficult to unravel in a linear fashion. In combination with poorly matched geometry between the pseudoknot and the ribosomal helicase, it may result in the pseudoknot blocking mRNA entry into the mRNA tunnel [115,118]. Chemical toeprinting experiments detected: (A) Ribosomal pausing at the pseudoknot, (B) a one base mRNA movement and (or) conformational change in the mRNA entry tunnel,

associated with transition of the aminoacyl tRNA from the A/T to the A/A state during accommodation. Thus, it was proposed, that accommodation may create tension in the mRNA between the decoding center of ribosome and the pseudoknot. The "9Å hypothesis" proposed that subsequent slip of mRNA in the 5' direction relieves this tension resulting in -1PRF (Figure 1.14) [119].

The 9Å model could be viewed as an extension of the "integrated model" described above. It places the -1PRF event at the aminoacyl tRNA selection step, before peptidyl transfer, thus accommodating the existing genetic and biochemical evidence.

In contrast, several groups have proposed that slippage may occur co-translocationally, and genetic and biochemical evidence suggested the importance of the P-site tRNA for -1PRF [120,121]. Whether these observations explain when -1PRF occurs, or merely reflect the fact that -1PRF includes simultaneous slippage of both A- and P-site tRNAs remains to be answered.

Programmed +1 Ribosomal Frameshifting

Programmed +1 Ribosomal Frameshifting (+1PRF) is another example of a translational recoding event. +1PRF involves slippage of the translating ribosome by one nucleotide in the 3' direction. Like Programmed -1 Ribosomal Frameshifting, +1PRF is also utilized by viruses and transposable elements to regulate the synthesis of structural and enzymatic proteins [122,123]. Functional +1PRF signals also were found in human, mouse [124], *E. coli* [125], and *S.cerevisiae* genomes [126,127].

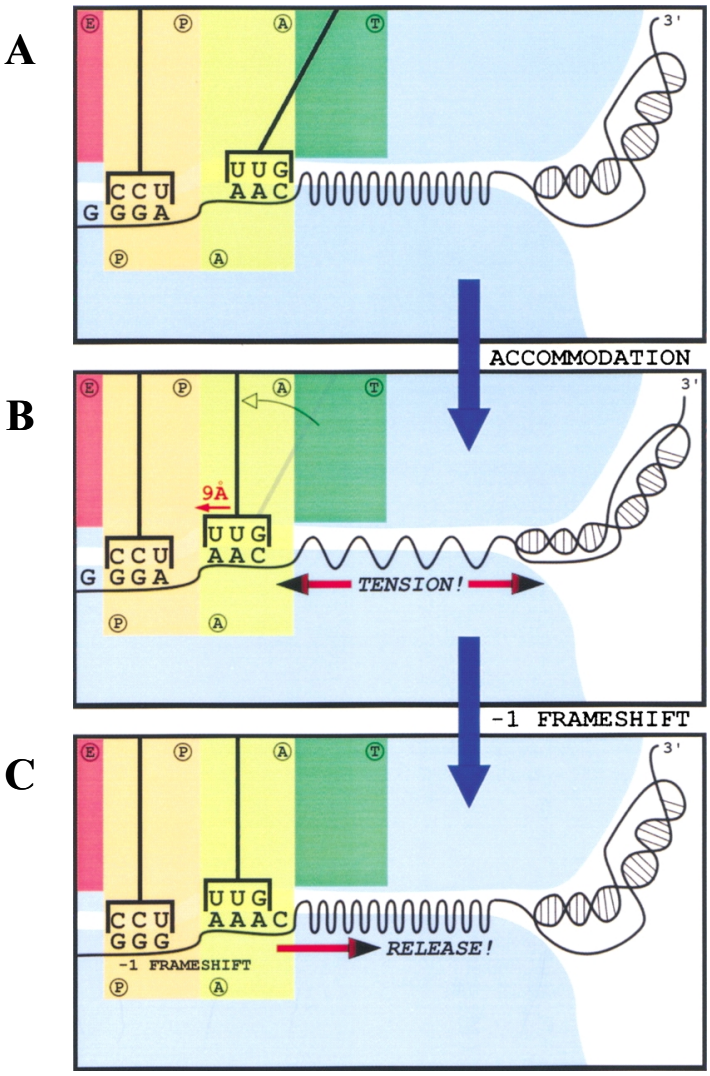

Figure 1.14. The 9-Å solution.

A. The 0-frame A- and P-site codons of a programmed –1 ribosomal frameshift signal are base-paired to cognate peptidyl- and aa-tRNAs occupying the P/P and A/T hybrid states respectively. B. Upon accommodation, the anticodon loop of the aa-tRNA moves 9 Å in the 5' direction, pulling the 3' mRNA sequence along with it. The mRNA pseudoknot is too large to enter the downstream tunnel, with the consequence that the linker region between the A-site codon and the mRNA pseudoknot is stretched, creating a localized region of tension in the linker region of mRNA. C. Decoupling of the A- and P-site codon-anticodon interactions from the 0-frame, and re-pairing in the –1 frame repositions the mRNA so as to relieve the tension. Adopted from Plant E., *et al* [119].

The frameshifting mechanisms of all known +1PRF signals are conserved. Like -1PRF, the +1PRF signal contains a heptameric slippery site, albeit the nature of the slippery site is completely different. Also, a downstream secondary structure is not required for efficient +1PRF. Protein sequencing of +1 frameshift products demonstrated the unambiguous incorporation of the 0-frame amino acid at the first codon and +1 frame amino acid at the second codon of the slippery site. These observations suggest that +1PRF happens before peptidyl transfer at the second codon, probably before or during A-site aminoacyl-tRNA selection [128]

+1PRF is kinetically driven by the presence of a codon decoded by a low abundance tRNA (hungry codon) at the A-site. For example, the slippery site of the Ty*1* retrotransposon is CUU AGG G (the incoming frame is indicated by spaces) [129]. The 0-frame AGG codon is decoded by the scarce $tRNA^{Arg}$, while the +1 frame GGC codon is decoded by the highly abundant $tRNA^{Gly}$ (Figure 1.15). The low abundance of the sense tRNA shifts the reaction of aminoacyl-tRNA selection toward the incorporation of a missense amino acid in the +1 frame. Amino acid starvation and genetic experiments support this hypothesis. Starvation by amino acid corresponding to the 0-frame codon induced +1PRF [130,131]. In contrast, overexpression of the hungry codon tRNA [129] or substitution of the hungry codon to a codon decoded by the high abundant isoaceptor tRNA eliminated frameshifting [114,128]. Thus from a kinetic point of view, the effects of the tRNA abundance could be seen as a type of kinetic partitioning [120]. The shortage of the 0-frame A-site tRNA promotes ribosomal pause and provides it time to slip. The following rapid

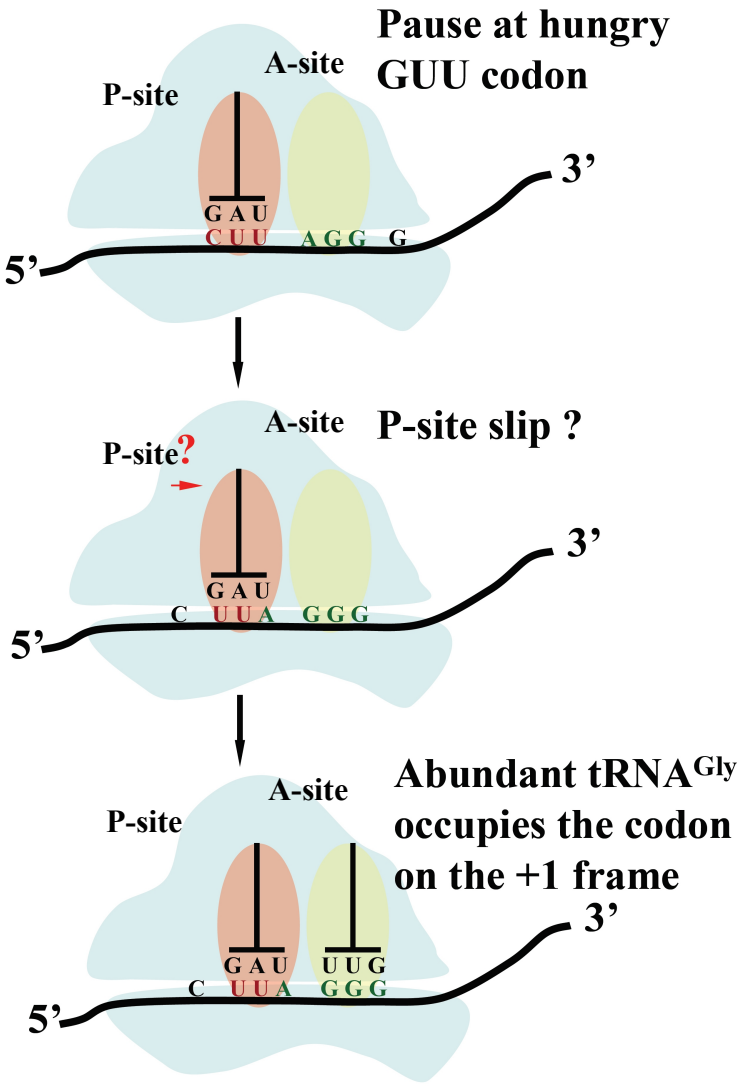

Figure 1.15. +1PRF.

A "hungry" AGG codon in the 0-frame of the heptameric CUU AGG C slippery site (the incoming frame is indicated by spaces) causes elongating ribosomes to pause while awaiting delivery of the rare CCU-tRNA^{Arg}. Slippage of the ribosome by one base in the 3′ direction during this pause allows the P-site tRNA to base-pair to the +1-frame GGC codon, creating a new A-site codon that corresponds to the highly abundant CCG-tRNA^{Gly}.

Figure 1.16. Kinetic model of +1PRF

Different ribosomal complexes designated as RS_{0-3}. Partial reactions are designated by the arabic numerals from 1 to 5. The changes in kinetic parameters that elevate rates of forward reactions (or decrease levels of the reverses reactions) in the left branch (and vice versa for the right branch) would elevate +1PRF level. For example, the rate of the 0-frame tRNA incorporation (1) is proportional would be proportional to the concentration of the RS_0 complex and concentration of the cognate tRNA. The slippage (3) is a first order reaction with rate proportional to the concentration of the RS_0 complex, and the rate constant. Thus abundance of the 0-frame tRNA would affect the ratio of reactions 1 and 3, in the agreement with observed effects of tRNA abundance on the +1PRF. It is obvious, that rate constant of the forward reaction (3) is determined by the stability of the codon anticodon duplex in the P-site of the RS_0 complex, and rate constant of the reverse reaction (-3) would depend on the stability of the codon anticodon duplex in the +1 frame. Rapid recognition of the +1 codon after P-site tRNA slippage followed by the irreversible peptidyl transfer works as an trap that prevents reverse reactions.

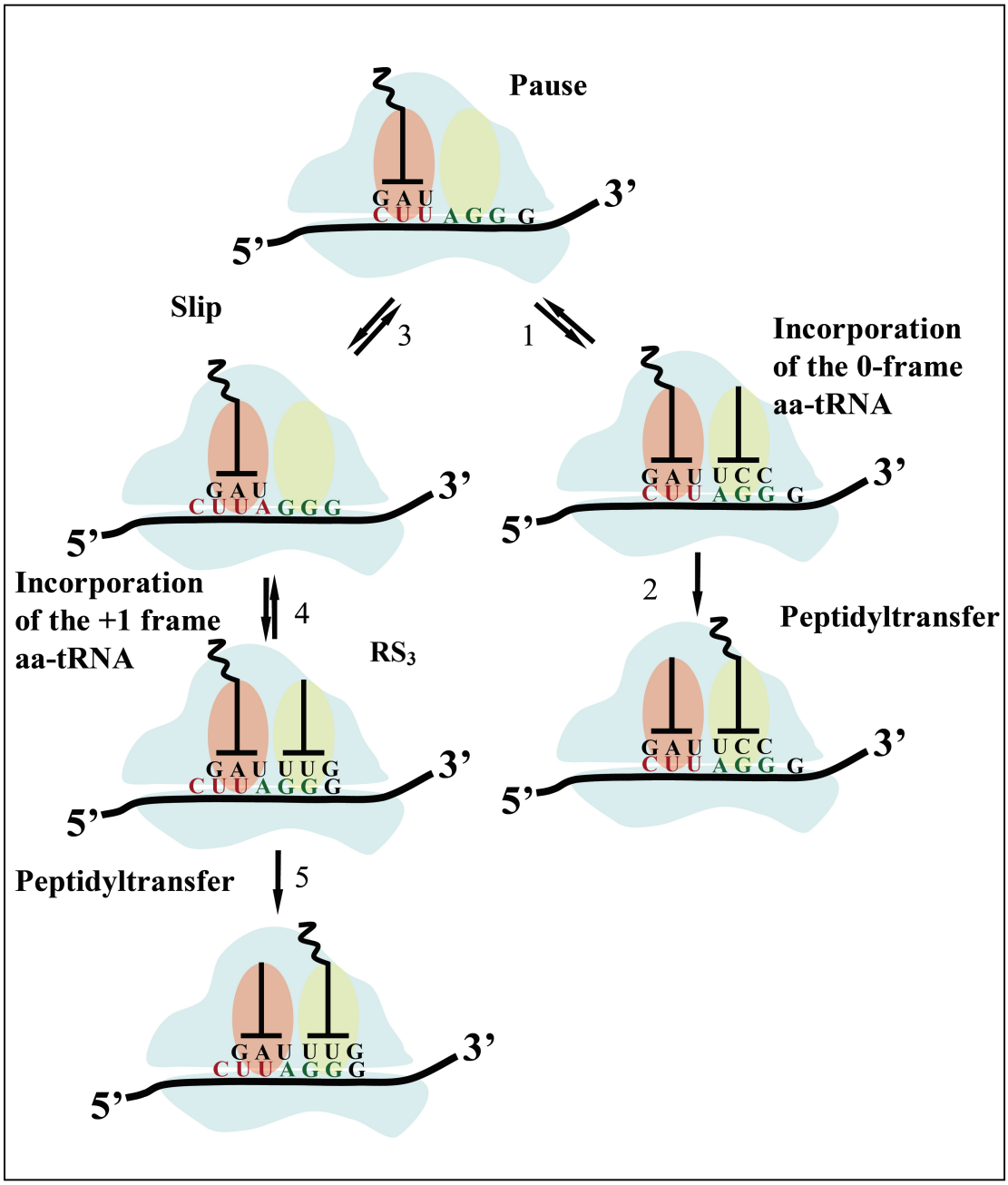
Pause
GAU
CUU AGG G
3'
5'
Slip
3
1
Incorporation
of the 0-frame
aa-tRNA
GAU UCC
CUU AGG G
3'
5'
GAU
CUUAGGG
3'
5'
2
Peptidyltransfer
Incorporation
of the +1 frame
aa-tRNA
4
RS3
GAU UCC
CUU AGG G
3'
5'
GAU UUG
CUUAGGG
3'
5'
Peptidyltransfer
5
GAU UUG
CUUAGGG
3'
5'

recognition of the +1 frame codon by abundant tRNAs, followed by the peptidyl transfer prevents slippage back to the 0-frame (Figure 1.16). The rate of slippage would depend on stability of the P-site tRNA complex and abundance of the 0 and +1 frame tRNAs. Also, in this model, the ratio of the 0-frame to the +1 frame aa-tRNA would determine the rate of the 0- and +1-frame recoding (reaction 1), thus defining the efficiency of frameshifting. The high abundance of the +1frame tRNA is required to increase rate of the +1frame codon decoding thus locking the ribosome in the new frame through the irreversible peptidyl transfer (reactions 4 and 5).

Several groups suggested that accommodation of +1 frame tRNA is preceded or accompanied by slippage of the P-site tRNA by one base prior incorporation of the A-site tRNA [120,132]. Substitution of the P-site leucine codon in the Ty*1* frameshift signal to any other leucine codon obliterated +1PRF frameshifting [87]. This notion is also supported by the observation that slippery site sequences of multiple +1PRF signals (e.g. the Ty*1* and Ty*3* retrotransposons of *S. cerevisiae*, *prfB* release factor of *E. coli* and *etc*.) allow the P-site tRNA to form a codon-anticodon duplex in the +1 frame. This notion is also supported by mutagenesis studies demonstrating that stability of the P-site interactions are critical for +1PRF efficiency [120,132]. Kinetically, the stability of the P-site tRNA:ribosome interaction is the major determinant of the slippage efficiency, thus also determining the efficiency of frameshifting.

Biological roles of the +1PRF and -1PRF

Programmed ribosomal frameshifting is a conditional event that allows translation of a downstream reading frame with a certain probability. +1PRF and -1PRF are used by viruses and retrotransposable elements to regulate expression of

their enzymatic and structural proteins. The L-A virus and Ty*1* retrotransposon of *S. cerevisiae* have long served as model systems for the studies -1PRF and +1PRF, respectively.

The genome of the L-A virus encodes two open reading frames connected by a -1PRF signal. The first frame encodes the *Gag* (capsid) protein, and the second encodes a viral RNA dependent RNA polymerase (RDRP). -1PRF is required for RDRP expression, and frameshifting efficiency defines the ratio of the capsid protein to viral polymerase [105]. Notably, viral polymerase is not only required for L-A replication and plus strand synthesis, but also nucleates capsid assembly. Alteration of frameshifting efficiency results in formation of incomplete viral particles, inhibiting L-A propagation [133]. The L-A virus has a satellite called M_1 that relies on L-A to supply capsid and RDRP. The single open reading frame of M_1 encodes a protein toxin that is exported into the surrounding media and kills M_1 minus cells, thus providing an easily detectable phenotype (Figure 1.17).

Like retroviruses, *Ty* elements of yeast replicate via an RNA intermediate. The Ty*1* frameshift signal connects two overlapping open reading frames (ORF) analogous to the retroviral *gag* and *pol* genes. Translation of the second frame (*pol*) is only possible as a result of +1PRF, which produces the *gag-pol* fusion protein [122,134]. Frameshifting efficiency defines the ratio of *gag* and *gag-pol*, which is critical for successful retrotransposition. Throughout our studies, we used programmed ribosomal frameshifting as a functional tool to characterize ribosomal components involved in maintaining correct reading frame and translational fidelity.

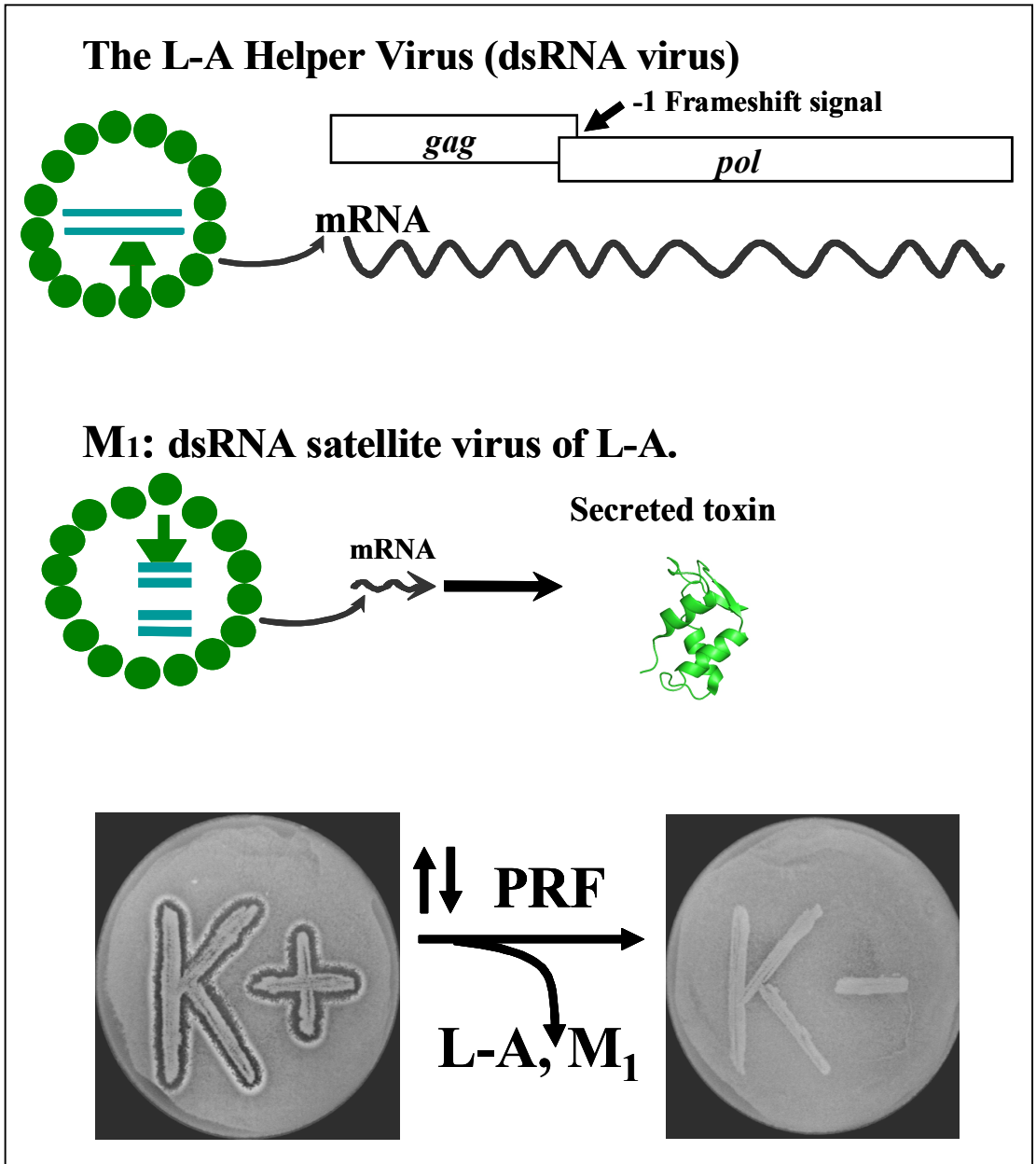

Figure 1.17. Killer virus system of yeast

A few examples of frameshift signals have been found in genomes of higher eukaryotes, however their significance is less clear. The regulation of polyamine biosynthesis via +1PRF is the most well studied, and appears to be a universally conserved regulatory mechanism in higher organisms that utilizes +1PRF. Arginine is a common polyamine precursor. It is converted into agmatine by agmatine decarboxylase. Agmatine is then transformed to putrescine by agmatinase. Alternatively, in the predominant pathway, arginase degrades arginine into ornithine, which is then converted into putrescine by ornithine decarboxylase. Then putrescine is converted into spermidine and spermine in a cascade of subsequent reactions (Figure 1.18, reviewed in Childs A.C., *et al* [135]).

The conversion of ornithine to putrescine is the limiting step of this pathway. Remarkably, ornithine decarboxylase expression is regulated in a feedback loop by antizyme [136]. The antizyme ORF is interrupted by a +1PRF signal, and translation of the downstream sequence is possible only as a result of +1PRF. Full length antizyme binds to ornithine decarboxylase and targets it for degradation by the 26S proteasome. The binding of antizyme also promotes dissociation of enzymatically active dimers of ornithine decarboxylase to enzymatically inactive monomers, resulting in a strong inhibition of ODC activity prior to degradation [137,138]. Early studies demonstrated that +1PRF efficiency depends on polyamine concentrations. High concentrations of polyamines promote increased levels of +1PRF and thus elevating antizyme expression [139,140]. This results in rapid degradation of ornithine decarboxylase and inhibition of the polyamine synthesis.

-1PRF signals have been identified in yeast [106], mouse [107-109], and human

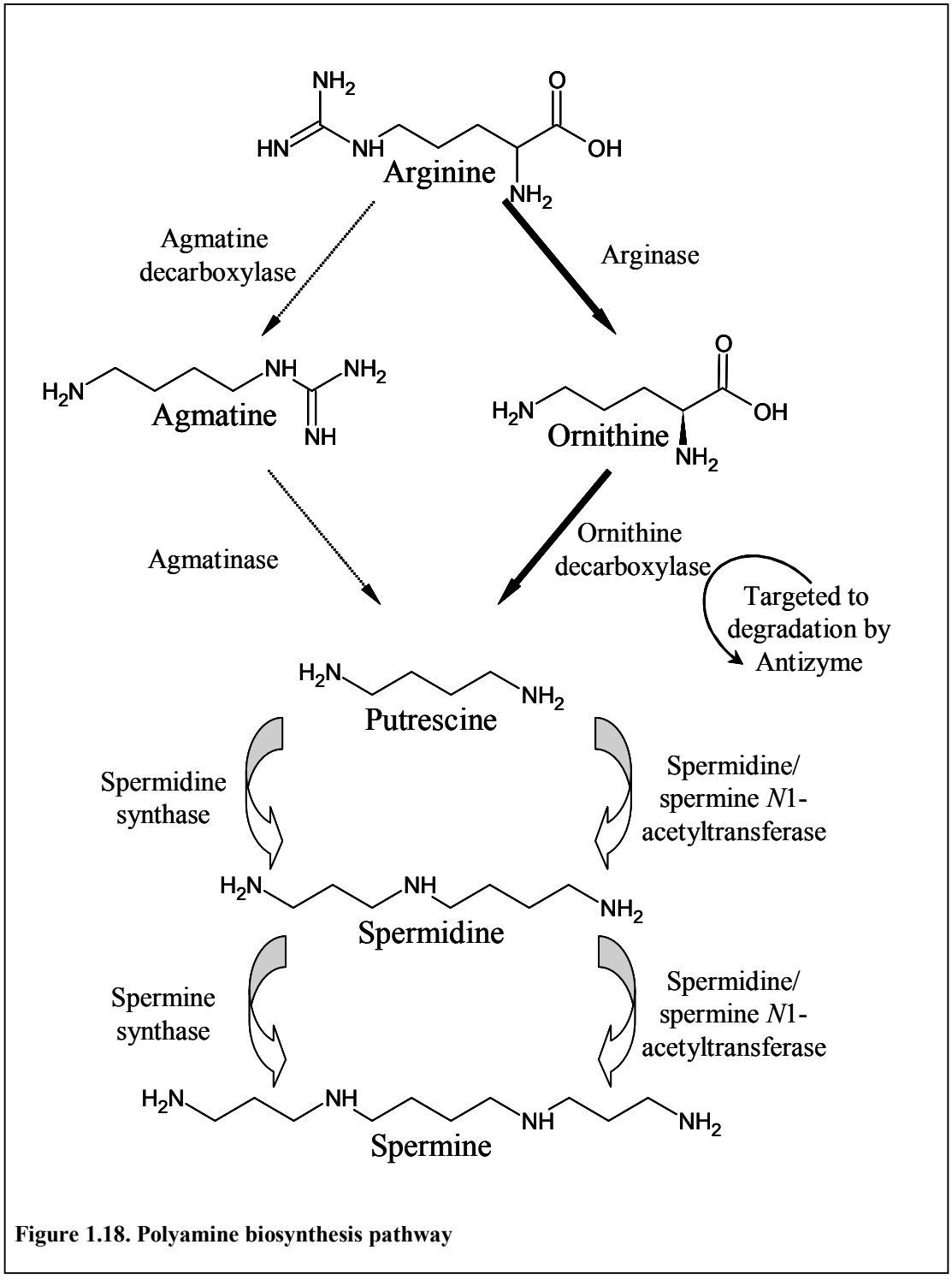

Figure 1.18. Polyamine biosynthesis pathway

genomes [107,110]. These include the mouse mucin domain containing gene *Muc1*, the mouse embryonal carcinoma differentiation regulated *Edr* gene, it's human orthologue PEG10, and the human paraneoplastic antigens Ma3 and Ma5. The presence of frameshifting product proteins in corresponding tissues has been demonstrated by western blotting and ability of these frameshift signals to promote -1PRF has been verified using artificial reporter systems. However, the functions of these genes and the significance of -1PRF signals remain unknown.

A search of the *S. cerevisiae* genome performed in our lab revealed the presence of multiple -1PRF signals [106]. Surprisingly, most of these signals do not direct the ribosome into new prolonged ORFs, but rather direct the ribosome to stop codons. Thus, -1PRF signals may act as conditional terminators of the protein synthesis, whose efficiency depends on frameshifting efficiency. It was proposed that the mRNA surveillance machinery would recognize such stop codons as premature termination codons, and that these mRNAs would be directed to degradation via the nonsense mediated decay (NMD) pathway. Thus -1PRF signals in eukaryotic genomes may work as mRNA destabilizing elements and therefore post transcriptionally regulate gene expression. This notion has been summarized in the "mRNA suicide" hypothesis [106,141]. In line with this hypothesis, experiments with an artificial reporter system containing -1PRF signals in the middle of the PGK1 reporter gene demonstrated an inverse relationship between mRNA stability and -1PRF efficiency [141]. Remarkably, microarray studies demonstrated that expression of approximately one third of the yeast genome is regulated via the NMD pathway [142-144]. It is currently unknown what fraction of these may be regulated via -1PRF. Importantly, "mRNA suicide" could not be unique to the -1PRF but also could be

triggered by +1 frameshifting. There are currently no observations that may support or argue against involvement of +1PRF in regulation of mRNA stability.

Nonsense mRNA Mediated Decay

The nonsense mRNA mediated decay (NMD) pathway degrades mRNAs in response to the presence of premature termination codons (PTC). NMD requires ongoing translation, a set of ubiquitous factors, Upf1p, Upf2p and Upf3p, and a wide range of accessory proteins, including those involved in termination and mRNA degradation. The Upf proteins recognize the presence of premature termination codon in conjunction with termination factors, targeting PTC containing mRNAs for degradation. The mechanisms by which the Upf proteins distinguish premature from normal stop codons remains unclear, and may vary between different organisms. In mammalian cells, premature termination codons must be > 59 nucleotides upstream of the most 3' exon - exon junction to be recognized by the NMD pathway [145]. In the nucleus, Upf3p interacts with the components of the splicesome and remains associated with mRNA after splicing and disassembly of the splicesome, thus marking the exon-exon junction [146,147]. Interactions between the terminating ribosome and Upf3p is thought to recruit the other Upf proteins, promoting mRNA decapping and degradation [148]. The mechanism of NMD in yeast is unclear and it is currently highly debated.

Thesis plan

X-ray crystal structures of the ribosome have greatly advanced our understanding of translation and provided positions and contacts of individual ribosomal components. These structures clearly demonstrated that ribosomes undergo multiple structural transitions during the elongation cycle. Currently, the dynamics of these transitions are still unknown. This work seeks to began to establish the connections between structure and function by identifying these components and uncovering the network of structural transitions that are responsible for information transfer between the active centers of the ribosome. Toward these ends, we used molecular genetics methods to identify functionally important residues in 5S rRNA and in ribosomal proteins L3 and L10. The mutants were characterized using genetic and biochemical methods. Chapter 2 discusses the role of ribosomal protein L3 in maintaining the conformation of the peptidyl transferase center and the aminoacyl-tRNA accommodation route. Chapter 3 describes saturation mutagenesis of 5S rRNA. Analysis of naturally occurring allelic variants of 5S rRNA suggests that this molecule may be involved in post transcriptional regulation of cellular gene expression via -1PRF coupled with the nonsense mediated decay pathway. Chapter 4 describes mutagenesis of ribosomal protein L10. The results of these experiments suggest that h38 and h89 participate in communication between the PTC and other active centers of the ribosome. Finally, Chapter 5 discusses these results in the context of X-ray crystal structures of the ribosome.

Chapter 2. Ribosomal protein L3

Introduction

Early in the history of modern yeast genetics, two mutants were independently identified based on separate phenotypes: resistance to the peptidyl transferase inhibitor trichodermin (*tcm1-1*) [149,150], and inability to maintain the M_1 killer virus (*mak8-1* = maintenance of killer) [151]. They were subsequently shown to be allelic to *RPL3*, the gene that encodes ribosomal protein L3, a 44 kDa essential large subunit ribosomal protein [152,153]. Independently, ribosome reconstitution experiments demonstrated that L3 is one of a few proteins required for peptidyl transferase center (PTC) activity [154], and that L3 and L24 are the only two proteins capable of initiating *in vitro* assembly of the *E. coli* 50S ribosomal subunit [155,156]. These early findings implicated L3 as a central component of peptidyl transfer activity, ribosome assembly, and as an important factor in the interaction between host cells and viruses.

An initial study of the *mak8-1* allele in the Dinman lab demonstrated that: (A) increased -1PRF efficiency constituted the basis for the loss of killer phenotype in *mak8-1* cells; and (B) the original *mak8-1* allele consisted of the double *rpl3* mutation W255C+P257T [157]. In a subsequent study, three additional single mutations were identified that were unable to maintain the killer virus (W255C, P257T, and I282T). The inability to propagate the killer virus in these strains was explained through elevated levels of -1PRF [158]. Biochemical analyses demonstrated that increased efficiency of -1PRF correlated with reduced rates of peptidyl transfer [158]. Importantly, the correlation between peptidyl transferase activity and -1PRF efficiencies was not

specific to *mak8-1*: these two properties also correlated in mutants of ribosomal protein L41 (*RPL41*) and histone deacetylase (*RPD3*) [159,160]. The molecular mechanism that couples -1PRF and peptidyl transferase activity is still unknown, however the existence of such a correlation suggests a functional link between -1PRF and peptidyl transfer.

Notably, the initial screen for mutant alleles that affected frame maintenance resulted in identification of the *mof6-1* allele of Rpd3. Expression of the *mof6-1* allele promoted increased levels of the -1PRF and resulted in loss of the killer phenotype [159,161]. Rpd3p is a part of the large histone deacetylation complex that includes the DNA binding protein Sin3p, and the regulatory proteins Sap30p and Ume6p [162]. Deacetylation of histones by Rpd3p promotes local chromatin condensation, resulting in repression of nearby PolII transcribed genes [163,164]. Remarkably, mutations in the *SIN3* and *SAP30* components of this complex that promote chromatin condensation also resulted in increased levels of -1PRF [159,165]. It is unclear how mutations in histone deacytelation complex promote the described phenotypes. One possibility is that these mutations may affect transcription of the ribosomal genes, including ribosomal proteins and rRNA. The resulting imbalance between ribosomal components may affect ribosomal biogenesis, resulting in formation of the 60S subunits that are different in their biochemical properties. However, the possibility of secondary effects has not been ruled out. The *RPD3* complex regulates transcription of a wide range of genes. It is possible that mutations in the *RPD3* complex may affect transcription levels of other components of the ribosome biogenesis machinery. Alternatively, the posttranscriptional regulation of mRNA stability via -1PRF and NMD pathway (Biological roles of the +1PRF and -1PRF, page 36) suggested the

existence of *trans*-acting factors that specifically regulate -1PRF efficiency. The identities of these factors are currently unknown; however it is possible that the histone deacetylation complex may mediate expression of these factors. Regerdless, the possible link between ribosomal biogenesis and -1PRF is intriguing.

Ribosomal protein L3 was also found to affect -1PRF. It contains two domains: a globular domain, located on the cytoplasmic side of the large ribosomal subunit, and a long extension that protrudes into the body of the large subunit toward the peptidyl transferase center. The globular domain of L3 forms extensive contacts with domain VI of 25S rRNA. It contacts h95 (at the tip of which is the sarcin-ricin loop (SRL)) and the GTPase associated center (h40-42). The base of the L3 extension interacts with the base of the h95. The middle section of the extension comes into close contact with helix 40, (part of the GTPase associated center), and with helixes 90, and 91. The distal portion of this domain contacts with the loop that connects helixes 89 and 90, and which forms the A-site region of the peptidyl transferase crevice. In the 3-D ribosomal structure, h95, h90-92, and h89 are stacked parallel to one another and form a continuous rRNA layer [166,167] (Figure 2.1). The *mak8-1* mutations are located in the tip of the extension, and tryptophan and proline residues contact with the loop that connects helixes 89 and 90. Notably, mutations in the same vicinity of the L3 proteins of *E. coli* and *Brachyspira spp.* also promoted resistance to tiamulin, a pleuromutilin antibiotic inhibitor

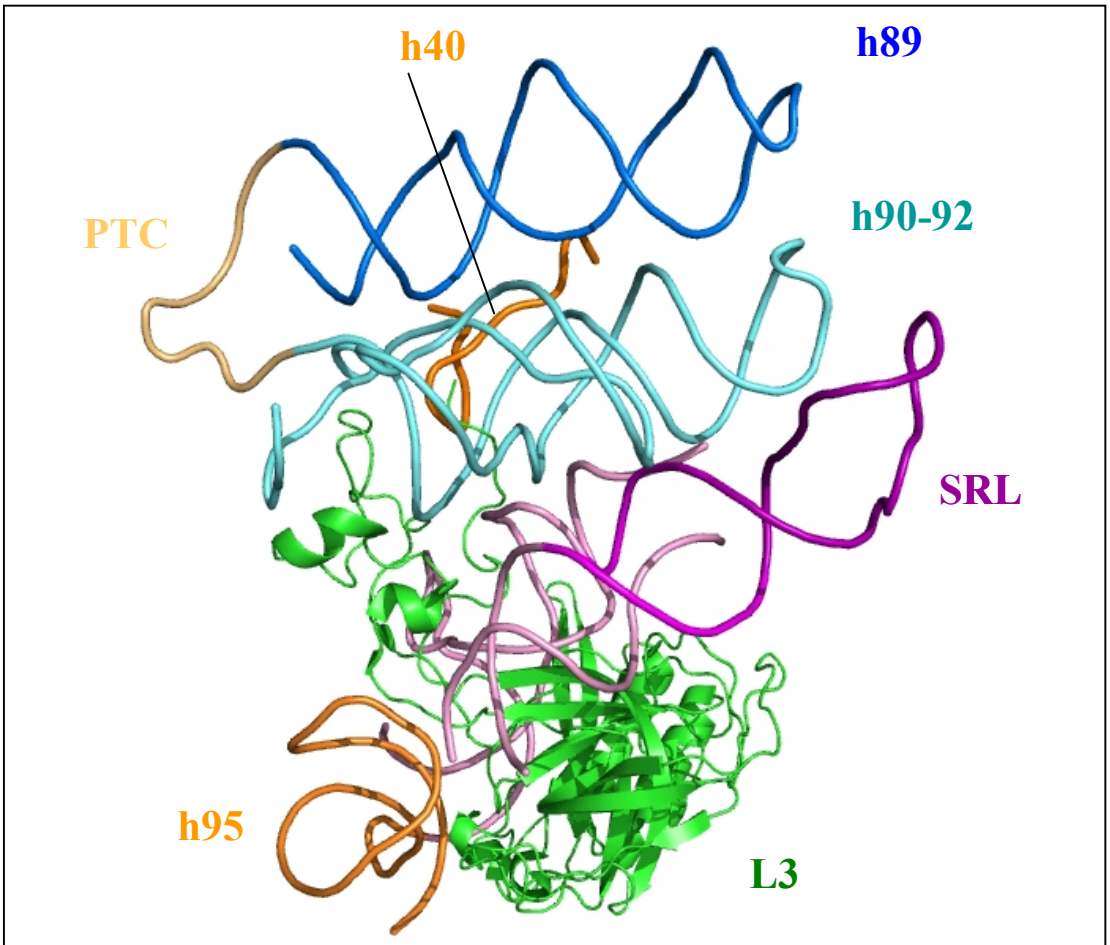

Figure 2.1. Position and contacts of ribosomal protein L3.

Ribosomal protein L3 contacts with the sarcin-ricin loop (SRL), the GTPase associated center (h40), helix 89, helixes 90-92, and helix 95 of 25S rRNA. The tip of the extension domain interacts with the peptidyl transferase center. (Based on the Cryo-EM structure of the *S. cerevisiae* ribosomes from Spahn C.M.T., *et al* [184].)

of peptidyl transfer [168], thus suggesting necessity of this domain for proper ribosomal function. Notably, previous studies in the Dinman lab demonstrated effects of peptidyl transferase inhibitors on the efficiency of -1PRF, thus linking peptidyl transfer and translational recoding [160,169]. Biochemical characterization of *rpl3* mutant strains showed altered levels of peptidyl transfer and -1PRF in these strains. These observations provoked more in-depth characterization of the *mak8-1* mutants. Toward this end, characterization of existing mutant alleles of L3 was conducted. Strains harboring mutant alleles of ribosomal protein L3 were characterized for their effects on cell propagation, protein synthesis and biochemical properties of mutant ribosomes. We found that mutations in L3 affected resistance to the peptidyl transferase inhibitors anisomycin and sparsomycin. Biochemical characterization demonstrated: (A) that elevated affinity for A-site tRNA is the underlying cause of anisomycin resistance in L3 mutants; (B) a correlation between increased affinity for aminoacyl-tRNA and elevated levels of -1PRF; (C) conformational changes in the vicinity of the PTC; and (D) altered DMS reactivity of the bases that form the "gates" through which the aminoacyl-tRNA passes during accommodation. These findings implicate ribosomal protein L3 in maintenance of the conformation the peptidyl transferase center and of the tRNA accommodation route.

Materials and methods.

Strains, media and genetic methods.

E. coli strain DH5α was used to amplify plasmid DNA. Protocols for transformation of yeast and *E.coli* and the YPAD, synthetic drop out medium (H-), and 4.7 MB plates for testing the killer phenotype were performed as previously

reported [170,171]. Strains used in this study are listed in the Appendix A, page 160. Doubling times were determined by fitting exponential sections of the growth curves to the equation: $y = y_0 e^{\frac{t \ln 2}{T}}$, where y is the OD_{595}, t is time and T is the doubling time. Drug sensitivities toward anisomycin and sparsomycin (Figure 2.2) were determined by dilution spot assays. Logarithmic dilutions starting from 10^5 CFU were spotted on plates with or without drug. Then plates were incubated at 30 °C for 3 days. The qualitative score was assigned by comparing the growth of mutant and wild type strains on media with and without the each drug. Positive scores were assigned to resistant strains and negative to sensitive strains.

In vivo methionine incorporation

In vivo methionine incorporation experiments to determine the rates of the protein synthesis were performed as described previously [172]. Briefly, 100 ml cell cultures were grown in media lacking methionine to an OD_{595} of 0.5-0.7. Then 5 μMoles of unlabeled methionine and 100 μCi of ^{35}S labeled methionine were added, resulting in a final specific activity of 20 mCi/mmole, and a concentration of 1 μCi/ml. Two 1 ml aliquots were collected every 10 minutes. The first aliquot was used for obtaining OD_{595} readings; and 200 μl of 50 % TCA was added to the second aliquot. The samples were incubated on ice for 20 minutes and then at 70 °C for 20 minutes. The samples were applied to GF-C glass filters, and filters were washed twice with 5 ml of 10 % TCA. Filters were dried and radioactivity was measured by liquid

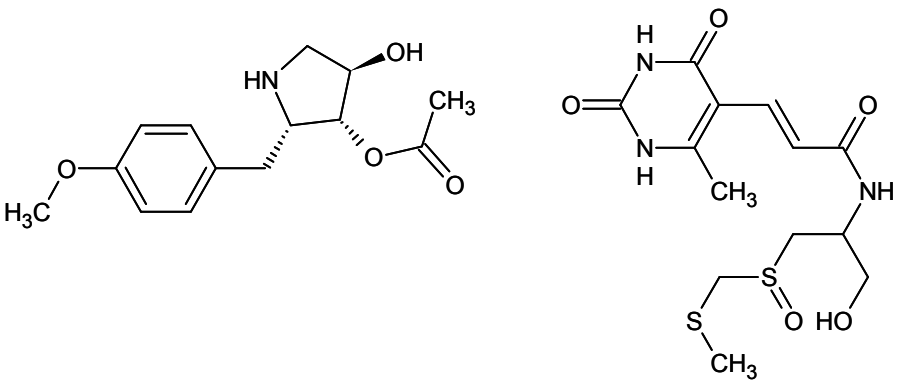

Figure 2.2. Structures of anisomycin and sparsomycin

scintillation counting. All time points were taken in triplicate. The obtained cpm counts were normalized by amount of cells in each sample measured as OD_{595} at each time point and plotted versus time. The rates of protein synthesis were calculated as the slope of the linear regression trendlines and expressed as counts per minute per 1 OU at 595 nm.

***In vivo* methylation of rRNA adenosines**

Unprotected adenosine bases in yeast rRNA were methylated in living cells with dimethylsulfate (DMS) using a modification of a previously described method [173]. Logarithmically growing yeast cells (10 ml, OD_{595} between 0.5 and 1.0) were pelleted by centrifugation, resuspended in 0.5ml of growth media, then DMS was added to concentrations of either 80 mM or 160 mM, and samples were incubated at room temperature for 2 minutes. Reactions were arrested by addition of ice cold β-mercaptoethanol to a final concentration of 0.7 M and 0.25 ml of ice cold water saturated with isoamyl alcohol. Control cells were not treated with DMS. Total nucleic acids were extracted by the Smash and Grab method described below. Reverse transcription reactions were performed at 45 ºC using 10 μg of rRNA, [^{32}P]-labeled oligonucleotides, and AMV reverse transcriptase (Roche). Strong stops one nucleotide 5' of modified bases were visualized by separating the reaction mixes through 6 % polyacrylamide-urea denaturing gels and subsequent autoradiography.

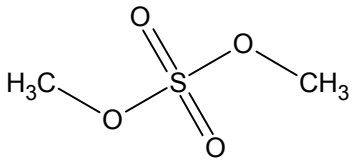

Figure 2.3. Structure of dimethyl sulfate.

Total RNA extraction (Smash and Grab)

Yeast cells (up to 50 O.U. at 595 nm) were suspended in 400 µl "Smash & Grab" buffer (10 mM Tris-HCl, pH 8.0, 100 mM NaCl, 1 mM EDTA, 1 % SDS, 2 % Triton X-100). Then one half volume of 0.5 mm glass beads and 400 µl Acid-Phenol/Chloroform (5:1, pH 4.9) were added to the cells. Nucleic acids were extracted by vortexing for 2 minutes, and debris was removed by centrifuged for 15 minutes at 14,000 rpm. The aqueous phase was collected and re-extracted with 400 µl Acid-Phenol/Chloroform. The extraction was performed one more time with Acid-Phenol/Chloroform and one time with Chloroform. The aqueous phase was collected and nucleic acids were precipitated by additing 0.1 volumes of 3 M $Na(CH_3COO)$ pH 5.2 and 2.5 volumes of 95 % ethanol. The nucleic acids were precipitated by incubating at -70 ºC for 30 minutes, and subsequent centrifugation for 15 minutes. Then, RNA pellets were washed with 1 ml 70 % ethanol, dried, and resuspended in 50 µl DEPC treated H_2O.

Purification of aa-synthetases

Aminoacyl-tRNA synthetases were purified as previously described with minor modifications [174]. Two pounds of frozen cake yeast (George R. Ruhl & Son, Inc., Hanover, MD) were placed in 500 ml of buffer A [0.2 M Tris-base, 0.3 M NH_4Cl, 20 mM $MgSO_4$, 1 mM EDTA, 0.15 M dextrose] and allowed to thaw and ferment overnight. Cells were disrupted by three passages through an ice-cooled Microfluidaser at ~18,000 lb/in^2, cell debris was removed by centrifugation at 4 °C in a Beckman JLA rotor at 10,000 rpm for 30 minutes, and 800 ml of supernatant was obtained. Fines and nucleic acids were precipitated by addition of polyethylenimine

(1.73 g/lb of cells, equivalent to 4.32 g/liter of lysate) over a period of 5 minutes with slow stirring. Precipitates were removed by centrifugation at 4 °C using a GSA rotor at 9,000 rpm for 40 minutes. Proteins in the supernatant were precipitated by addition of 472 g of ammonium sulfate per liter of extract (70 % saturation), and precipitates were collected by centrifugation in a GSA rotor at 12,000 rpm for 45 minutes at room temperature. The pellet from this step was suspended in 43.75 ml of buffer C [30 mM potassium phosphate, pH 7.2, 1 mM EDTA, 1 mM DTE, 0.01 mM PMSF] per 100 g of pellet and subsequently dialyzed in 2 liters of buffer C overnight with two changes of buffer. The extract then was clarified by centrifugation in a GSA rotor at 12,000 rpm for 45 minutes at 4 °C. The supernatant was diluted 2.5 times with buffer C and fractionated through a Sephadex CM50 column equilibrated with buffer C. The column was washed with buffer D [30 mM potassium phosphate, pH 7.2, 1 mM EDTA, 0.01 mM PMSF, 10 % glycerol] with 50 mM KCl. The proteins were eluted from the column using a series of step gradients composed of buffer D containing 150 mM, 300 mM, and 500 mM KCl. The material eluted by buffer D with 150 mM KCl contains phenylalanyl-tRNA synthetase activity. Proteins were precipitated by addition of 472 g/liter of ammonium sulfate, and pellets were suspended in buffer D containing 50 mM KCl. Extracts were dialyzed against 1 liter with two changes of buffer D50 for 10 h, after which they were clarified by centrifugation in a GSA rotor at 12,000 rpm for 45 minutes at 4 °C. The obtained preparations of aa-tRNA synthetases were aliquoted and flash frozen in liquid nitrogen.

Synthesis of aa-tRNA and Ac-aa-tRNA and HPLC purification

Yeast phenylalanyl-tRNAs were aminoacylated by scaling up a previously described method [175]. The reaction mix (5 ml) contained 300 mM Tris-HCl, pH 7.6, 100 mM KCl, 20 mM $MgCl_2$, 0.4 mM ATP, 40 µM [^{14}C]Phe [496 mCi/mmole], plus 5 mg of tRNA-Phe and 475 µl of aminoacyl-tRNA synthetases (D150) purified as described above. Reaction mixtures were incubated for 30 minutes at 30 °C, and proteins were removed by extraction with acid-phenol-chloroform. [^{14}C]Phe-tRNA was separated from uncharged tRNA and free [^{14}C]Phe by high-performance liquid chromatography (HPLC) as previously described [176] with the following modifications. Samples were loaded onto a 4.6x250 mm JT Baker wide-pore butyl column equilibrated with buffer A [20 mM $NH_4(CH_3COO)$, 10 mM $MgCl_2$, 400 mM NaCl; pH 5.0] at 1 ml/min. The column was washed with 10 ml of buffer A, creating conditions under which free phenylalanine and aminoacyladenylate are eluted from the column. Uncharged tRNAs were eluted by isocratic elution with 19 ml at 15 % of buffer B [20 mM $NH_4(CH_3COOH)$, 10 mM $MgCl_2$, 400 mM NaCl, 60 % methanol; pH 5.0). [^{14}C]Phe-tRNA was eluted using a step gradient to 100 % of buffer B. Elution of aminoacyl-tRNA was monitored by $OD_{260/280}$ readings, and [^{14}C]Phe-tRNA peak and concentrations were determined by scintillation counting. The presence of aminoacyl-tRNA in the eluted material was confirmed by gel filtration through G-25 spin columns and by nonenzymatic hydrolysis of ester bonds at basic pH [177]. Ac-[^{14}C]tRNA was obtained in a similar manner. Yeast phenylalanyl tRNA was charged with [^{14}C]Phe as above and extracted with phenol. The [^{14}C]Phe-tRNA was acetylated by addition of 64 µl of acetic anhydride at 15 minutes intervals for 1 h

on ice [176]. The reaction mix was clarified by centrifugation at 15,000 rpm for 3 minutes, and Ac-[^{14}C]Phe-tRNA was purified by HPLC as described above.

Isolation of ribosomes

Yeast ribosomes were isolated using a modification of a previously published protocol [176]. Briefly, cells were grown in YPAD medium to an OD_{595} of 0.8, collected by centrifugation, and washed twice with cold 120 mM KCl. Cells were suspended to concentrations of 1 g/ml in buffer A [20 mM Tris-HCl, pH 7.5 at 4 °C, 5 mM $Mg(CH_3COO)_2$, 50 mM KCl, 10 % glycerol, 1 mM PMSF, 1 mM DTE], and one-half volume of glass beads (0.5 mm) were added. Then cells were disrupted at 4 °C with a Mini BeadBeater for 2 minutes at maximum speed. Extracts were transferred to 4ml centrifuge tubes, and glass beads were washed twice with 1 ml of buffer A. Washes were combined with extracts and spun in an MSL-50 rotor (Beckman) for 25 minutes at 20,000 rpm. Supernatants were transferred to 4 ml polycarbonate tubes containing 1 ml of a cushion of buffer B [20 mM Tris-HCl, pH 7.5 at 4 °C, 5 mM $Mg(CH_3COO)_2$, 50 mM KCl, 25 % glycerol, 1 mM PMSF, 1 mM DTE], and ribosomes were sedimented by centrifugation at 4 °C for 2 h at 50,000 rpm using the MSL-50 rotor. Fines from ribosome pellets were gently washed off with buffer C [50 mM Tris-HCl, pH 7.5 at 4 °C, 5 mM $Mg(CH_3COO)_2$, 50 mM NH_4Cl, 0.1 mM PMSF, 0.1 mM DTE, 25 % glycerol]. Ribosomes were suspended in buffer C at concentrations of 2 to 10 pmol/µl (1 OD_{260} = 20 pmol) and stored frozen at –80 °C.

tRNA binding

The tRNA binding assay is based mainly on the work of Nierhaus and Synetos laboratories. Multiple repetitions of tRNA binding experiments demonstrated uniform

rules of tRNA binding to the ribosome. tRNA binding can be predicted based on the nature of the tRNA and ribosomal state during the tRNA binding reaction. These rules are summarized in the Figure 2.4 [178].

Ac-Phe-tRNA was used as a substrate in the P-site binding assay. Acetylation of the primary amino group of phenylalanine mimics the peptide bond, and the ribosome recognizes this substrate as a peptidyl-tRNA [176,179]. Thus, according to the rules (Figure 2.4), this substrate would directly bind to the P-site of the empty ribosomes. The A-site binding assay starts with pre-incubation of the ribosomes with poly U and an excess of deacylated tRNA. Deacylated tRNA first occupies the P-site of the ribosome, and then fills the E-site, thus resulting in formation of the poly U charged ribosomes with pre-occupied P and E sites (Figure 2.4). Following the tRNA binding rules, the aminoacyl-tRNA binds to the A-site of this complex (Figure 2.4, P and E-sites are occupied). Early studies of translational apparatus demonstrated that eEF-1 co-purifies with non salt washed ribosomes. During the binding reaction, Phe-tRNA forms the ternary complex eEF-1:GTP:Phe-tRNA, which subsequently binds to the A-site. The joint efforts of two groups demonstrated that eEF-1 is present in excess in preparations of the non salt washed ribosomes, and that eEF-1 does not limit tRNA binding or peptidyl transfer (which involves aa-tRNA binding as a partial reaction) [176,180,181].

The assays were performed at equilibrium, as was determined by the time dependence of tRNA binding. Aminoacyl-tRNA binding to the A-site of the ribosome was carried out as previously described [182] in reaction mixtures (50 μl) containing

State of the ribosome	Added tRNA	Binding event
Empty ribosome with mRNA 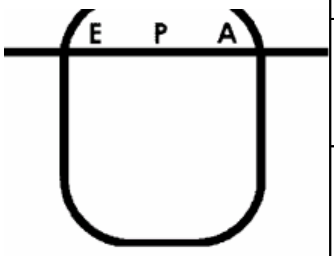	Deacylated tRNA	Binds directly to the P site.
	Peptidyl-tRNA	Binds directly to the P site.
	Aminoacyl-tRNA :EF-Tu:GTP	Binds directly to the A site
Deacylated tRNA at the P site 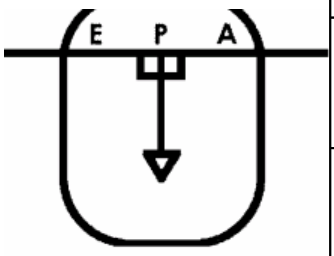	Deacylated tRNA	Binds directly to the E site
	Peptidyl-tRNA	Does not bind
	Aminoacyl-tRNA :EF-Tu:GTP	Binds directly to the A site
P and E-sites are occupied 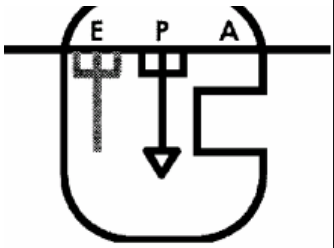	Deacylated tRNA	Does not bind
	Peptidyl-tRNA	Does not bind
	Aminoacyl-tRNA :EF-Tu:GTP	Binds directly to the A site

Figure 2.4. Uniform rules of tRNA binding

80 mM Tris-HCl, pH 7.4, 160 mM NH_4Cl, 11 mM $Mg(CH_3COO)_2$, 6 mM β-mercaptoethanol, 0.4 mM GTP, and 2 mM spermidine, 0.4 μg/ml of poly(U), and 12 - 25 pmol of ribosomes. The reaction mixtures were preincubated with uncharged tRNA (4:1 tRNA/ribosomes) at 30 °C for 15 minutes to ensure full occupation of P- and E-sites by uncharged tRNA, after which various quantities (4 – 264 pmol) of [^{14}C]Phe-tRNA or Ac-[^{14}C]Phe-tRNA were added. Reaction mixtures were incubated at 30 °C for an additional 20 minutes to allow formation of [^{14}C]Phe-tRNA-80S-poly(U) complexes. Aliquots were then applied to nitrocellulose membranes, filters were washed with 2 ml of binding buffer, and radioactivity was measured by scintillation counting. Background levels of radioactivity were determined using a blank sample and subtracted from the test samples. Acetyl-aminoacyl-tRNA binding assays were performed in a similar way, but deacylated tRNA was omitted from pre-incubation mix.

Data analysis

Data obtained in the tRNA binding experiments were plotted onto Scatchard plots according to the single binding site equation: $\frac{v}{[tRNA]} = K_a - K_a v$, where $v = [tRNA \bullet RS]/[RS_0]$ and represents the number of bound tRNA molecules per ribosome, $[tRNA]$ is the concentration of unbound tRNA, and K_a is the apparent association constant. The plot v vs. $v/[tRNA]$ represents a straight line and provides K_a as the negative slope. Plots for different mutants were normalized to the percentage of active ribosomes in each preparation, and K_a values were determined as the slopes of linear regression trend lines [183].

Computational analysis of the ribosome structure.

Cryo-electron microscopy (cryo-EM) reconstruction of *Saccharomyces cerevisiae* ribosomal proteins threaded onto the X-ray crystal structure of the *H. marismortui* 50S ribosomal subunit [184] was visualized using Pymol [185].

Results

Expression of mutant forms of L3 affects rates of cell growth, protein synthesis and antibiotic resistance.

In an effort to understand the consequences of expressing mutant forms of L3 on cell growth and division, *RPL3::HIS3* gene knockout strains harboring plasmid-borne wild-type or mutant alleles of *rpl3* were inoculated into standard defined medium lacking tryptophan (H-trp) to OD_{550} ~0.01, and growth rates were determined by measuring optical densities of aliquots taken at 1h intervals. The growth curves are shown in Figure 2.5. The results demonstrated that the I282T mutant had the least effect on cell doubling times (~110 min, compared to ~92 min for cells expressing the wild type gene, see Figure 2.5, Figure 2.6 and Table 1). More significantly, expression of the peptidyl transferase center-proximal mutants, i.e., W255C, P257T, and *mak8-1* (W255C + P257T) had dramatic effects on cell growth rates (doubling times of ~150 min, ~130 min and ~155 min respectively, Table 1 and Figure 2.6).

As the gene in question encodes a ribosomal protein, we assayed the effects of the mutations on protein synthesis by examining rates of [^{35}S]methionine incorporation into the TCA-precipitable fraction of cell lysates. The results of these

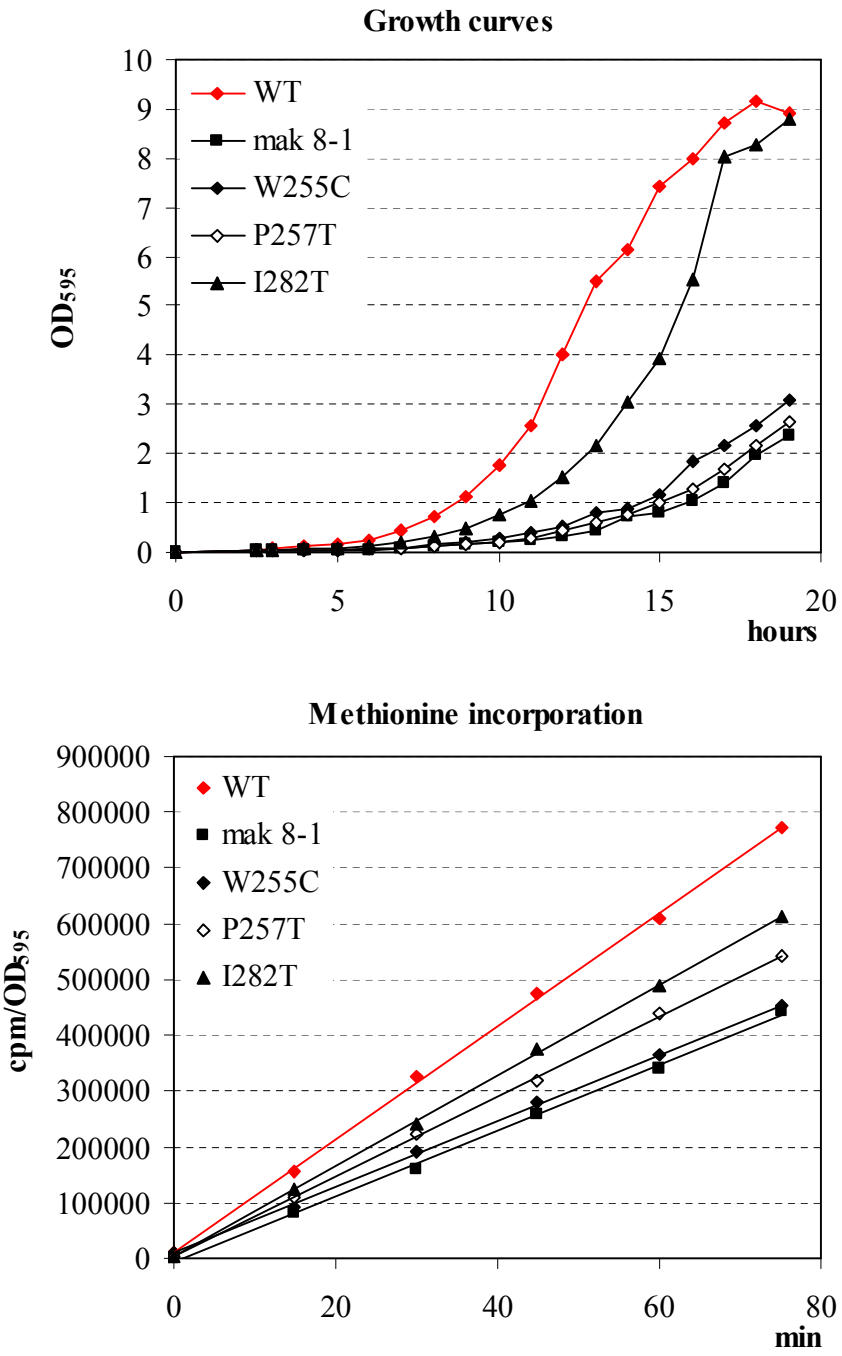

Figure 2.5. Growth curves and rates of protein synthesis of L3 mutants.

Plasmid-borne alleles of *RPL3* were expressed in isogenic *RPL3::HIS3* gene disruption backgrounds. Growth curves and rates of methionine incorporation were measured as described in the Materials and methods (page 50). Exponential trendlines for logarifmic parts of the growth curves are shown in the Figure 2.6.

A

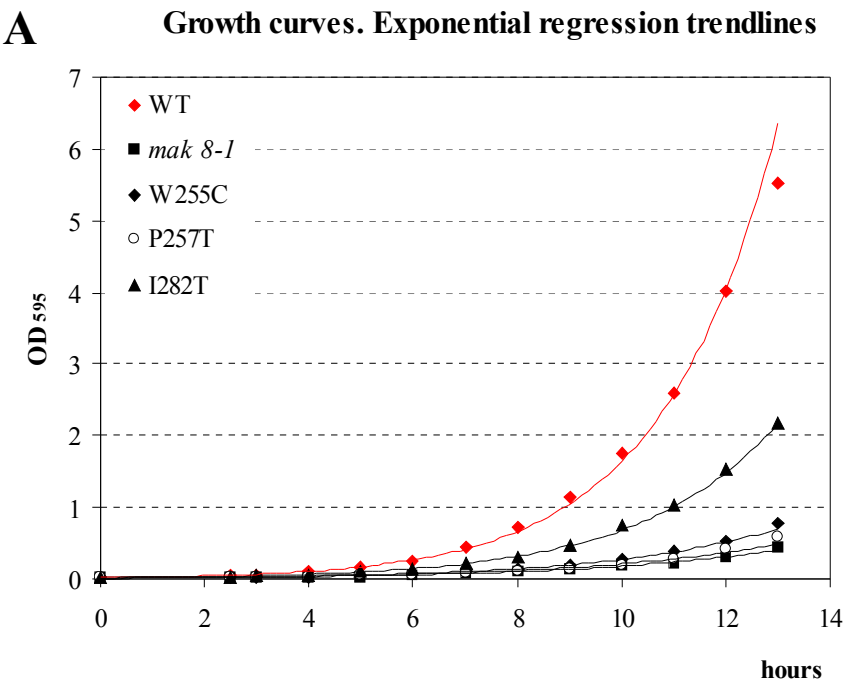

B

Strain	y_0	a (ln2/T), h^{-1}	R^2
WT	0.0179	0.4515	0.9986
mak 8-1	0.0124	0.2687	0.9834
P257T	0.0116	0.3165	0.9846
I282T	0.0146	0.3850	0.9973
W255C	0.0129	0.2800	0.9855

Figure 2.6. Doubling time calculations

Panel A shows the exponential regression trendlines according to the equation $y = y_0 e^{ax}$. The obtained trendline parameters (B) have been used to calculate doubling time according to the equation: $a = \frac{\ln 2}{T}$.

	WT	G15C	P18S	I282T	P257T	W255C	*mak8-1*
Dbl. time, min	92	-	-	110	130	150	155
Prot. syn, cpm/min.	10331	-	-	8196	7233	6118	5762
Anisomycin	0	0	+3	+2	+2	+4	+4
K_a for aa-tRNA to the A-site ($x10^6$ M^{-1})	1.1	7.1	4.3	-	-	7.3	-
Sparsomycin	0	-	-	0	-2	-2	-2
K_a for peptidyl-tRNA to the P-site ($x10^6$ M^{-1})	$\leq$0.9	-	-	$\leq$ 2.4	7.9	3.7	9.8
Pep-transferase [158]	WT	-	-	**â**	**â â**	**â â â**	**â â â**
-1PRF, % [158,182]	8.8	14.4	-	13.2	13.9	14.2	14.5

Table 1. Summary of properties of *rpl3* mutants

Doubling times were calculated as described in Materials and methods (page 49). The rates of protein synthesis were calculated as a slope of the linear regression trendlines and expressed as cpm per minute per 1 OD of the cells at 595 nm (page 50). Drug sensitivities were assessed by dilutions spot assay and quantitative scores were assigned. Positive scores correspond to resistant and negative scores to sensitive phenotypes. The aminoacyl-tRNA affinities were measured as described in Materials and methods (page 57). -1PRF efficiencies are from Meskauskas A., *et al* [182], and Meskauskas A., *et al* [158]. The rates of the peptidyl transfer (Pep-transferase are cited from Meskauskas A., *et al* [158]). Dashes indicate that a given parameter has not been evaluated that in a particular strain.

experiments are shown in Figure 2.5 and Table 1. The results indicate that, with respect to protein synthesis, the mutants exhibited a pattern similar to those observed with regard to growth rates, i.e., WT > I282T > P257T > W255C > *mak8-1* (10331,8196,7233,6118, and 5762 cpm/min/OU_{595} correspondingly).

To reveal effects of the L3 mutant alleles on ribosomal function, a pharmacogenetic approach was employed. Strains were tested for resistance/hypersensitivity to two peptidyl transferase inhibitors, anisomycin and sparsomycin. Anisomycin is a competitive inhibitor of the peptidyl transferase reaction and interferes with binding of A-site substrate. It binds in the vicinity of the peptidyl transferase center, and the *p*-methoxyphenyl group of anisomycin fills the hydrophobic crevice normally occupied by the peptidyl moiety of aminoacyl-tRNA (Figure 2.7) [186]. We found that, mutant L3 alleles promoted resistance to anisomycin. The *mak8-1* and W255C alleles showed maximum resistance and were assigned a score of +4 (see Materials and methods page 49, and Figure 2.8). Sparsomycin is a peptidyl transferase inhibitor that mostly affects the P-site. It requires a P-site substrate for stable interaction with the ribosome, and does not binds to the ribosomes in the absence of a peptidyl-tRNA [187]. The pyrimidine ring of sparsomycin is sandwiched between the CCA end of the P-site tRNA and helix 91 of 25S rRNA.(A2637 in *H. marismortui* Figure 2.9). The tail of the molecule is pointed toward the active site crevice and partially occupies the aminoacyl-tRNA binding pocket (Figure 2.7) [186]. Three strains (*mak8-1*, W255C and P257T) were hypersensitive to sparsomycin and were assigned score of -2 and (Figure 2.8).

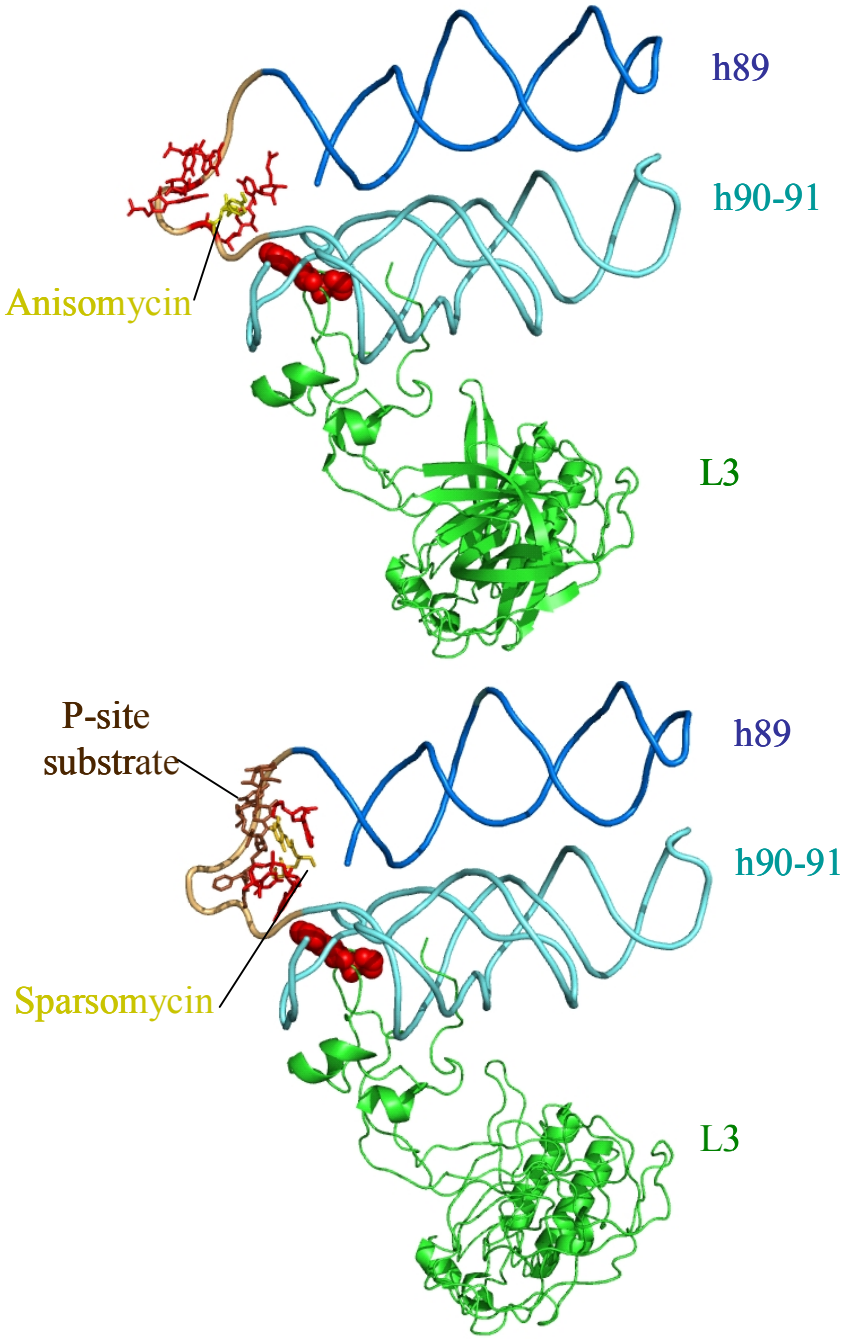

Figure 2.7. Anisomycin and sparsomycin binding sites.

Anisomycin and sparsomycin bind at the peptidyl transferase center. The bases that interact with drug molecules are shown as the red stick models. The amino acid residues W255 and P257 of ribosomal protein L3 are shown as red spheres.

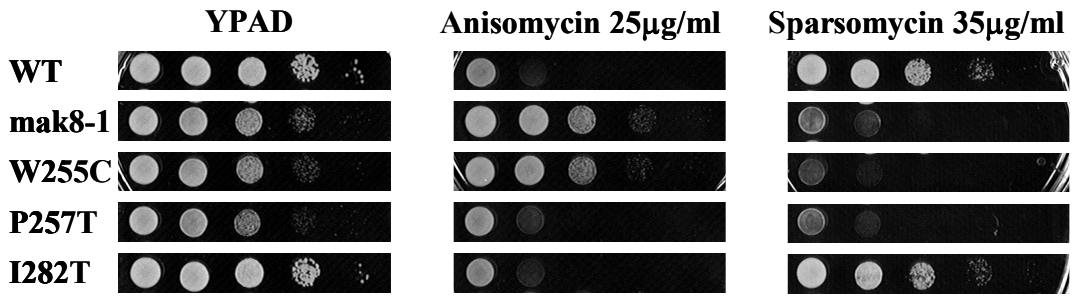

Figure 2.8. Strains containing mutant forms of L3 have altered drug sensitivity phenotypes.

Mid-log phase cultures of isogenic strains harboring various plasmid-borne *RPL3* alleles were spotted in 10-fold dilutions onto YPAD alone (No Drug), YPAD containing anisomycin (25μg/ml), or YPAD plus sparsomycin (35 μg/ml). Cells were grown at 30 °C for three days.

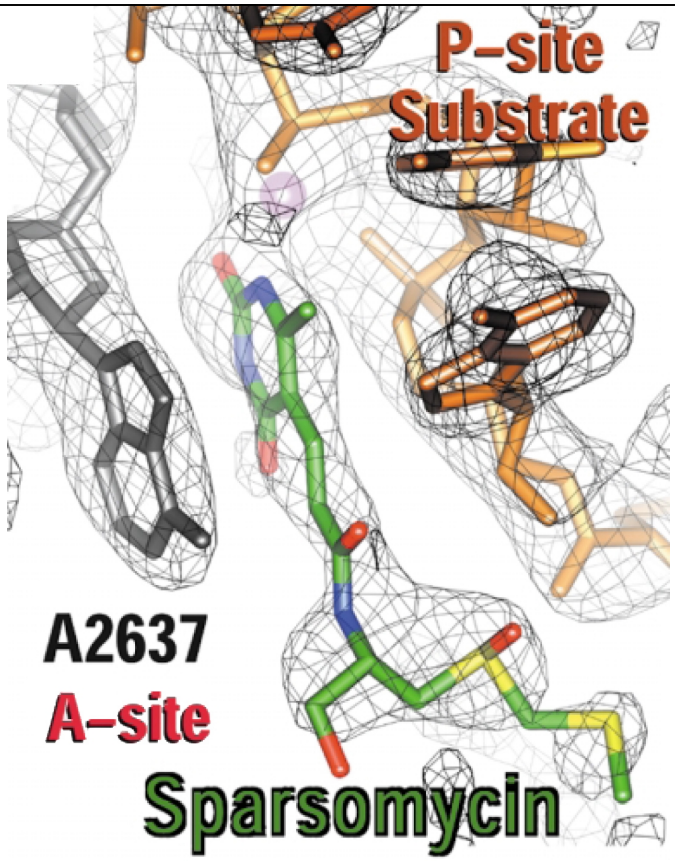

Figure 2.9. Interactions of sparsomycin with the P-site substrate

The sparsomycin ring is sandwiched between C75 and A76 of the P-site tRNA, and A2637 (*H. marismortui*). The tail of the molecule is pointed toward the A-site crevice. Modified from Hansen J.L., *et al* [186].

Mutant forms of L3 promote increased ribosome affinities for tRNAs

Observations that mutations in ribosomal protein L3 affect sensitivity to peptidyl transferase specific drugs suggest that these mutations may affect how ribosomes functionally interact with tRNAs. To test this hypothesis, filter binding assays were used to monitor the affinities of wild-type and mutant ribosomes for tRNAs using [^{14}C]Phe–tRNA^{Phe} and [^{14}C]Ac-Phe–tRNA^{Phe}, which have been previously demonstrated to bind exclusively to the A- and P-sites respectively [188]. An inherent complication in the biochemical comparison of different samples is that specific activities of the samples vary from preparation to preparation. Thus, the absolute amounts of bound tRNA are not directly comparable between samples, and do not reflect affinity of the tRNA to ribosomes. The widespread error in analysis of tRNA-ribosome interactions derives from the fact that yield activities of samples have not been controlled, and tRNA affinities have been described as amounts of bound tRNA at the single substrate concentration [189-191]. To overcome this problem, experiments were conducted over a range of tRNA concentrations and Ka values were calculated by Scatchard plot analysis. Peptidyl-tRNA binding analysis demonstrated that the sparsomycin sensitive mutant ribosomes generally have higher affinities for Ac-Phe–tRNA^{Phe} (Figure 2.10). These results are in agreement with the previous suggestion that elevated affinity of the P-site for tRNA aggravates the effect of sparsomycin [192]. The effects of P-site tRNA affinity on sparsomycin sensitivity could be explained by a mechanism of inhibition of the peptidyl transferase by sparsomycin. Sparsomycin is a mixed noncompetitive inhibitor and

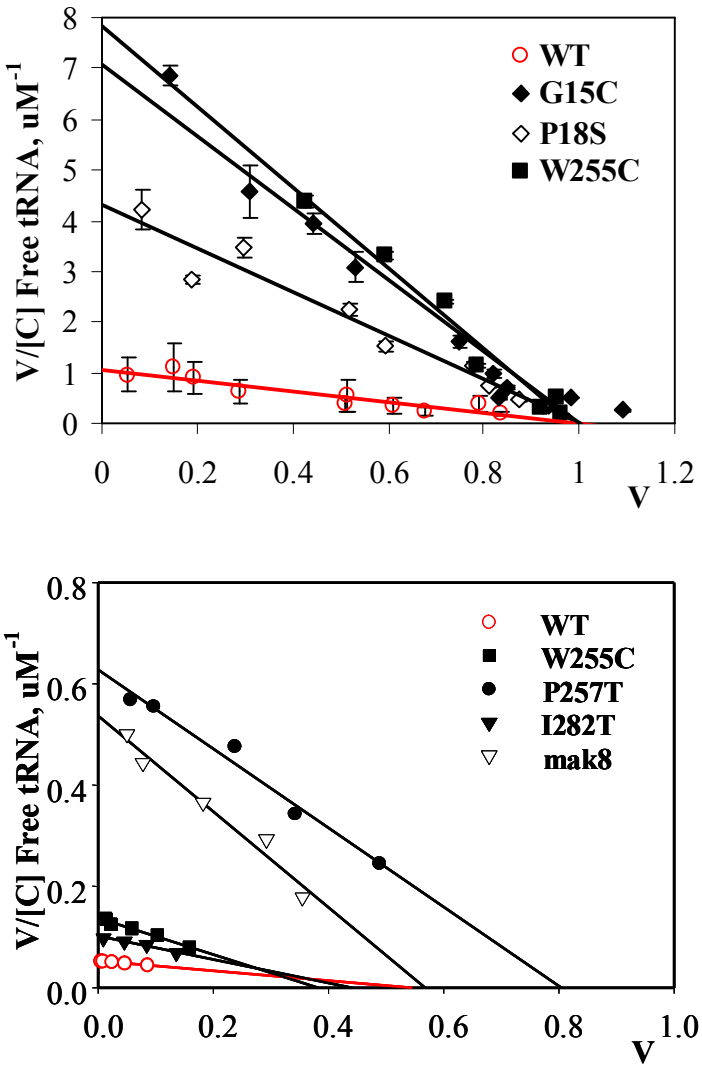

Figure 2.10. Characterization affinities for aa-tRNAs and peptidyl-tRNA by wild-type and mutant ribosomes.

Ribosomes isolated from yeast cells expressing the wild-type, G15, P18S, W255C, P257T, I282T, and mak8-1 mutant forms of L3 were used for assays. tRNA binding was carried out as described in Materials and methods (page 57). Data were plotted onto Scatchard plot and K_a values were determined as the slopes of linear regression trendlines. The A-site binding data was normalized to the amount of active ribosomes determined as the intersection with the abscissa axis on the initial Scatchard plot. The P-site binding data was not normalized to illustrate amount of the active ribosomes.

requires a P-site substrate for efficient binding. During the elongation cycle, the P-site is always occupied either by peptidyl-tRNA or deacylated tRNA. However, the flexibility of the acceptor end of the P-site tRNA may influence the ability of sparsomycin to interact with the ribosome by affecting the number of the possible conformations, or half-lives of the ribosome conformations to which sparsomycin may bind. While no direct data describing dynamics of the P-site tRNA are available, we hypothesize that the L3 mutants may stiffen the acceptor end of the P-site tRNA (which translates in increased [Ac]Phe-tRNA affinity), thus promoting formation of the sparsomycin:ribosome complex.

To reveal the functionally important groups of ribosomal protein L3, a library of randomly generated *rpl3* alleles was screened for resistance to anisomycin, resulting in the identification of 43 new *rpl3* alleles [182]. Since anisomycin prevents binding of aa-tRNAs [193,194], mutants resistant to this drug might be expected to have increased affinities for aa-tRNAs. To test this model, aa-tRNA binding affinities to the A-site were determined for ribosomes purified from a few selected strains identified in the prior screens for anisomycin resistance and loss of the killer phenotype, taking care to block non-specific binding to ribosomal P- and E- sites by pre-incubating ribosomes with uncharged tRNAs. The results of these experiments are represented in the form of a Scatchard plot in Figure 2.10, and summarized in Table 1. This analysis reveals that Ka's of wild-type, G15C, P18S, and W255C ribosomes for aa-tRNAs are 1.1×10^6 M^{-1}, 7.1×10^6 M^{-1}, 4.3×10^6 M^{-1} and 7.3×10^6 M^{-1} respectively. Thus, as predicted, the anisomycin resistant strains have increased A-site affinities for aa-tRNA.

The *mak8-1* form of L3 has an effect on the structure of the large subunit rRNA.

The observation that ribosomes containing mutant forms of L3 had decreased peptidyl transferase activities [158] was suggestive of an underlying structural defect. To test this hypothesis, the effects of the *mak8-1* form of the protein on the structure of 25S rRNA were probed *in vivo* by treating cells with the RNA methylating agent DMS. In this method, unpaired adenine and cytosine bases are the most reactive and are typically most sensitive to structural changes [195,196]. Modification by DMS is detected as strong stops in reverse transcriptase primer extension assays one nucleotide 5' of the site of methylation. Primers 25-4, 25-6, and 25-7 (see Appendix C and Table 11) were used to determine the methylation patterns of 25S rRNAs from isogenic strains expressing wild-type L3 or *mak8-1* through an approximately 400 nucleotide stretch of domain V, comprising 25S rRNA nucleotides positions 2650 to 3040. The results show that expression of the *mak8-1* form of L3 affects the structure of the 25S rRNA in a number of discrete regions. In particular, nucleotides in the loop region of helix 85 (A2690–A2704) were better protected from DMS attack in *mak8-1* ribosomes relative to wild-type (Figure 2.11 and Figure 2.12). Though the enhanced protection of these residues in *mak8-1* ribosomes was modest, this pattern was observed in every repetition of this experiment. We suggest that the reason for the weak pattern of enhanced protection originates from the *in vivo* nature of the assay which probes all of the ribosomes in the cell in every different stage of elongation; each of these has a different status with regard to interactions with elongation factors and tRNAs. The observed pattern of enhanced protection in helix 85 suggests that the

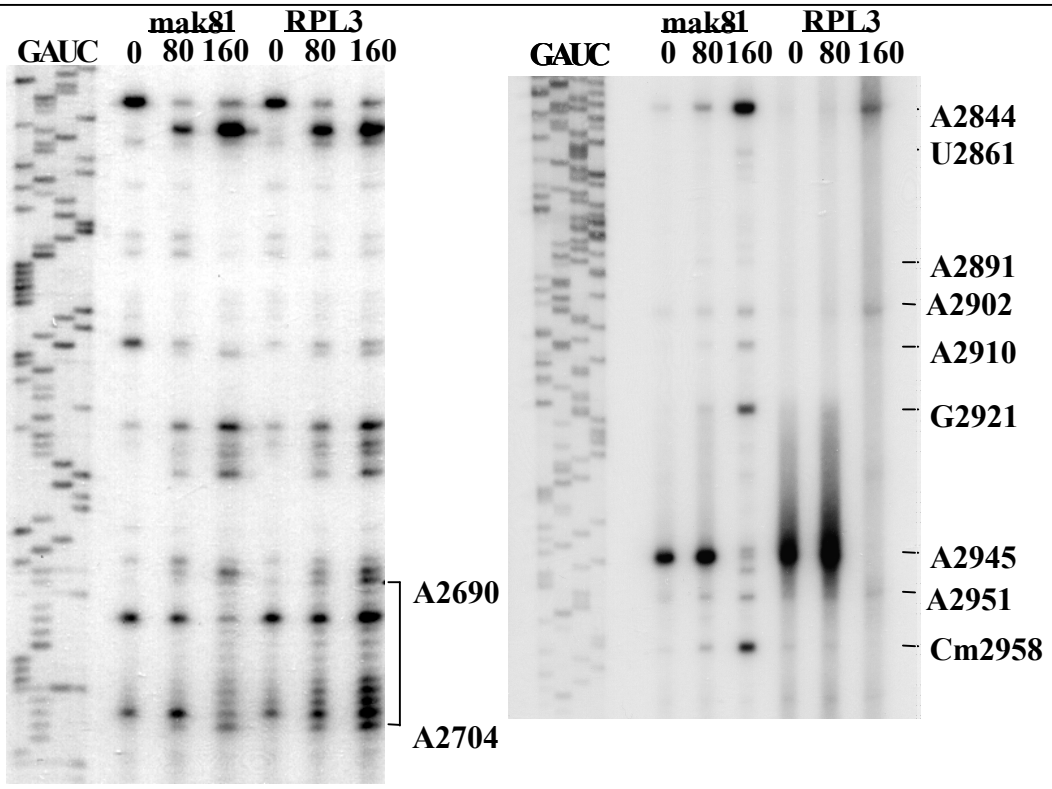

Figure 2.11. The mak8-1 form of L3 affects the structure of the 25S rRNA.

Isogenic wild-type (*RPL3*) and *mak8-1* cells were treated with DMS *in vivo*. Reverse transcriptase extensions of [^{32}P]-labeled primers were performed using extracted rRNAs as templates, the reactions were separated through 6 % urea-polyacrylamide denaturing gels, and visualized by autoradiography. Autoradiograms of the primer extension reactions using Oligo 25-4 and Oligo 25-7 are shown. Sequencing ladders are reverse labeled so as to reflect the sense strand of 25S rRNA in the indicated 5' to 3' directions. DMS concentrations are shown in mM. Specific protected or deprotected bases are indicated.

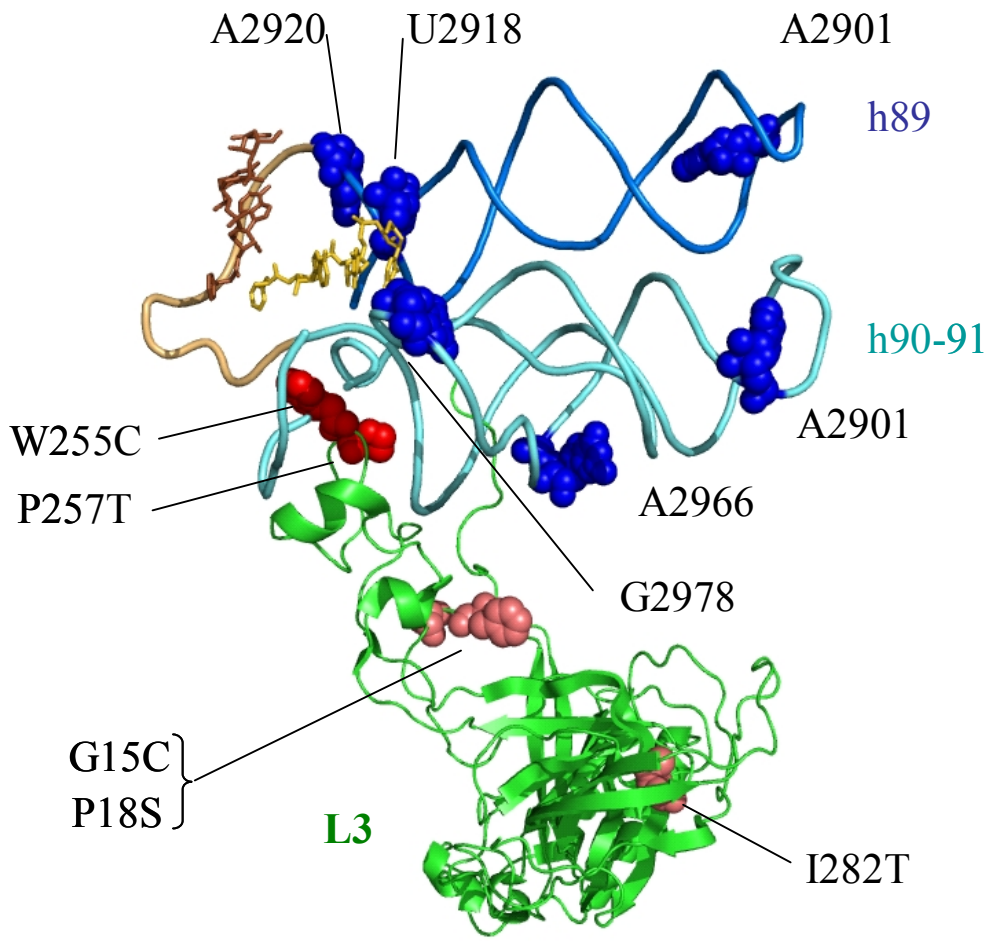

Figure 2.12. Position of L3 mutants in the ternary ribosomal structure.

The yeast ribosomal rRNA and proteins were modeled in the context of the crystal structure of *H. marismortui* ribosome. The body of L3 is located on the surface side of the large subunit, while the tip of the protein protrudes toward the peptidyl transferase center. The A site substrate is depicted in yellow and the P site substrate is in brown. The residues that exhibit altered DMS reactivity in *mak8-1* strain are indicated in blue.

difference is due to altered interaction of *mak8-1* ribosomes with another factor, most likely the T-loop of the peptidyl-tRNA, which has been shown to interact with the loop region of helix 85 in the *T. thermophilus* large subunit [44]. This finding is in agreement with observed correlation between increased affinities for peptidyl-tRNA and sparsomycin sensitivity, which suggests that altered interactions between the P-site tRNA and ribosome is the underlying cause of drug phenotypes. In contrast, expression of the *mak8-1* form of L3 resulted in strongly enhanced deprotection patterns of specific bases in helices 89, 90 and 91, suggesting intrinsic differences in ribosomal structure (Figure 2.12). For example, A2844 in the distal loop of helix 89 became accessible to DMS modification. A similar pattern in the proximal arm and distal loop in helix 91 appears to render A2891 and A2910 hypersensitive to methylation by DMS. Hypermethylation was observed at position G2921 in the A-loop, the *E. coli* counterpart of which (G2554) is a cross-link site to a puromycin derivative [197]. Moderate levels of deprotection were also observed at positions A2951 (the analogous *E. coli* U2584 is a footprint site for P-site tRNA [197]), and the naturally methylated C2958. For unknown reasons, the strong reproducible stop at A2945 disappeared at higher DMS concentrations. This pattern was observed reproducibly observed in the *in vivo* DMS modification experiments with these strains, but has not been found in *in vitro* structure probing experiments conducted in our laboratory. These results may be due to probing of multiple conformations of the ribosomes *in vivo*, and (or) from effects of DMS modifications on RNA stability in the subsequent extraction step. However, regardless of the possible origin of this stop, since it occurred in both wild-type and *mak8-1* samples, it is probably not informative in terms of comparison between the two alleles.

Discussion

Although accumulating evidence indicates that rRNA is the main, and perhaps only, catalytic component of the ribosome, mutational analysis has long ascribed significant functional relevance to several ribosomal proteins [198-201]. The effects of expression of *RPL3* mutants on tRNA binding, resistance to PTC specific translation inhibitors and structural changes indicate that L3 belongs to this class of ribosomal proteins. The questions are whether the functional effects of the mutations characterized in this study are due to changes in rRNA structure conferred by the mutant proteins, or might L3 be directly involved in structural transitions during the elongation cycle? To address this, a new characterization of existing L3 mutants was conducted. We found that mutations in ribosomal protein L3 affect resistance to the peptidyl transferase inhibitors anisomycin and sparsomycin. There are several explanations for how mutations in L3 can result in anisomycin resistant and sparsomycin sensitive phenotypes. First, drug resistance or sensitivity may arise from decreased affinity of the inhibitor-ribosome interaction. This mechanism of resistance toward peptidyl transfer inhibitors was previously observed for tiamulin and avilamycin [168,202]. Examination of the X-ray crystal structure of the *H. marismortui* large subunit shows that two of the anisomycin resistant mutants, W255C and P257T, are located close to the peptidyl transferase center (Figure 2.12) and thus may directly affect PTC conformation and drug resistance. rRNA structure probing of *mak8-1* ribosomes confirms this notion demonstrating that A2951 (PTC, in *S. cerevisiae, E. coli* 2585) is deprotected in the *mak8-1* strain. Remarkably, it has been previously demonstrated that lack of post transcriptional modification of this base affects the level of sparsomycin sensitivity [203]. Recently, the X-ray structure of *H. marismortui*

ribosomes complexed with sparsomycin demonstrated that U2584 and U2585 (in *E. coli, S. cerevisiae* bases U2952 and U2953) are part of the sparsomycin binding pocket. *In vitro* structure probing experiments of W255C strain with CMCT conducted in our group also demonstrated protection of one of those residues - U2953 in the mutant strain [204]. Thus these results suggest that L3 mutants promote an altered conformation of the PTC.

Our observations suggest a role for L3 and (or) L3 contacting elements in activation of the peptidyl transferase center. The induced fit hypothesis of PTC activation suggests that movements of bases in positions 2583–2585 (in *E. coli, S. cerevisiae* 2951-2953) and U2506 (in *E. coli, S. cerevisiae* U2874) serves to reorganize the geometry of the PTC and make the ester group of the peptidyl-tRNA accessible for nucleophilic attack [39].When the PTC is in the "uninduced" (non-active) state, U2585 (in *E. coli, S. cerevisiae* U2953) is buried inside of the ribosome, and its Watson-Crick face is protected by U2506 (in *E. coli, S. cerevisiae* U2874). A2583 (in *E. coli, S. cerevisiae* A2951) stacks with U2584 (in *E. coli, S. cerevisiae* U2952), and A2583 is available for modification. Upon transition to the active state, U2506 (in *E. coli, S. cerevisiae* U2874) moves toward the P-site, exposing the Watson-Crick face U2585 (in *E. coli, S. cerevisiae* U2953) making this base accessible for modification. The observed mild hypermethylation of A2951 may result from the distorted position of U2874 (in *S. cerevisiae*), which partially shields the Watson-Crick face of A2951 (in *S. cerevisiae*) in the "uninduced" conformation. We hypothesize that mutations in L3 promote the "uninduced" PTC conformation and impede the transition into the "active" state (Figure 2.13). This hypothesis is in a good agreement with observed

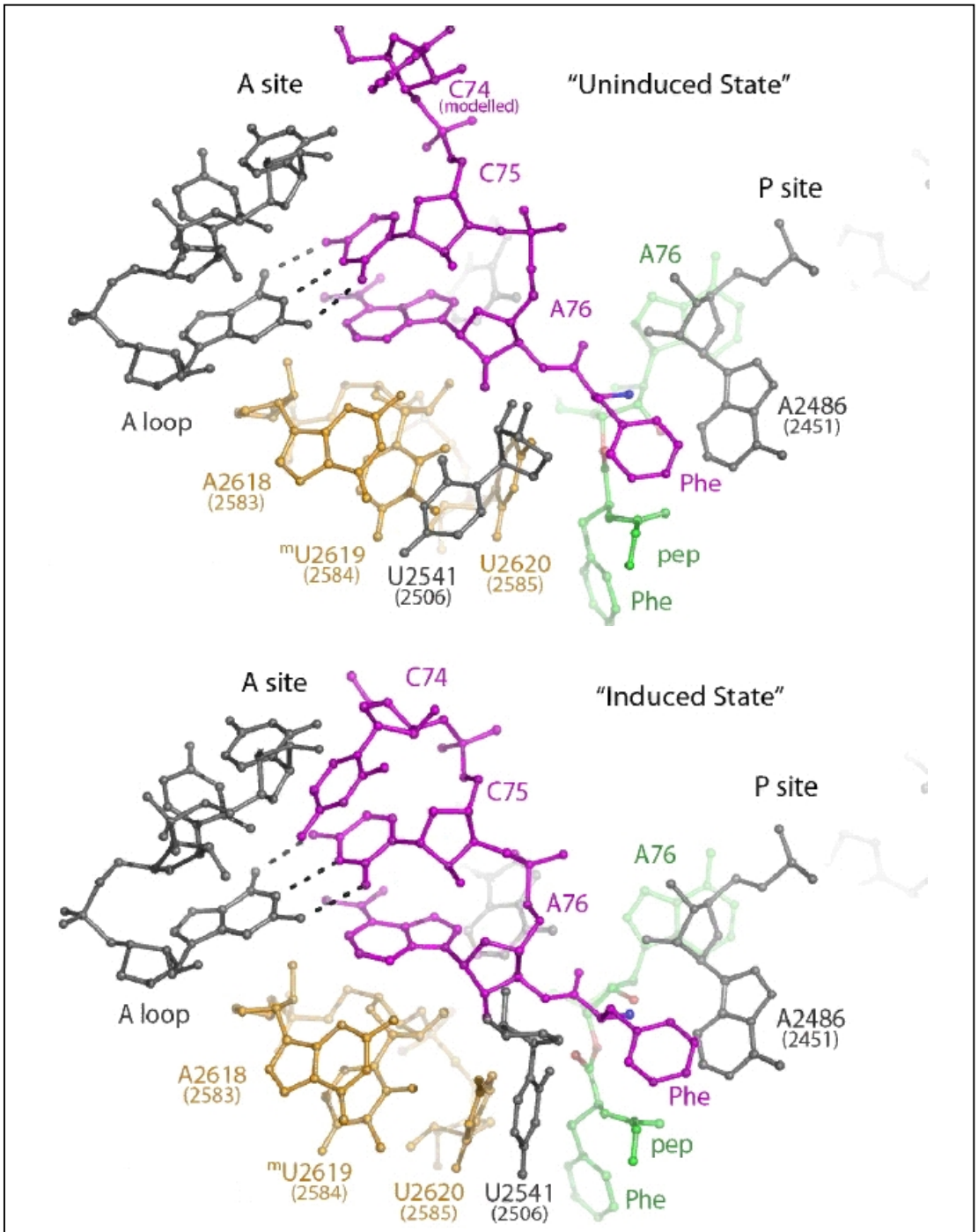

Figure 2.13. Conformational transitions in the PTC associated with adoption of the induced conformation.

Adopted from Schmeing,T.M., *et al* [39]

defects of W255C, P257T, and mak8-1 ribosomes in the puromycin reaction (Table 1) [158]. Puromycin fails to trigger the "active" conformation, and rates of peptidyl transfer with puromycin are a few orders of magnitude lower than with native aa-tRNA. Thus, the puromycin reaction likely occurs as a result of spontaneous activation of the PTC due to random sampling of conformations by the ribosome. The stiffened conformations of U2506, U2584 and U2585 (in *E. coli, S. cerevisiae* U2874, U2952 and U2953) in the uniduced state, *i.e.* in the L3 mutants, would encumber these oscillations resulting in a decrease in the observed rate of puromycin reaction.

Regarding sparsomycin resistance, the rRNA structure probing experiments suggest that L3 mutants promote an altered conformation of the sparsomycin binding site. This (1) may promote increased affinity of ribosomes for sparsomycin, and/or (2) impede PTC activation and work in synergy with sparsomycin, to prevent PTC transition into the “induced” state. The increased affinity for peptidyl-tRNA observed in our biochemical experiments may aggravate these effects by increasing the apparent K_a for sparsomycin (as discussed in Results section, page 69) [53].

The observed anisomycin effects and structure probing data complete the puzzle. Anisomycin is a competitive inhibitor of peptidyl transfer when puromycin and CCA-Phe fragments are used as A-site substrates [193,205]. X-ray crystal structures show that anisomycin binds in the A-site crevice and sterically interferes with the peptidyl moiety of aminoacyl-tRNA. The comparisons of the crystal structures of the ribosome at different stages of aminoacyl tRNA selection demonstrated that this pocket is unoccupied before accommodation [24,25,44]. These observations suggest that anisomycin interferes with positioning of the 3’ end of the aminoacyl-tRNA and specifically inhibits tRNA accommodation. The locations of the anisomycin resistant

mutants suggest a different resistance mechanism than for sparsomycin. Although W255 and P257 are located close to the PTC, the position of other anisomycin resistant mutants makes it unlikely that they directly affect anisomycin binding. The P18S substitution is located in the middle of the L3 extension, and I282T is located in the globular domain of L3 (for a full list of An^r mutants of L3 see Meskauskas A., *et al* [182]). Since anisomycin is a competitive inhibitor of the peptidyl transferase reaction and CCA-Phe binding [193], the increased rates of the forward reactions of the tRNA selection pathway would result in increased occupation of peptidyl transferase center by the acceptor end of A-site tRNA, thus promoting anisomycin resistance. The biochemical characterizations of the An^r strains demonstrated a direct correlation between anisomycin resistance and affinity for Phe-$tRNA^{Phe}$ (Table 1), and subsequent characterization of other L3 mutant strains reinforced this notion [204]. The X-ray crystal structure and results of structure probing experiments provide insights into which stages of aminoacyl-tRNA selection may be affected. Intriguingly, the W255 and P257 amino acid residues contact C2942 (in *S. cerevisiae*). This base forms the second of two "accommodation gates". The chemical probing experiments demonstrated altered DMS reactivity of the nucleotide bases in helix 89 (U2861 and A2863in *S. cerevisiae*) and at the tip of the sarcin-ricin loop (A2844 in *S. cerevisiae*, Figure 2.12). The base of helix 89 forms the second gate that must be passed by the acceptor end of an aminoacyl-tRNA during accommodation [37]. An open conformation of these gates would decrease the pause associated with the gates and increase the rate of accommodation. Alternatively an altered sarcin ricin loop (SRL) structure may promote increased rates of GTPase activation, and subsequently accommodation. Both mechanisms would result in anisomycin resistance.

We suggest that the effects of *mak8-1,* W255C, and P257T forms of L3 on tRNA accommodation and conformation of the PTC are functionally linked. The accommodation simulation and the induced fit model of PTC activation together suggest that accommodation of aa-tRNA triggers changes in PTC conformation. It is tempting to hypothesize that L3 (and/or L3 contacting elements) are involved in inducing conformational changes in the PTC upon accommodation. First, the W255 and P257 amino acid residues contact C2941 (in *S. cerevisiae*), the residue that forms the second gate, and with C2944 (in *S. cerevisiae*). C2941 (in *S. cerevisiae*) flips in the opposite direction and faces toward the peptidyl transferase center. Remarkably, the position of C2941 differs between the "uninduced" and "induced" conformations of the ribosome. The primary amino group of C2941 (in *S. cerevisiae*) is within 3.9Å of the 3' OH of U2874 (in *S. cerevisiae,* distance in *H. marismortui* structure). However these two groups may come within hydrogen bonding distance during transition into the "induced" conformation. We propose that movement of these bases associated with accommodation brings the amino group of C2941 (in *S. cerevisiae*) closer to the 3' OH of U2874 (in *S. cerevisiae*), allowing formation of this hydrogen bond. Formation of the bond promotes/secures the flipped conformation of U2874 (in *S. cerevisiae*) thus switching/locking the PTC conformation in the “induced state” and preparing it for peptidyl transfer.

Accommodation, which is driven by energetically unfavorable conformation of the aminoacyl-tRNA, promotes movement of the gate bases [37]. This movement provides the activation energy required for the subsequent flip of U2874 (in *S. cerevisiae*) and movement of U2952 and U2953 (in *S. cerevisiae*) during PTC activation. The subsequent formation of the hydrogen bond between the primary

amine of C2941 (in *S. cerevisiae*) and the 3' OH of U2874 (in *S.cerevisiae*) stabilizes/promotes the flipped conformation of U2874 (in *S. cerevisiae*). Subsequent formation of base pairing interactions between the CCA-end of the aminoacyl-tRNA and 25S rRNA stabilizes the active conformation of the ribosome by putting it in a more stable "energy well", thus preventing the return to the "uniduced" state.

In this chapter, a biochemical characterization of the L3 mutants has been presented. We demonstrated that ribosomal protein L3 affects aminoacyl-tRNA selection either through conformational changes in active centers of the ribosome, or through active participation in structural transitions during the elongation cycle. We proposed a model that links accommodation and PTC activation, and suggested that (1) process of accommodation triggers an active conformation of the PTC, and (2) L3 and (or) L3 contacting elements may be involved in induction of the active PTC conformation.

Chapter 3. 5S rRNA

Introduction

The eukaryotic ribosome is a 4.0-megadalton complex composed of four ribosomal RNAs (5S, 5.8S, 18S, and 25S) and multiple proteins. Initial studies of ribosomes granted a majority of the catalytic functions to the ribosomal proteins and assigned merely a scaffolding role to rRNA. Subsequent biochemical and structural studies reversed this model toward assigning an active role to the ribosomal RNA. The elucidation of ribosome structures at atomic resolution clearly confirmed the active role of rRNA in ribosome function demonstrating that the active centers of the ribosome are solely composed of RNA [40,43,166,206]. The A- and the P-sites, the majority of inter subunit interfaces, the peptidyl transferase, decoding and the GTPase associated centers are all composed of the 5S, 18S, and 25S rRNA. Furthermore, rRNA is responsible for proper tRNA selection, peptide bond formation and GTPase activation [40,166,207,208]. Those functions are performed by 18S and 25S rRNAs [166,207]. The functions of the two small ribosomal rRNAs, 5S and 5.8S, are less well understood.

As the role of rRNA in protein biosynthesis became more apparent in recent years, we chose to focus on the role of 5S rRNA in ribosome function and translational fidelity. In the ternary ribosomal structure, 5S rRNA connects the active centers of ribosome. The “top” part of 5S rRNA is composed of domains II and III (Figure 3.1). These domains form the upper part of the central protuberance of the large subunit together with ribosomal proteins L5 and L11 (Figure 3.2). The central

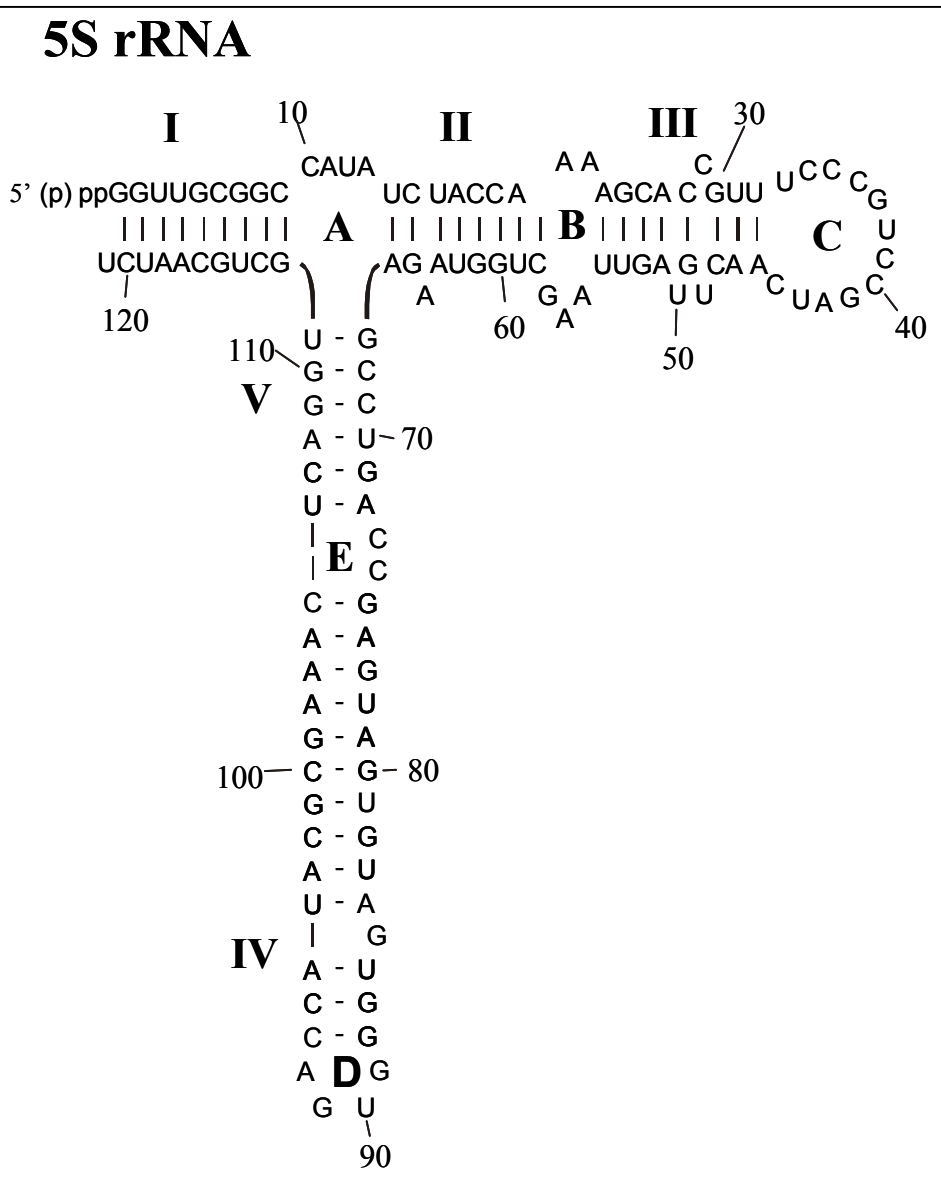

Figure 3.1. Secondary structure of 5S rRNA.

5S rRNA is composed of five domains (designated by roman numerals), separated by bulges (designated by letters).

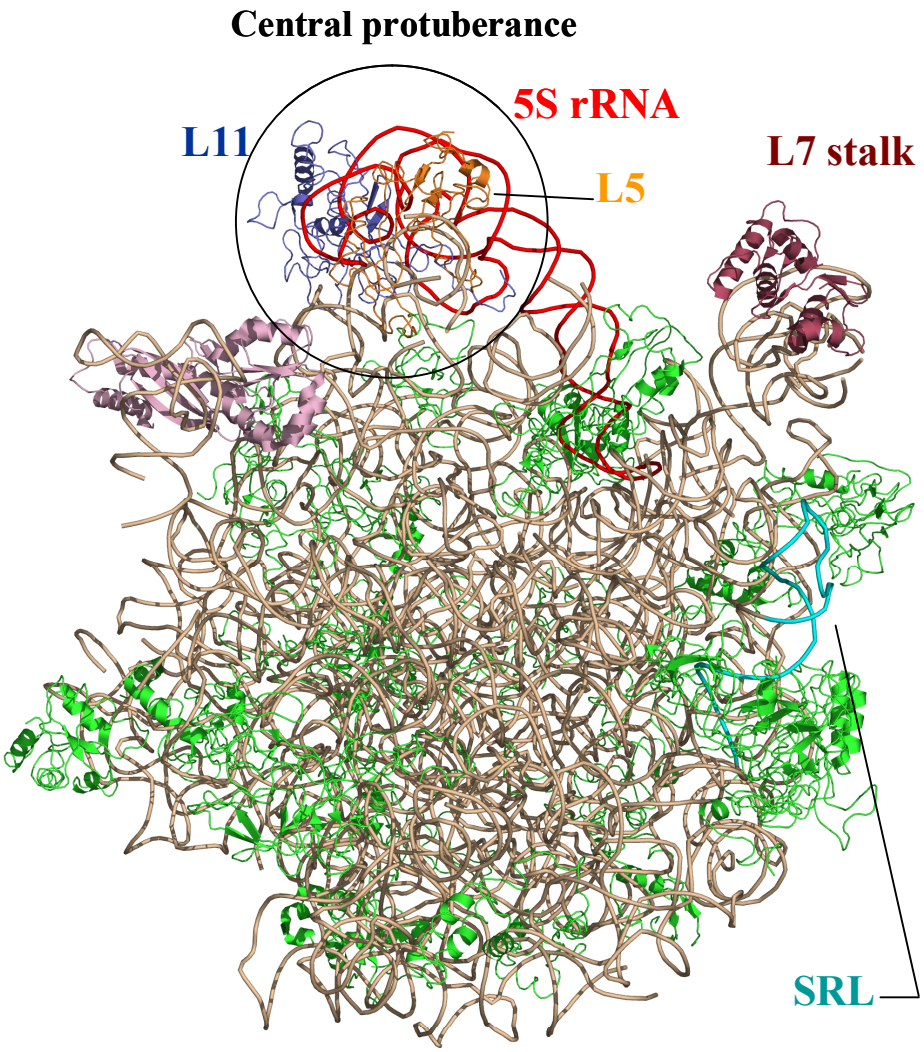

Figure 3.2. Anatomy of the large subunit.

The central protuberance on the large subunit is circled. The 5S rRNA (red) together with ribosomal proteins L5 (orange) and L11 (blue) form the main mass of the central protuberance. The L7 stalk (raspberry) and SRL (cyan) are shown for orientation. (Based on the Cryo-EM structure of the *S. cerevisiae* ribosomes from Spahn C.M.T., *et al* [184].)

protuberance establishes contacts with the small subunit through three intersubunit bridges: B1a, B1b, and B1c. Bridges B1b and B1c connect L11 with ribosomal protein S15 on the small subunit [59]. Domain V of 5S rRNA lies at the base of the triple junction of the molecule (Figure 3.1), and interacts with the A-site finger (ASF, h38, Figure 3.1) [44,59]. Structurally the A-site finger protrudes along the horizontal axis of the large subunit and connects the peptidyl transferase center (through helix 80 and the P-loop) with the small subunit. The apical part of h38 contacts small subunit protein S13 to form the B1a bridge. The B1a bridge is evolutionarily conserved and is present in ribosomes from all kingdoms except mitochondria[v]. The positions and contacts of the B1 bridges change during the elongation cycle. Binding of elongation factor eEF-2, which catalyzes translocation, promotes a ratchet-like movement of the small subunit by approximately 30° [62,209]. Upon this rotation, the B1a bridge disappears and bridges B1b and B1c are reformed at another position, establishing new contacts with the small subunit. Deletion of the B1a bridge in *E. coli* results in increased levels of stop codon suppression, +1 ribosomal frameshifting, and decreased rates of EF-G activation [210]. This rotation was implicated in defining ribosomal binding sites, thus defining the selectivity of the ribosome to the particular elongation factor. It is thought that at the start of the elongation cycle the ribosome adopts a "locked" conformation, which favors EF-Tu binding and allows accurate aa-tRNA selection. During or after aa-tRNA selection or peptidyl transfer the ribosome transitions to the "unlocked" state. This state promotes EF-G recruitment and allows movement of the mRNA by 3 bases in 3' direction during translocation. The subsequent movement of the small subunit presumably puts the ribosome into the

[v] Interestingly, mitochondrial ribosomes are the only ribosomes that also lack 5S rRNA.

locked state, thus preparing it for the next round of the elongation cycle. It is likely, that this movement promotes GTP hydrolysis by EF-G which in turn results in dissociation of the elongation factor from the ribosome. Deletion analysis of h38 demonstrated that disruption of the tip of the helix, which participates in formation of the B1 bridges, inhibits EF-G activation and promotes mis-sense incorporation. Notably, it was demonstrated that ribosomal protein L5, which interacts with the opposite side of 5S rRNA, and is spatially close to h38, helps to stabilize P-site tRNA:ribosome interactions, and that mutations in L5 affected efficiencies of +1 and -1PRF. While the mechanism of these observations in unknown, the proximity of h38 suggests that L5 (or L5 contacting elements) could be involved in these conformational changes, or that it could help to maintain the structure of the surrounding areas required for the ribosome transitions. We hypothesize that the B1 bridges and the central protuberance could be involved in coordination of factor selection and regulation of their activities.

The 5S rRNA"toe" (domain IV, Figure 3.1) makes contact with the triple junction formed by h39, h89 and L10. As described above, helix 38 interacts with the peptidyl-tRNA through the P-loop and h80. Interestingly, helix 89 forms the gates though which the acceptor end of the incoming A-site tRNA slides into the peptidyl transferase center [37]. Functional analysis of *Thermus aquaticus* ribosomes depleted of 5S rRNA suggested that 5S provides either a structural or functional link between domains II and V of 25S rRNA[vi]. These observations reinforced our hypothesis that

[vi] h39 is part of the domain II; the peptidyl transferase center and h89 composed entirely by the domain V of 25S rRNA

thr central protuberance and 5S rRNA act to link the different active centers of the ribosome, and between large and small subunits.

To address these hypotheses, we conducted an analysis of a library of 5S rRNA alleles mutagenized to near saturation. Previous genetic analysis of 5S rRNA was hindered by the presence of four genomic repeats of 5S rRNA. In this work, we devised a system allowing expression of mutant alleles as the only source of 5S rRNA. Surprisingly, it was found that all but seven of 246 mutant 5S rRNA alleles tested were incompatible with viability when expressed as the sole form of the molecule. Genetic analyses suggested that the viable alleles might affect the binding of peptidyl-tRNA to ribosomes, and rRNA chemical protection experiments using ribosomes isolated from these strains revealed changes in chemical protection patterns in both 5S and 25S rRNA. A bioinformatic analysis revealed the apparent presence of multiple 5S rRNA alleles in the genomes of all eukaryotes examined. The previous observation of allele-specific semi-dominant phenotypes in 5S mutant analysis [211] led us to ask whether naturally occurring variants of this molecule might also affect translational fidelity. Overexpression of naturally occurring 5S rDNA variants in a wild-type *RDN1* background indeed resulted in allele-specific changes in programmed −1 and +1 ribosomal frameshifting, suggesting that changes in the expression patterns of endogenous allelic 5S rRNA variants may be used to alter gene expression.

Materials and Methods

Strains, plasmids and genetic methods

E. coli strain DH5α was used to amplify plasmids, and *E. coli* transformations were performed using a standard calcium chloride method as described previously [212]. Yeast cells were transformed using the alkali cation method [170]. YPAD, YPG, SD, synthetic complete medium (H-) and 4.7 MB plates for testing the killer phenotype were used as described previously [213]. Plasmid shuffling techniques using 5-flouroorotic acid (5-FOA) were performed as previously described [214]. For dilution spot assays, growing yeast cells in mid-logarithmic phase were initially diluted to 2×10^7 colony forming units (CFU)/ml. Subsequently, 10^5 CFU (5 µl) aliquots, and tenfold dilutions from the same cultures thereof were spotted either onto rich medium and incubated at 15, 30 and 37 °C, or incubated at 30 °C on rich medium containing anisomycin (10µg/ml) or sparsomycin (30 µg/ml). Assays for programmed ribosomal frameshifting followed previously described protocols [116,211]. These involve the use of 0-frame control and −1 or +1 ribosomal frameshift test vectors in which the production of a reporter enzyme (either firefly luciferase of β-galactosidase) is dependent upon a programmed ribosomal frameshift event. Percentage of frameshifting is calculated by dividing the enzymatic activities measured from cells expressing the frameshift test plasmids by those from cells expressing the 0-frame controls, and multiplying the resulting values by 100 %. The nonsense suppression of the UAA stop codon has been measured with the dual luciferase reporter system. This assay is essentially the same as the dual luciferase frameshifting assay. In this reporter

the frameshift signal has been replaced by the stop codon and translation of the second luciferase is possible only as result of the stop codon readthrough (Figure 3.3).

Ty*1* retrotransposition assays were performed using pJEF1105 as previously described [215]. Briefly, transcription of a *neo*^{r}-tagged Ty*1* cDNA clone was induced by incubation in 2 % galactose at 20 °C for 3 days, after which cells that had lost pJEF1105 were identified by screening for growth on dextrose-containing medium in the presence of 5-FOA. The cells were then grown in liquid culture overnight, and tenfold dilutions of mid-log cells were spotted onto a medium containing 100 μg/ml Gentcin (Life Technologies, Gaithersburg, Md.) to select for cells in which retrotransposition had occurred, or onto rich medium as a control.

The pJD180 series of plasmids contain one complete *RDN1* repeat cloned into the pRS400 series [216], the pJD106 and pJD209 series consist of high copy vectors containing variants of the 5S rDNA gene, and the pJD211 series harbor a single copy of the 35S rDNA operon [217]. The pJD373 series of plasmids is based on the pJD211 series, and contain the C1495U allele in helix 44 of 18S rDNA, which was previously shown to confer a recessive hygromycin-resistant phenotype on yeast cells [218]. Standard oligonucleotide site directed mutagenesis was used to generate the naturally occurring allelic 5S rRNA yeast variants (*RDN5-2* through *RDN5-7*) and the *RDN5-Ooc* and *RDN5-Som* hybrids of yeast and *Xenopus* 5S rRNAs using the *RDN5-1* allele cloned into pRS424, a high copy TRP1-2μ vector [216] as a template.

Generation of the *rdn1ΔΔ* yeast strain JD1111, and of strains harboring mutant alleles of 5S rDNA on a *2μ-TRP1* vector were performed previously described [211]. This strain was based on NOY891 [217], which was subsequently found

Bi-cistronic dual luciferase reportes

0-frame dual luciferase reporter

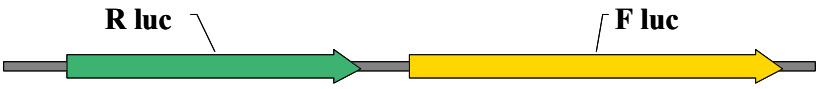

Recoding dual luciferase reporter

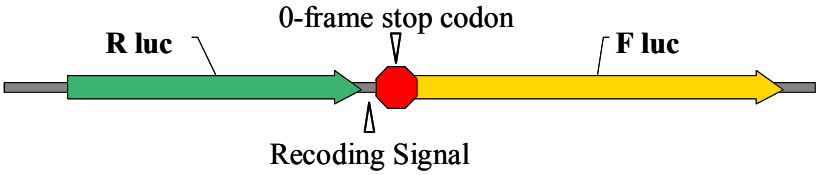

$$\text{Recoding efficiency} = \frac{\text{F luc}_{-1}/\text{R luc}_{-1}}{\text{F luc}_0/\text{R luc}_0} * 100\%$$

Mono-cistronic β-gal reporters

0-frame β-gal reporter

Recoding β-gal reporter

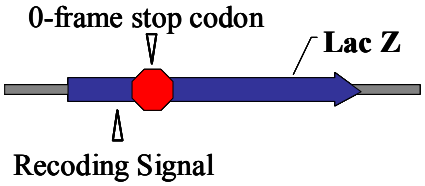

$$\text{Recoding efficiency} = \frac{\beta\text{-gal}_{-1}}{\beta - \text{gal}_0} * 100\%$$

Figure 3.3. Translational recoding reporter systems.

The bi-cistronic dual luciferase and mono-cistronic β-gal systems were used. Both reporter systems allow translation of the sequence downstream from a recoding signal (Firefly luciferase for dual luciferase, and the majority of the lac-Z ORF for the β -gal reporter) only as result of translational recoding event.

to contain four telomere proximal 5S rDNA repeats on chromosome XII [219]. These repeats are deleted in NOY1049 [219]. Strain JD932 has a complete, wild-type *RDN1* locus.

Library generation

To construct a new series of strains lacking the chromosomal 5S rDNA repeats, NOY1049 (*MATa ade2-1 ura3-1 trp1-1 his3-11 leu2-3, 112 can1-100 ΔrDNA::his3::hisG* + pNOY353 (GAL7-35S rDNA, 5S rDNA, *TRP1*, 2μ, amp^r, Appendix A, page 161) was transformed with pJD180.Ura. To promote spontaneous loss of *TRP1* plasmid (pNOY353) transformants were incubated in liquid standard defined medium lacking uracil (-ura) for 4 days, streaked for single colonies on –ura solid medium, and subsequently replica plated onto medium lacking tryptophan (-trp). Trp^- auxotrophs were picked and designated JD1248 (*MATa ade2-1 ura3-1 trp1-1 his3-11 leu2-3, 112 can1-100 ΔrDNA::his3::hisG* + pJD180.URA). The observed rate of loss of tryptophan prototrophy was approximately 10 %. JD1253 (*MATa ade2-1 ura3-1 trp1-1 his3-11 leu2-3, 112 can1-100 ΔrDNA::his3::hisG* + pJD180.URA [LA-HN M_1]) was created by introducing the L-A and M_1 viruses into JD1248 cells by cytoduction using a previously described technique [133].

Cytoduction is essentially a mating process that went until the cytoplasmic fusion state, but had not proceeded to the nuclei fusion state. JD1248 strain was grown on YPAD plates containing a gradient of ethidium bromide from 0 to 10 mg/ml to promote mitochondria loss. Cells lacking mitochondria (rho^0) were selected by the inability to grow on a non-fermentable carbon source (glycerol, YPG media). Then rho^0 strain was crossed with JD759 (*MATα kar1-1 arg1 thr(i,x)* L-A HN M_1).

JD759 strain harbors the *kar1-1* allele of an essential protein required for karyogamy. This mutation delays the nuclear fusion thus making it possible to obtain intermediates of the mating process that have not progressed to the nuclear fusion state. Strains obtained in JD759xJD1248 cross were selected against the JD759 donor strain by growth on -Arg media. Diploids were identified by the growth on media lacking non essential amino acids (SD). JD1248 colonies with successful cytoplasmic transfer (rho^+) were identified by the ability to grow on YPG media. The presence of the L-A and M_1 viruses in these strains were confirmed by the killer assay. Briefly, the cells were replica plated 4.7 MB Killer media plates that had been seeded with a lawn (0.5 OU at OD_{595} per 100 mm plate) of 5x47 killer indicator yeast cells (M_1 minus, Appendix A, page 161). Then plates were incubated at 18º C for 2 to 3 days and presence of the killer phenotype was scored as a zone of growth inhibition surrounding Killer positive colonies. The resulting killer positive strain was designated JD1253.

The JD1253 strain was used to generate stains expressing mutant 5S alleles using the plasmid shuffling technique. Plasmid shuffle is the substitution of one plasmid for another. JD1253 was transformed with pJD373.Leu harboring 5.8S, 18S and 23S rRNA genes, and with one of the 246 variants of pJD106.Trp harboring different 5S rRNA alleles (Appendix B, page 166). Transformants were selected on media lacking tryptophan and leucine. pJD373.Leu has a recessive hygromycin resistance mutation (U1759C) in 18S rRNA, thus allowing negative selection against recombinants between pJD373.Leu and pJD180.Ura on hygromycin containing media. Spontaneous loss of the pJD180.Ura plasmid was promoted by growth on H-Trp-Leu media (containing uracil). Cells were passaged on H-Trp-Leu media three

times, and were subsequently streaked for single colonies on medium lacking tryptophan and leucine, and containing 5-flouroorotic acid (5-FOA) [220] and hygromycin (300 μg/ml) to negatively select against pD180.Ura. 5S rRNA from these obtained strains was sequenced to confirm presence of the mutant alleles.

rRNA sequencing

Expression of mutant 5S rRNA was confirmed by a modified single base primer extension method [221]. In essence, this is a standard primer extension method in which sequencing dNTPs/ddNTP mix was substituted for mix of three dNTPs and one ddNTP. Excess of ddNTP and the absence of the corresponding dNTP ensures nearly 100 % termination at the first base complimentary to the ddNTP, and does not continue beyond this base regardless of downstream sequence. Thus the base 3' of the primer can be unambiguously identified as a single base extension using a reaction mix containing the corresponding ddNTP. The extension reactions in the three other mixes continue to the nucleotide complementary to ddNTP in the reaction mix. Thus this method allows detection of even minor contamination by wild type 5S rRNA allele. Oligonucleotides complementary to 5S rRNA (Appendix C, page 174) were labeled with γ[^{32}P]ATP using T4 polynucleotide kinase, and annealed with 5S rRNA isolated from purified ribosomes. Primer extension reactions were performed using AMV reverse transcriptase (Roche) in a buffer containing 50 mM Tris–HCl pH 8.3, 60 mM NaCl, 6 mM magnesium acetate, 10 mM DTT, and chain terminating mixes containing 0.25 mM dNTPs (three of the four) plus 0.25 mM ddNTP (the fourth). Reactions were incubated at 45 °C for 30 minutes, terminated by the addition of 2 × formamide sequencing dye, heated to 90 °C, quenched on ice and fractionated by

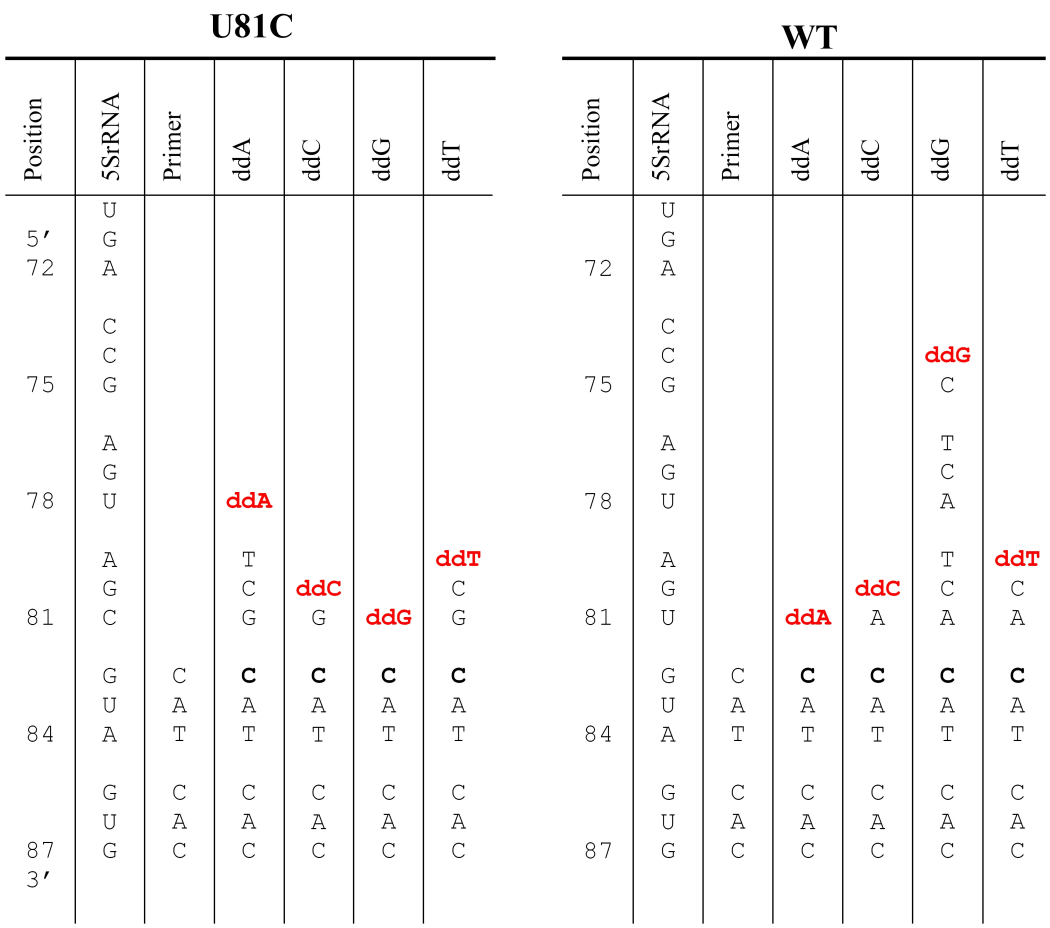

Figure 3.4. rRNA sequencing.

Example of a single base rRNA sequencing assay at position 81 for a wild type and U81C strains. The expected stops from non reacted primers are designated by black bold. The stops resulted from ddNTP incorporation is designated by red bold.

electrophoresis thorough 12 % polyacrylamide urea denaturing gels. Labeled bands were visualized by autoradiography

Chemical protection analyses

Chemical probing with dimethylsulphate (DMS), 1-cyclohexyl-3-(2-morpholinoethyl) carbodiimide metho-p-toluene (CMCT), and kethoxal (Figure 2.3 and Figure 3.5), followed by RT primer extension analysis of modified RRNAs were performed as previously described [222]. The following primers (numbered according to first transcribed base) were used: 2,957, 3,057, 1,231, 1,343 and 1,112 for *S.cerevisiae* 25S rRNA, and 99 for 5S rRNA (Table 11).

Bioinformatic methods

Genbank was first queried for 5S rRNA sequences according to species. The resulting sequences were then used in BLAST searches [223] to identify homologous sequences in the NCBI nucleotide database. Sequences were hand curated to identify those that 1) were represented by multiple independent Genbank accession entries, and 2) did not contain overly large deletions of sequence (i.e. did not appear to be truncation products or pseudogenes). The resulting sequences were then aligned with one another using ClustalW [224].

Results

Generation and characterization of 5S rRNA mutants

Examination of the yeast strain used for a previous 5S rRNA saturation mutagenesis study [211] revealed that it contained four genomic copies of the 5S

Kethoxal

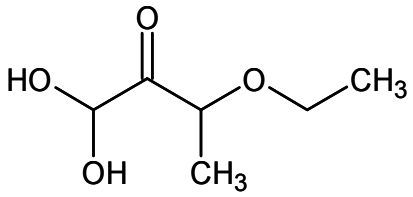

CMCT

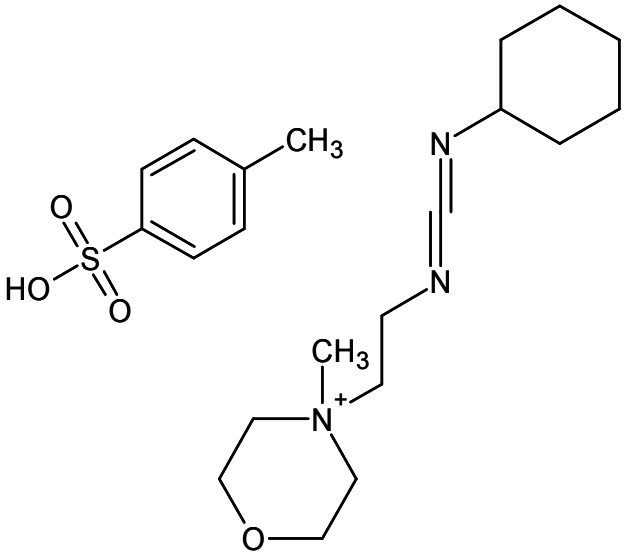

Figure 3.5. Structures of kethoxal and CMCT

rRNA gene. To express mutant forms of 5S rRNA in the absence of the wild type molecule, strain NOY1049 in which the chromosomal 5S rDNA repeats were completely deleted was obtained from the laboratory of M.Nomura [219]. This strain was subjected to two additional rounds of genetic manipulation to create a new parental strain designated JD1253 (as described in Material and methods, page 92). Subsequent attempts to obtain 5SrRNA mutant strains by the plasmid shuffle method [214] failed due to high rates of recombination between the wild type and mutant forms of the 5S gene. Direct sequence analysis of 5S rRNAs from those strains demonstrated the absence of expression of the mutant allele. In order to minimize recombination and select cells containing only mutant forms of 5S rRNA, a rigorous selection scheme involving negative selection for both the wild-type *RDN1* gene and the plasmid on which it was encoded was devised (see Materials and methods, page 92). Having established the new strain and selection protocol, we examined the effects of all 246 5S rRNA alleles [211] on cell growth and viability. Surprisingly, only seven of the alleles supported viability: all the others were unviable when expressed as the sole form of 5S rRNA. The seven viable alleles were A20C, C69U, A76U, A79G, U81C, A84U and C93U (Figure 3.6). The new mutant strains were first characterized with regard to their growth rates at different temperatures. In general, expression of each of the seven functional 5S rRNA mutant alleles was associated with significantly reduced growth rates at 30 °C compared to wild type. Although some of the mutants may have been slightly temperature-sensitive, they were surprisingly resistant to cold (Figure 3.7).

Figure 3.6. Direct rRNA sequence analyses of 5S rRNA mutants.

rRNAs were extracted from ribosomes purified from JD1253 cells expressing wild-type or mutant forms of 5S rRNA. Oligonucleotides complementary to 5S rRNA were labeled with $\gamma[^{32}P]$ATP using T4 polynucleotide kinase, and annealed with 5S rRNA isolated from purified ribosomes. Primer-extension reactions were performed using AMV reverse transcriptase, fractionated by electrophoresis through denaturing 12 % polyacrylamide-urea gels, and labeled bands were visualized by autoradiography

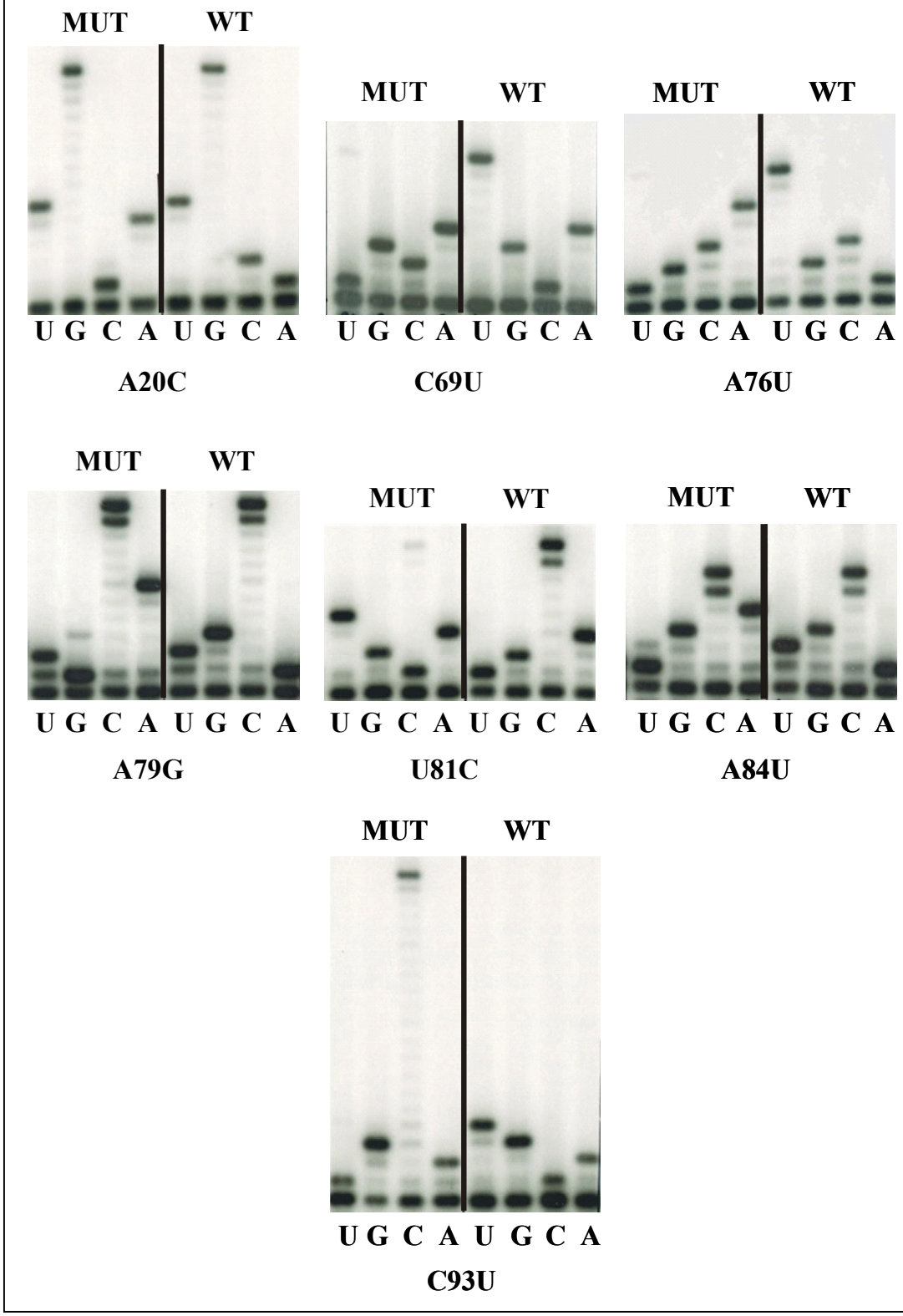
MUT
WT
U G C A U G C A
A20C
MUT
WT
U G C A U G C A
C69U
MUT
WT
U G C A U G C A
A76U
MUT
WT
U G C A U G C A
A79G
MUT
WT
U G C A U G C A
U81C
MUT
WT
U G C A U G C A
A84U
MUT
WT
U G C A U G C A
C93U

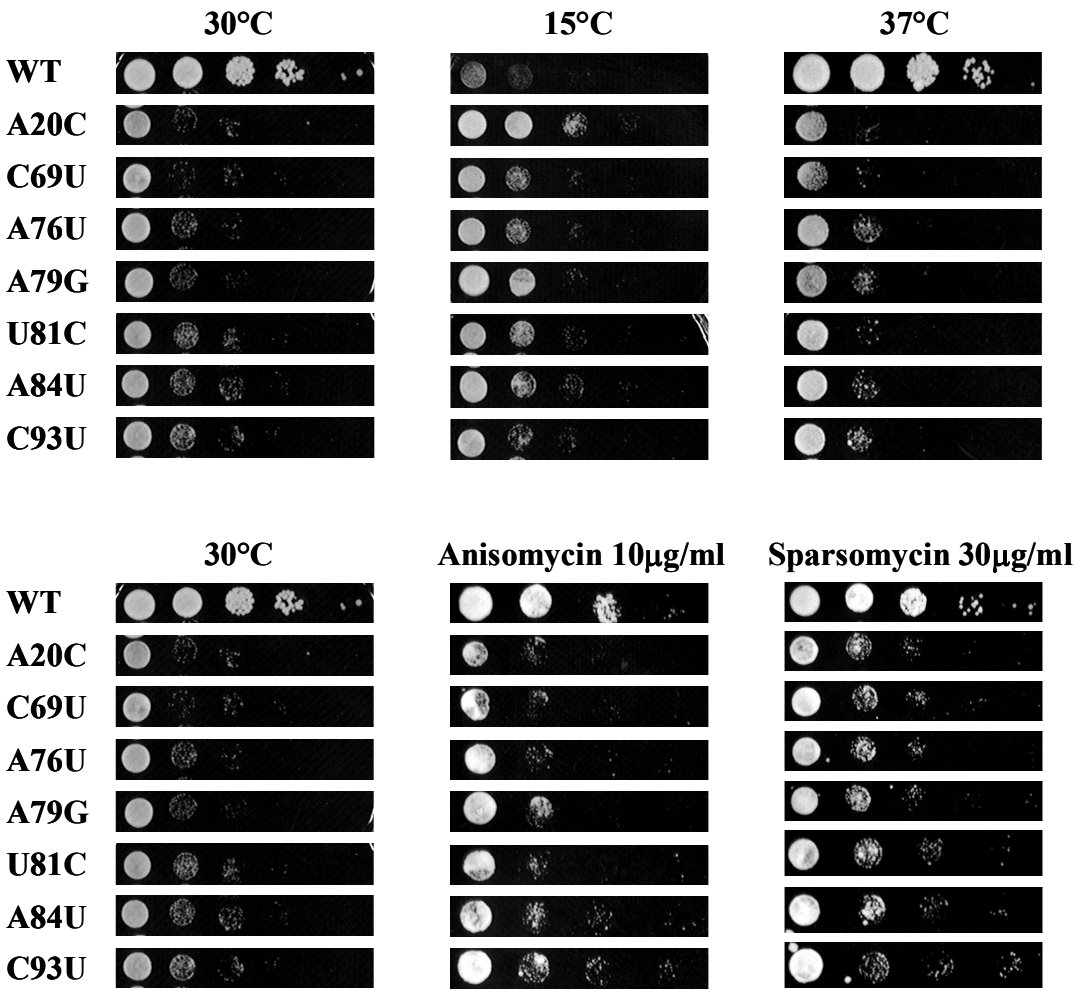

Figure 3.7. Growth phenotypes of 5S rRNA mutants.

Mid-logarithmically growing JD1253 cells were diluted to 2×10^7 colony forming units (CFU)/ml. Subsequently, aliquots (5 µl) containing 10^4 CFU, and tenfold dilutions from the same cultures were spotted either onto rich medium (YPAD) and incubated at 15, 30, and 37 °C, or onto YPAD containing anisomycin (10 µg/ml) or sparsomycin (30 µg/ml) and incubated at 30 °C.

Translational inhibitors provide expedient probes for changes in ribosome function (reviewed in Ogle J.M. and Ramakrishnan V.[22]). The seven mutant 5S rRNA strains were characterized with regard to anisomycin and sparsomycin sensitivity. Both drugs bind in the vicinity of the peptidyl transferase center [186] and severely inhibit peptidyl transferase activity [193,225]. Though the results with anisomycin were generally equivocal, sparsomycin actually improved the growth of all of the mutants (Figure 3.7). Anisomycin binds to the A-site hydrophobic crevice, which is occupied by the peptidyl moiety of the aminoacyl-tRNA in the absence of the drug. In contrast, sparsomycin mainly contacts the peptidyl-tRNA, but also extends into the A-site crevice. The observed drug phenotypes suggest that these mutations in 5S rRNA altered the conformation and/or functionality of the P-site, but did not affect the A-site tRNA.

Programmed ribosomal frameshifting (PRF) provides a powerful tool to monitor translational fidelity [116]. The PRF signals from two endogenous yeast viruses, L–A (which utilizes a −1PRF mechanism) and the Ty*1* retrotransposable element (which uses +1PRF) were employed to monitor the effects of the 5S alleles on these processes using dual-luciferase reporter plasmids [226]. All seven of the viable mutants promoted no changes in −1PRF, and had no effect on the "Killer" phenotype. In contrast, a few of the mutants promoted modest but statistically significant changes in +1PRF. Ty*1* retrotransposition frequencies were most strongly reduced by those alleles that promoted the largest increases in +1PRF (Figure 3.8), thus confirming the biological significance of observed changes in levels of +1 frameshifting.

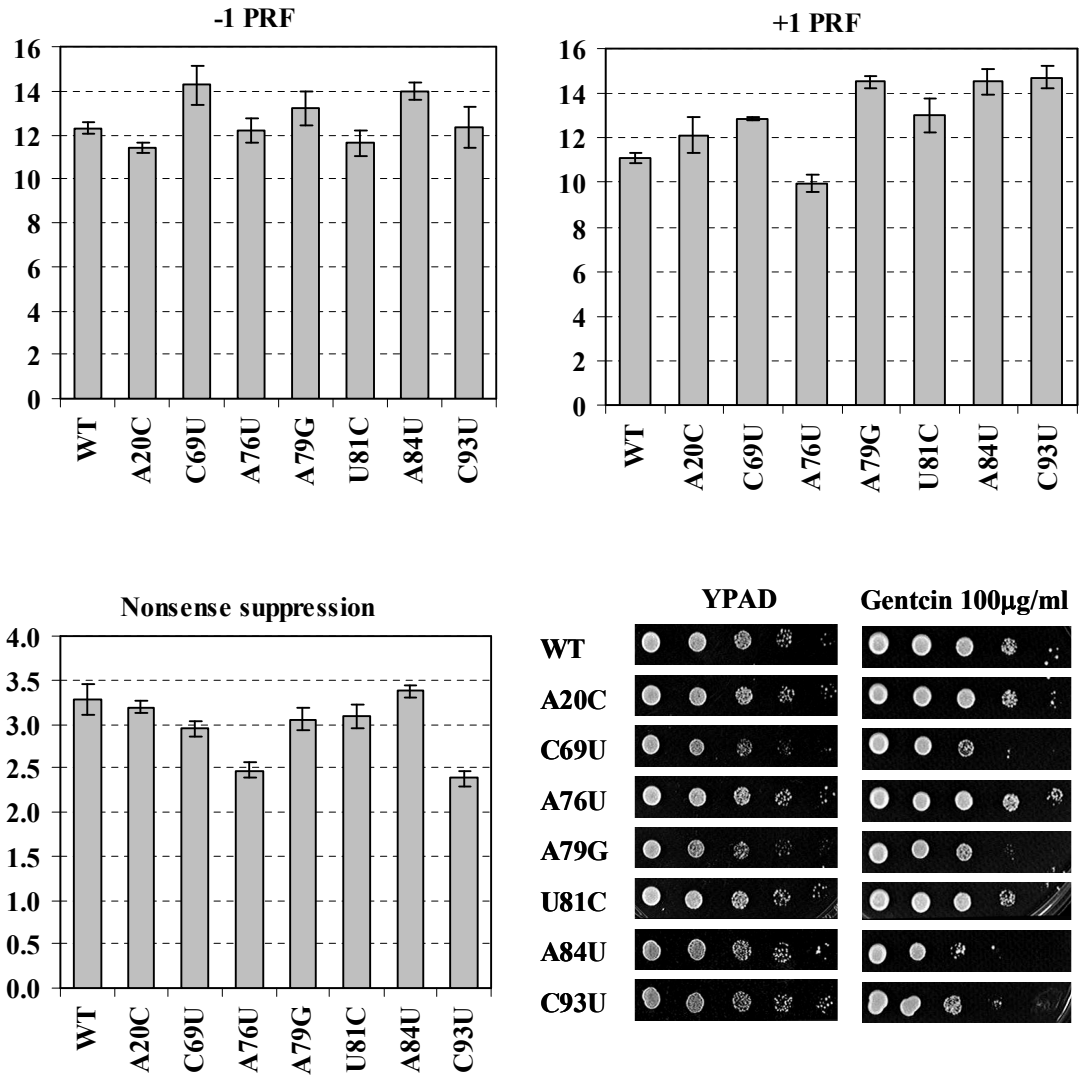

Figure 3.8. Efficiency of translational recoding events.

Translational recoding efficiencies are not affected in most of the viable 5S mutants. However, while changes in +1PRF efficiencies (plotted as percent of frameshifting) are small but biologically significant and affected the efficiency of Ty*1* retrotransposition (shown at the right bottom panel).

In the context of current PRF models, -1PRF is kinetically driven by accommodation of A-site tRNA, while +1 frameshifting is primary affected by conformation and status of the P-site. The observed PRF and viral maintenance phenotypes reinforce the notion that mutations in 5S rRNA primary affect the P-site of the ribosome.

Structural characterization of ribosomes containing mutant forms of 5S rRNA

Isolated ribosomes containing only mutant forms of 5S rRNA were probed *in vitro* for structural changes in 25S and 5S rRNAs using three base-specific reagents: dimethylsulfate (DMS), kethoxal, and 1-cyclohexyl-3-(2-morpholinoethyl) carbodiimide metho-p-toluene (CMCT). DMS preferentially donates a methyl group to hydrogen bond accepting ring nitrogens of C, G and A residues [196,227]; kethoxal reacts with the N1 and N2 amine of solvent exposed G residues [228,229], and CMCT reacts with non-interacting N1 and N3 nitrogens of G and U residues, respectively [230]. Base modifications by these reagents cause n−1 reverse transcriptase stops, allowing for identification of base-specific changes in rRNA structure. Reverse transcription analysis was employed to monitor structural changes in domains II, V and VI of 25S rRNA, and throughout the entire length of 5S rRNA.

The results of these studies revealed that the mutants showed structural changes in both 5S and 25S rRNAs. Figure 3.9 shows representative autoradiograms from these studies, and Figure 3.10 depicts the bases in question in relation to two-dimensional representations of 5S rRNA and helix 95 of the 25S rRNA. The

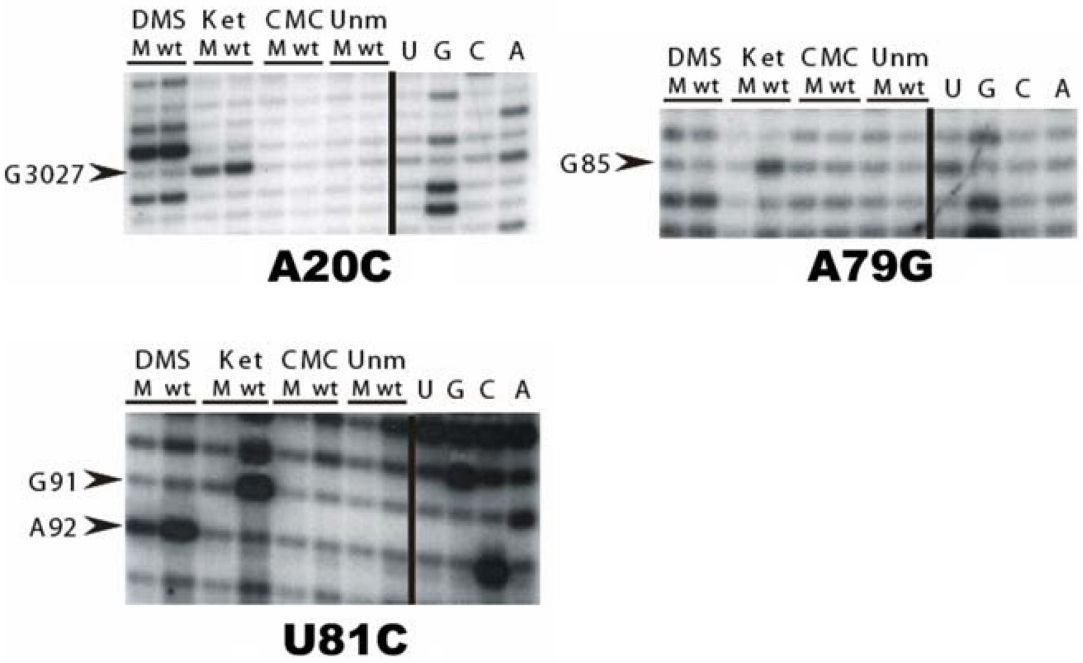

Figure 3.9. Chemical protection analyses.

Ribosomes purified from JD1253 cells expressing either wild-type or mutant 5S rRNAs were chemically probed with DMS, kethoxal and CMCT. The representative autoradiograms depicting probing of 5S rRNA (U81C and A79G) and 25S rRNA (A20C) are shown. M indicates corresponding *RDN5* mutant, wt indicates ribosomes containing expressing *RDN5-1*allele, and Unm an unmodified control.

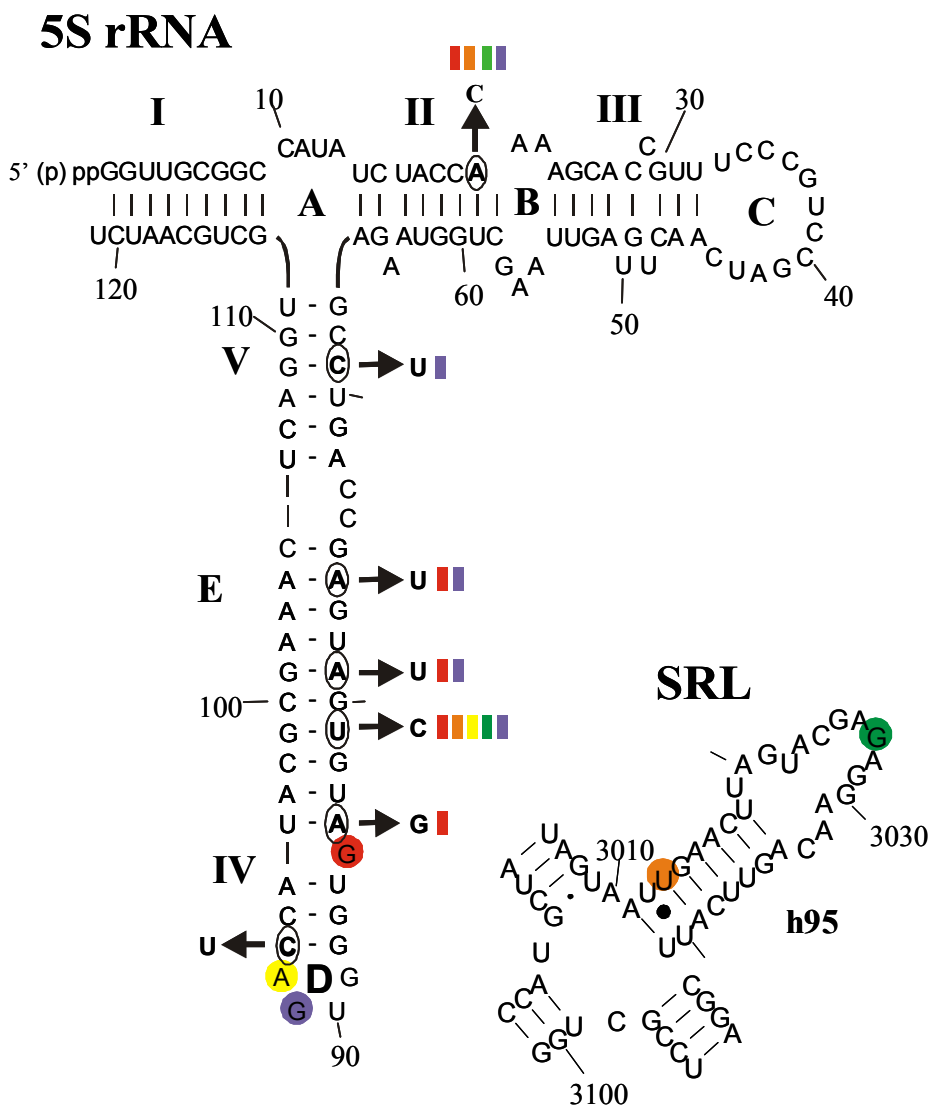

Figure 3.10. Summary of the chemical protection analyses.

Ribosomes purified from JD1253 cells expressing either wild-type or mutant 5S rRNAs were chemically probed with DMS, kethoxal and CMCT. The products of reverse transcriptase primer extension reactions were subjected to PAGE analysis on denaturing PA-urea gels, and visualized by autoradiography. Color code shows summary of the effects of pure mutants mapped onto 5S rRNA and the helix 95-sarcin/ricin loop (SRL) region of 25S rRNA. The open circles indicate positions of wild-type bases, and the arrows indicate the relevant mutant alleles. The color-coded bars indicate which mutant 5S rRNAs alter the chemical reactivities of other similarly coded, circled, bases in 5S and 25S rRNAs

reactivities of three bases in 5S rRNA were specifically altered by the mutations. In particular, in all of the mutants (with the exception of C69U), G85, which is normally unpaired, was protected from chemical modification. Allele-specific effects were also observed with regard to G91 and A92, which lie in the loop D region of the molecule: all of the mutants except A84G promoted increased protection at position G91, while only U81C altered the protection pattern of A92. Two of the 5S rRNA mutants also had effects on 25S rRNA. Specifically, the A20C and U81C alleles conferred protection of G3027, and weaker but consistent reactivity at position U3013. Interestingly, G3027 is located in the sarcin/ricin loop (SRL), which is involved in elongation factor binding (Figure 3.10).

Naturally occurring allelic variants of 5S rRNA specifically inhibit programmed −1 ribosomal frameshifting

Eukaryotic genomes contain >100 copies of rDNA genes. It is generally assumed either that they are all identical, or that minor differences are inconsequential. Alternatively, it is possible that allelic 5S rDNA variants may have been functionally selected for. To examine this issue, GenBank was searched for species-specific 5S rDNA alleles that fulfilled the following criteria (1) each variant had to be represented by multiple independent entries, and (2) obvious pseudogenes (e.g., those containing large deletions or insertions) were rejected. These searches revealed the presence of multiple 5S rDNA alleles in every genome examined. Specifically, the *S. cerevisiae* genome contains at least seven different allelic variants, *Homo sapiens* has ≥13, *Xenopus laevis* includes ≥6, *Mus musculus* contains ≥16, and

Drosophila melanogaster has ≥11 (Figure 3.11). To test the hypothesis that different forms of 5S rRNA may differentially affect translational fidelity, site-directed mutagenesis was used to create the seven naturally occurring yeast 5S rRNA allelic variants [vii], and these were expressed from high-copy-number 2μ vectors. All but the "wild-type" (*RDN5-1*) variants of the molecule were inviable, either as the sole form of 5S rRNA (in JD1253 cells), or in the presence of four chromosomal copies (in JD1111 cells) (data not shown). Intriguingly, expression of the *RDN5-7* variant in a wild-type *RDN1* strain background (JD932) resulted in significant inhibition of −1PRF (Figure 3.12).

Effects of hybrid yeast/Xenopus 5S rRNAs on programmed ribosomal frameshifting

Early studies of 5S rRNA in *X. laevis* revealed that ribosomes isolated from oocytes and somatic cells contained different forms of 5S rRNA [231]. In light of the observation that 5S rRNA allelic variants can have differential effects on translational fidelity, we hypothesize that *Xenopus* may use the two different forms of 5S rRNAs to post-transcriptionally regulate gene expression during the embryonic development program. To examine this question, yeast 5S rRNA clones were mutagenized to mimic the *Xenopus* oocyte and somatic 5S rRNA variants. Specifically, bases in yeast 5S rRNA at positions 30, 48, 54, 56 and 57 were altered to the corresponding residues in either *Xenopus* somatic (*RDN5-som*), or oocyte (*RDN5-ooc*) 5S rRNAs (Figure 3.11). Although both forms were inviable in JD1253

[vii] Recent addition to SGD database describes seven copies of 5S rDNAin *S.cerevisiae* genome. The SGD allele *RDN5-1* corresponds to the *RDN5-1* allele in this study, and SGD alleles *RDN5-2 – RDN5-7* identical, having the same sequence as *RDN5-2* allele described here.

Alignments of *S. cerevisiae* 5S rRNA allelic variants.

```
RDN5-1    GGTTGCGGCCATATCTACCAGAAAGCACCGTTTCCCGTCCGATCAACTGTAGTTAAGCTG 60
RDN5-7    GGTTGCGGCCATATCTACCAGAAAGCACCGTTTCCCGTCCGATCAACTGT-GTTAAGCTG 59
RDN5-3    GGTTGCGGCCATATCTACCAGAA-GCACCGTTTCCCGTCCGATCAACTGTAGTTAAGCTG 59
RDN5-2    GGTTGCGG  CCATATCTACCAGAAAGCACCGTTTCCCGTCCGATCAACTGTAGTTAAGCTG 60
RDN5-6    GGTTGCGGCCATATCTACCAGAAAGCACCGTTTCCCGTCCGATCAACTGTAGTTAAGCTG 60
RDN5-5    GGTTGCGGCCATATCTACCAGAAAGCACCGTTTCCCGTCCGATCAACTGTAGTTAAGCTG 60
RDN5-4    GGTTGCGGCCATATCTACCAGAAAGCACCGTTCTCCGTCCGATCAACTGTAGTTAAGCTG 60
          ********************** ********  *************** *********

RDN5-1    GTAAGAGCCTGACCGAGTAGTGTAGTGGGTGACCATACGCGAAACTCAGGTGCTGCAATC 120
RDN5-7    GTA-GAGCCTGACCGAGTA-TGTAGTGGGTGACCATACGCGAAACTCAGGTGCTGCAATC 117
RDN5-3    GTAAGAGCCTGACCGAGTAGTGTAGTGGGTGACCATACGCGAAACTCAGGTGCTGCAATC 119
RDN5-2    GTAAGAGCCTGACCGAGTAGTGTAGTGGGTGACCATACGCGAAACTCAGGTGCTGCAGT- 119
RDN5-6    GTAAGAGCCTGACCGAGTAGTGTAGTGGGTGACCATACGCGAAACTCAGGTGCTGCA--- 117
RDN5-5    GTAAGAGCCTGACCGAGTAGTGTAGTGGGTGACCATACGCGAAACTCAGGTGCTGCATTC 120
RDN5-4    GTAAGAGCCTGACCGAGTAGTGTAGTGGGTGACCATACGCGAAACTCAGGTGCTGCAATC 120
          *** *************** ************************************

RDN5-1    T 121
RDN5-7    T 118
RDN5-3    T 120
RDN5-2    -
RDN5-6    -
RDN5-5    T 121
RDN5-4    T 121
```

Alignment of *X. lavae* 5S rRNA allelic variants.

```
RDN5-ooc  GCCTACGGCCACACCACCCTGAAAGTGCCTGATCTCGTCTGATCTCAGAAGCGATACAGG 60
RDN5-som  GCCTACGGCCACACCACCCTGAAAGTGCCCGATCTCGTCTGATCTCGGAAGCCAAGCAGG 60
          ***************************** *************** ***** *  ****

RDN5-ooc  GTCGGGCCTGGTTAGTACCTGGATGGGAGACCGCCTGGGAATACCAGGTGTCGTAGGCTT 120
RDN5-som  GTCGGGCCTGGTTAGTACTTGGATGGGAGACCGCCTGGGAATACCAGGTGTCGTAGGCTT 120
          ****************** ****************************************

RDN5-ooc  -
RDN5-som  T 121
```

Figure 3.11. Allelic variants of 5S rRNAs in eukaryotic genomes.

Conservation of multiple 5S rDNA alleles in eukaryotic genomes. GenBank was first queried for 5S rRNA sequences according to species, and the resulting sequences were used in BLAST searches (Altschul et al.) to identify homologous sequences in the database. Sequences were hand curated to ensure their validity, and then aligned with one another. RDN5-som and RDN5-ooc show the sequences of the hybrid yeast/Xenopus clones. Color coding is used to denote base substitutions.

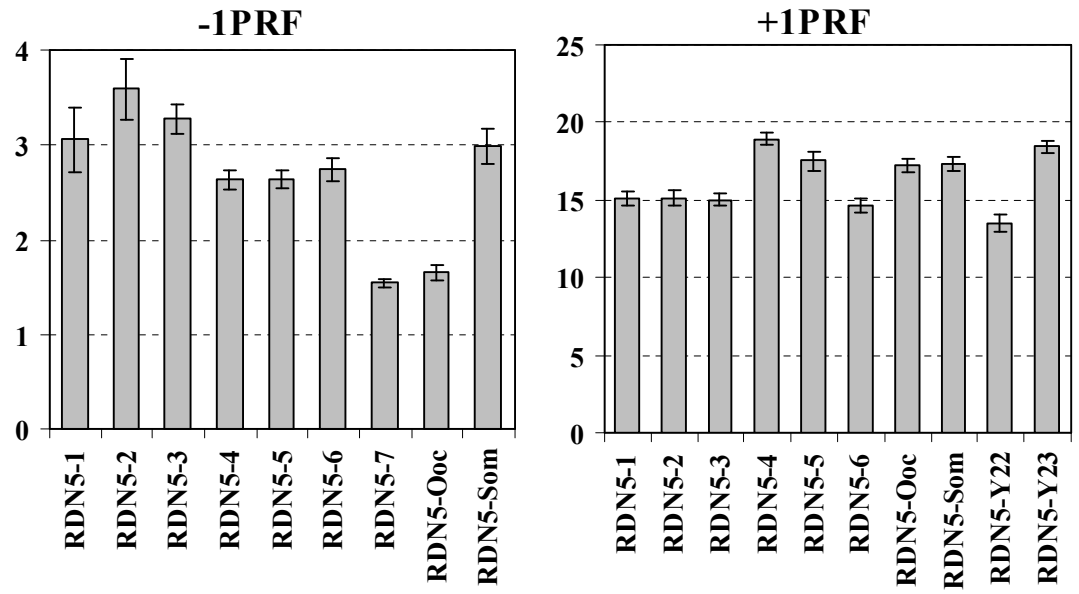

Figure 3.12. Semi-dominant effects of naturally occurring yeast and hybrid yeast/Xenopus 5S rRNA alleles on L–A directed −1, and Ty*1* promoted +1PRF.

Using the yeast *RDN5-1* allele cloned into a high-copy-number 2μ vector, oligonucleotide-primed site-directed mutagenesis was used to create the other six naturally occurring yeast *RDN5* alleles (*RDN5-2* to *RDN5-7*), and the hybrid yeast/Xenopus *RDN5-ooc* and *RDN5-som* alleles (see Figure 3.11). These alleles were episomally expressed in JD932 cells, a wild-type yeast strain containing a full complement of chromosomal rDNA genes. Programmed −1 and +1 ribosomal frameshifting efficiencies were monitored with β-gal reporter plasmids as described in Materials and methods, page 89, and plotted as percent of frameshifting.

and JD1111 strain backgrounds, overexpression of *RDN5-ooc* in JD932D background promoted significant and specific inhibition of −1PRF in the context of the wild-type RDN1 locus (Figure 3.12). The potential significance of these findings is discussed below.

Discussion

This study represents the first structure/function analysis of 5S rRNA in a eukaryotic system. Having established a new yeast strain and selection protocol, we examined the effects of all 246 5S rRNA alleles [211] on cell growth and viability. The observation that only seven of the alleles were viable when expressed as the sole form of 5S rRNA can be interpreted in several ways. First, it could imply that 5S rRNA plays a critical role in ensuring the proper functioning of the ribosome. Alternatively, the mutations in 5S rRNA may result in a lethal phenotype not associated with protein synthesis. All rRNAs except 5S rRNA are transcribed by the RNA polymerase I as a single 35S transcript. In the nucleolus, pre-rRNA is modified and cleaved in the cascade of subsequent reactions that produces 25S, 18S and 5.8S rRNA [232,233]. In contrast, *RDN5* is transcribed by the RNA polymerase III from an internal promoter located within first 20 nucleotides of the coding sequence and the 5' end of 5S rRNA is defined by the transcription start site [234,235]. Subsequent trimming of the five nucleotides from 3' end by the SNIP complex produces the mature molecule [236]. Transcription of 5S rRNA is autoregulated by a feedback mechanism that involves TFIIIA [237] and ribosomal protein L5 [238,239]. TFIIIA is an essential transcription factor for RNA polymerase III and is required for transcription of Pol III genes including 5S rRNA [240,241]. After transcription, TFIIIA binds the newly transcribed 5S rRNA and

forms a 7S complex [242-244]. Formation of the complex exposes a nuclear export signal of the TFIIIA and triggers nuclear export of the 7S complex through the Ran pathway [245]. In the cytoplasm, ribosomal protein L5 promotes release of TFIIIA and formation of the L5:5S rRNA complex [246]. Binding of 5S rRNA exposes the L5 nuclear localization signal and activates nuclear import of the RNA-protein complex [247,248]. This feedback loop regulates L5 and 5S rRNA expression and ensures stoichiometric proportions of L5 and 5S rRNA in the nucleus (Figure 3.13). Regions of the protein – RNA interactions span a substantial part of the 5S rRNA molecule. L5 interacts with helix III and loop C of 5S rRNA [249], and 7S complex formation requires helices II through IV (Figure 3.10) [246]. Integrity of the feedback regulation loop is essential for viability and development of *Xenopus lavae* oocytes and for viability of *S. cerevisiae* [250,251]. Therefore mutations in the promoter region and regions of 5S rRNA, which are required for L5 and TFIIIA interaction, may result in lethality unassociated with protein synthesis.

Identification of seven mutants that were viable as the sole forms of 5S rRNA has made possible the first structure/function analysis of this molecule in a eukaryotic system. Functionally, the ability of these mutants to antagonize the effects of sparsomycin, which increases binding of peptidyl-tRNA to the P-site [205,252], suggests that they may promote decreased binding of peptidyl-tRNAs; similar observations were made with mutant forms of ribosomal protein L5 [169]. A20 and C69

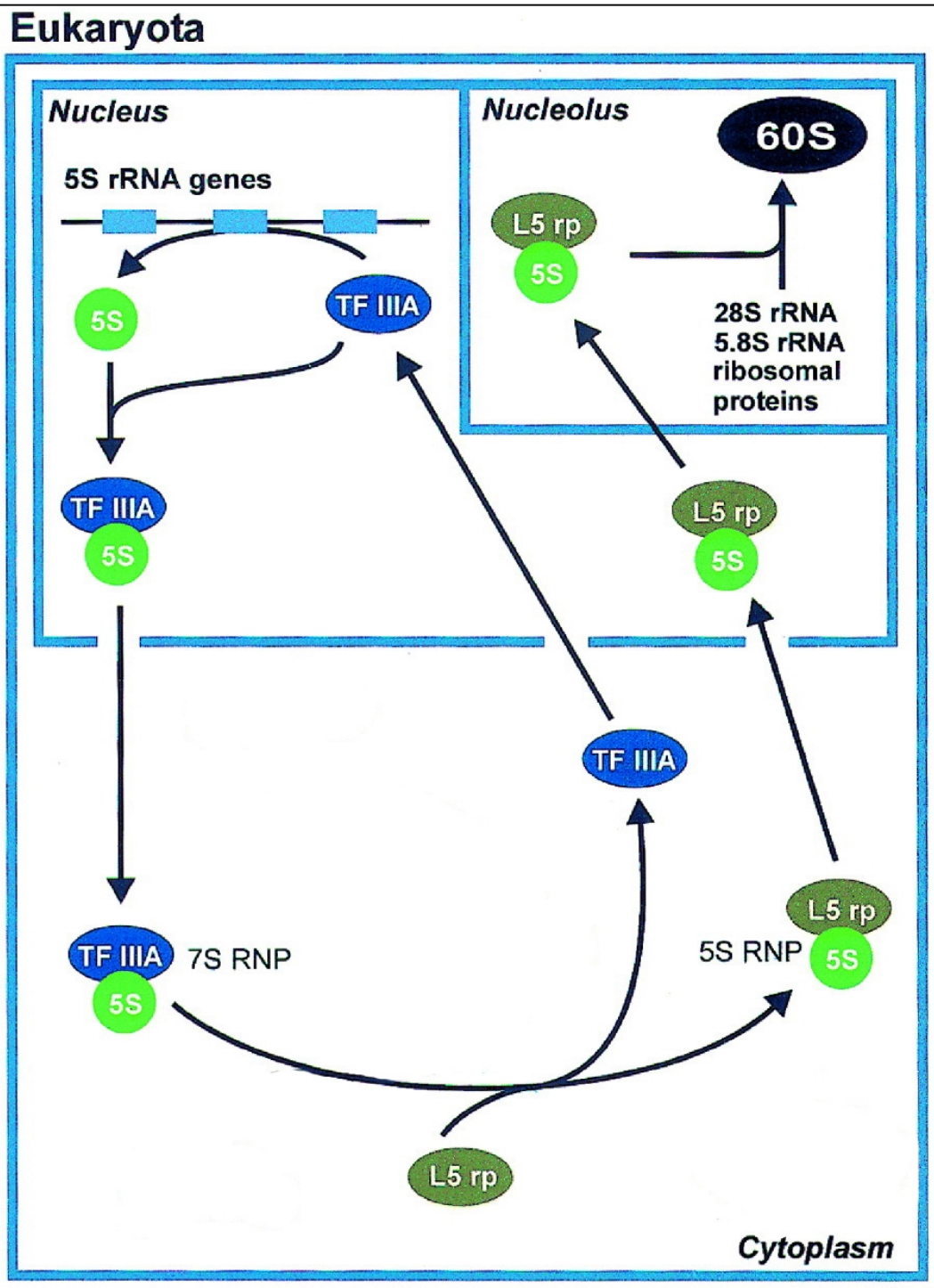

Figure 3.13. The autoregulation loop of 5S rRNA and TFIIIA.

Modified from Szymanski M., *et al* [253].

are located within the L5 binding site (Figure 3.14), thus 5S:L5 interactions may promote sparsomycin resistance through a similar mechanism. Interestingly, C69U, A76U, A79G, U81G and A84C are all clustered in the region that interacts with the A-site finger (h38, Figure 3.14) [184]. The base of the A-site finger contacts with h39 and the P-loop (h80), thus connecting 5S rRNA to the peptidyl transferase center and the P-site. Therefore, these mutants may promote sparsomycin resistance by affecting the structure/function of the peptidyl transferase center. Surprisingly, these mutants did not show any anisomycin associated phenotypes, implying that 5S specifically interacts and communicates with the P-site but not with the A-site of the ribosome. The last mutant, C93U is located in the D-loop of 5S rRNA (Figure 3.14). Though the D-loop contacts several important regions on the ribosome, including h89, h41 and ribosomal protein L10, it is remote from the P-site associated structural components. Thus the observed effect of C93U is on +1PRF and anisomycin resistance is probably indirect.

Chemical protection studies amend this hypothesis. All of the mutations influenced chemical reactivities of nucleotides G85 and G91 in 5S rRNA (Figure 3.10). G85 is located in the A site finger binding region and G91 is a part of the D-loop. There are only two partial exceptions to this rule: C69U substitution does not affect G85 but resulted in de-protection of G91, and G84 does not affect G91 but influences the chemical reactivity of G85. Thus mutations resulting in sparsomycin resistance are either located in the areas of interactions between 5S rRNA and L5, or the A-site finger (h38), or influence the structure of L5 and the h38 binding regions.

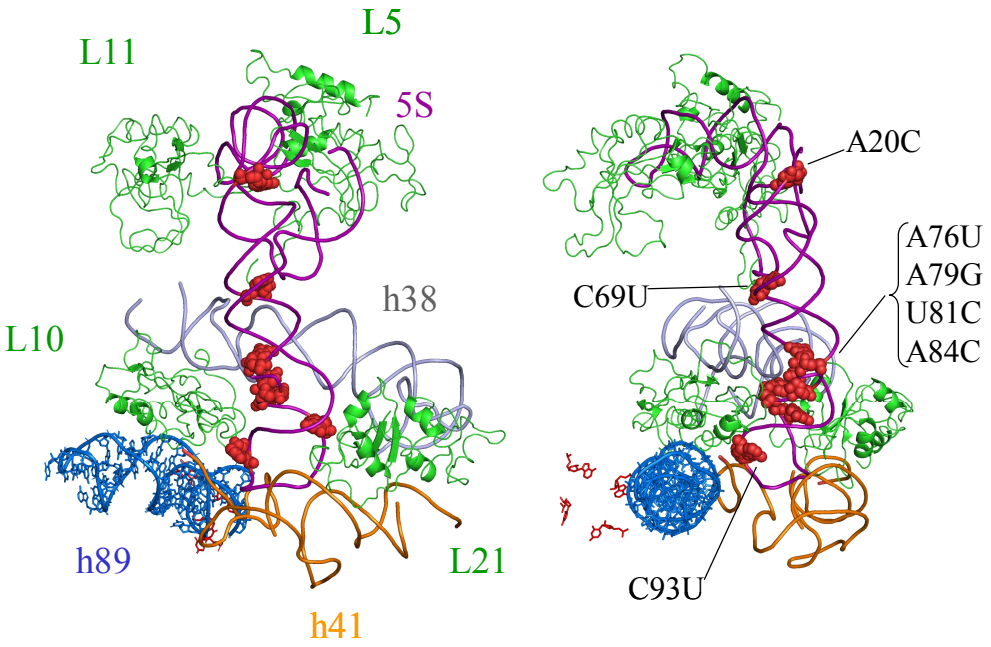

Figure 3.14. Position of the viable mutations of 5S rRNA in the 3D ribosomal structure.

The viable 5S rRNA mutants (red spheres) interact with ribosomal protein L5 (A20C), h41 (depicted in yellow, C93U) and clustered in the region of contact with h38 (shown in gray, mutants A76U, A79G, U81C and A84C). Bases of the inner core of the PTC are shown by red stick models. Helix 89 is shown in blue. (Based on the Cryo-EM structure of the *S. cerevisiae* ribosomes from Spahn C.M.T., *et al* [184].)

These observations together suggest that 5S rRNA, L5 and the A-site finger (h38) contacts are important for proper functioning of the peptidyl transferase center, as previously observed in cells expressing mutant derivatives of ribosomal protein L5 [169]. The observation that 5S rRNA alleles also affect Ty*1* retrotransposition and +1PRF, which requires slippage of the peptidyl-tRNA are consistent with this conclusion. It is possible that 5S rRNA participates in a structural rearrangement pathway that promotes a communication between the P-site, the PTC, and the other active centers of ribosome through the contacts with L5 and helix 38.

Intriguingly, two mutants A20C and U81C affected protection of nucleotides located in the sarcin-ricin loop (U3013 and G3027 Figure 3.10)[viii]. These findings suggest that the SRL and GTPase associated center are influenced by 5S rRNA, most likely through mutual interactions with h38.

As a final consideration, why do multiple 5S rDNA alleles appear to be retained in eukaryotic genomes? We found that the *RDN5-7* allele had a semi-dominant effect on L–A directed −1PRF. This is the first demonstration that a naturally occurring allele of a ribosomal component can affect this aspect of translational fidelity. We recently demonstrated that -1PRF signals may act as mRNA destabilizing elements and influence mRNA stability by the efficiency of frameshifting [141]. A search of the yeast genome database identified a large number of functional -1PRF signals that can potentially act as mRNA destabilizing elements and thus regulate gene expression [106]. We hypothesize that at least some 5S rRNA sequence variants may have been evolutionarily selected to allow for fine tuning of

[viii] The sarcin-ricin loop is located on the solvent side of the large subunit and it is a functionally important component of the factor binding site. Cleavage of the sarcin-ricin loop results in irreversible association of translation factors with ribosome and inhibition of protein synthesis.

gene expression at the post-transcriptional level. Interestingly, the 5S rRNA-ribosomal protein L5 complex is assembled onto large subunits late in ribosome biogenesis, and this complex can be dissociated from and re-associated onto core large subunits [239,254]. Thus, different versions of 5S rRNA could be added onto newly synthesized core 60S subunits, allowing cells to rapidly alter the -1PRF efficiency of newly synthesized ribosomes and thus regulate stability of actively translated mRNA.

Studies using the yeast/Xenopus hybrids lend support to this suggestion. Expression of *RDN5-ooc* allele resulted in two-fold inhibition of -1PRF in the presence of wild type 5S rRNA. In *X. lavae,* expression of two alleles of 5S rRNA, oocyte and somatic, is strictly regulated during development. An unfertilized egg contains only the oocyte form of 5S rRNA. At this stage only a minor fraction of 5S rRNA is incorporated into the ribosomes and a majority of 5S is stored in the cytoplasm in a complex with TFIIIA. Upon fertilization, the oocyte form of 5S rRNA is transferred into the nucleus and it is incorporated into newly assembled ribosomes. Release of TFIIIA activates transcription of 5S rRNA, most of which is the somatic form. During development, the somatic form of 5S rRNA is gradually substituted in place by the oocyte version. As a result, somatic cells do not contain of oocyte the form 5S rRNA. Expression of the somatic form of 5S rRNA may result in increased levels of -1PRF, which would serve to destabilize -1PRF containing messages. Thus the switch between the different forms of 5S rRNA could be responsible for the rapid degradation of maternal mRNAs during oocyte development [255,256].

In conclusion, the first analysis of 5S rRNA in a eukaryotic system has been presented. Our observations suggest that 5S rRNA is an important functional component of the ribosome. We demonstrated that 5S rRNA may be involved in communication between P-site and other functional centers of the ribosome, likely through interactions with the A-site finger and ribosomal protein L5. Analysis of expression of naturally occurring alleles in *S. cerevisiae*, suggests that 5S rRNA may be involved in post transcriptional regulation of gene expression via the NMD pathway.

Chapter 4. Ribosomal protein L10

Introduction

Ribosomal protein L10 was initially identified in yeast in a screen for mutants that were synthetically lethal with a deletion of subunit 6 of cytochrome bc1 [257]. Subsequent genetic studies demonstrated that *QSR1*, as it was named, was essential for protein synthesis and allelic to *RPL10* [258,259]. L10 is required for formation of 80S ribosomes, and mutations in *RPL10* specifically affect large subunit maturation and subunit joining [260,261]. Studies of ribosomal export demonstrated that L10 incorporation is the last step required for production of mature 60S subunits. Nearly mature large subunits, lacking L10, are exported from the nucleus to the cytoplasm in complex with an export adapter protein called Nmd3p via the Crm1p pathway [262,263]. Upon export, a complex formed by L10 and Sqt1p binds to the large subunit, promoting release of Nmd3p followed by incorporation of L10 [264]. Release of Nmd3p from the large subunit requires L10 and GTP hydrolysis by the G-protein Lsg1p [265]. Mutations that affect Lsg1p activation, or replacement of GTP with non-hydrolysable GTP analogs traps Nmp3p in the complex with L10, Sqt1p, and the large subunit [266]. It is thought that Sqt1 plays a dual role: (A) it co-translationally binds L10 and acts as a chaperone by stabilizing newly synthesized L10 [267]; and (B) it provides a scaffold for interactions between L10 and the large subunit [266] .

These observations suggest that L10 may itself play a major role in subunit joining and translation, and (or) that L10 integration into the large subunit promotes conformational changes which distinguish mature from pre-mature ribosomes. The

cryo-EM structure of the 80S yeast ribosome showed that there are no contacts between small subunit components and L10 [59], thus making direct involvement of L10 in subunit joining unlikely. In the ternary ribosome structure, L10 protrudes from the cytoplasmic side of the large subunit starting from the base of the L7/L12 stalk toward the peptidyl transferase center. L10 is sandwiched between h38 and h89, and its tip interacts with h39 [59]. The contacts that L10 makes with h38, h39 and the P-loop establish its connection with the peptidyl transferase center. Interestingly, domain V of 5S rRNA makes contact with a junction formed by L10, h38 and h39, but does not establish direct contact with L10 (Figure 4.1). The L10 protein of yeast is larger then bacterial homologs, and its C-terminal domain together with an extension of h38 forms a large unresolved mass next to the L7/L12 stalk [59]. Thus, elucidation of the functional role of L10 may reveal structural and conformational features required for subunit joining, translation initiation and subunit maturation.

Toward the goal of furthering our understanding of L10, we randomly mutagenazied *RPL10* and screened a primary library of mutants for the inability to maintain the killer phenotype. This approach was based on the rationale that propagation of the L-A and M_1 viruses of yeast depends on multiple factors such as -1PRF, the correct ratio of 40/60S subunits, and the efficiency of protein synthesis. Thus we reasoned that this approach would result in identification of mutants that affect multiple stages of protein synthesis. This screen identified 56 new *rpl10* alleles. Genetic analyses demonstrated the effects of the mutant *rpl10* alleles on

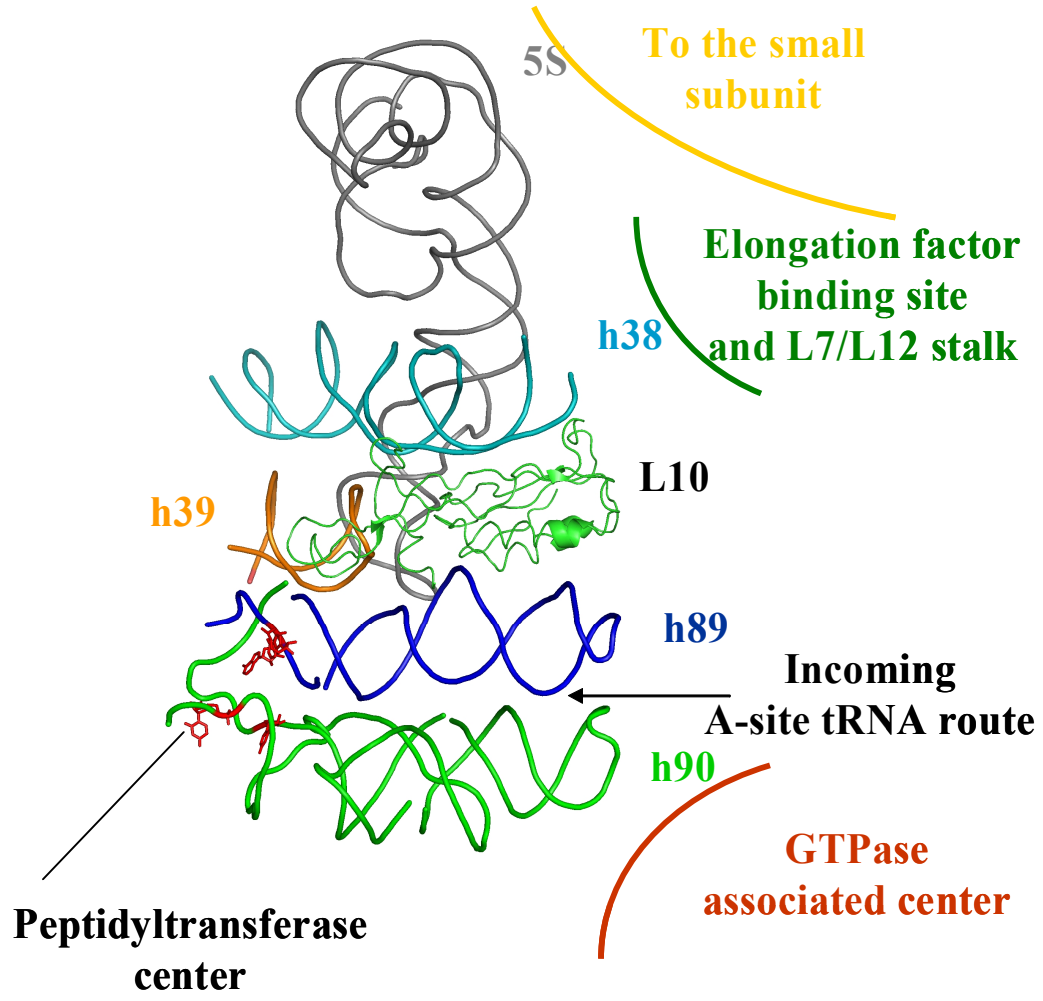

Figure 4.1. Position of L10 in the ternary ribosomal structure

L10 is sandwiched between h38 and h89. The PTC proximal region of L10 is restricted by h38. The C-terminal part of L10 (unresolved in this structure) contacts with the L7/L12 stalk. (Based on the Cryo-EM structure of the *S. cerevisiae* ribosomes from Spahn C.M.T., *et al* [184].)

sensitivity/resistance to cold (15 °C), heat (37 °C), anisomycin, and paromomycin (Figure 2.2 and Figure 4.2). Efficiencies of -1PRF and non-programmed suppression of the UAA nonsense codon were measured using a dual-luciferase reporter system. Biochemical characterization demonstrated effects of *rpl10* alleles on ribosome biogenesis and affinities for aminoacyl-tRNA. These analyses: (A) reveal functionally important regions of ribosomal protein L10; and (B) suggested that h38 (the "A-site finger") and the loop at the base of helix 89 (components of the "accommodation gates") are required for proper ribosomal function and aminoacyl-tRNA selection.

Material and methods

Strains, media and genetic methods

Yeast and *E. coli* media were prepared as previously described [171,212]. Yeast transformation, cytoduction and Killer virus maintenance assays were conducted as previously described [170,268]. *E. coli* DH5α was used to amplify plasmid DNA. Strains used in this study are listed in the Appendix A, page 162. Specifically, JD1238 (*MATa rpl10::Kan met15Δ0 leu2Δ0 ura3Δ0 his3Δ0* pJD429.URA, L-A HN M_1) was used as a parental strain for the expression of *RPL10* alleles. Cold, heat and drug resistance were measured by dilution spot assays. Cell cultures were grown at 30°C to mid-logarithmic phase, and then 10 fold dilutions of cell (from 10^5 to 10 CFU) in 5µl aliquots were spotted on appropriate media and grown for 3 – 5 days. Qualitative scores were assigned to describe growth under different conditions. Positive scores

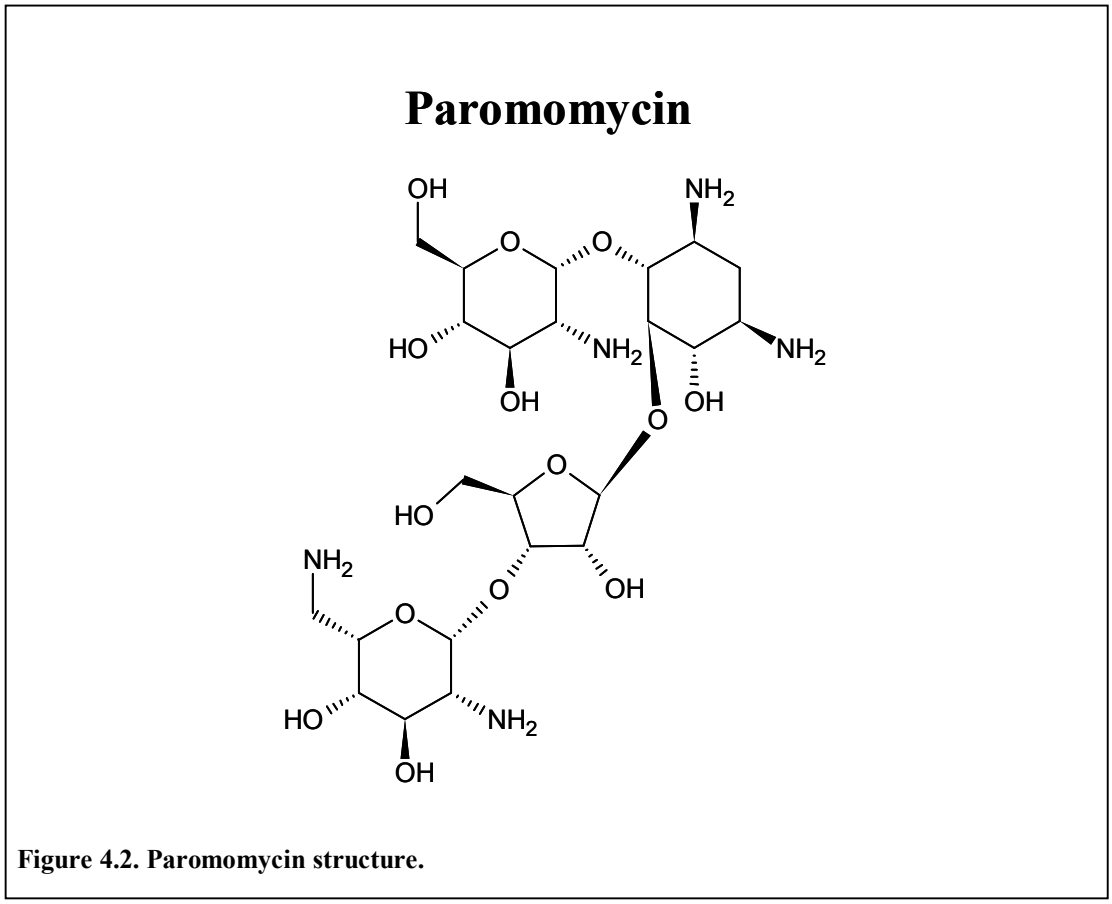

Figure 4.2. Paromomycin structure.

were assigned to resistant strains and negative scores were assigned to sensitive strains. Efficiencies of -1PRF and nonsense suppression were measured using a dual luciferase reporter system as previously described [226]. Reporter plasmids are listed in Appendix B, page 165.

Random mutagenesis of *RPL10*

A library of plasmid-borne *rpl10* mutants was constructed using the error-prone PCR and gap repair method [269]. Mutagenesis primers (70 nucleotides) for PCR were designed to be complementary to the 5' and 3' untranslated regions of *RPL10* and included translational start and stop codons: (forward, RPL10_RMF; reverse, RPL10_RMR, Appendix C, page 177). Random mutagenesis was performed with the GeneMorph II PCR random mutagenesis kit with template concentrations optimized to generate between one and four mutations per *RPL10* coding sequence. pJD589 was digested with StuI. The linearized plasmid lacking the *RPL10* coding sequence was purified by Tris-acetate-EDTA-agarose gel electrophoresis and cotransformed with the randomly PCR-mutagenized *RPL10* coding sequences into JD1238 cells. After 3 days of growth on selective medium (H-trp), cells that had lost the wild-type *RPL10*-containing plasmids were selected by replica plating onto 5-fluoroorotic acid (5-FOA)-containing medium [214]. Colonies were arrayed onto H-trp plates and subsequently replica plated onto a lawn of 5x47 cells (*MAT*a/*MAT*α *his1*/+ *trp1*/+ *ura3*/+ K^{-}, Appendix A, page 160) to identify K^{-} colonies. Approximately 3000 colonies were screened. Plasmids were rescued into *E.coli* from yeast strains that had lost the killer phenotype. Plasmids were reintroduced into JD1238 cells and rescored for the inability to maintain the killer phenotype. This procedure was performed three

times, in order to prevent identification of false positive strains due to spontaneous Killer virus loss. Only those strains that were confirmed as unable to maintain killer phenotype were selected as new *rpl10* alleles.

Polysome profiles

50 ml cell cultures were grown in YPAD media to OD_{595} of 0.5-0.7. Cells were rapidly mixed with 50ml of ice cold buffer L [20 mM Tris-base, 50 mM KCl, and 12 mM $MgCl_4$, 1 mM DTT, 200 μg/ml cycloheximide] and collected by centrifugation using a table top centrifuge at 4000 rpm for 10 minutes at 4 °C. Cell pellets were re-suspended in 50 ml of ice cold buffer L and again collected by centrifugation for a second time. Cells were then re-suspended in ~1 ml of buffer L and mixed with equal volumes of 0.5 mm glass beads. Cells were disrupted in a Mini Beadbeater at 4 °C using 4 pulses of 1 minute each with 2 minutes intervals allowing for cooling. Cell debris was removed by centrifugation in a microcentrifuge at 15000 rpm for 15 minutes at 4 °C. Supernatants were collected, and 6 OU at OD_{280} in 200 μl were applied to the top of a 13 ml sucrose gradient. Linear 7-47 % sucrose gradients were prepared by mixing buffers A [20 mM Tris-base, 50 mM KCl, 12 mM $MgCl_4$, 1 mM DTT, 200 μg/ml cycloheximide, 7 % sucrose] and B [20 mM Tris-base, 50 mM KCl, 12 mM $MgCl_4$, 1 mM DTT, 200 μg/ml cycloheximide, 47 % sucrose]. Cell lysates were separated by centrifugation in SW-41Ti rotor at 40000 rpm for 3 h at 4 ˚C. Gradients were subsequently developed using an ISCO-5 gradient fractionator. Continuous OD_{254} readings were recorded and resulting hard copy charts were digitized. The red-ink curves were extracted using the color selection tool in Adobe Photoshop.

aa-tRNA synthesis and aa-tRNA binding

Synthesis of aminoacyl-tRNA and aminoacyl-tRNA binding experiments were performed as described in Chapter 2, page 56.

Analysis of aa-tRNA binding data

The field of ribosomal biochemistry was established in a period from late 1960 to the early 1970's. At that time, data analysis was hindered by a lack of computational resources. Thus researchers were forced to use linearization approaches to analyze these non-linear data. In the ribosome-ligand interaction field, the reciprocal approach, often referred as the Scatchard plot, became widely utilized and became the *de facto* standard [183,252,270-272]. In this approach, the single site binding isotherm equation is transformed into:

$$[tRNA \bullet RS] = [RS_0] - K_d \frac{[tRNA \bullet RS]}{[tRNA]} \quad \text{or} \quad \frac{[tRNA \bullet RS]}{[tRNA]} = K_a[RS_0] - K_a[RS \bullet tRNA],$$

where $[RS_0]$ is initial concentration of the ribosomes, $[tRNA \bullet RS]$ is the concentration of the complex of tRNA and ribosomes, and $[tRNA]$ is the free tRNA concentration. Division of both sides of equation by $[RS_0]$ and subsequent substitution of $v = [tRNA \bullet RS]/[RS_0]$ yields: $v = 1 - K_d v/[tRNA]$ or $\frac{v}{[tRNA]} = K_a - K_a v$. In the first case the plot of $v/[tRNA]$ vs. v is linear with a negative slope equal to K_d. In the second case, charting v vs. $v/[tRNA]$ also provides K_a as a negative slope. Both methods proved to be useful in the absence of computationally unattainable alternatives. However, both approaches distort the data and grossly violate assumptions of the linear regression. First, the linear regression

assumes that the point distribution is normal and that the standard deviation is the same at every point on the abscissa. Obviously these transformations disturb the data point distribution. Secondly, the transformations introduce the error in the abscissa coordinates. Since the linear regression algorithm (sum of least squares) minimizes vertical distances between data points and the fitted curve, it is erroneous to use it due to error introduced both into both abscissa and ordinate coordinates. In addition this approach hinders analysis of multiple binding sites and adjustments for non-specific binding [273].

In our previous work on ribosomal protein L3 we illustrated the validity of our biochemical methods and their compatibility with historically accepted analytical methods. Since adequate computational resources are now available there is no reason to continue utilizing Scatchard plot analysis. Thus in this study, nonlinear regression analysis of binding data was done by SigmaPlot 9.0 and GraphPad Prism 4.0 software. Two models have been used: 1) binding with ligand depletion and 2) binding with ligand depletion and non specific binding. In case of ligand depletion, the concentration of free ligand is significantly different from the initial ligand concentration. Application of $[tRNA] = [tRNA_0] - [tRNA \bullet RS]$ and $[RS] = [RS_0] - [tRNA \bullet RS]$ substitutions to the K_d definition equation ($K_d = \frac{[RS] * [tRNA]}{[tRNA \bullet RS]}$; $[tRNA \bullet RS] = \frac{[RS] * [tRNA]}{K_d}$) yields:

$[tRNA \bullet RS]^2 - [tRNA \bullet RS]([RS_0] + [tRNA_0] + K_d]) + [RS_0][tRNA_0] = 0$. Solution of the second order equation results: $[tRNA \bullet RS] = \frac{-b - \sqrt{b^2 - 4c}}{2}$, where

$b = -([RS_0] + [tRNA_0] + K_d])$, and $c = [RS_0][tRNA_0]$. The binding data have been fitted into this equation constraining $[RS_0]$ and K_d to positive values.

The non specific binding with ligand depletion model is similar to the ligand depletion model. Assuming that the dissociation constant for non specific binding is much higher than for the $[tRNA \bullet RS]$ complex, the binding isotherm for nonspecific binding can be viewed as linear in the range of $[tRNA]$ concentrations used. Thus, $[tRNA \bullet RS] = \frac{[RS] * [tRNA]}{K_d} + NS[tRNA]$. Application of $[tRNA] = [tRNA_0] - [tRNA \bullet RS]$ and $[RS] = [RS_0] - [tRNA \bullet RS]$ substitutions to this equation produces:

$$[tRNA \bullet RS]^2 - [tRNA \bullet RS]([RS_0] + [tRNA_0] + K_d]) + [RS_0][tRNA_0] = 0$$

Solution of the second order equation results in: $[tRNA \bullet RS] = \frac{-b - \sqrt{b^2 - 4ac}}{2a}$, where $b = -([RS_0] + [tRNA_0] + K_d + K_d NS + 2[tRNA_0]NS)$, $a = 1 + NS$, and $c = [tRNA_0](K_d NS + [tRNA_0]NS + [RS_0])$. The binding data have been fitted into this equation with $[RS_0]$, K_d, and NS constrained to positive values. Then using the obtained results, data have been plotted on Scatchard plot for visualization purposes.

Results

Identification of new *rpl10* alleles by random mutagenesis

Previous studies identified *rpl10* alleles affecting large subunit maturation and association. Together with L10's position in the 3-D ribosomal structure, these

findings encouraged us to pursue an in depth analysis of L10 function. Previously known *rpl10* alleles were identified by their temperature sensitive phenotypes. Examination of these alleles in a new strain background, that better mimics genomic expression of L10, revealed that they had no effects on virus maintenance and resistance toward translational inhibitors [274]. To identify mutants that affect these processes, a large-scale mutagenesis project involving both random and site-specific PCR mutagenesis was devised. Mutants were primarily screened for loss of the M_1 virus based on the rationalization that this approach would yield alleles that promoted translational defects. To this end, the coding region of *RPL10* was subjected to random PCR mutagenesis (avg. 1-4 mutations per PCR product) and screened for loss of the killer phenotype as described in the Materials and methods. The mutant *RPL10-HIS3* plasmids were rescued from killer minus strains, passaged through *E. coli*, re-introduced into *rpl10Δ* cells, and re-scored for their abilities to promote M_1 virus loss. Approximately 15 % of the mutants were lethal as determined by their inability to grow in the presence of 5-FOA (data not shown). Due to an ~10 % intrinsic rate of killer loss in the JD1293 strain background, the plasmid rescue and reintroduction procedure was performed three times to avoid false positive results. In the end, the mutations responsible for conferring K^- phenotype were identified by DNA sequence analysis. In a screen of >3,000 colonies, 56 killer minus mutants were identified. These included 35 single mutations, 19 double mutations, 1 triple mutation, and 1 C-terminal 7 amino acid deletion mutant. The large number of alleles with single amino acid substitutions allowed exclusion of alleles with multiple mutations from subsequent analysis. Among the single mutants, multiple substitutions were found at positions 7, 9, 40, 93, 94 and 145. Regions with high

frequencies of mutations were mainly located at the N-terminal and middle parts of the protein. These regions span amino acids 7-17, 59-94, and 144-152.

Temperature and drug specific phenotypes

Spot assays of 10-fold dilutions were used to determine relative degrees of cold, heat, anisomycin, and paromomycin resistance. The results are shown in Figure 4.3 and Figure 4.4. We have not observed a direct correlation between temperature, drug resistance and killer loss. One cold sensitive and two cold resistant strains were found. Surprisingly, no heat sensitive mutants were identified (Table 2 and Figure 4.3).

Thirteen anisomycin resistant and four sensitive strains were identified. In the ternary ribosomal structure, anisomycin resistant/sensitive mutants are located in the region where L10 interacts with h89 and h38/39. Residues R7, Y9 and L152 contact with helix 89. Amino acids K15, Y17, P93 and F94 are located on the surface of L10 that interacts with h38, and V26 lies in the base of the residues P93 and F94. I120 is positioned in a tip of L10 close to the junction between helixes 38 and 39. Interestingly, G81 is located on the solvent side of the ribosome and does not contact any other parts of the 60S subunit in the mature ribosomal particle (Table 2, Figure 4.4, and Figure 4.5).

Paromomycin resistance was used to probe for defects associated with interactions between the small and large subunits. Paromomycin increases incorporation of mis-sense tRNAs and suppression of termination [275,276]. It binds to the small subunit, near the decoding center, and promotes structural transitions

Figure 4.3. Heat and cold resistance phenotypes of L10 mutant strains.

Strains harboring mutant alleles of ribosomal protein L10 were grown to mid-logarithmic phase and spotted in ten fold dilutions on YPAD media. Subsequently, plates were incubated at 15 °C, 30 °C and 37 °C for three to five days and scored as described in Materials and methods, page 122.

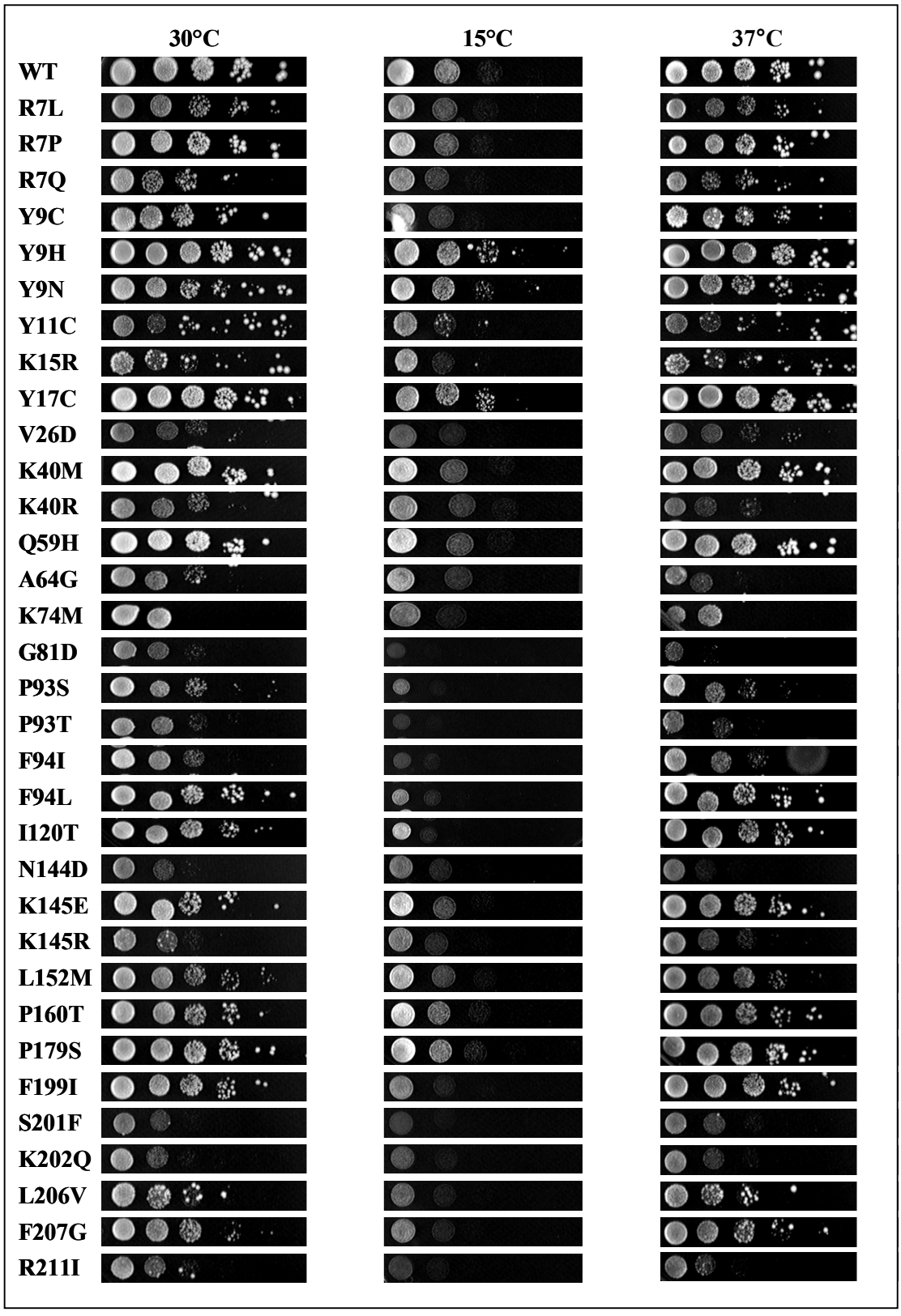
30°C
15°C
37°C
WT
R7L
R7P
R7Q
Y9C
Y9H
Y9N
Y11C
K15R
Y17C
V26D
K40M
K40R
Q59H
A64G
K74M
G81D
P93S
P93T
F94I
F94L
I120T
N144D
K145E
K145R
L152M
P160T
P179S
F199I
S201F
K202Q
L206V
F207G
R211I

Figure 4.4. Anisomycin and paromomycin resistance phenotypes of L10 mutant strains.

Strains harboring mutant alleles of ribosomal protein L10 were grown to mid-logarithmic phase and spotted in ten fold dilutions on media containing anisomycin (10 μg/ml), paromomycin (3 mg/ml), and control media without drug. Plates were subsequently incubated at 30 °C for three days and scored as described in Materials and methods, page 122.

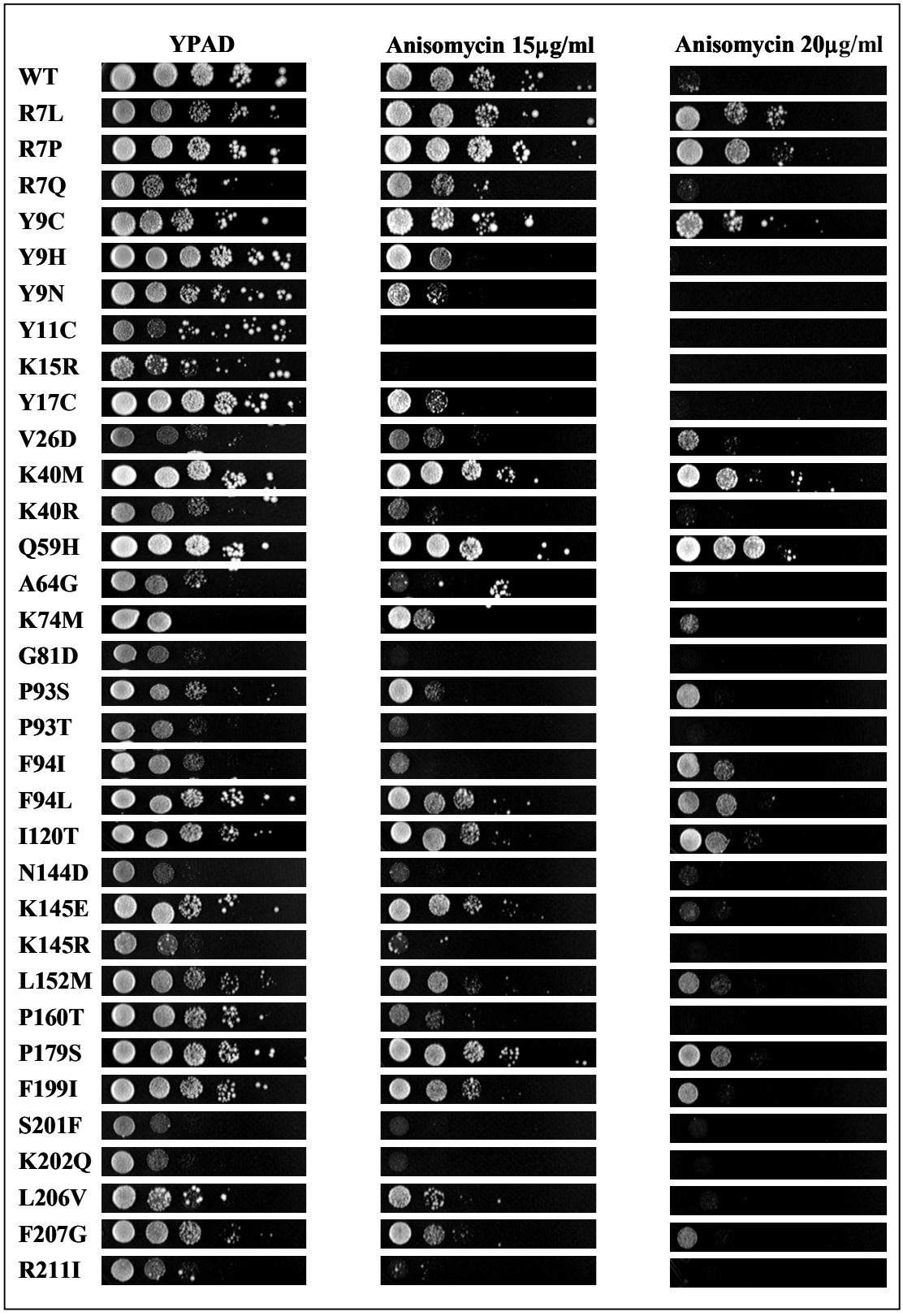
YPAD
Anisomycin 15µg/ml
Anisomycin 20µg/ml
WT
R7L
R7P
R7Q
Y9C
Y9H
Y9N
Y11C
K15R
Y17C
V26D
K40M
K40R
Q59H
A64G
K74M
G81D
P93S
P93T
F94I
F94L
I120T
N144D
K145E
K145R
L152M
P160T
P179S
F199I
S201F
K202Q
L206V
F207G
R211I

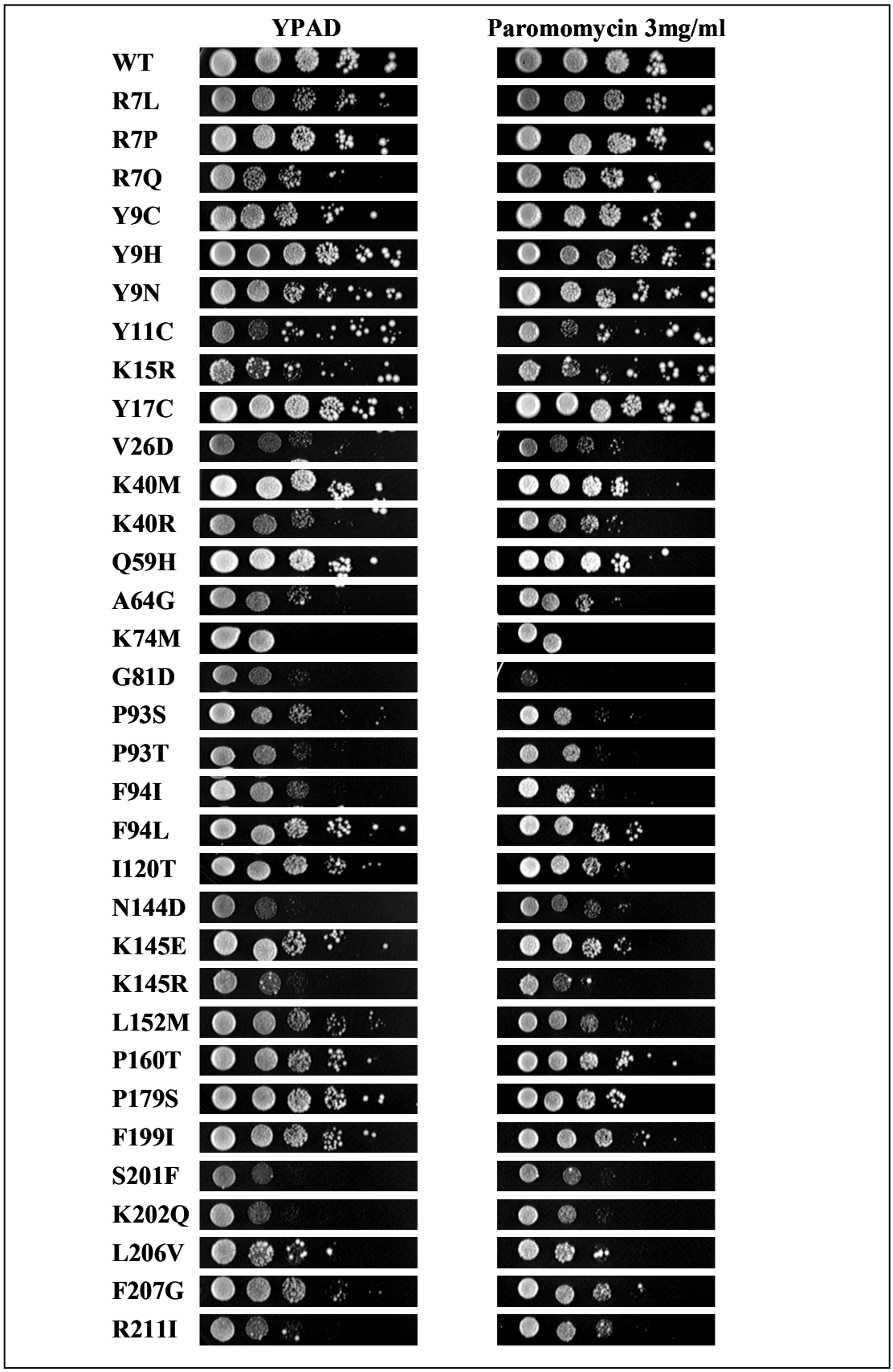
YPAD
Paromomycin 3mg/ml
WT
R7L
R7P
R7Q
Y9C
Y9H
Y9N
Y11C
K15R
Y17C
V26D
K40M
K40R
Q59H
A64G
K74M
G81D
P93S
P93T
F94I
F94L
I120T
N144D
K145E
K145R
L152M
P160T
P179S
F199I
S201F
K202Q
L206V
F207G
R211I

Mutaion	Cold (15^0C)	Heat (37^0C)	Anisomycin	Paromomycin
WT	N/A	N/A	N/A	N/A
R7L	0	0	+2	0
R7P	0	0	+2	0
R7Q	0	0	0	0
Y9C	0	0	+1	0
Y9H	+1	0	-1	0
Y9N	0	0	-1	0
Y11C	0	0	0	0
K15R	0	0	0	0
Y17C	+0.5	0	-1	0
V26D	0	0	+0.5	0
K40M	0	0	+2	0
K40R	0	0	0	0
Q59H	0	0	+3	0
A64G	0	0	0	0
K74M	0	0	0	0
G81D	0	0	-0.5	-2

Mutaion	Cold (15^0C)	Heat (37^0C)	Anisomycin	Paromomycin
P93S	-0.5	0	+1	0
P93T	0	0	0	0
F94I	0	0	+2	0
F94L	0	0	+1	0
I120T	0	0	+2	0
N144D	0	0	0	+1
K145E	0	0	0	0
K145R	0	0	0	0
L152M	0	0	+1	0
P160T	0	0	0	0
P179S	0	0	+2	0
F199I	0	0	+1	0
S201F	0	0	0	0
K202Q	0	0	0	0
L206V	0	0	0	0
E207G	0	0	0	0
R211I	0	0	0	0

Table 2. Temperature and drug sensitivity phenotypes of L10 mutants

Positive values represent a resistance, while negative values represent sensitivity to a specific condition compared to its own and wild-type growth at 30 ºC on the media without drug. A value of 0 indicates absence of specific phenotype. The values expressed as $\log_{10}$ difference as scored by dilution spot assays.

associated with formation of the codon-anticodon duplex [276,277]. Interestingly, paromomycin improved the growth of the N144D allele (Figure 4.4). Only one paromomycin sensitive strain (G81D) was identified, which also promoted anisomycin sensitivity.

Programmed -1 ribosomal frameshifting and nonsense suppression

Altered efficiencies of -1PRF is one of the common causes of the loss of the M_1 virus and Killer phenotype. -1 PRF efficiencies were determined for the all of the new *rpl10* alleles. Wild type level of -1PRF was 8.3 $\pm$ 0.16%. Surprisingly most of the *rpl10* alleles did not show significant changes in -1PRF efficiencies. Three alleles (K15R, K145E and P178S) promoted decreased levels of -1PRF, six alleles (Y9C, Y9H, Y11C, K74M, G81D and P93S) promoted increased levels of frameshifting, and 24 strains exhibited wild type efficiencies (Figure 4.6). Therefore, loss of the killer virus in most of the strains could not be attributed to the changes in -1PRF.

Efficiency of non programmed nonsense codon suppression was measured in all *rpl10* strains using the dual-luciferase system. The results are summarized in the Figure 4.7. The wild type level of nonsense suppression was determined to be 2.7 %. Among the mutants, 11 strains had elevated levels of nonsense suppression, and 7 strains were hyper-accurate. The levels of nonsense suppression varied significantly between strains. The greatest level of NS was observed in the P179S mutant (2.2 fold of wild-type). The lowest levels were observed in the Y9C and F94I mutants (0.42- and 0.23- fold of wild type accordingly). Interestingly, mutants that most affected

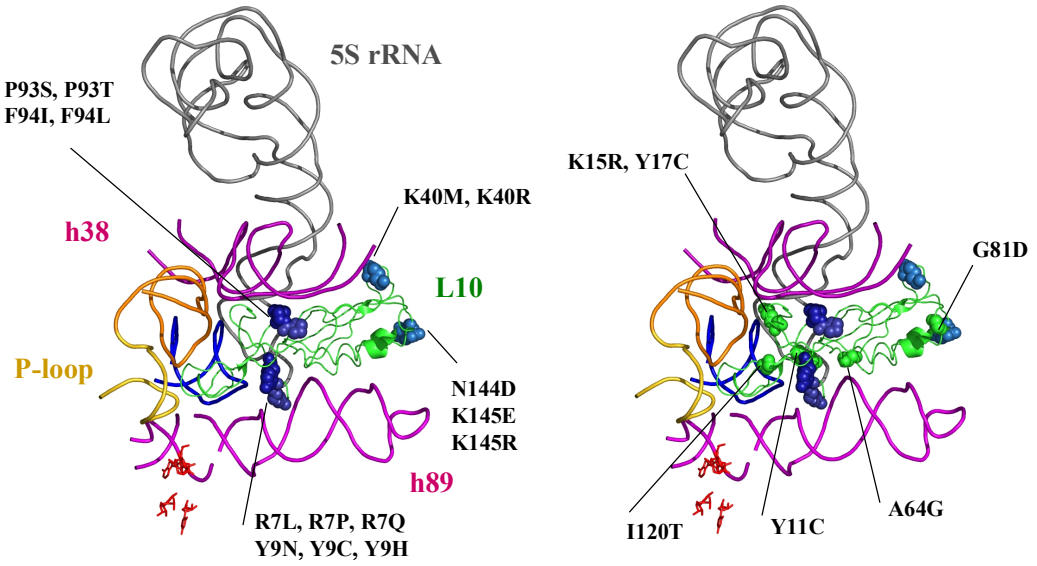

Figure 4.5. Position of new rpl10 mutants in ternary ribosomal structure.

Ribosomal protein L10 (green) is sandwiched between h38 and h89. The tip of L10 contacts with h39 (blue) and P-loop (h80). The inner core of the peptidyl transferase center is represented by the red sticks models. Mutations in L10 that promote loss of the killer phenotype are shown as spheres. (Based on the Cryo-EM structure of the *S. cerevisiae* ribosomes from Spahn C.M.T., *et al* [184].)

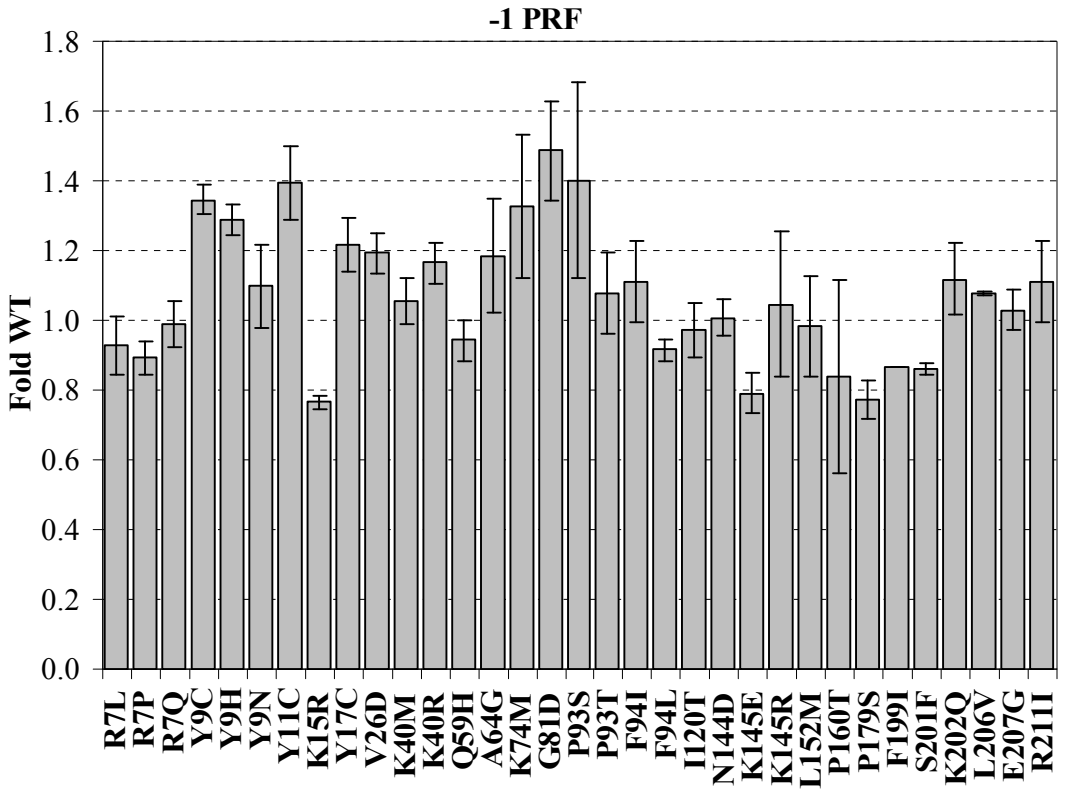

Figure 4.6. -1PRF efficiencies of the new rpl10 alleles

The library of *rpl10* alleles was examined for efficiencies of -1PRF. The -1PRF efficiency of wild-type was 8.3 ± 0.16 %. The data are presented as fold of wild-type, and the error bars represent standard error. Frameshifting efficiencies less than 0.8 and greater than 1.2 are considered as significantly different from WT.

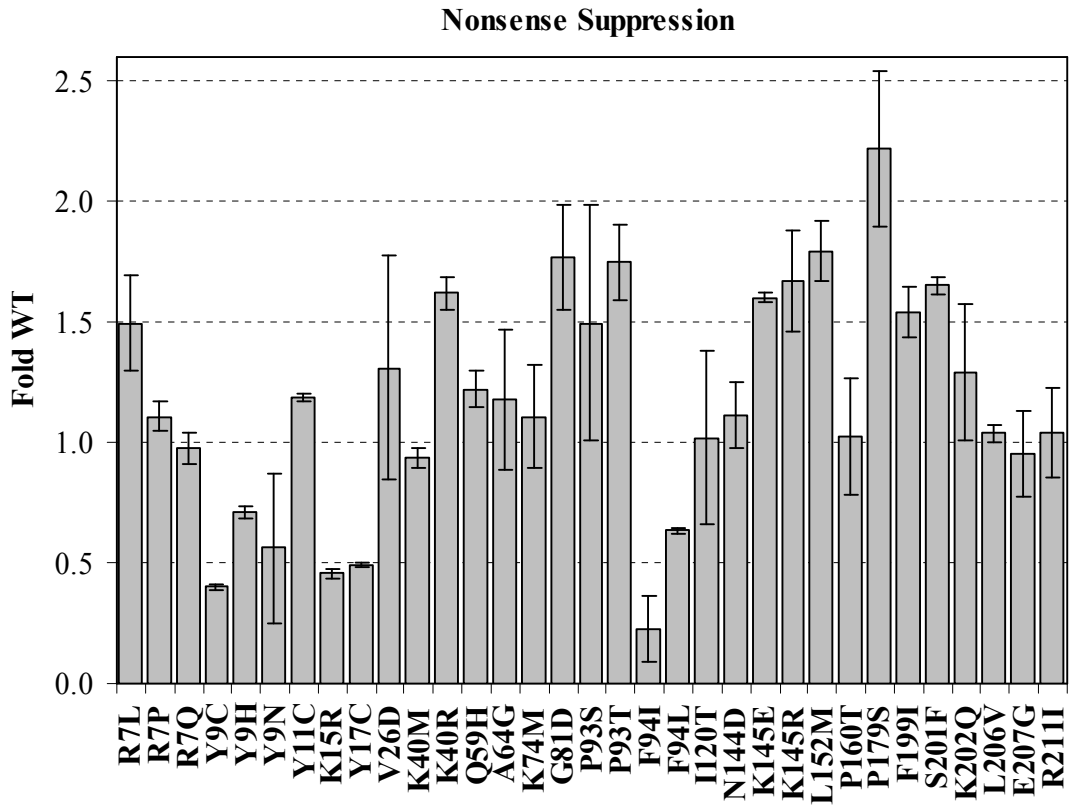

Figure 4.7. Nonsense suppression efficiencies of new rpl10 alleles

Nonsense suppression efficiencies were examined for the library of *rpl10*. The nonsense suppression efficiency of wild-type was 2.7 ± 0.11 %. The data are presented as fold of wild-type, and the error bars represent standard error.

nonsense suppression are closely clustered in the four regions of the protein: 7-17, 81-94, 144-152, and 199-201.

Biochemical characterization of the new *rpl10* alleles

Previous studies demonstrated an important role for L10 in large subunit maturation [264,266]. Sucrose gradient analyses were performed on a subset of strains harboring L10 mutants to reveal their effects on ribosomal biogenesis. A total of 16 strains were examined. This analysis revealed two types of effects. First, the R7L, R7Q, G81D, P93S, P93T, F94I, K145I, and K145R mutants demonstrated the presence of halfmers in their polysomal fractions (Figure 4.8). The halfmers indicate the presence of initiation intermediates. During initiation, the 43S complex recruits the mRNA (thus forming 48S complex) and the 60S subunit. Insufficient 60S production or production of defective 60S subunits that are deficient in their ability to form 80S ribosomes pause initiation at the 48S complex stage. Accumulation of this intermediate is detected as halfmers on polysome profiles. The assembly of the 48S complexes on actively translated mRNAs results in formation of complexes with intermediate sedimentation coefficients relative to the polysome peaks. Second, strains Y9C, R7P and R7Q had reduced levels of 60S subunits, also indicating 60S biogenesis defect. Previous studies demonstrated that the N-terminal region of L10 is required for interaction with Sqt1p. Therefore, at least some of these mutants may affect later stages of ribosome biogenesis, e.g. interactions with Lsg1p and Nmd3p, or result in formation of partially active 60S ribosomal subunits. Notably, the extents of the halfmer defects were determined by the nature of amino acid substitution,

Figure 4.8. Sucrose gradient profiles of the L10 mutants strains

Cell lysates were separated by centrifugation in a SW-41Ti rotor at 40000 rpm for 3 h at 4 °C. Gradients were subsequently developed using an ISCO-5 gradient fractionator. Continuous OD_{254} readings were recorded and resulting hard copy charts were digitized. The red-ink curves were extracted using the color selection tool in Adobe Photoshop. The positions of the 40S, 60S, 80S and polysomal peaks are indicated on every profile. Halfmers may be seen as peaks immediately following the 80S and polysomal peaks.

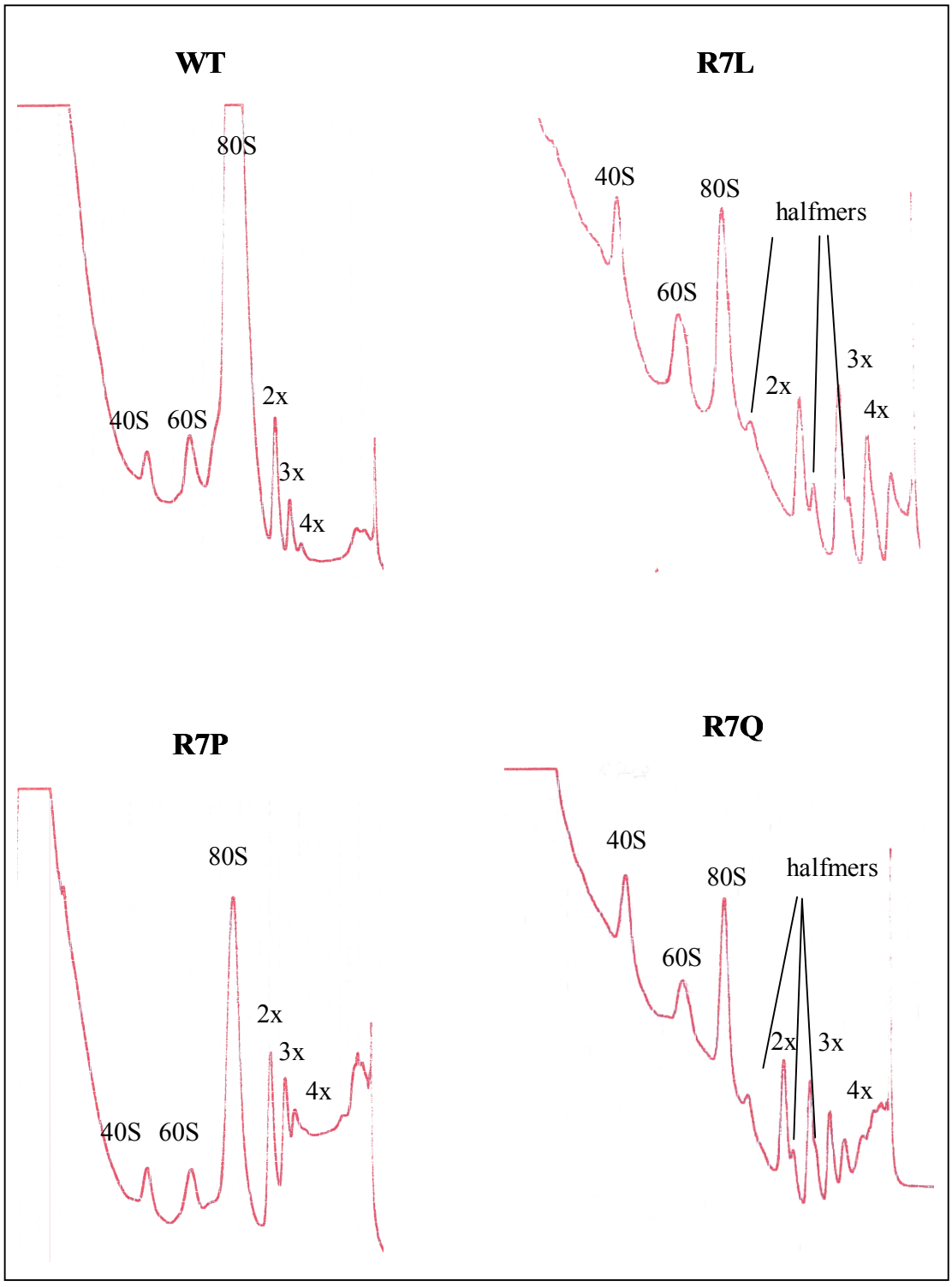
WT
80S
40S
60S
2x
3x
4x
R7L
40S
80S
halfmers
60S
2x
3x
4x
R7P
80S
2x
3x
4x
40S
60S
R7Q
40S
80S
halfmers
60S
2x
3x
4x

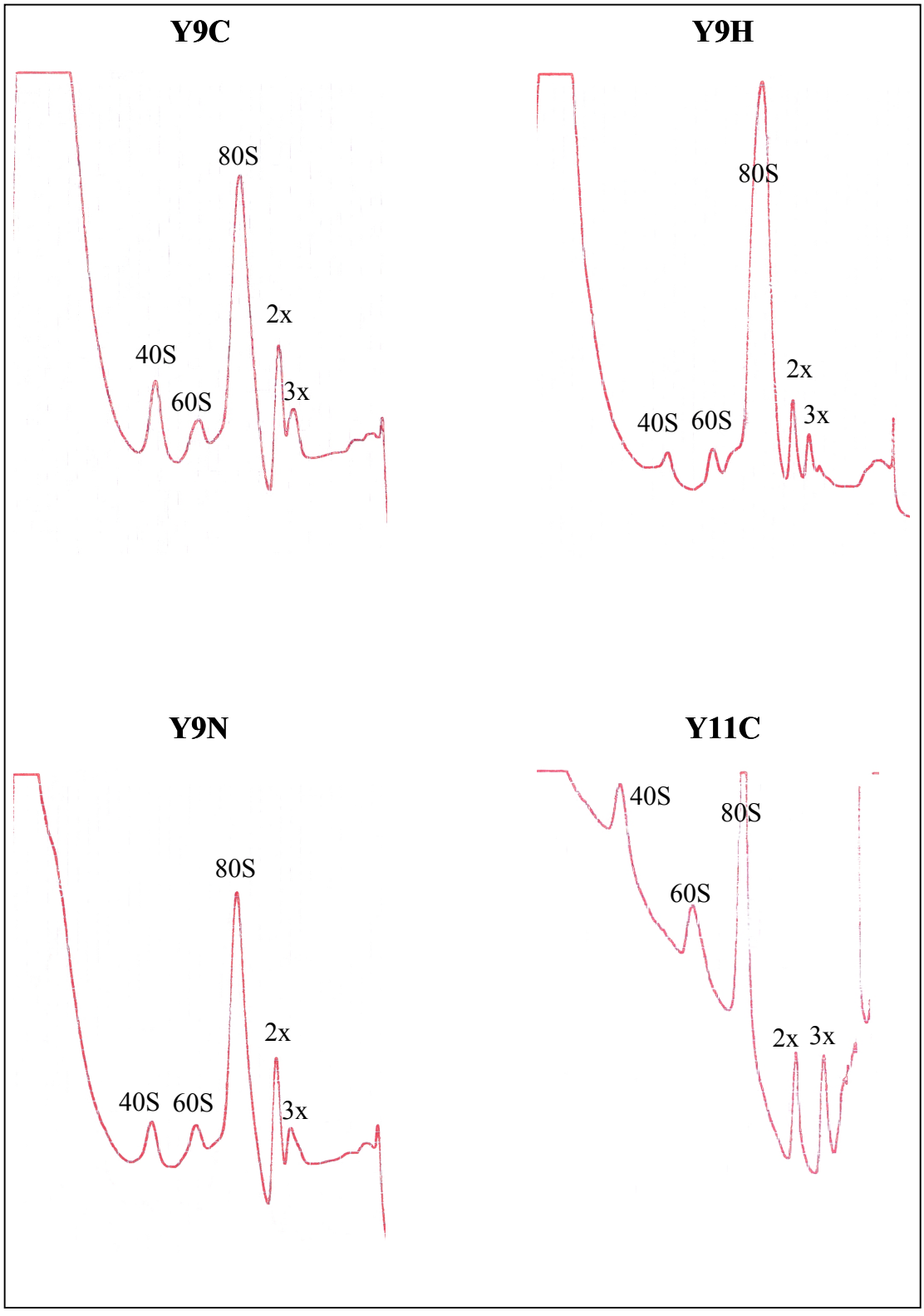
Y9C
80S
2x
40S
60S
3x
Y9H
80S
2x
40S
60S
3x
Y9N
80S
2x
40S
60S
3x
Y11C
40S
80S
60S
2x
3x

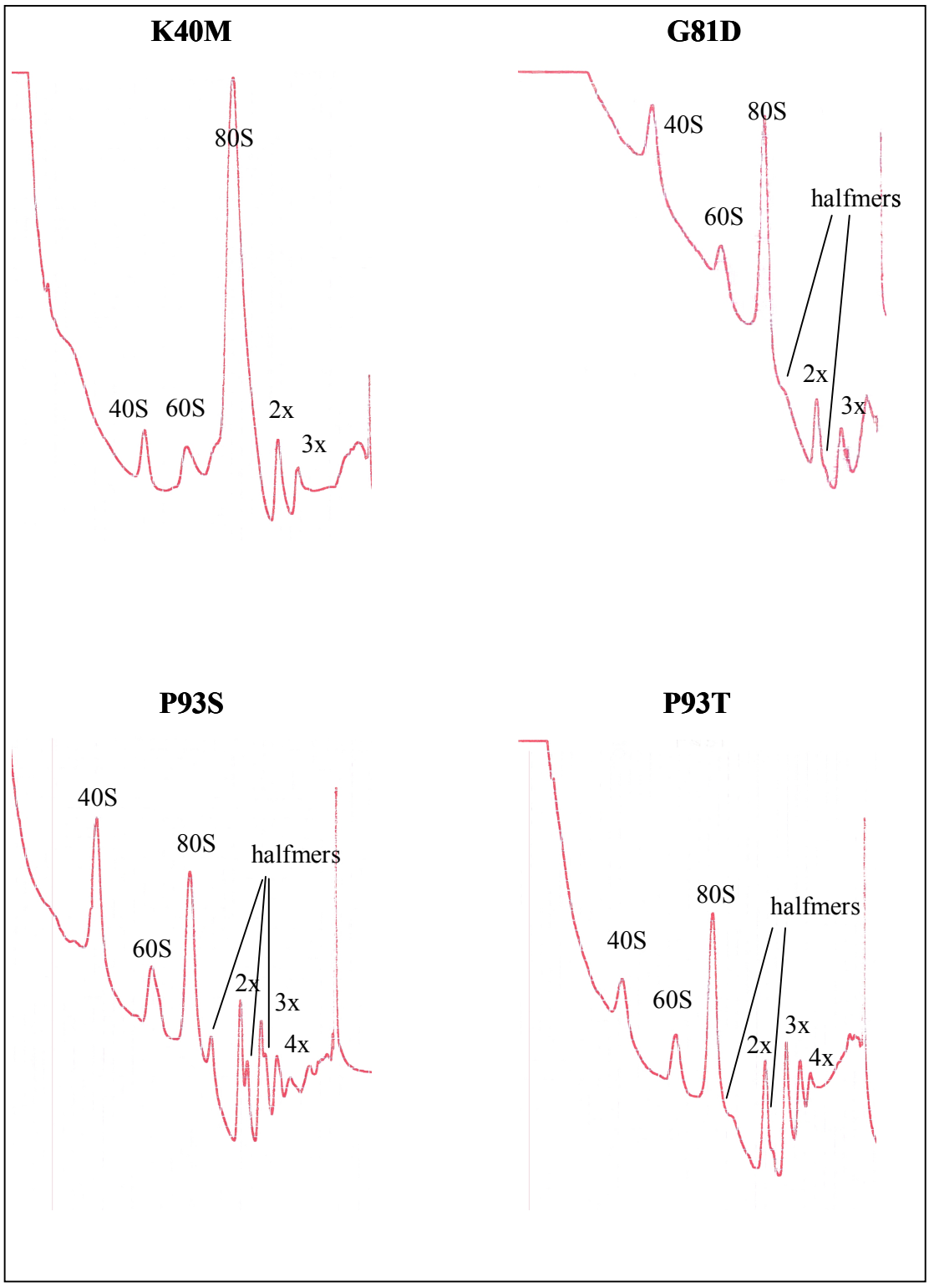
K40M
80S
40S
60S
2x
3x
G81D
40S
80S
60S
halfmers
2x
3x
P93S
40S
80S
halfmers
60S
2x
3x
4x
P93T
80S
halfmers
40S
60S
2x
3x
4x

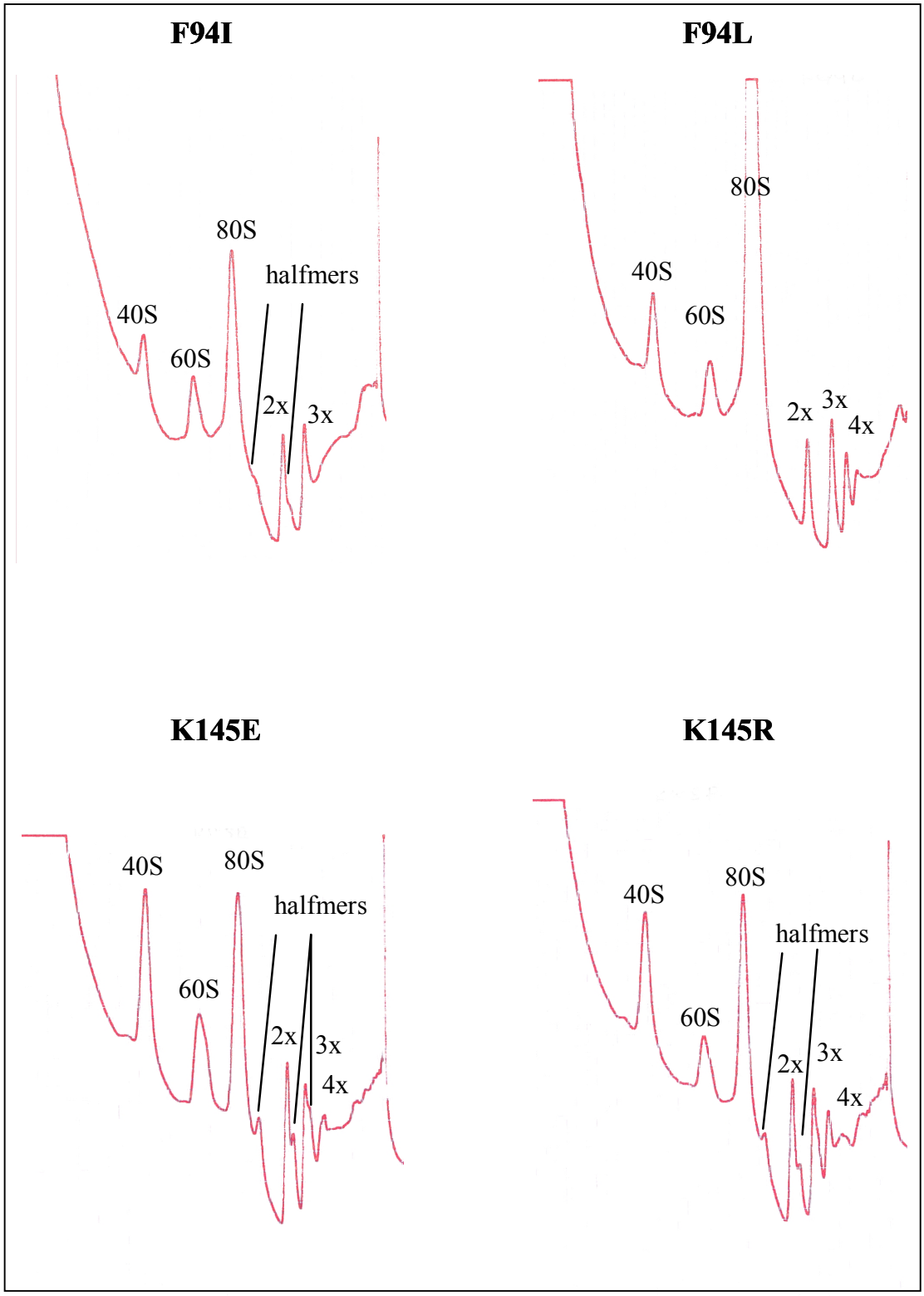
F94I
40S
60S
80S
halfmers
2x
3x
F94L
40S
60S
80S
2x
3x
4x
K145E
40S
60S
80S
halfmers
2x
3x
4x
K145R
40S
60S
80S
halfmers
2x
3x
4x

rather than by position. For example, P93S promoted a severe halfmer defect, while the analogous substitution to threonine resulted in very mild defect. Similar results were observed for multiple mutations at positions 7, 9, 93 and 94 (Figure 4.8).

The correlation observed in the L3 mutants (described in Chapter 2) between anisomycin resistance and increased affinity for A-site tRNA ecouraged us to characterize this parameter. Aminoacyl-tRNA association constants with the A-site were determined for ribosomes purified from five strains (WT, R7Q, Y9C, Y9H, and P93S). Strains were selected based on two criteria: first, by position in the ternary ribosomal structure, and secondly by their degree of anisomycin resistance. Interestingly, no direct correlation between anisomycin resistance and affinity for aminoacyl-tRNA was observed. The R7Q strain that does not exibit anisomycin dependent phenotype, and the anisomycin sensitive strain Y9H, had the same K_a as wild-type. One anisomycin resistant strain - P93S had an elevated affinity for the A-site tRNA, but another resistant strain Y9C had a decreased K_a (Figure 4.9 and Table 3).

Discussion

This study describes the generation and characterization of the library of *rpl10* alleles that promote loss of the Killer phenotype. Measurements of -1PRF demonstrated that loss of the killer is not due to changes in the -1PRF but rather due to the 60S biogenesis defect. However, mutants with seemingly normal polysome profiles and wild type levels of -1PRF suggested that killer virus loss can be promoted by another unknown mechanism. A similar observation was made with *mak* (*maintenance of killer*) mutants of yeast [161].

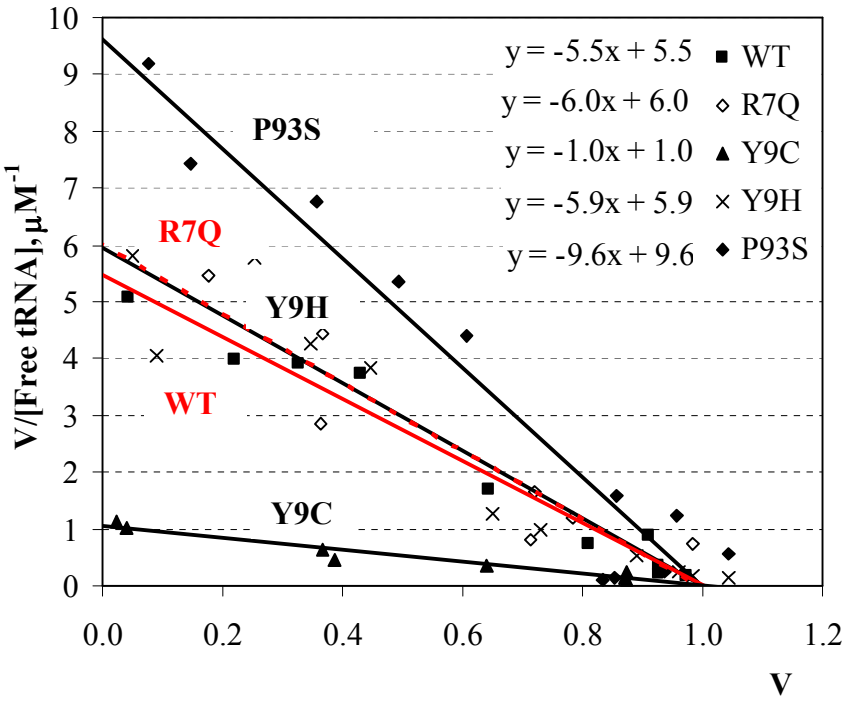

Figure 4.9. Scatchard plot analysis of Phe-tRNA binding to ribosomes from the different *rpl10* strains.

Aminoacyl-tRNA binding to the A-site of the ribosome was carried out as previously described [183]. The reaction mixtures were preincubated with uncharged tRNA at 30°C for 15min to ensure full occupation of P- and E-sites by uncharged tRNA, after which various quantities of (4 – 264 pmoles) of [^{14}C]Phe-tRNA were added. Reaction mixtures were incubated at 30 °C for an additional 15 minutes to allow formation of [^{14}C]Phe-tRNA-80S-poly(U) complexes. Aliquots were then applied onto nitrocellulose membranes, filters were washed with 2ml of binding buffer, and radioactivity was measured by scintillation counting. Background levels of radioactivity were determined using a blank sample and subtracted from the test samples. The A-site binding data was normalyzed to the amount of the active ribosomes, which was initially determined as intersection with the abscissa axis on the Scatchard plot.

	Kd, μMoles	-1PRF	NS	Anisomycin	Paromomycin	15^0C	37^0C	Halfmers
WT	0.09 +/-0.01	1	1	N/A	N/A	N/A	N/A	No
R7Q	0.10 +/-0.04	0.98 +/-0.06	0.97 +/-0.06	0	0	0	0	-
Y9C	0.65 +/-0.14	1.34 +/-0.04	0.40 +/-0.01	+1	0	0	0	No
Y9H	0.11 +/-0.02	1.28 +/-0.04	0.71 +/-0.02	-1	0	+1	0	No
P93S	0.05 +/-0.01	1.40 +/-0.28	1.49 +/-0.48	+1	0	-0.5	0	Yes

Table 3. Summary of properties of rpl10 mutants

The -1PRF and nonsense suppression efficiencies expressed as a fold of wild type. Drug and temperature sensitivity scores were assigned as Materials and methods, page 122.

The positions of the mutated residues in the 3-D ribosomal structure point to important components of L10 and critical regions of L10-ribosome interactions. The mutations were clustered in the regions of the protein that make contacts with helices 89 and 38. Of the 22 mutant residues whose locations could be mapped in the 3-D ribosomal structure, 8 make contacts with h89 (R7L, R7P, R7Q, Y9C, Y9H, Y9N, Y11C and A64G) and 6 interact with h38 (K40M, K40R, P93S, P93T, F94I and F94L). Seven of these alleles were anisomycin resistant (R7L, R7P, Y9C, K40M, P93S, F94I, and F94L), and two were anisomycin sensitive (Y9H and Y9N). Notably, every mutant residue located near h89 either directly interacts with bases in the bulge at the base of h89 or makes contacts with residues of L10 that interact with the bulge (Figure 4.5). This bulge is involved in formation of the first of the "accommodation gates", which are thought to direct movement of the acceptor end of the A-site tRNA during the accommodation stage of aa-tRNA selection [37]. The loop connecting h89 and h90 forms the A-site side of the peptidyl transferase center and the anisomycin binding site (Figure 2.7). Thus, these residues may affect both accommodation and the conformation of the peptidyl transferase center. As was previously observed with the mutants of *rpl3*, altered conformation of these gates was hypothesized to promote increased affinities for aminoacyl-tRNAs resulting in anisomycin resistance via a competitive mechanism. Notably, another cluster of L10 mutants (residues 93-94) interacts with h38, and in the ternary structure those mutants are close to the residues interacting with the h89. Thus, we hypothesized that this group of L10 mutants promote the observed anisomycin specific phenotypes through a similar competitive mechanism. To test this hypothesis, the aminoacyl-tRNA affinities for ribosomes from strains with different degrees of anisomycin sensitivity were measured. The WT

and R7Q strains (no anisomycin phenotype), the anisomycin sensitive Y9H mutant, and the anisomycin resistant strain Y9C and P93S were examined. Ribosomes from R7Q strain have the same aa-tRNA affinities as wild type ribosomes, while ribosomes from the resistant mutant Y9C had a lower affinity for aa-tRNA, and ribosomes from the P93S resistant strain had increased affinity for aa-tRNA compared to wild type ribosomes. Lastly, ribosomes from the anisomycin sensitive Y9H strain were found to have the same affinity for the aa-tRNA as wild type (Table 3 and Figure 4.9). Thus, anisomycin resistance as applied to L10 is not linked with aa-tRNA affinity, implying that the mechanism of anisomycin resistance is different from that of L3. One alternative is that the rate of accomodation may be affected; however the effects could also be masked by altered efficiencies of the upstream reactions or by the changed stability of the ribosome-tRNA complex. For example, decreased rates of the initial aa-tRNA binding and (or) codon recognition could accompany the increased rates of accommodation. Our tRNA binding assay measures "total" binding and is unable access the rates of the individual steps of the aa-tRNA selection. Thus the observed changes in aa-tRNA affinities may result from a combination of altered rates of accommodation and changes in the preceding steps. Alternatively, it is possible that these mutations affect the conformation of the anisomycin binding site, and thus the affinity of the ribosome for anisomycin. A similar effect was previously observed for tualimin and trichodermin [149,168].

Previous analysis of an A-site finger (h38) deletion in *E.coli* demonstrated that the A-site finger is required for fine tuning of EF-G GTPase activation[210] . Thus, the observed effects on aa-tRNA binding and anisomycin resistance may result from increased rates of GTPase activation in these mutants. This hypothesis can be tested

by assessing rates of the GTPase activation and GTP hydrolysis by the elongation factors eEF-1 and eEF-2.

The current study also demonstrated effects of the L10 mutations on termination codon recognition. Altered levels of nonsense suppression suggest that these mutations: (A) may disrupt communication between the decoding center and the large subunit; or (B) may affect functions associated with release factors. Interestingly, two alleles, G81D and N144D, promoted a paromomycin specific phenotype. Paromomycin binds in the decoding center on the small subunit and promotes nonsense suppression. Notably, in the ternary ribosomal structure G81D and N144D are close to each other and are located on the solvent side of the ribosome. While no specific contacts between L10 and eEF-2 were observed in the Cryo-EM reconstruction of yeast ribosomes, that study did reveal a large unresolved "mass" composed of the tip of h38 and the C-terminal domain of L10 [184]. This "mass" contacts the L7/L12 stalk, which serves as an entry site for incoming translation factors. It is possible that conformational changes promoted by the G81D and N144D mutations are translated to the eEF-1 binding site, and thus may affect the fidelity of protein synthesis. Thus, the mutations near the solvent side of the ribosome may affect nonsense suppression by altering the ability of the ribosome to discriminate between elongation and termination factors. The proximity of this unresolved mass both to the elongation factor binding site and central protuberance suggests that L10 may functionally connect the factor binding site and small subunit. Identification of 8 mutants in this domain that promote Killer virus loss suggests a functional relevance of the C-terminus of L10. Notably, P179S, F199I, and S201F were hypoaccurate promoting increased levels of nonsense suppression.

A recent study demonstrated an effect of the A-site finger on the level of stop codon read through [210]. Thus, altered levels of nonsense suppression in L10 that establish contacts with h38 may result from altered A-site finger/L10 interactions. While it is currently unclear how mutations in L10 may cause such effects, the future structure probing experiment and biochemical characterization of the partial reactions of aminoacyl-tRNA selection and eRF1 binding may reveal the underlying mechanism (and structural prerequisites) of eRF1 recognition. Involvement of h38 in maintenance of the translational fidelity, as well as the position of the unresolved C-terminal region of L10 between central protuberance and L7/L12 stalk, implies functional significance of h38. It is possible that h38 and L10 serve as a bridge between the factor binding site and the small subunit via the B1a bridge, or through the central protuberance. Alternatively, h38 may communicate with the h89 through L10, which forms a continious RNA structure with h90-92 and GTPase associated center (h42). Deletion of the h38 tip in *E. coli* resulted in decreased rates of EF-G activation, thus suggesting the possibility of a link between GTPase activation and B1 bridge formation. Chemical probing of this region coupled with further biochemical characterization including monitoring of: (A) GTPase rates in these strains, and (B) the effects of codon-anticodon mismatching on rates of initial binding and codon recognition may further our understanding of the elongation factor function and role of the ribosome in aa-tRNA selection.

L10 also plays the critical role in 60S subunit biogenesis. It is the last protein incorporated into the large ribosomal subunit, and is required for subunit joining and displacement of the export adapter Nmd3p. Thus, elucidation of these L10-associated functions can help to reveal (A) structural/conformational features required for large

subunit function and (or) activation, and (B) structural rearrangements that distinguish premature 60S subunits from active ribosomes. Recent studies demonstrated roles for Nmd3p, Sqt1p and Lsg1p in L10 incorporation, 60S export, and maturation [264,266]. A subsequent study demonstrated that Arx1p and Rei1p are also involved in 60S export [278]. However, the exact interplay between these factors is unknown. Further characterization of the L10 mutants with defects in ribosome biogenesis may shed light on these interactions and provide a deeper insight in the processes of ribosome maturation/activation.

Here we have described random mutagenesis of ribosomal protein L10. The new *rpl10* alleles were characterized with regard to cold, heat, anisomycin, and paromomycin associated phenotypes. Efficiencies of translational recoding events (-1PRF and NS) were measured using dual luciferase reporter systems. This characterization demonstrated that loss of the M_1 virus is not due to changes in -1PRF efficiency. In a subset of strains, loss of the killer virus correlated with defects in subunit maturation and (or) joining, as evidenced by the presence of halfmers in sucrose gradient profiles. Further characterization of these strains may help to determine the sequence of events required for L10 incorporation and (or) displacement of pNmd3, as well as activation of the large subunit. Biochemical characterization showed that anisomycin resistance in L10 strains is not linked with changes in aa-tRNA affinity, and that the mechanism of anisomycin resistance is different from that observed with ribosomal protein

L3. Further characterization of these strains may help to unravel the functional relationships between h38, h89 and the peptidyl-transferase center.

Chapter 5. What is next?

Further directions

Genetic studies followed by functional/structural characterization are a proven approach for unraveling mechanisms of action of protein-RNA complexes. With regard to the results presented in this dissertation, we have presented functional analyses of ribosomal proteins L3 and L10, and 5S ribosomal rRNA. There are many possible directions along which this work can be extended, and multiple ways to test the proposed hypotheses.

Ribosomal protein L3

In this study, we proposed that accommodation triggers adoption of the active conformation by the peptidyl transferase center. There are few approaches that may be used to test this idea. First, since we proposed specific functions for the gate nucleotides (C2942, C2944 and C2943 in *S. cerevisiae*) and for the nucleotides that contact with tip of the L3, site specific mutagenesis of these bases may provide further insight into their functions. For example substitution of C2942 to U would prevent formation of the hydrogen bond between the primary amino group of C2942 with the 2' OH ribose of U2874 (in *S. cerevisiae*). Additionally, mutagenesis of the gate bases, for example purine to pyrimidine substitutions, would directly affect gate sizes, which should affect accommodation efficiency. Chemical modifications of these strains coupled with characterization of tRNA affinities for A- and P-sites, and rates of peptidyl transfer could provide help in determining their roles and interplay between these bases.

Biophysical experiments aimed toward directly examining the structural dynamics of the peptidyltransferase center would allow real time monitoring of changes in base conformation and flexibility. Fluorescent techniques have proved to be extremely useful in these types of analyses. One possible approach would be to use fluorescently labeled tRNA substrates and ribosomal components. Measurements of FRET, fluorescence half-lives, shifts in fluorescence parameters, *etc.* may provide insight into the conformational dynamics of the PTC during the process of accommodation and adoption of the "induced" state. There are a few potential targets for fluorescent labeling. Fluorescent labeling of A- and P-site tRNAs has been successfully used to determine the conformational transitions of the tRNAs during aa-tRNA selection and translocation by FRET [60,279]. Examination of PTC dynamics would be technically similar, and comparison of the mutant and wild type ribosomes may provide insight into the molecular mechanisms underlying the observed phenotypes. Fluorescence quenching is another method. It is based on notion that conformational changes in the immediate vicinity of a fluorophore may quench or brighten fluorescence. In the translation field this technique has been applied to observe conformational transitions in the D-loop of the tRNA upon binding with ribosomes [280,281]. The introduction of the fluorophores (for example proflavine) into the acceptor end of the tRNA or 25S rRNA would enable real time monitoring of the conformational transitions around labeled bases.

As a final thought, elucidation of the atomic resolution structures of these mutants in complex with different ligands (A- and P-site substrates and TSA analogs) would provide direct observation of structural roles of the C2942, C2944 and C2943 bases. While this approach must await the efforts of the X-ray crystallographers, it

would definitively describe the interplay between bases and amino acid residues of interest.

5S rRNA

The effects of naturally occurring allelic variants on the -1PRF efficiencies suggests that 5S rRNA may be involved in post transcriptional regulation of cellular gene expression via the NMD pathway. The plausibility of this hypothesis is based on the validity of the "mRNA suicide" idea. Thus a definitive demonstration of the role of -1PRF in regulation of *bona fide* cellular mRNA stability must necessarily precede attempts to reveal the physiological significance of 5S rRNA alleles on -1PRF efficiency. This could be achieved by monitoring of mRNA decay rates under conditions that promote different levels of -1PRF. These could be achieved by (A) using of NMD deficient strains (for example *upf1Δ*), (B) using alleles of ribosomal components that promote altered levels of the frameshifting, and (C) using drugs that specifically affect -1PRF, *i.*e. anisomycin.

Ribosomal protein L10

In this work, we describe the generation and characterization of a library of *rpl10* alleles. We have completed the initial analysis of these alleles, creating a toolbox for subsequent studies. There are multiple avenues that now may be followed with this project. First, strains with multiple defects in ribosome biogenesis were identified. Further characterization of these strains may help unravel the relationship between factors involved in the large subunit export during the last steps of ribosome maturation.

Phenotypic and biochemical characterizations revealed that mechanism of anisomycin sensitivity/resistance is likely to be uncoupled from affinity for aa-tRNA. Pursuing this line of inquiry would contribute to furthering our understanding of ribosome function. Structural characterization of these mutants using RNA modifying agents will help to determine rRNA bases and structural groups affected by the L10 mutants. Site specific mutagenesis of 25S rRNA that interact with L10, specifically bulges in h89 and h38, may also shed light on their functions. Moreover, the bulge in helix 38 is a good candidate as a critical element involved in communication between the GTPase associated center and the small subunit.

Appendix A: Strains

Table 4. List of strains used in the L3 study.

Strain name	Description
5X47	*MAT*a/*MAT*α *his1*/+ *trp1*/+ *ura3*/+ K^-
JD1090	*MAT*α *ura3-52 lys2-801 trp1Δ leu2 his3 RPL3*::*HIS3 pJD166.ura* [*L-AHNB* M_1]
JD1228	*MAT*α *ura3-52 lys2-801 trp1δ leu2= his3 RPL3::HIS3* pJD166.WT.trp
JD 1229	*MAT*α *ura3-52 lys2-801 trp1δ leu2= his3 RPL3::HIS3* pJD166.mak8.trp
JD1230	*MAT*α *ura3-52 lys2-801 trp1δ leu2= his3 RPL3::HIS3* pJD166_P257T.trp
JD1231	*MAT*α *ura3-52 lys2-801 trp1δ leu2= his3 RPL3::HIS3* pJD166.I282T.trp
JD1232	*MAT*α *ura3-52 lys2-801 trp1δ leu2= his3 RPL3::HIS3* pJD166.W255C.trp
JD1228.G15C	*MAT*α *ura3-52 lys2-801 trp1δ leu2= his3 RPL3::HIS3* pJD166.G15C.trp
JD1228.P18S	*MAT*α *ura3-52 lys2-801 trp1δ leu2= his3 RPL3::HIS3* pJD166.P18S.trp

Table 5. List of strains used in the 5S study.

Strain name	Description
5X47	*MATa*/*MATα his1*/+ *trp1*/+ *ura3*/+ K^-
JD759	*MATα* ***kar1-1*** *arg1 thr(i,x)* L-A HN M_1
JD932D	*MATα ade 2-1 trp1-1 ura3-1 leu2-3,112 his3-11,15 can1-100* [L-AHN M_1]
JD1111	*MATa ade2-1 ura3-1 leu2-3 his3-11 trp1 can1-100 rdn1ΔΔ::HIS3* pJD106.URA pJD211.LEU [LA-HN M_1]
JD1248	*MATa ade2-1 ura3-1 trp1-1 his3-11 leu2-3, 112 can1-100 ΔrDNA::his3::hisG* + pJD180.URA
JD1253	*MATa ade2-1 ura3-1 trp1-1 his3-11 leu2-3, 112 can1-100 ΔrDNA::his3::hisG* + pJD180.URA [LA-HN M_1]
NOY1049	*MATa ade2-1 ura3-1 trp1-1 his3-11 leu2-3, 112 can1-100 ΔrDNA::his3::hisG* + pNOY353 (GAL7-35S rDNA, 5S rDNA, *TRP1*, 2μ, amp^r)

Table 6. List of strains used in the L10 study

Strain name	Description
5X47	*MATa*/*MATα his1*/+ *trp1*/+ *ura3*/+ K^-
JD579	*MATα* ***kar1-1*** *arg1 thr(i,x)* L-A HN M_1
JD1293	*MATa rpl10::Kan met15Δ0 leu2Δ0 ura3Δ0 his3Δ0* pJD429.URA, L-A HN M_1
JD1308	*MATa rpl10::Kan met15Δ0 leu2Δ0 ura3Δ0 his3Δ0* pJD586.HIS, L-A HN M_1
JD1308.R7L	*MATa rpl10::Kan met15Δ0 leu2Δ0 ura3Δ0 his3Δ0* pJD586.R7L.HIS
JD1308.R7P	*MATa rpl10::Kan met15Δ0 leu2Δ0 ura3Δ0 his3Δ0* pJD586.R7P.HIS
JD1308.R7Q	*MATa rpl10::Kan met15Δ0 leu2Δ0 ura3Δ0 his3Δ0* pJD586.R7Q.HIS
JD1308.Y9C	*MATa rpl10::Kan met15Δ0 leu2Δ0 ura3Δ0 his3Δ0* pJD586.Y9C.HIS
JD1308.Y9H	*MATa rpl10::Kan met15Δ0 leu2Δ0 ura3Δ0 his3Δ0* pJD586.Y9H.HIS
JD1308.Y9N	*MATa rpl10::Kan met15Δ0 leu2Δ0 ura3Δ0 his3Δ0* pJD586.Y9N.HIS
JD1308.Y11C	*MATa rpl10::Kan met15Δ0 leu2Δ0 ura3Δ0 his3Δ0* pJD586.Y11C.HIS
JD1308.K15R	*MATa rpl10::Kan met15Δ0 leu2Δ0 ura3Δ0 his3Δ0* pJD586.K15R.HIS
JD1308.Y17C	*MATa rpl10::Kan met15Δ0 leu2Δ0 ura3Δ0 his3Δ0* pJD586.Y17C.HIS
JD1308.V26D	*MATa rpl10::Kan met15Δ0 leu2Δ0 ura3Δ0 his3Δ0* pJD586.V26D.HIS
JD1308.K40M	*MATa rpl10::Kan met15Δ0 leu2Δ0 ura3Δ0 his3Δ0* pJD586.K40M.HIS
JD1308.K40R	*MATa rpl10::Kan met15Δ0 leu2Δ0 ura3Δ0 his3Δ0* pJD586.K40R.HIS
JD1308.Q59H	*MATa rpl10::Kan met15Δ0 leu2Δ0 ura3Δ0 his3Δ0* pJD586.Q59H.HIS
JD1308.A64G	*MATa rpl10::Kan met15Δ0 leu2Δ0 ura3Δ0 his3Δ0* pJD586.A64G.HIS
JD1308.K74M	*MATa rpl10::Kan met15Δ0 leu2Δ0 ura3Δ0 his3Δ0* pJD586.K74M.HIS
JD1308.G81D	*MATa rpl10::Kan met15Δ0 leu2Δ0 ura3Δ0 his3Δ0* pJD586.G81D.HIS
JD1308.P93S	*MATa rpl10::Kan met15Δ0 leu2Δ0 ura3Δ0 his3Δ0* pJD586.P93S.HIS
JD1308.P93T	*MATa rpl10::Kan met15Δ0 leu2Δ0 ura3Δ0 his3Δ0* pJD586.P93T.HIS
JD1308.F94I	*MATa rpl10::Kan met15Δ0 leu2Δ0 ura3Δ0 his3Δ0*

	pJD586.F94I.HIS
JD1308.F94L	*MATa rpl10::Kan met15Δ0 leu2Δ0 ura3Δ0 his3Δ0* pJD586.F94L.HIS
JD1308.I120T	*MATa rpl10::Kan met15Δ0 leu2Δ0 ura3Δ0 his3Δ0* pJD586.I120T.HIS
JD1308.N144D	*MATa rpl10::Kan met15Δ0 leu2Δ0 ura3Δ0 his3Δ0* pJD586.N144D.HIS
JD1308.K145E	*MATa rpl10::Kan met15Δ0 leu2Δ0 ura3Δ0 his3Δ0* pJD586.K145E.HIS
JD1308.K145R	*MATa rpl10::Kan met15Δ0 leu2Δ0 ura3Δ0 his3Δ0* pJD586.K145R.HIS
JD1308.L152M	*MATa rpl10::Kan met15Δ0 leu2Δ0 ura3Δ0 his3Δ0* pJD586.L152M.HIS
JD1308.P160T	*MATa rpl10::Kan met15Δ0 leu2Δ0 ura3Δ0 his3Δ0* pJD586.P160T.HIS
JD1308.P179S	*MATa rpl10::Kan met15Δ0 leu2Δ0 ura3Δ0 his3Δ0* pJD586.P179S.HIS
JD1308.F199I	*MATa rpl10::Kan met15Δ0 leu2Δ0 ura3Δ0 his3Δ0* pJD586.F199I.HIS
JD1308.S201F	*MATa rpl10::Kan met15Δ0 leu2Δ0 ura3Δ0 his3Δ0* pJD586.S201F.HIS
JD1308.K202Q	*MATa rpl10::Kan met15Δ0 leu2Δ0 ura3Δ0 his3Δ0* pJD586.K202Q.HIS
JD1308.L206V	*MATa rpl10::Kan met15Δ0 leu2Δ0 ura3Δ0 his3Δ0* pJD586.L206V.HIS
JD1308.F207G	*MATa rpl10::Kan met15Δ0 leu2Δ0 ura3Δ0 his3Δ0* pJD586.F207G.HIS
JD1308.R211I	*MATa rpl10::Kan met15Δ0 leu2Δ0 ura3Δ0 his3Δ0* pJD586.R211I.HIS

Appendix B: Plasmids

Table 7. List of plasmids used in L3 study

Plasmid name	Parental vector	Description
pJD166	pRS316 [282,283]	A *RPL3* expressing plasmid encoding wild type form of L3 from *URA*-based vector [158].
pJD166.*mak8-1*	pJD166	A *RPL3* expressing plasmid encoding *mak8-1* allele of L3 from *Trp*-based vector [158].
pJD166.G15C	pJD166	A *RPL3* expressing plasmid encoding G15C allele of L3 from *Trp*-based vector.
pJD166.P18S	pJD166	A *RPL3* expressing plasmid encoding P18S allele of L3 from *Trp*-based vector.
pJD166.P257T	pJD166	A *RPL3* expressing plasmid encoding P257T allele of L3 from *Trp*-based vector [158].
pJD166.W255C	pJD166	A *RPL3* expressing plasmid encoding W255C allele of L3 from *Trp*-based vector [158].
pJD166.I282T	pJD166	A *RPL3* expressing plasmid encoding I282T allele of L3 from *Trp*-based vector [158].

Table 8. List of reporter plasmids

Plasmid name	Parental vector	Description
pJEF1105		Ty*1* retrotransposition reporter
pJD170.0	pRS306 [282,283]	A zero frame monocistronic β- galactosidase reporter
pJD179.-1	pRS306	A -1PRF (L-A frameshift signal) monocistronic β- galactosidase reporter
pJD205.0	pRS305 [282,283]	A zero frame monocistronic β- galactosidase reporter
pJD205.-1	pRS305	A -1PRF (L-A frameshift signal) monocistronic β- galactosidase reporter
pJD205.+1	pRS305	A +1PRF (Ty*1* frameshift signal) monocistronic β- galactosidase reporter
pJD357	p2mc [284]	A zero frame control dual luciferase reporter (DLR) expressing bicistronic mRNA encoding a fusion of *Renilla* and firefly luciferase [226].
pJD376	p2mci [284]	A -1PRF (L-A frameshift signal) dual luciferase reporter (DLR) expressing bicistronic mRNA encoding a fusion of *Renilla* and firefly luciferase [226]
pJD431	pJD357	A non-sense codon (UAA) suppression dual luciferase reporter (DLR) expressing bicistronic mRNA encoding a fusion of *Renilla* and firefly luciferase [226]

Table 9. List of plasmids harboring RDN alleles

Plasmid name	Parental vector	Description
pJD106.URA	pRS426 [282,283]	pRS426 harboring wild-type allele of 5S rRNA
pJD180.URA	pRS426	pRS426 harboring wild-type alleles of 5S, 5.8S, 18S and 25S rRNA
pJD211.LEU	pRS425 [282,283]	pRS425 harboring wild-type alleles of 5.8S, 18S and 25S rRNA
pJD373.LEU	pRS425	pRS425 harboring wild-type alleles of 5.8S and 25S, and *Hyg*^{r} (U1759C) allele of 18S rRNA
pJD209	pRS424 [282,283]	pRS424 harboring wild-type allele of 5S rRNA
pJD209.RDN5-2	pJD209	pJD209 harboring RDN5-2 allele of 5S rRNA
pJD209.RDN5-3	pJD209	pJD209 harboring RDN5-3 allele of 5S rRNA
pJD209.RDN5-4	pJD209	pJD209 harboring RDN5-4 allele of 5S rRNA
pJD209.RDN5-5	pJD209	pJD209 harboring RDN5-5 allele of 5S rRNA
pJD209.RDN5-6	pJD209	pJD209 harboring RDN5-6 allele of 5S rRNA
pJD209.RDN5-7	pJD209	pJD209 harboring RDN5-7 allele of 5S rRNA
pJD209.RDN5-Ooc	pJD209	pJD209 harboring RDN5-Ooc allele of 5S rRNA
pJD209.RDN5-Som	pJD209	pJD209 harboring RDN5-Som allele of 5S rRNA
pJD209	pJD209	pJD209 harboring wild-type allele of 5S rRNA
pJD209.G1A	pJD209	pJD209 harboring G1A allele of 5S rRNA
pJD209.G1U	pJD209	pJD209 harboring G1U allele of 5S rRNA
pJD209.G2A	pJD209	pJD209 harboring G2A allele of 5S rRNA
pJD209.G2U	pJD209	pJD209 harboring G2U allele of 5S rRNA
pJD209.G2C	pJD209	pJD209 harboring G2C allele of 5S rRNA
pJD209.U3A	pJD209	pJD209 harboring U3A allele of 5S rRNA
pJD209.U3C	pJD209	pJD209 harboring U3C allele of 5S rRNA
pJD209.U4A	pJD209	pJD209 harboring U4A allele of 5S rRNA
pJD209.U4C	pJD209	pJD209 harboring U4C allele of 5S rRNA
pJD209.G5A	pJD209	pJD209 harboring G5A allele of 5S rRNA
pJD209.G5U	pJD209	pJD209 harboring G5U allele of 5S rRNA
pJD209.G5C	pJD209	pJD209 harboring G5C allele of 5S rRNA
pJD209.C6A	pJD209	pJD209 harboring C6A allele of 5S rRNA
pJD209.C6U	pJD209	pJD209 harboring C6U allele of 5S rRNA
pJD209.G7U	pJD209	pJD209 harboring G7U allele of 5S rRNA
pJD209.G7C	pJD209	pJD209 harboring G7C allele of 5S rRNA

pJD209.G8A	pJD209	pJD209 harboring G8A allele of 5S rRNA
pJD209.G8U	pJD209	pJD209 harboring G8U allele of 5S rRNA
pJD209.G8C	pJD209	pJD209 harboring G8C allele of 5S rRNA
pJD209.C9U	pJD209	pJD209 harboring C9U allele of 5S rRNA
pJD209.C9G	pJD209	pJD209 harboring C9G allele of 5S rRNA
pJD209.C10A	pJD209	pJD209 harboring C10A allele of 5S rRNA
pJD209.C10U	pJD209	pJD209 harboring C10U allele of 5S rRNA
pJD209.A11C	pJD209	pJD209 harboring A11C allele of 5S rRNA
pJD209.A11G	pJD209	pJD209 harboring A11G allele of 5S rRNA
pJD209.U12C	pJD209	pJD209 harboring U12C allele of 5S rRNA
pJD209.A13C	pJD209	pJD209 harboring A13C allele of 5S rRNA
pJD209.U14A	pJD209	pJD209 harboring U14A allele of 5S rRNA
pJD209.U14C	pJD209	pJD209 harboring U14C allele of 5S rRNA
pJD209.C15A	pJD209	pJD209 harboring C15A allele of 5S rRNA
pJD209.C15U	pJD209	pJD209 harboring C15U allele of 5S rRNA
pJD209.U16A	pJD209	pJD209 harboring U16A allele of 5S rRNA
pJD209.U16C	pJD209	pJD209 harboring U16C allele of 5S rRNA
pJD209.A17C	pJD209	pJD209 harboring A17C allele of 5S rRNA
pJD209.C18U	pJD209	pJD209 harboring C18U allele of 5S rRNA
pJD209.C19A	pJD209	pJD209 harboring C19A allele of 5S rRNA
pJD209.C19U	pJD209	pJD209 harboring C19U allele of 5S rRNA
pJD209.C19G	pJD209	pJD209 harboring C19G allele of 5S rRNA
pJD209.A20C	pJD209	pJD209 harboring A20C allele of 5S rRNA
pJD209.A20G	pJD209	pJD209 harboring A20G allele of 5S rRNA
pJD209.G21A	pJD209	pJD209 harboring G21A allele of 5S rRNA
pJD209.G21U	pJD209	pJD209 harboring G21U allele of 5S rRNA
pJD209.DG21	pJD209	pJD209 harboring DG21 allele of 5S rRNA
pJD209.A22U	pJD209	pJD209 harboring A22U allele of 5S rRNA
pJD209.A22C	pJD209	pJD209 harboring A22C allele of 5S rRNA
pJD209.A22G	pJD209	pJD209 harboring A22G allele of 5S rRNA
pJD209.A23U	pJD209	pJD209 harboring A23U allele of 5S rRNA
pJD209.A23C	pJD209	pJD209 harboring A23C allele of 5S rRNA
pJD209.A23G	pJD209	pJD209 harboring A23G allele of 5S rRNA
pJD209.A24U	pJD209	pJD209 harboring A24U allele of 5S rRNA
pJD209.A24C	pJD209	pJD209 harboring A24C allele of 5S rRNA
pJD209.G25A	pJD209	pJD209 harboring G25A allele of 5S rRNA
pJD209.G25U	pJD209	pJD209 harboring G25U allele of 5S rRNA
pJD209.G25C	pJD209	pJD209 harboring G25C allele of 5S rRNA
pJD209.C26U	pJD209	pJD209 harboring C26U allele of 5S rRNA
pJD209.A27C	pJD209	pJD209 harboring A27C allele of 5S rRNA
pJD209.A27G	pJD209	pJD209 harboring A27G allele of 5S rRNA
pJD209.C28A	pJD209	pJD209 harboring C28A allele of 5S rRNA
pJD209.C28U	pJD209	pJD209 harboring C28U allele of 5S rRNA
pJD209.C29A	pJD209	pJD209 harboring C29A allele of 5S rRNA
pJD209.C29U	pJD209	pJD209 harboring C29U allele of 5S rRNA
pJD209.G30A	pJD209	pJD209 harboring G30A allele of 5S rRNA
pJD209.G30U	pJD209	pJD209 harboring G30U allele of 5S rRNA

pJD209.G30C	pJD209	pJD209 harboring G30C allele of 5S rRNA
pJD209.U31A	pJD209	pJD209 harboring U31A allele of 5S rRNA
pJD209.U31C	pJD209	pJD209 harboring U31C allele of 5S rRNA
pJD209.U32A	pJD209	pJD209 harboring U32A allele of 5S rRNA
pJD209.U32C	pJD209	pJD209 harboring U32C allele of 5S rRNA
pJD209.U33A	pJD209	pJD209 harboring U33A allele of 5S rRNA
pJD209.U33C	pJD209	pJD209 harboring U33C allele of 5S rRNA
pJD209.U33G	pJD209	pJD209 harboring U33G allele of 5S rRNA
pJD209.C34A	pJD209	pJD209 harboring C34A allele of 5S rRNA
pJD209.C34G	pJD209	pJD209 harboring C34G allele of 5S rRNA
pJD209.C35U	pJD209	pJD209 harboring C35U allele of 5S rRNA
pJD209.C35G	pJD209	pJD209 harboring C35G allele of 5S rRNA
pJD209.DC36	pJD209	pJD209 harboring DC36 allele of 5S rRNA
pJD209.C36A	pJD209	pJD209 harboring C36A allele of 5S rRNA
pJD209.C36U	pJD209	pJD209 harboring C36U allele of 5S rRNA
pJD209.C36G	pJD209	pJD209 harboring C36G allele of 5S rRNA
pJD209.G37A	pJD209	pJD209 harboring G37A allele of 5S rRNA
pJD209.G37U	pJD209	pJD209 harboring G37U allele of 5S rRNA
pJD209.G37C	pJD209	pJD209 harboring G37C allele of 5S rRNA
pJD209.U38A	pJD209	pJD209 harboring U38A allele of 5S rRNA
pJD209.U38C	pJD209	pJD209 harboring U38C allele of 5S rRNA
pJD209.U38G	pJD209	pJD209 harboring U38G allele of 5S rRNA
pJD209.C39A	pJD209	pJD209 harboring C39A allele of 5S rRNA
pJD209.C39U	pJD209	pJD209 harboring C39U allele of 5S rRNA
pJD209.C39G	pJD209	pJD209 harboring C39G allele of 5S rRNA
pJD209.C40A	pJD209	pJD209 harboring C40A allele of 5S rRNA
pJD209.C40U	pJD209	pJD209 harboring C40U allele of 5S rRNA
pJD209.C40G	pJD209	pJD209 harboring C40G allele of 5S rRNA
pJD209.G41A	pJD209	pJD209 harboring G41A allele of 5S rRNA
pJD209.G41U	pJD209	pJD209 harboring G41U allele of 5S rRNA
pJD209.G41C	pJD209	pJD209 harboring G41C allele of 5S rRNA
pJD209.A42C	pJD209	pJD209 harboring A42C allele of 5S rRNA
pJD209.U43C	pJD209	pJD209 harboring U43C allele of 5S rRNA
pJD209.U43G	pJD209	pJD209 harboring U43G allele of 5S rRNA
pJD209.C44A	pJD209	pJD209 harboring C44A allele of 5S rRNA
pJD209.C44U	pJD209	pJD209 harboring C44U allele of 5S rRNA
pJD209.A45U	pJD209	pJD209 harboring A45U allele of 5S rRNA
pJD209.A45C	pJD209	pJD209 harboring A45C allele of 5S rRNA
pJD209.A46U	pJD209	pJD209 harboring A46U allele of 5S rRNA
pJD209.A46C	pJD209	pJD209 harboring A46C allele of 5S rRNA
pJD209.C47A	pJD209	pJD209 harboring C47A allele of 5S rRNA
pJD209.C47U	pJD209	pJD209 harboring C47U allele of 5S rRNA
pJD209.C47G	pJD209	pJD209 harboring C47G allele of 5S rRNA
pJD209.U48A	pJD209	pJD209 harboring U48A allele of 5S rRNA
pJD209.U48C	pJD209	pJD209 harboring U48C allele of 5S rRNA
pJD209.G49A	pJD209	pJD209 harboring G49A allele of 5S rRNA
pJD209.G49C	pJD209	pJD209 harboring G49C allele of 5S rRNA

pJD209.U50A	pJD209	pJD209 harboring U50A allele of 5S rRNA
pJD209.U50C	pJD209	pJD209 harboring U50C allele of 5S rRNA
pJD209.A51U	pJD209	pJD209 harboring A51U allele of 5S rRNA
pJD209.A51C	pJD209	pJD209 harboring A51C allele of 5S rRNA
pJD209.G52A	pJD209	pJD209 harboring G52A allele of 5S rRNA
pJD209.G52C	pJD209	pJD209 harboring G52C allele of 5S rRNA
pJD209.U53A	pJD209	pJD209 harboring U53A allele of 5S rRNA
pJD209.U53C	pJD209	pJD209 harboring U53C allele of 5S rRNA
pJD209.U54A	pJD209	pJD209 harboring U54A allele of 5S rRNA
pJD209.U54C	pJD209	pJD209 harboring U54C allele of 5S rRNA
pJD209.A55U	pJD209	pJD209 harboring A55U allele of 5S rRNA
pJD209.A55C	pJD209	pJD209 harboring A55C allele of 5S rRNA
pJD209.A56C	pJD209	pJD209 harboring A56C allele of 5S rRNA
pJD209.G57A	pJD209	pJD209 harboring G57A allele of 5S rRNA
pJD209.G57U	pJD209	pJD209 harboring G57U allele of 5S rRNA
pJD209.G57C	pJD209	pJD209 harboring G57C allele of 5S rRNA
pJD209.C58U	pJD209	pJD209 harboring C58U allele of 5S rRNA
pJD209.C58G	pJD209	pJD209 harboring C58G allele of 5S rRNA
pJD209.U59A	pJD209	pJD209 harboring U59A allele of 5S rRNA
pJD209.U59C	pJD209	pJD209 harboring U59C allele of 5S rRNA
pJD209.G60A	pJD209	pJD209 harboring G60A allele of 5S rRNA
pJD209.G60U	pJD209	pJD209 harboring G60U allele of 5S rRNA
pJD209.G61A	pJD209	pJD209 harboring G61A allele of 5S rRNA
pJD209.G61U	pJD209	pJD209 harboring G61U allele of 5S rRNA
pJD209.G61C	pJD209	pJD209 harboring G61C allele of 5S rRNA
pJD209.U62C	pJD209	pJD209 harboring U62C allele of 5S rRNA
pJD209.A63U	pJD209	pJD209 harboring A63U allele of 5S rRNA
pJD209.A63C	pJD209	pJD209 harboring A63C allele of 5S rRNA
pJD209.A64U	pJD209	pJD209 harboring A64U allele of 5S rRNA
pJD209.A64C	pJD209	pJD209 harboring A64C allele of 5S rRNA
pJD209.G65U	pJD209	pJD209 harboring G65U allele of 5S rRNA
pJD209.A66G	pJD209	pJD209 harboring A66G allele of 5S rRNA
pJD209.G67A	pJD209	pJD209 harboring G67A allele of 5S rRNA
pJD209.G67C	pJD209	pJD209 harboring G67C allele of 5S rRNA
pJD209.C68U	pJD209	pJD209 harboring C68U allele of 5S rRNA
pJD209.C68G	pJD209	pJD209 harboring C68G allele of 5S rRNA
pJD209.C69A	pJD209	pJD209 harboring C69A allele of 5S rRNA
pJD209.C69U	pJD209	pJD209 harboring C69U allele of 5S rRNA
pJD209.C69G	pJD209	pJD209 harboring C69G allele of 5S rRNA
pJD209.U70A	pJD209	pJD209 harboring U70A allele of 5S rRNA
pJD209.U70C	pJD209	pJD209 harboring U70C allele of 5S rRNA
pJD209.G71A	pJD209	pJD209 harboring G71A allele of 5S rRNA
pJD209.G71U	pJD209	pJD209 harboring G71U allele of 5S rRNA
pJD209.G71C	pJD209	pJD209 harboring G71C allele of 5S rRNA
pJD209.A72C	pJD209	pJD209 harboring A72C allele of 5S rRNA
pJD209.C73A	pJD209	pJD209 harboring C73A allele of 5S rRNA
pJD209.C73U	pJD209	pJD209 harboring C73U allele of 5S rRNA

pJD209.C73G	pJD209	pJD209 harboring C73G allele of 5S rRNA
pJD209.C74A	pJD209	pJD209 harboring C74A allele of 5S rRNA
pJD209.C74U	pJD209	pJD209 harboring C74U allele of 5S rRNA
pJD209.G75A	pJD209	pJD209 harboring G75A allele of 5S rRNA
pJD209.G75U	pJD209	pJD209 harboring G75U allele of 5S rRNA
pJD209.A76U	pJD209	pJD209 harboring A76U allele of 5S rRNA
pJD209.A76C	pJD209	pJD209 harboring A76C allele of 5S rRNA
pJD209.A76G	pJD209	pJD209 harboring A76G allele of 5S rRNA
pJD209.G77U	pJD209	pJD209 harboring G77U allele of 5S rRNA
pJD209.G77C	pJD209	pJD209 harboring G77C allele of 5S rRNA
pJD209.U78C	pJD209	pJD209 harboring U78C allele of 5S rRNA
pJD209.A79U	pJD209	pJD209 harboring A79U allele of 5S rRNA
pJD209.G80U	pJD209	pJD209 harboring G80U allele of 5S rRNA
pJD209.G80C	pJD209	pJD209 harboring G80C allele of 5S rRNA
pJD209.U81C	pJD209	pJD209 harboring U81C allele of 5S rRNA
pJD209.G82A	pJD209	pJD209 harboring G82A allele of 5S rRNA
pJD209.G82C	pJD209	pJD209 harboring G82C allele of 5S rRNA
pJD209.U83C	pJD209	pJD209 harboring U83C allele of 5S rRNA
pJD209.A84U	pJD209	pJD209 harboring A84U allele of 5S rRNA
pJD209.A84C	pJD209	pJD209 harboring A84C allele of 5S rRNA
pJD209.A84G	pJD209	pJD209 harboring A84G allele of 5S rRNA
pJD209.G85A	pJD209	pJD209 harboring G85A allele of 5S rRNA
pJD209.G85U	pJD209	pJD209 harboring G85U allele of 5S rRNA
pJD209.U86A	pJD209	pJD209 harboring U86A allele of 5S rRNA
pJD209.U86C	pJD209	pJD209 harboring U86C allele of 5S rRNA
pJD209.G87A	pJD209	pJD209 harboring G87A allele of 5S rRNA
pJD209.G87C	pJD209	pJD209 harboring G87C allele of 5S rRNA
pJD209.G88U	pJD209	pJD209 harboring G88U allele of 5S rRNA
pJD209.G88C	pJD209	pJD209 harboring G88C allele of 5S rRNA
pJD209.G89A	pJD209	pJD209 harboring G89A allele of 5S rRNA
pJD209.G89C	pJD209	pJD209 harboring G89C allele of 5S rRNA
pJD209.U90C	pJD209	pJD209 harboring U90C allele of 5S rRNA
pJD209.G91A	pJD209	pJD209 harboring G91A allele of 5S rRNA
pJD209.G91U	pJD209	pJD209 harboring G91U allele of 5S rRNA
pJD209.G91C	pJD209	pJD209 harboring G91C allele of 5S rRNA
pJD209.A92U	pJD209	pJD209 harboring A92U allele of 5S rRNA
pJD209.A92C	pJD209	pJD209 harboring A92C allele of 5S rRNA
pJD209.C93A	pJD209	pJD209 harboring C93A allele of 5S rRNA
pJD209.C93U	pJD209	pJD209 harboring C93U allele of 5S rRNA
pJD209.C94A	pJD209	pJD209 harboring C94A allele of 5S rRNA
pJD209.C94U	pJD209	pJD209 harboring C94U allele of 5S rRNA
pJD209.A95U	pJD209	pJD209 harboring A95U allele of 5S rRNA
pJD209.A95C	pJD209	pJD209 harboring A95C allele of 5S rRNA
pJD209.U96A	pJD209	pJD209 harboring U96A allele of 5S rRNA
pJD209.U96C	pJD209	pJD209 harboring U96C allele of 5S rRNA
pJD209.A97C	pJD209	pJD209 harboring A97C allele of 5S rRNA
pJD209.C98A	pJD209	pJD209 harboring C98A allele of 5S rRNA

pJD209.C98U	pJD209	pJD209 harboring C98U allele of 5S rRNA
pJD209.C98G	pJD209	pJD209 harboring C98G allele of 5S rRNA
pJD209.G99A	pJD209	pJD209 harboring G99A allele of 5S rRNA
pJD209.G99U	pJD209	pJD209 harboring G99U allele of 5S rRNA
pJD209.C100U	pJD209	pJD209 harboring C100U allele of 5S rRNA
pJD209.G101A	pJD209	pJD209 harboring G101A allele of 5S rRNA
pJD209.G101C	pJD209	pJD209 harboring G101C allele of 5S rRNA
pJD209.A102U	pJD209	pJD209 harboring A102U allele of 5S rRNA
pJD209.A102C	pJD209	pJD209 harboring A102C allele of 5S rRNA
pJD209.A102G	pJD209	pJD209 harboring A102G allele of 5S rRNA
pJD209.A103U	pJD209	pJD209 harboring A103U allele of 5S rRNA
pJD209.A103C	pJD209	pJD209 harboring A103C allele of 5S rRNA
pJD209.A104U	pJD209	pJD209 harboring A104U allele of 5S rRNA
pJD209.A104G	pJD209	pJD209 harboring A104G allele of 5S rRNA
pJD209.C105A	pJD209	pJD209 harboring C105A allele of 5S rRNA
pJD209.C105U	pJD209	pJD209 harboring C105U allele of 5S rRNA
pJD209.C105G	pJD209	pJD209 harboring C105G allele of 5S rRNA
pJD209.U106A	pJD209	pJD209 harboring U106A allele of 5S rRNA
pJD209.U106C	pJD209	pJD209 harboring U106C allele of 5S rRNA
pJD209.C107A	pJD209	pJD209 harboring C107A allele of 5S rRNA
pJD209.C107U	pJD209	pJD209 harboring C107U allele of 5S rRNA
pJD209.C107G	pJD209	pJD209 harboring C107G allele of 5S rRNA
pJD209.A108U	pJD209	pJD209 harboring A108U allele of 5S rRNA
pJD209.A108C	pJD209	pJD209 harboring A108C allele of 5S rRNA
pJD209.G109A	pJD209	pJD209 harboring G109A allele of 5S rRNA
pJD209.G109C	pJD209	pJD209 harboring G109C allele of 5S rRNA
pJD209.G110A	pJD209	pJD209 harboring G110A allele of 5S rRNA
pJD209.G110U	pJD209	pJD209 harboring G110U allele of 5S rRNA
pJD209.G110C	pJD209	pJD209 harboring G110C allele of 5S rRNA
pJD209.U111C	pJD209	pJD209 harboring U111C allele of 5S rRNA
pJD209.G112C	pJD209	pJD209 harboring G112C allele of 5S rRNA
pJD209.C113U	pJD209	pJD209 harboring C113U allele of 5S rRNA
pJD209.U114C	pJD209	pJD209 harboring U114C allele of 5S rRNA
pJD209.G115A	pJD209	pJD209 harboring G115A allele of 5S rRNA
pJD209.G115U	pJD209	pJD209 harboring G115U allele of 5S rRNA
pJD209.C116A	pJD209	pJD209 harboring C116A allele of 5S rRNA
pJD209.C116U	pJD209	pJD209 harboring C116U allele of 5S rRNA
pJD209.A117U	pJD209	pJD209 harboring A117U allele of 5S rRNA
pJD209.A117C	pJD209	pJD209 harboring A117C allele of 5S rRNA
pJD209.A118U	pJD209	pJD209 harboring A118U allele of 5S rRNA
pJD209.A118C	pJD209	pJD209 harboring A118C allele of 5S rRNA
pJD209.U119C	pJD209	pJD209 harboring U119C allele of 5S rRNA
pJD209.C120U	pJD209	pJD209 harboring C120U allele of 5S rRNA
pJD209.U121C	pJD209	pJD209 harboring U121C allele of 5S rRNA

Table 10. List of plasmids harboring RPL10 alleles

Plasmid name	Parental vector	Description
pJD429	pRS426	pRS426 harboring wild-type allele of *RPL10*
pJD589	pRS313 [282,283]	pRS313 harboring wild-type allele of *RPL10*
pJD589.R7L	pJD589	pRS313 harboring R7L allele of *RPL10*
pJD589.R7P	pJD589	pRS313 harboring R7P allele of *RPL10*
pJD589.R7Q	pJD589	pRS313 harboring R7Q allele of *RPL10*
pJD589.Y9C	pJD589	pRS313 harboring Y9C allele of *RPL10*
pJD589.Y9H	pJD589	pRS313 harboring Y9H allele of *RPL10*
pJD589.Y9N	pJD589	pRS313 harboring Y9N allele of *RPL10*
pJD589.Y11C	pJD589	pRS313 harboring Y11C allele of *RPL10*
pJD589.K15R	pJD589	pRS313 harboring K15R allele of *RPL10*
pJD589.Y17C	pJD589	pRS313 harboring Y17C allele of *RPL10*
pJD589.V26D	pJD589	pRS313 harboring V26D allele of *RPL10*
pJD589.K40M	pJD589	pRS313 harboring K40M allele of *RPL10*
pJD589.K40R	pJD589	pRS313 harboring K40R allele of *RPL10*
pJD589.Q59H	pJD589	pRS313 harboring Q59H allele of *RPL10*
pJD589.A64G	pJD589	pRS313 harboring A64G allele of *RPL10*
pJD589.K74M	pJD589	pRS313 harboring K74M allele of *RPL10*
pJD589.G81D	pJD589	pRS313 harboring G81D allele of *RPL10*
pJD589.P93S	pJD589	pRS313 harboring P93S allele of *RPL10*
pJD589.P93T	pJD589	pRS313 harboring P93T allele of *RPL10*
pJD589.F94I	pJD589	pRS313 harboring F94I allele of *RPL10*
pJD589.F94L	pJD589	pRS313 harboring F94L allele of *RPL10*
pJD589.I120T	pJD589	pRS313 harboring I120T allele of *RPL10*
pJD589.N144D	pJD589	pRS313 harboring N144D allele of *RPL10*
pJD589.K145E	pJD589	pRS313 harboring K145E allele of *RPL10*
pJD589.K145R	pJD589	pRS313 harboring K145R allele of *RPL10*
pJD589.L152M	pJD589	pRS313 harboring L152M allele of *RPL10*
pJD589.P160T	pJD589	pRS313 harboring P160T allele of *RPL10*
pJD589.P179S	pJD589	pRS313 harboring P179S allele of *RPL10*
pJD589.F199I	pJD589	pRS313 harboring F199I allele of *RPL10*
pJD589.S201F	pJD589	pRS313 harboring S201F allele of *RPL10*
pJD589.K202Q	pJD589	pRS313 harboring K202Q allele of *RPL10*
pJD589.L206V	pJD589	pRS313 harboring L206V allele of *RPL10*
pJD589.F207G	pJD589	pRS313 harboring F207G allele of *RPL10*
pJD589.R211I	pJD589	pRS313 harboring R211I allele of *RPL10*

Appendix C: Primers

Table 11. List of primers used in structure probing experiments .

Primer name	Sequence
5-1	AGATTGCAGCACCTGAGTTTCG
18-1	CAAAATCAAGAAAGAGC
25-2	GACTTCCATGGCCACCG
25-4	TAAAGGATCGATAGGCC
25-5	TCAAAAAGCAATGTCGC
25-6	AACCTGTCTCACGACGG
25-7	CCTGATCAGACAGCCGC
99	AGATTGCAGCACCTGAGTTTCG
1,112	CTTACCAAAAATGGCCC
1,231	GACTTCCATGGCCACCG
1,343	GGGCATCATATCAACCC
2,957	AACCTGTCTCACGACGG
3,057	CCTGATCAGACAGCCGC

Table 12. Primers used for direct sequencing of 5S rRNA.

Primer name	Sequence
N001	AAAAAAAAGAAATAABGATTGCAGCACCTGA
N002	AAAAAAAGAAATAAAHATTGCAGCACCTGAG
N003	AAAAAAGAAATAAAGBTTGCAGCACCTGAGT
N004	AAAAAGAAATAAAGAVTGCAGCACCTGAGTT
N005	AAAAGAAATAAAGATVGCAGCACCTGAGTTT
N006	AAAGAAATAAAGATTHCAGCACCTGAGTTTC
N007	AAGAAATAAAGATTGDAGCACCTGAGTTTCG
N008	AGAAATAAAGATTGCBGCACCTGAGTTTCGC
N009	GAAATAAAGATTGCAHCACCTGAGTTTCGCG
N010	AAATAAAGATTGCAGDACCTGAGTTTCGCGT
N011	AATAAAGATTGCAGCBCCTGAGTTTCGCGTA
N012	ATAAAGATTGCAGCADCTGAGTTTCGCGTAT
N013	TAAAGATTGCAGCACDTGAGTTTCGCGTATG
N014	AAAGATTGCAGCACCVGAGTTTCGCGTATGG
N015	AAGATTGCAGCACCTHAGTTTCGCGTATGGT
N016	AGATTGCAGCACCTGBGTTTCGCGTATGGTC
N017	GATTGCAGCACCTGAHTTTCGCGTATGGTCA
N018	ATTGCAGCACCTGAGVTTCGCGTATGGTCAC
N019	TTGCAGCACCTGAGTVTCGCGTATGGTCACC
N020	TGCAGCACCTGAGTTVCGCGTATGGTCACCC
N021	GCAGCACCTGAGTTTDGCGTATGGTCACCCA
N022	CAGCACCTGAGTTTCHCGTATGGTCACCCAC
N023	AGCACCTGAGTTTCGDGTATGGTCACCCACT
N024	GCACCTGAGTTTCGCHTATGGTCACCCACTA
N025	CACCTGAGTTTCGCGVATGGTCACCCACTAC
N026	ACCTGAGTTTCGCGTBTGGTCACCCACTACA
N027	CCTGAGTTTCGCGTAVGGTCACCCACTACAC
N028	CTGAGTTTCGCGTATHGTCACCCACTACACT
N029	TGAGTTTCGCGTATGHTCACCCACTACACTA
N030	GAGTTTCGCGTATGGVCACCCACTACACTAC
N031	AGTTTCGCGTATGGTDACCCACTACACTACT
N032	GTTTCGCGTATGGTCBCCCACTACACTACTC
N033	TTTCGCGTATGGTCADCCACTACACTACTCG
N034	TTCGCGTATGGTCACDCACTACACTACTCGG
N035	TCGCGTATGGTCACCDACTACACTACTCGGT
N036	CGCGTATGGTCACCCBCTACACTACTCGGTC
N037	GCGTATGGTCACCCADTACACTACTCGGTCA
N038	CGTATGGTCACCCACVACACTACTCGGTCAG
N039	GTATGGTCACCCACTBCACTACTCGGTCAGG
N040	TATGGTCACCCACTADACTACTCGGTCAGGC
N041	ATGGTCACCCACTACBCTACTCGGTCAGGCT
N042	TGGTCACCCACTACADTACTCGGTCAGGCTC
N043	GGTCACCCACTACACVACTCGGTCAGGCTCT
N044	GTCACCCACTACACTBCTCGGTCAGGCTCTT

N045	TCACCCACTACACTADTCGGTCAGGCTCTTA
N046	CACCCACTACACTACVCGGTCAGGCTCTTAC
N047	ACCCACTACACTACTDGGTCAGGCTCTTACC
N048	CCCACTACACTACTCHGTCAGGCTCTTACCA
N049	CCACTACACTACTCGHTCAGGCTCTTACCAG
N050	CACTACACTACTCGGVCAGGCTCTTACCAGC
N051	ACTACACTACTCGGTDAGGCTCTTACCAGCT
N052	CTACACTACTCGGTCBGGCTCTTACCAGCTT
N053	TACACTACTCGGTCAHGCTCTTACCAGCTTA
N054	ACACTACTCGGTCAGHCTCTTACCAGCTTAA
N055	CACTACTCGGTCAGGDTCTTACCAGCTTAAC
N056	ACTACTCGGTCAGGCVCTTACCAGCTTAACT
N057	CTACTCGGTCAGGCTDTTACCAGCTTAACTA
N058	TACTCGGTCAGGCTCVTACCAGCTTAACTAC
N059	ACTCGGTCAGGCTCTVACCAGCTTAACTACA
N060	CTCGGTCAGGCTCTTBCCAGCTTAACTACAG
N061	TCGGTCAGGCTCTTADCAGCTTAACTACAGT
N062	CGGTCAGGCTCTTACDAGCTTAACTACAGTT
N063	GGTCAGGCTCTTACCBGCTTAACTACAGTTG
N064	GTCAGGCTCTTACCAHCTTAACTACAGTTGA
N065	TCAGGCTCTTACCAGDTTAACTACAGTTGAT
N066	CAGGCTCTTACCAGCVTAACTACAGTTGATC
N067	AGGCTCTTACCAGCTVAACTACAGTTGATCG
N068	GGCTCTTACCAGCTTBACTACAGTTGATCGG
N069	GCTCTTACCAGCTTABCTACAGTTGATCGGA
N070	CTCTTACCAGCTTAADTACAGTTGATCGGAC
N071	TCTTACCAGCTTAACVACAGTTGATCGGACG
N072	CTTACCAGCTTAACTBCAGTTGATCGGACGG
N073	TTACCAGCTTAACTADAGTTGATCGGACGGG
N074	TACCAGCTTAACTACBGTTGATCGGACGGGA
N075	ACCAGCTTAACTACAHTTGATCGGACGGGAA
N076	CCAGCTTAACTACAGVTGATCGGACGGGAAA
N077	CAGCTTAACTACAGTVGATCGGACGGGAAAC
N078	AGCTTAACTACAGTTHATCGGACGGGAAACG
N079	GCTTAACTACAGTTGBTCGGACGGGAAACGG
N080	CTTAACTACAGTTGAVCGGACGGGAAACGGT
N081	TTAACTACAGTTGATDGGACGGGAAACGGTG
N082	TAACTACAGTTGATCHGACGGGAAACGGTGC
N083	AACTACAGTTGATCGHACGGGAAACGGTGCT
N084	ACTACAGTTGATCGGBCGGGAAACGGTGCTT
N085	CTACAGTTGATCGGADGGGAAACGGTGCTTT
N086	TACAGTTGATCGGACHGGAAACGGTGCTTTC
N087	ACAGTTGATCGGACGHGAAACGGTGCTTTCT
N088	CAGTTGATCGGACGGHAAACGGTGCTTTCTG
N089	AGTTGATCGGACGGGBAACGGTGCTTTCTGG
N090	GTTGATCGGACGGGABACGGTGCTTTCTGGT
N091	TTGATCGGACGGGAABCGGTGCTTTCTGGTA

N092	TGATCGGACGGGAAADGGTGCTTTCTGGTAG
N093	GATCGGACGGGAAACHGTGCTTTCTGGTAGA
N094	ATCGGACGGGAAACGHTGCTTTCTGGTAGAT
N095	TCGGACGGGAAACGGVGCTTTCTGGTAGATA
N096	CGGACGGGAAACGGTHCTTTCTGGTAGATAT
N097	GGACGGGAAACGGTGDTTTCTGGTAGATATG
N098	GACGGGAAACGGTGCVTTCTGGTAGATATGG
N099	ACGGGAAACGGTGCTVTCTGGTAGATATGGC
N100	CGGGAAACGGTGCTTVCTGGTAGATATGGCC
N101	GGGAAACGGTGCTTTDTGGTAGATATGGCCG
N102	GGAAACGGTGCTTTCVGGTAGATATGGCCGC
N103	GAAACGGTGCTTTCTHGTAGATATGGCCGCA
N104	AAACGGTGCTTTCTGHTAGATATGGCCGCAA
N105	AACGGTGCTTTCTGGVAGATATGGCCGCAAC
U106	AGATTGCAGCACCTG
C107	AGATTGCAGCACCT
A108	AGATTGCAGCACC
G109	AGATTGCAGCAC
G110	AGATTGCAGCA
U111	AGATTGCAGC

Table 13. List of primers used for random mutagenesis of RPL10

Primer name	Sequence
RPL10_RMF	TTCCGCAAGTGCTTTTGGAGTGGGACTTTCAAACTTTAAAGTA CAGTATATCAAATAACTAATTCAAGATGGCTAGAAGG
RPL10_RMR	AATTACTGTTTAATAAACTAGAATTTAAATCAAAAAAATTTCT CTTTTAAGTTAGTTCAAATGTTTGAAAAGAACTTAGG

Reference List

1. Noller,H.F., Yusupov,M.M., Yusupova,G.Z., Baucom,A., Lieberman,K., Lancaster,L., Dallas,A., Fredrick,K., Earnest,T.N. & Cate,J.H. Structure of the ribosome at 5.5 Å resolution and its interactions with functional ligands. *Cold Spring Harb. Symp. Quant. Biol.* **66**, 57-66 (2001).

2. Ban,N., Nissen,P., Hansen,J., Capel,M., Moore,P.B. & Steitz,T.A. Placement of protein and RNA structures into a 5 Å-resolution map of the 50S ribosomal subunit. *Nature* **400**, 841-847 (1999).

3. Shatkin,A.J. Capping of eucaryotic mRNAs. *Cell* **9**, 645-653 (1976).

4. Rao,M.S., Hirsch,F., Wu,B.C., Spohn,W.H. & Busch,H. Comparative studies on the '5'-cap' and in vitro translational activity of cytoplasmic and nuclear poly A(+) RNA1. *Mol. Cell Biochem.* **15**, 3-13 (1977).

5. Merrick,W.C. Cap-dependent and cap-independent translation in eukaryotic systems. *Gene* **332**, 1-11 (2004).

6. Kozak,M. Initiation of translation in prokaryotes and eukaryotes. *Gene* **234**, 187-208 (1999).

7. Grifo,J.A., Tahara,S.M., Morgan,M.A., Shatkin,A.J. & Merrick,W.C. New initiation factor activity required for globin mRNA translation. *J. Biol. Chem.* **258**, 5804-5810 (1983).

8. Craig,A.W., Haghighat,A., Yu,A.T. & Sonenberg,N. Interaction of polyadenylate-binding protein with the eIF4G homologue PAIP enhances translation. *Nature* **392**, 520-523 (1998).

9. Le,H., Tanguay,R.L., Balasta,M.L., Wei,C.C., Browning,K.S., Metz,A.M., Goss,D.J. & Gallie,D.R. Translation initiation factors eIF-iso4G and eIF-4B interact with the poly(A)-binding protein and increase its RNA binding activity. *J. Biol. Chem.* **272**, 16247-16255 (1997).

10. Grifo,J.A., Tahara,S.M., Leis,J.P., Morgan,M.A., Shatkin,A.J. & Merrick,W.C. Characterization of eukaryotic initiation factor 4A, a protein involved in ATP-dependent binding of globin mRNA. *J. Biol. Chem.* **257**, 5246-5252 (1982).

11. Tahara,S.M., Morgan,M.A. & Shatkin,A.J. Binding of inosine-substituted mRNA to reticulocyte ribosomes and eukaryotic initiation factors 4A and 4B requires ATP. *J. Biol. Chem.* **258**, 11350-11353 (1983).

12. Pestova,T.V., Borukhov,S.I. & Hellen,C.U. Eukaryotic ribosomes require initiation factors 1 and 1A to locate initiation codons. *Nature* **394**, 854-859 (1998).

13. Kozak,M. Role of ATP in binding and migration of 40S ribosomal subunits. *Cell* **22**, 459-467 (1980).

14. Sachs,A.B., Sarnow,P. & Hentze,M.W. Starting at the beginning, middle, and end: translation initiation in eukaryotes. *Cell* **89**, 831-838 (1997).

15. Jan,E. & Sarnow,P. Factorless ribosome assembly on the internal ribosome entry site of cricket paralysis virus. *J. Mol. Biol.* **324**, 889-902 (2002).

16. Pestova,T.V., Lomakin,I.B. & Hellen,C.U. Position of the CrPV IRES on the 40S subunit and factor dependence of IRES/80S ribosome assembly. *EMBO Rep.* **5**, 906-913 (2004).

17. Costa-Mattioli,M., Svitkin,Y. & Sonenberg,N. La autoantigen is necessary for optimal function of the poliovirus and hepatitis C virus internal ribosome entry site in vivo and in vitro. *Mol. Cell. Biol.* **24**, 6861-6870 (2004).

18. Lu,H., Li,W., Noble,W.S., Payan,D. & Anderson,D.C. Riboproteomics of the hepatitis C virus internal ribosomal entry site. *J. Proteome. Res.* **3**, 949-957 (2004).

19. Spirin,A.S. Ribosomes. Springer, (2000).

20. Nierhaus,K.H. The allosteric three-site model for the ribosomal elongation cycle: features and future. *Biochemistry* **29**, 4997-5008 (1990).

21. Rodnina,M.V. & Wintermeyer,W. Fidelity of aminoacyl-tRNA selection on the ribosome: kinetic and structural mechanisms. *Annu. Rev. Biochem.* **70**, 415-435 (2001).

22. Ogle,J.M. & Ramakrishnan,V. Structural insights into translational fidelity. *Annu. Rev. Biochem.* **74**, 129-177 (2005).

23. Rodnina,M.V., Gromadski,K.B., Kothe,U. & Wieden,H.J. Recognition and selection of tRNA in translation. *FEBS Lett.* **579**, 938-942 (2005).

24. Stark,H., Rodnina,M.V., Rinke-Appel,J., Brimacombe,R., Wintermeyer,W. & van Heel,M. Visualization of elongation factor Tu on the Escherichia coli ribosome. *Nature* **389**, 403-406 (1997).

25. Stark,H., Rodnina,M.V., Wieden,H.J., Zemlin,F., Wintermeyer,W. & van Heel,M. Ribosome interactions of aminoacyl-tRNA and elongation factor Tu in the codon-recognition complex. *Nat. Struct. Biol.* **9**, 849-854 (2002).

26. Pape,T., Wintermeyer,W. & Rodnina,M. Induced fit in initial selection and proofreading of aminoacyl-tRNA on the ribosome. *EMBO J.* **18**, 3800-3807 (1999).

27. Thompson,R.C. & Karim,A.M. The accuracy of protein biosynthesis is limited by its speed: high fidelity selection by ribosomes of aminoacyl-tRNA ternary complexes containing GTP[γ S]. *Proc. Natl. Acad. Sci. U. S. A.* **79**, 4922-4926 (1982).

28. Karim,A.M. & Thompson,R.C. Guanosine 5'-O-(3-thiotriphosphate) as an analog of GTP in protein biosynthesis. The effects of temperature and polycations on the accuracy of initial recognition of aminoacyl-tRNA ternary complexes by ribosomes. *J. Biol. Chem.* **261**, 3238-3243 (1986).

29. Wintermeyer,W., Peske,F., Beringer,M., Gromadski,K.B., Savelsbergh,A. & Rodnina,M.V. Mechanisms of elongation on the ribosome: dynamics of a macromolecular machine. *Biochem. Soc. Trans.* **32**, 733-737 (2004).

30. Ogle,J.M., Brodersen,D.E., Clemons,W.M., Jr., Tarry,M.J., Carter,A.P. & Ramakrishnan,V. Recognition of cognate transfer RNA by the 30S ribosomal subunit. *Science* **292**, 897-902 (2001).

31. Rodnina,M.V., Fricke,R., Kuhn,L. & Wintermeyer,W. Codon-dependent conformational change of elongation factor Tu preceding GTP hydrolysis on the ribosome. *EMBO J.* **14**, 2613-2619 (1995).

32. Rodnina,M.V., Pape,T., Fricke,R., Kuhn,L. & Wintermeyer,W. Initial binding of the elongation factor Tu.GTP.aminoacyl-tRNA complex preceding codon recognition on the ribosome. *J. Biol. Chem.* **271**, 646-652 (1996).

33. Nissen,P., Kjeldgaard,M., Thirup,S., Polekhina,G., Reshetnikova,L., Clark,B.F. & Nyborg,J. Crystal structure of the ternary complex of Phe-tRNAPhe, EF-Tu, and a GTP analog. *Science* **270**, 1464-1472 (1995).

34. Abel,K., Yoder,M.D., Hilgenfeld,R. & Jurnak,F. An α to β conformational switch in EF-Tu. *Structure.* **4**, 1153-1159 (1996).

35. Romero,G., Chau,V. & Biltonen,R.L. Kinetics and thermodynamics of the interaction of elongation factor Tu with elongation factor Ts, guanine nucleotides, and aminoacyl-tRNA. *J. Biol. Chem.* **260**, 6167-6174 (1985).

36. Pape,T., Wintermeyer,W. & Rodnina,M.V. Complete kinetic mechanism of elongation factor Tu-dependent binding of aminoacyl-tRNA to the A site of the E. coli ribosome. *EMBO J.* **17**, 7490-7497 (1998).

37. Sanbonmatsu,K.Y., Joseph,S. & Tung,C.S. Simulating movement of tRNA into the ribosome during decoding. *Proc. Natl. Acad. Sci. U. S. A.* **102**, 15854-15859 (2005).

38. Green,R., Switzer,C. & Noller,H.F. Ribosome-catalyzed peptide-bond formation with an A-site substrate covalently linked to 23S ribosomal RNA. *Science* **280**, 286-289 (1998).

39. Schmeing,T.M., Huang,K.S., Strobel,S.A. & Steitz,T.A. An induced-fit mechanism to promote peptide bond formation and exclude hydrolysis of peptidyl-tRNA. *Nature* **438**, 520-524 (2005).

40. Nissen,P., Hansen,J., Ban,N., Moore,P.B. & Steitz,T.A. The structural basis of ribosome activity in peptide bond synthesis. *Science* **289**, 920-930 (2000).

41. Valle,M., Zavialov,A., Li,W., Stagg,S.M., Sengupta,J., Nielsen,R.C., Nissen,P., Harvey,S.C., Ehrenberg,M. & Frank,J. Incorporation of aminoacyl-tRNA into the ribosome as seen by cryo-electron microscopy. *Nat. Struct. Biol.* **10**, 899-906 (2003).

42. Yarus,M., Valle,M. & Frank,J. A twisted tRNA intermediate sets the threshold for decoding. *RNA*. **9**, 384-385 (2003).

43. Ban,N., Nissen,P., Hansen,J., Moore,P.B. & Steitz,T.A. The complete atomic structure of the large ribosomal subunit at 2.4 Å resolution. *Science* **289**, 905-920 (2000).

44. Yusupov,M.M., Yusupova,G.Z., Baucom,A., Lieberman,K., Earnest,T.N., Cate,J.H. & Noller,H.F. Crystal structure of the ribosome at 5.5 Å resolution. *Science* **292**, 883-896 (2001).

45. Steitz,T.A. & Moore,P.B. RNA, the first macromolecular catalyst: the ribosome is a ribozyme. *Trends Biochem. Sci.* **28**, 411-418 (2003).

46. Katunin,V.I., Muth,G.W., Strobel,S.A., Wintermeyer,W. & Rodnina,M.V. Important contribution to catalysis of peptide bond formation by a single ionizing group within the ribosome. *Mol. Cell* **10**, 339-346 (2002).

47. Weinger,J.S., Parnell,K.M., Dorner,S., Green,R. & Strobel,S.A. Substrate-assisted catalysis of peptide bond formation by the ribosome. *Nat. Struct. Mol. Biol.* **11**, 1101-1106 (2004).

48. Trobro,S. & Aqvist,J. Mechanism of peptide bond synthesis on the ribosome. *Proc. Natl. Acad. Sci. U. S. A.* **102**, 12395-12400 (2005).

49. Sievers,A., Beringer,M., Rodnina,M.V. & Wolfenden,R. The ribosome as an entropy trap. *Proc. Natl. Acad. Sci. U. S. A.* **101**, 7897-7901 (2004).

50. Beringer,M., Bruell,C., Xiong,L., Pfister,P., Bieling,P., Katunin,V.I., Mankin,A.S., Bottger,E.C. & Rodnina,M.V. Essential mechanisms in the catalysis of peptide bond formation on the ribosome. *J. Biol. Chem.* **280**, 36065-36072 (2005).

51. Erlacher,M.D., Lang,K., Wotzel,B., Rieder,R., Micura,R. & Polacek,N. Efficient ribosomal peptidyl transfer critically relies on the presence of the ribose 2'-OH at A2451 of 23S rRNA. *J. Am. Chem. Soc.* **128**, 4453-4459 (2006).

52. Quiggle,K., Kumar,G., Ott,T.W., Ryu,E.K. & Chladek,S. Donor site of ribosomal peptidyltransferase: investigation of substrate specificity using 2'(3')-O-(N-acylaminoacyl)dinucleoside phosphates as models of the 3' terminus of N-acylaminoacyl transfer ribonucleic acid. *Biochemistry* **20**, 3480-3485 (1981).

53. Hausner,T.P., Geigenmuller,U. & Nierhaus,K.H. The allosteric three-site model for the ribosomal elongation cycle. New insights into the inhibition mechanisms of aminoglycosides, thiostrepton, and viomycin. *J. Biol. Chem.* **263**, 13103-13111 (1988).

54. Gnirke,A., Geigenmuller,U., Rheinberger,H.J. & Nierhaus,L.H. The allosteric three-site model for the ribosomal elongation cycle. Analysis with a heteropolymeric mRNA. *J. Biol. Chem.* **264**, 7291-7301 (1989).

55. Moazed,D. & Noller,H.F. Intermediate states in the movement of transfer RNA in the ribosome. *Nature* **342**, 142-148 (1989).

56. Sharma,D., Southworth,D.R. & Green,R. EF-G-independent reactivity of a pre-translocation-state ribosome complex with the aminoacyl tRNA substrate puromycin supports an intermediate (hybrid) state of tRNA binding. *RNA*. **10**, 102-113 (2004).

57. Blanchard,S.C., Kim,H.D., Gonzalez,R.L., Jr., Puglisi,J.D. & Chu,S. tRNA dynamics on the ribosome during translation. *Proc. Natl. Acad. Sci. U. S. A.* **101**, 12893-12898 (2004).

58. Agrawal,R.K., Penczek,P., Grassucci,R.A., Burkhardt,N., Nierhaus,K.H. & Frank,J. Effect of buffer conditions on the position of tRNA on the 70 S ribosome as visualized by cryoelectron microscopy. *J. Biol. Chem.* **274**, 8723-8729 (1999).

59. Spahn,C.M., Gomez-Lorenzo,M.G., Grassucci,R.A., Jorgensen,R., Andersen,G.R., Beckmann,R., Penczek,P.A., Ballesta,J.P. & Frank,J. Domain movements of elongation factor eEF2 and the eukaryotic 80S ribosome facilitate tRNA translocation. *EMBO J.* **23**, 1008-1019 (2004).

60. Puglisi,J.D., Blanchard,S.C. & Green,R. Approaching translation at atomic resolution. *Nat. Struct. Biol.* **7**, 855-861 (2000).

61. Moore,P.B. Molecular mimicry in protein synthesis? *Science* **270**, 1453-1454 (1995).

62. Valle,M., Zavialov,A., Sengupta,J., Rawat,U., Ehrenberg,M. & Frank,J. Locking and unlocking of ribosomal motions. *Cell* **114**, 123-134 (2003).

63. Kapp,L.D. & Lorsch,J.R. The molecular mechanics of eukaryotic translation. *Annu. Rev. Biochem.* **73**, 657-704 (2004).

64. Arkov,A.L., Freistroffer,D.V., Ehrenberg,M. & Murgola,E.J. Mutations in RNAs of both ribosomal subunits cause defects in translation termination. *EMBO J.* **17**, 1507-1514 (1998).

65. Caskey,C.T., Beaudet,A.L., Scolnick,E.M. & Rosman,M. Hydrolysis of fMet-tRNA by peptidyl transferase. *Proc. Natl. Acad. Sci. U. S. A.* **68**, 3163-3167 (1971).

66. Scolnick,E., Tompkins,R., Caskey,T. & Nirenberg,M. Release factors differing in specificity for terminator codons. *Proc. Natl. Acad. Sci. U. S. A.* **61**, 768-774 (1968).

67. Freistroffer,D.V., Pavlov,M.Y., MacDougall,J., Buckingham,R.H. & Ehrenberg,M. Release factor RF3 in E.coli accelerates the dissociation of release factors RF1 and RF2 from the ribosome in a GTP-dependent manner. *EMBO J.* **16**, 4126-4133 (1997).

68. Grentzmann,G., Brechemier-Baey,D., Heurgue,V., Mora,L. & Buckingham,R.H. Localization and characterization of the gene encoding release factor RF3 in Escherichia coli. *Proc. Natl. Acad. Sci. U. S. A.* **91**, 5848-5852 (1994).

69. Kristensen,O., Reshetnikova,L., Nissen,P., Siboska,G., Thirup,S. & Nyborg,J. Isolation, crystallization and X-ray analysis of the quaternary complex of Phe-tRNA(Phe), EF-Tu, a GTP analog and kirromycin. *FEBS Lett.* **399**, 59-62 (1996).

70. Hansson,S., Singh,R., Gudkov,A.T., Liljas,A. & Logan,D.T. Crystal structure of a mutant elongation factor G trapped with a GTP analogue. *FEBS Lett.* **579**, 4492-4497 (2005).

71. Konecki,D.S., Aune,K.C., Tate,W. & Caskey,C.T. Characterization of reticulocyte release factor. *J. Biol. Chem.* **252**, 4514-4520 (1977).

72. Song,H., Mugnier,P., Das,A.K., Webb,H.M., Evans,D.R., Tuite,M.F., Hemmings,B.A. & Barford,D. The crystal structure of human eukaryotic release factor eRF1-mechanism of stop codon recognition and peptidyl-tRNA hydrolysis. *Cell* **100**, 311-321 (2000).

73. Vestergaard,B., Van,L.B., Andersen,G.R., Nyborg,J., Buckingham,R.H. & Kjeldgaard,M. Bacterial polypeptide release factor RF2 is structurally distinct from eukaryotic eRF1. *Mol. Cell* **8**, 1375-1382 (2001).

74. Klaholz,B.P., Pape,T., Zavialov,A.V., Myasnikov,A.G., Orlova,E.V., Vestergaard,B., Ehrenberg,M. & van Heel,M. Structure of the Escherichia coli ribosomal termination complex with release factor 2. *Nature* **421**, 90-94 (2003).

75. Rawat,U.B., Zavialov,A.V., Sengupta,J., Valle,M., Grassucci,R.A., Linde,J., Vestergaard,B., Ehrenberg,M. & Frank,J. A cryo-electron microscopic study of ribosome-bound termination factor RF2. *Nature* **421**, 87-90 (2003).

76. Ito,K., Ebihara,K. & Nakamura,Y. The stretch of C-terminal acidic amino acids of translational release factor eRF1 is a primary binding site for eRF3 of fission yeast. *RNA.* **4**, 958-972 (1998).

77. Stansfield,I., Jones,K.M., Kushnirov,V.V., Dagkesamanskaya,A.R., Poznyakovski,A.I., Paushkin,S.V., Nierras,C.R., Cox,B.S., Ter Avanesyan,M.D. & Tuite,M.F. The products of the SUP45 (eRF1) and SUP35 genes interact to mediate translation termination in Saccharomyces cerevisiae. *EMBO J.* **14**, 4365-4373 (1995).

78. Ito,K., Ebihara,K., Uno,M. & Nakamura,Y. Conserved motifs in prokaryotic and eukaryotic polypeptide release factors: tRNA-protein mimicry hypothesis. *Proc. Natl. Acad. Sci. U. S. A.* **93**, 5443-5448 (1996).

79. Ito,K., Uno,M. & Nakamura,Y. A tripeptide 'anticodon' deciphers stop codons in messenger RNA. *Nature* **403**, 680-684 (2000).

80. Uno,M., Ito,K. & Nakamura,Y. Polypeptide release at sense and noncognate stop codons by localized charge-exchange alterations in translational release factors. *Proc. Natl. Acad. Sci. U. S. A.* **99**, 1819-1824 (2002).

81. Ito,K., Frolova,L., Seit-Nebi,A., Karamyshev,A., Kisselev,L. & Nakamura,Y. Omnipotent decoding potential resides in eukaryotic translation termination factor eRF1 of variant-code organisms and is modulated by the interactions of amino acid sequences within domain 1. *Proc. Natl. Acad. Sci. U. S. A.* **99**, 8494-8499 (2002).

82. Lozupone,C.A., Knight,R.D. & Landweber,L.F. The molecular basis of nuclear genetic code change in ciliates. *Curr. Biol.* **11**, 65-74 (2001).

83. Scarlett,D.J., McCaughan,K.K., Wilson,D.N. & Tate,W.P. Mapping functionally important motifs SPF and GGQ of the decoding release factor RF2 to the Escherichia coli ribosome by hydroxyl radical footprinting. Implications for macromolecular mimicry and structural changes in RF2. *J. Biol. Chem.* **278**, 15095-15104 (2003).

84. Seit-Nebi,A., Frolova,L., Justesen,J. & Kisselev,L. Class-1 translation termination factors: invariant GGQ minidomain is essential for release activity and ribosome binding but not for stop codon recognition. *Nucleic Acids Res.* **29**, 3982-3987 (2001).

85. Frolova,L.Y., Tsivkovskii,R.Y., Sivolobova,G.F., Oparina,N.Y., Serpinsky,O.I., Blinov,V.M., Tatkov,S.I. & Kisselev,L.L. Mutations in the highly conserved GGQ motif of class 1 polypeptide release factors abolish

ability of human eRF1 to trigger peptidyl-tRNA hydrolysis. *RNA.* **5**, 1014-1020 (1999).

86. Zavialov,A.V., Buckingham,R.H. & Ehrenberg,M. A posttermination ribosomal complex is the guanine nucleotide exchange factor for peptide release factor RF3. *Cell* **107**, 115-124 (2001).

87. Farabaugh,P.J. Programmed translational frameshifting. *Annu. Rev. Genet.* **30**, 507-528 (1996).

88. Gesteland,R.F. & Atkins,J.F. Recoding: dynamic reprogramming of translation. *Annu. Rev. Biochem.* **65**, 741-768 (1996).

89. Allmang,C. & Krol,A. Selenoprotein synthesis: UGA does not end the story. *Biochimie* (2006).

90. Hubert,N., Walczak,R., Sturchler,C., Myslinski,E., Schuster,C., Westhof,E., Carbon,P. & Krol,A. RNAs mediating cotranslational insertion of selenocysteine in eukaryotic selenoproteins. *Biochimie* **78**, 590-596 (1996).

91. Krzycki,J.A. The direct genetic encoding of pyrrolysine. *Curr. Opin. Microbiol.* **8**, 706-712 (2005).

92. Beier,H. & Grimm,M. Misreading of termination codons in eukaryotes by natural nonsense suppressor tRNAs. *Nucleic Acids Res.* **29**, 4767-4782 (2001).

93. Nilsson,M. & Ryden-Aulin,M. Glutamine is incorporated at the nonsense codons UAG and UAA in a suppressor-free Escherichia coli strain. *Biochim. Biophys. Acta* **1627**, 1-6 (2003).

94. Bock,A. Molecular biology. Invading the genetic code. *Science* **292**, 453-454 (2001).

95. Kuchino,Y., Hanyu,N., Tashiro,F. & Nishimura,S. Tetrahymena thermophila glutamine tRNA and its gene that corresponds to UAA termination codon. *Proc. Natl. Acad. Sci. U. S. A* **82**, 4758-4762 (1985).

96. Hanyu,N., Kuchino,Y., Nishimura,S. & Beier,H. Dramatic events in ciliate evolution: alteration of UAA and UAG termination codons to glutamine codons due to anticodon mutations in two Tetrahymena tRNAs. *EMBO J.* **5**, 1307-1311 (1986).

97. Kwok,Y. & Wong,J.T. Evolutionary relationship between Halobacterium cutirubrum and eukaryotes determined by use of aminoacyl-tRNA synthetases as phylogenetic probes. *Can. J. Biochem.* **58**, 213-218 (1980).

98. Weiss,W.A. & Friedberg,E.C. Normal yeast tRNA(CAGGln) can suppress amber codons and is encoded by an essential gene. *J. Mol. Biol.* **192**, 725-735 (1986).

99. Weiss,W.A., Edelman,I., Culbertson,M.R. & Friedberg,E.C. Physiological levels of normal tRNA(CAGGln) can effect partial suppression of amber mutations in the yeast Saccharomyces cerevisiae. *Proc. Natl. Acad. Sci. U. S. A.* **84**, 8031-8034 (1987).

100. Martin,R., Phillips-Jones,M.K., Watson,F.J. & Hill,L.S. Codon context effects on nonsense suppression in human cells. *Biochem. Soc. Trans.* **21**, 846-851 (1993).

101. Valente,L. & Kinzy,T.G. Yeast as a sensor of factors affecting the accuracy of protein synthesis. *Cell Mol. Life Sci.* **60**, 2115-2130 (2003).

102. Marra,M.A., Jones,S.J., Astell,C.R., Holt,R.A., Brooks-Wilson,A., Butterfield,Y.S., Khattra,J., Asano,J.K., Barber,S.A., Chan,S.Y., Cloutier,A., Coughlin,S.M., Freeman,D., Girn,N., Griffith,O.L., Leach,S.R., Mayo,M., McDonald,H., Montgomery,S.B., Pandoh,P.K., Petrescu,A.S., Robertson,A.G., Schein,J.E., Siddiqui,A., Smailus,D.E., Stott,J.M., Yang,G.S., Plummer,F., Andonov,A., Artsob,H., Bastien,N., Bernard,K., Booth,T.F., Bowness,D., Czub,M., Drebot,M., Fernando,L., Flick,R., Garbutt,M., Gray,M., Grolla,A., Jones,S., Feldmann,H., Meyers,A., Kabani,A., Li,Y., Normand,S., Stroher,U., Tipples,G.A., Tyler,S., Vogrig,R., Ward,D., Watson,B., Brunham,R.C., Krajden,M., Petric,M., Skowronski,D.M., Upton,C. & Roper,R.L. The Genome sequence of the SARS-associated coronavirus. *Science* **300**, 1399-1404 (2003).

103. Jacks,T., Power,M.D., Masiarz,F.R., Luciw,P.A., Barr,P.J. & Varmus,H.E. Characterization of ribosomal frameshifting in HIV-1 gag-pol expression. *Nature* **331**, 280-283 (1988).

104. Somogyi,P., Jenner,A.J., Brierley,I. & Inglis,S.C. Ribosomal pausing during translation of an RNA pseudoknot. *Mol. Cell. Biol.* **13**, 6931-6940 (1993).

105. Dinman,J.D., Icho,T. & Wickner,R.B. A -1 ribosomal frameshift in a double-stranded RNA virus of yeast forms a gag-pol fusion protein. *Proc. Natl. Acad. Sci. U. S. A.* **88**, 174-178 (1991).

106. Jacobs,J.L., Belew T.A. & Dinman,J.D. www.dinmanlab.umd.edu/prfdb/. Unpublished .

107. Manktelow,E., Shigemoto,K. & Brierley,I. Characterization of the frameshift signal of Edr, a mammalian example of programmed -1 ribosomal frameshifting. *Nucleic Acids Res.* **33**, 1553-1563 (2005).

108. Shigemoto,K., Brennan,J., Walls,E., Watson,C.J., Stott,D., Rigby,P.W. & Reith,A.D. Identification and characterisation of a developmentally regulated mammalian gene that utilises -1 programmed ribosomal frameshifting. *Nucleic Acids Res.* **29**, 4079-4088 (2001).

109. Levitin,F., Baruch,A., Weiss,M., Stiegman,K., Hartmann,M.L., Yoeli-Lerner,M., Ziv,R., Zrihan-Licht,S., Shina,S., Gat,A., Lifschitz,B., Simha,M., Stadler,Y., Cholostoy,A., Gil,B., Greaves,D., Keydar,I., Zaretsky,J., Smorodinsky,N. & Wreschner,D.H. A novel protein derived from the MUC1 gene by alternative splicing and frameshifting. *J. Biol. Chem.* **280**, 10655-10663 (2005).

110. Wills,N.M., Moore,B., Hammer,A., Gesteland,R.F. & Atkins,J.F. A functional -1 ribosomal frameshift signal in the human paraneoplastic Ma3 gene. *J. Biol. Chem.* **281**, 7082-7088 (2006).

111. Harger,J.W., Meskauskas,A., Nielsen,J., Justice,M.C. & Dinman,J.D. Ty1 retrotransposition and programmed +1 ribosomal frameshifting require the integrity of the protein synthetic translocation step. *Virology* **286**, 216-224 (2001).

112. Hudak,K.A., Hammell,A.B., Yasenchak,J., Tumer,N.E. & Dinman,J.D. A C-terminal deletion mutant of pokeweed antiviral protein inhibits programmed +1 ribosomal frameshifting and Ty1 retrotransposition without depurinating the sarcin/ricin loop of rRNA. *Virology* **279**, 292-301 (2001).

113. Tumer,N.E., Parikh,B.A., Li,P. & Dinman,J.D. The pokeweed antiviral protein specifically inhibits Ty1-directed +1 ribosomal frameshifting and retrotransposition in Saccharomyces cerevisiae. *J. Virol.* **72**, 1036-1042 (1998).

114. Weiss,R. & Gallant,J. Mechanism of ribosome frameshifting during translation of the genetic code. *Nature* **302**, 389-393 (1983).

115. Dinman,J.D., Richter,S., Plant,E.P., Taylor,R.C., Hammell,A.B. & Rana,T.M. The frameshift signal of HIV-1 involves a potential intramolecular triplex RNA structure. *Proc. Natl. Acad. Sci. U. S. A.* **99**, 5331-5336 (2002).

116. Harger,J.W., Meskauskas,A. & Dinman,J.D. An "integrated model" of programmed ribosomal frameshifting. *Trends Biochem. Sci.* **27**, 448-454 (2002).

117. Plant,E.P., Perez-Alvarado,G.C., Jacobs,J.L., Mukhopadhyay,B., Hennig,M. & Dinman,J.D. A three-stemmed mRNA pseudoknot in the SARS coronavirus frameshift signal. *PLoS. Biol.* **3**, e172 (2005).

118. Yusupova,G.Z., Yusupov,M.M., Cate,J.H. & Noller,H.F. The path of messenger RNA through the ribosome. *Cell* **106**, 233-241 (2001).

119. Plant,E.P., Jacobs,K.L., Harger,J.W., Meskauskas,A., Jacobs,J.L., Baxter,J.L., Petrov,A.N. & Dinman,J.D. The 9-Å solution: how mRNA pseudoknots promote efficient programmed -1 ribosomal frameshifting. *RNA.* **9**, 168-174 (2003).

120. Baranov,P.V., Gesteland,R.F. & Atkins,J.F. P-site tRNA is a crucial initiator of ribosomal frameshifting. *RNA.* **10**, 221-230 (2004).

121. Hansen,T.M., Baranov,P.V., Ivanov,I.P., Gesteland,R.F. & Atkins,J.F. Maintenance of the correct open reading frame by the ribosome. *EMBO Rep.* **4**, 499-504 (2003).

122. Farabaugh,P.J., Zhao,H. & Vimaladithan,A. A novel programed frameshift expresses the POL3 gene of retrotransposon Ty3 of yeast: frameshifting without tRNA slippage. *Cell* **74**, 93-103 (1993).

123. Wang,X., Wong,S.M. & Liu,D.X. Identification of Hepta- and Octo-Uridine stretches as sole signals for programmed +1 and -1 ribosomal frameshifting during translation of SARS-CoV ORF 3a variants. *Nucleic Acids Res.* **34**, 1250-1260 (2006).

124. Matsufuji,S., Matsufuji,T., Miyazaki,Y., Murakami,Y., Atkins,J.F., Gesteland,R.F. & Hayashi,S. Autoregulatory frameshifting in decoding mammalian ornithine decarboxylase antizyme. *Cell* **80**, 51-60 (1995).

125. Craigen,W.J. & Caskey,C.T. Expression of peptide chain release factor 2 requires high-efficiency frameshift. *Nature* **322**, 273-275 (1986).

126. Ivanov,I.P., Gesteland,R.F. & Atkins,J.F. Evolutionary specialization of recoding: frameshifting in the expression of S. cerevisiae antizyme mRNA is via an atypical antizyme shift site but is still +1. *RNA.* **12**, 332-337 (2006).

127. Shah,A.A., Giddings,M.C., Parvaz,J.B., Gesteland,R.F., Atkins,J.F. & Ivanov,I.P. Computational identification of putative programmed translational frameshift sites. *Bioinformatics.* **18**, 1046-1053 (2002).

128. Peter,K., Lindsley,D., Peng,L. & Gallant,J.A. Context rules of rightward overlapping reading. *New Biol.* **4**, 520-526 (1992).

129. Belcourt,M.F. & Farabaugh,P.J. Ribosomal frameshifting in the yeast retrotransposon Ty: tRNAs induce slippage on a 7 nucleotide minimal site. *Cell* **62**, 339-352 (1990).

130. Lindsley,D. & Gallant,J. On the directional specificity of ribosome frameshifting at a "hungry" codon. *Proc. Natl. Acad. Sci. U. S. A.* **90**, 5469-5473 (1993).

131. Weiss,R.B. & Gallant,J.A. Frameshift suppression in aminoacyl-tRNA limited cells. *Genetics* **112**, 727-739 (1986).

132. Curran,J.F. Analysis of effects of tRNA:message stability on frameshift frequency at the Escherichia coli RF2 programmed frameshift site. *Nucleic Acids Res.* **21**, 1837-1843 (1993).

133. Dinman,J.D. & Wickner,R.B. Ribosomal frameshifting efficiency and gag/gag-pol ratio are critical for yeast M1 double-stranded RNA virus propagation. *J. Virol.* **66**, 3669-3676 (1992).

134. Clare,J.J., Belcourt,M. & Farabaugh,P.J. Efficient translational frameshifting occurs within a conserved sequence of the overlap between the two genes of a yeast Ty1 transposon. *Proc. Natl. Acad. Sci. U. S. A.* **85**, 6816-6820 (1988).

135. Childs,A.C., Mehta,D.J. & Gerner,E.W. Polyamine-dependent gene expression. *Cell. Mol. Life Sci.* **60**, 1394-1406 (2003).

136. Heller,J.S., Fong,W.F. & Canellakis,E.S. Induction of a protein inhibitor to ornithine decarboxylase by the end products of its reaction. *Proc. Natl. Acad. Sci. U. S. A.* **73**, 1858-1862 (1976).

137. Hayashi,S. & Murakami,Y. Rapid and regulated degradation of ornithine decarboxylase. *Biochem. J.* **306 (Pt 1)**, 1-10 (1995).

138. Murakami,Y., Matsufuji,S., Kameji,T., Hayashi,S., Igarashi,K., Tamura,T., Tanaka,K. & Ichihara,A. Ornithine decarboxylase is degraded by the 26S proteasome without ubiquitination. *Nature* **360**, 597-599 (1992).

139. Balasundaram,D., Dinman,J.D., Tabor,C.W. & Tabor,H. SPE1 and SPE2: two essential genes in the biosynthesis of polyamines that modulate +1 ribosomal frameshifting in Saccharomyces cerevisiae. *J. Bacteriol.* **176**, 7126-7128 (1994).

140. Balasundaram,D., Dinman,J.D., Wickner,R.B., Tabor,C.W. & Tabor,H. Spermidine deficiency increases +1 ribosomal frameshifting efficiency and inhibits Ty1 retrotransposition in Saccharomyces cerevisiae. *Proc. Natl. Acad. Sci. U. S. A.* **91**, 172-176 (1994).

141. Plant,E.P., Wang,P., Jacobs,J.L. & Dinman,J.D. A programmed -1 ribosomal frameshift signal can function as a cis-acting mRNA destabilizing element. *Nucleic Acids Res.* **32**, 784-790 (2004).

142. Lelivelt,M.J. & Culbertson,M.R. Yeast Upf proteins required for RNA surveillance affect global expression of the yeast transcriptome. *Mol. Cell. Biol.* **19**, 6710-6719 (1999).

143. Mendell,J.T., Sharifi,N.A., Meyers,J.L., Martinez-Murillo,F. & Dietz,H.C. Nonsense surveillance regulates expression of diverse classes of mammalian transcripts and mutes genomic noise. *Nat. Genet.* **36**, 1073-1078 (2004).

144. He,F., Li,X., Spatrick,P., Casillo,R., Dong,S. & Jacobson,A. Genome-wide analysis of mRNAs regulated by the nonsense-mediated and 5' to 3' mRNA decay pathways in yeast. *Mol. Cell* **12**, 1439-1452 (2003).

145. Sun,X., Moriarty,P.M. & Maquat,L.E. Nonsense-mediated decay of glutathione peroxidase 1 mRNA in the cytoplasm depends on intron position. *EMBO J.* **19**, 4734-4744 (2000).

146. Kim,V.N., Kataoka,N. & Dreyfuss,G. Role of the nonsense-mediated decay factor hUpf3 in the splicing-dependent exon-exon junction complex. *Science* **293**, 1832-1836 (2001).

147. Kashima,I., Yamashita,A., Izumi,N., Kataoka,N., Morishita,R., Hoshino,S., Ohno,M., Dreyfuss,G. & Ohno,S. Binding of a novel SMG-1-Upf1-eRF1-eRF3 complex (SURF) to the exon junction complex triggers Upf1 phosphorylation and nonsense-mediated mRNA decay. *Genes Dev.* **20**, 355-367 (2006).

148. Maquat,L.E. Nonsense-mediated mRNA decay: splicing, translation and mRNP dynamics. *Nat. Rev. Mol. Cell Biol.* **5**, 89-99 (2004).

149. Jimenez,A. & Vazquez,D. Quantitative binding of antibiotics to ribosomes from a yeast mutant altered on the peptidyl-transferase center. *Eur. J. Biochem.* **54**, 483-492 (1975).

150. Schindler,D., Grant,P. & Davies,J. Trichodermin resistance--mutation affecting eukaryotic ribosomes. *Nature* **248**, 535-536 (1974).

151. Wickner,R.B. Chromosomal and nonchromosomal mutations affecting the "killer character" of Saccharomyces cerevisiae. *Genetics* **76**, 423-432 (1974).

152. Fried,H.M. & Warner,J.R. Cloning of yeast gene for trichodermin resistance and ribosomal protein L3. *Proc. Natl. Acad. Sci. U. S. A.* **78**, 238-242 (1981).

153. Wickner,R.B., Ridley,S.P., Fried,H.M. & Ball,S.G. Ribosomal protein L3 is involved in replication or maintenance of the killer double-stranded RNA genome of Saccharomyces cerevisiae. *Proc. Natl. Acad. Sci. U. S. A.* **79**, 4706-4708 (1982).

154. Schulze,H. & Nierhaus,K.H. Minimal set of ribosomal components for reconstitution of the peptidyltransferase activity. *EMBO J.* **1**, 609-613 (1982).

155. Tumminia,S.J., Hellmann,W., Wall,J.S. & Boublik,M. Visualization of protein-nucleic acid interactions involved in the *in vitro* assembly of the *Escherichia coli* 50S ribosomal subunit. *J. Mol. Biol.* **235**, 1239-1250 (1994).

156. Nowotny,V. & Nierhaus,K.H. Initiator proteins for the assembly of the 50S subunit from Escherichia coli ribosomes. *Proc. Natl. Acad. Sci. U. S. A.* **79**, 7238-7242 (1982).

157. Peltz,S.W., Hammell,A.B., Cui,Y., Yasenchak,J., Puljanowski,L. & Dinman,J.D. Ribosomal protein L3 mutants alter translational fidelity and

promote rapid loss of the yeast killer virus. *Mol. Cell. Biol.* **19**, 384-391 (1999).

158. Meskauskas,A., Harger,J.W., Jacobs,K.L. & Dinman,J.D. Decreased peptidyltransferase activity correlates with increased programmed -1 ribosomal frameshifting and viral maintenance defects in the yeast Saccharomyces cerevisiae. *RNA.* **9**, 982-992 (2003).

159. Meskauskas,A., Baxter,J.L., Carr,E.A., Yasenchak,J., Gallagher,J.E., Baserga,S.J. & Dinman,J.D. Delayed rRNA processing results in significant ribosome biogenesis and functional defects. *Mol. Cell. Biol.* **23**, 1602-1613 (2003).

160. Dinman,J.D., Ruiz-Echevarria,M.J., Czaplinski,K. & Peltz,S.W. Peptidyl-transferase inhibitors have antiviral properties by altering programmed -1 ribosomal frameshifting efficiencies: development of model systems. *Proc. Natl. Acad. Sci. U. S. A.* **94**, 6606-6611 (1997).

161. Dinman,J.D. & Wickner,R.B. Translational maintenance of frame: mutants of Saccharomyces cerevisiae with altered -1 ribosomal frameshifting efficiencies. *Genetics* **136**, 75-86 (1994).

162. Struhl,K. Histone acetylation and transcriptional regulatory mechanisms. *Genes Dev.* **12**, 599-606 (1998).

163. Vannier,D., Balderes,D. & Shore,D. Evidence that the transcriptional regulators SIN3 and RPD3, and a novel gene (SDS3) with similar functions, are involved in transcriptional silencing in S. cerevisiae. *Genetics* **144**, 1343-1353 (1996).

164. Rundlett,S.E., Carmen,A.A., Kobayashi,R., Bavykin,S., Turner,B.M. & Grunstein,M. HDA1 and RPD3 are members of distinct yeast histone deacetylase complexes that regulate silencing and transcription. *Proc. Natl. Acad. Sci. U. S. A.* **93**, 14503-14508 (1996).

165. Sun,Z.W. & Hampsey,M. A general requirement for the Sin3-Rpd3 histone deacetylase complex in regulating silencing in Saccharomyces cerevisiae. *Genetics* **152**, 921-932 (1999).

166. Cate,J.H., Yusupov,M.M., Yusupova,G.Z., Earnest,T.N. & Noller,H.F. X-ray crystal structures of 70S ribosome functional complexes. *Science* **285**, 2095-2104 (1999).

167. Klein,D.J., Moore,P.B. & Steitz,T.A. The roles of ribosomal proteins in the structure assembly, and evolution of the large ribosomal subunit. *J. Mol. Biol.* **340**, 141-177 (2004).

168. Pringle,M., Poehlsgaard,J., Vester,B. & Long,K.S. Mutations in ribosomal protein L3 and 23S ribosomal RNA at the peptidyl transferase centre are

associated with reduced susceptibility to tiamulin in Brachyspira spp. isolates. *Mol. Microbiol.* **54**, 1295-1306 (2004).

169. Meskauskas,A. & Dinman,J.D. Ribosomal protein L5 helps anchor peptidyl-tRNA to the P-site in Saccharomyces cerevisiae. *RNA.* **7**, 1084-1096 (2001).

170. Ito,H., Fukuda,Y., Murata,K. & Kimura,A. Transformation of intact yeast cells treated with alkali cations. *J. Bacteriol.* **153**, 163-168 (1983).

171. Wickner,R.B. & Leibowitz,M.J. Chromosomal genes essential for replication of a double-stranded RNA plasmid of Saccharomyces cerevisiae: the killer character of yeast. *J. Mol. Biol.* **105**, 427-443 (1976).

172. Carr-Schmid,A., Durko,N., Cavallius,J., Merrick,W.C. & Kinzy,T.G. Mutations in a GTP-binding motif of eukaryotic elongation factor 1A reduce both translational fidelity and the requirement for nucleotide exchange. *J. Biol. Chem.* **274**, 30297-30302 (1999).

173. Mereau,A., Fournier,R., Gregoire,A., Mougin,A., Fabrizio,P., Luhrmann,R. & Branlant,C. An in vivo and in vitro structure-function analysis of the Saccharomyces cerevisiae U3A snoRNP: protein-RNA contacts and base-pair interaction with the pre-ribosomal RNA. *J. Mol Biol.* **273**, 552-571 (1997).

174. von der Haar F. Purification of aminoacyl-tRNA synthetases. *Methods Enzymol.* **59**, 257-267 (1979).

175. von der Haar F. Affinity elution: principles and applications to purification of aminoacyl-tRNA synthetases. *Methods Enzymol.* **34**, 163-171 (1974).

176. Triana-Alonso,F.J., Spahn,C.M., Burkhardt,N., Rohrdanz,B. & Nierhaus,K.H. Experimental prerequisites for determination of tRNA binding to ribosomes from Escherichia coli. *Methods Enzymol.* **317**, 261-276 (2000).

177. Kaneko,I. & Doi,R.H. Alteration of valyl-sRNA during sporulation of bacillus subtilis. *Proc. Natl. Acad. Sci. U. S. A.* **55**, 564-571 (1966).

178. Marquez,V., Wilson,D.N. & Nierhaus,K.H. Functions and interplay of the tRNA-binding sites of the ribosome. *Biochem. Soc. Trans.* **30**, 133-140 (2002).

179. Odinzov,V.B. & Kirillov,S.V. Interaction of N-acetyl-phenylalanyl-tRNAPhe with 70S ribosomes of Escherichia coli. *Nucleic Acids Res.* **5**, 3871-3879 (1978).

180. Rheinberger,H.J., Geigenmuller,U., Wedde,M. & Nierhaus,K.H. Parameters for the preparation of Escherichia coli ribosomes and ribosomal subunits active in tRNA binding. *Methods Enzymol.* **164**, 658-670 (1988).

181. Synetos,D. & Coutsogeorgopoulos,C. Studies on the catalytic rate constant of ribosomal peptidyltransferase. *Biochim. Biophys. Acta* **923**, 275-285 (1987).

182. Meskauskas,A., Petrov,A.N. & Dinman,J.D. Identification of functionally important amino acids of ribosomal protein L3 by saturation mutagenesis. *Mol. Cell. Biol.* **25**, 10863-10874 (2005).

183. Schilling-Bartetzko,S., Franceschi,F., Sternbach,H. & Nierhaus,K.H. Apparent association constants of tRNAs for the ribosomal A, P, and E sites. *J. Biol. Chem.* **267**, 4693-4702 (1992).

184. Spahn,C.M.T., Beckmann,R., Eswar,N., Penczek,P.A., Sali,A., Blobel,G. & Frank,J. Structure of the 80S ribosome from Saccharomyces cerevisiae - tRNA-ribosome and subunit-subunit interactions. *Cell* **107**, 373-386 (2001).

185. DeLano,W.L. The PyMOL Molecular Graphics System, www.pymol.org. 2002.

186. Hansen,J.L., Moore,P.B. & Steitz,T.A. Structures of five antibiotics bound at the peptidyl transferase center of the large ribosomal subunit. *J. Mol. Biol.* **330**, 1061-1075 (2003).

187. Monro,R.E., Celma,M.L. & Vazquez,D. Action of sparsomycin on ribosome-catalysed peptidyl transfer. *Nature* **222**, 356-358 (1969).

188. Triana,F., Nierhaus,K.H. & Chakraburtty,K. Transfer RNA binding to 80S ribosomes from yeast: evidence for three sites. *Biochem. Mol. Biol. Int.* **33**, 909-915 (1994).

189. Chan,Y.L., Dresios,J. & Wool,I.G. A pathway for the transmission of allosteric signals in the ribosome through a network of RNA tertiary interactions. *J. Mol. Biol.* **355**, 1014-1025 (2006).

190. Velichutina,I.V., Dresios,J., Hong,J.Y., Li,C., Mankin,A., Synetos,D. & Liebman,S.W. Mutations in helix 27 of the yeast Saccharomyces cerevisiae 18S rRNA affect the function of the decoding center of the ribosome. *RNA.* **6**, 1174-1184 (2000).

191. Panopoulos,P., Dresios,J. & Synetos,D. Biochemical evidence of translational infidelity and decreased peptidyltransferase activity by a sarcin/ricin domain mutation of yeast 25S rRNA. *Nucleic Acids Res.* **32**, 5398-5408 (2004).

192. Porse,B.T., Kirillov,S.V., Awayez,M.J., Ottenheijm,H.C. & Garrett,R.A. Direct crosslinking of the antitumor antibiotic sparsomycin, and its derivatives, to A2602 in the peptidyl transferase center of 23S-like rRNA within ribosome-tRNA complexes. *Proc. Natl. Acad. Sci. U. S. A.* **96**, 9003-9008 (1999).

193. Pestka,S., Rosenfeld,H., Harris,R. & Hintikka,H. Studies on transfer ribonucleic acid-ribosome complexes. XXI. Effect of antibiotics on peptidyl-puromycin synthesis by mammalian polyribosomes. *J. Biol. Chem.* **247**, 6895-6900 (1972).

194. Carrasco,L., Barbacid,M. & Vazquez,D. The trichodermin group of antibiotics, inhibitors of peptide bond formation by eukaryotic ribosomes. *Biochim. Biophys. Acta* **312**, 368-376 (1973).

195. Qu,H.L., Michot,B. & Bachellerie,J.P. Improved methods for structure probing in large RNAs: a rapid 'heterologous' sequencing approach is coupled to the direct mapping of nuclease accessible sites. Application to the 5' terminal domain of eukaryotic 28S rRNA. *Nucleic Acids Res.* **11**, 5903-5920 (1983).

196. Lempereur,L., Nicoloso,M., Riehl,N., Ehresmann,C., Ehresmann,B. & Bachellerie,J.P. Conformation of yeast 18S rRNA. Direct chemical probing of the 5' domain in ribosomal subunits and in deproteinized RNA by reverse transcriptase mapping of dimethyl sulfate-accessible. *Nucleic Acids Res.* **13**, 8339-8357 (1985).

197. Mueller,F., Sommer,I., Baranov,P., Matadeen,R., Stoldt,M., Wohnert,J., Gorlach,M., van Heel,M. & Brimacombe,R. The 3D arrangement of the 23 S and 5 S rRNA in the Escherichia coli 50 S ribosomal subunit based on a cryo-electron microscopic reconstruction at 7.5 Å resolution. *J. Mol. Biol.* **298**, 35-59 (2000).

198. Deusser,E., Stoffler,G. & Wittmann,H.G. Ribosomal proteins. XVI. Altered S4 proteins in Escherichia coli revertants from streptomycin dependence to independence. *Mol. Gen. Genet.* **109**, 298-302 (1970).

199. Funatsu,G. & Wittmann,H.G. Ribosomal proteins. 33. Location of amino-acid replacements in protein S12 isolated from Escherichia coli mutants resistant to streptomycin. *J. Mol. Biol.* **68**, 547-550 (1972).

200. O'Connor,M., Gregory,S.T. & Dahlberg,A.E. Multiple defects in translation associated with altered ribosomal protein L4. *Nucleic Acids Res.* **32**, 5750-5756 (2004).

201. Stoffler,G., Deusser,E., Wittmann,H.G. & Apirion,D. Ribosomal proteins. XIX. Altered S5 ribosomal protein in an Escherichia coli revertant from strptomycin dependence to independence. *Mol. Gen. Genet.* **111**, 334-341 (1971).

202. Kofoed,C.B. & Vester,B. Interaction of avilamycin with ribosomes and resistance caused by mutations in 23S rRNA. *Antimicrob. Agents Chemother.* **46**, 3339-3342 (2002).

203. Tan,G.T., DeBlasio,A. & Mankin,A.S. Mutations in the peptidyl transferase center of 23 S rRNA reveal the site of action of sparsomycin, a universal inhibitor of translation. *J. Mol. Biol.* **261**, 222-230 (1996).

204. Meskauskas,A. & Dinman,J.D. Unpublished .

205. Pestka,S. Studies on the formation of transfer ribonucleic acid-ribosome complexes. XI. Antibiotic effects on phenylalanyl-oligonucleotide binding to ribosomes. *Proc. Natl. Acad. Sci. U. S. A.* **64**, 709-714 (1969).

206. Ban,N., Freeborn,B., Nissen,P., Penczek,P., Grassucci,R.A., Sweet,R., Frank,J., Moore,P.B. & Steitz,T.A. A 9 Å resolution X-ray crystallographic map of the large ribosomal subunit. *Cell* **93**, 1105-1115 (1998).

207. Wilson,D.N. & Nierhaus,K.H. The ribosome through the looking glass. *Angew. Chem. Int. Ed. Engl.* **42**, 3464-3486 (2003).

208. Noller,H.F. RNA structure: Reading the ribosome. *Science* **309**, 1508-1514 (2005).

209. Baram,D. & Yonath,A. From peptide-bond formation to cotranslational folding: dynamic, regulatory and evolutionary aspects. *FEBS Lett.* **579**, 948-954 (2005).

210. Sergiev,P.V., Kiparisov,S.V., Burakovsky,D.E., Lesnyak,D.V., Leonov,A.A., Bogdanov,A.A. & Dontsova,O.A. The conserved A-site finger of the 23S rRNA: just one of the intersubunit bridges or a part of the allosteric communication pathway? *J. Mol. Biol.* **353**, 116-123 (2005).

211. Smith,M.W., Meskauskas,A., Wang,P., Sergiev,P.V. & Dinman,J.D. Saturation mutagenesis of 5S rRNA in Saccharomyces cerevisiae. *Mol. Cell. Biol.* **21**, 8264-8275 (2001).

212. Sambrook J., Fritsch E.F. & Maniatis T. Molecular cloning, a laboratory manual. Cold Spring Harbor Laboratory Press, (1987).

213. Wickner,R.B. & Leibowitz,M.J. Two chromosomal genes required for killing expression in killer strains of Saccharomyces cerevisiae. *Genetics* **82**, 429-442 (1976).

214. Rose,M.D., Winston,F. & Hieter,P. Methods in yeast genetics. Cold Spring Harbor Laboratory Press, Cold Spring Harbor, N.Y., (1990).

215. Boeke,J.D., Eichinger,D., Castrillon,D. & Fink,G.R. The Saccharomyces cerevisiae genome contains functional and nonfunctional copies of transposon Ty1. *Mol Cell Biol.* **8**, 1432-1442 (1988).

216. Christianson,T.W., Sikorski,R.S., Dante,M., Shero,J.H. & Hieter,P. Multifunctional yeast high-copy-number shuttle vectors. *Yeast* **110**, 119-122 (1992).

217. Oakes,M., Aris,J.P., Brockenbrough,J.S., Wai,H., Vu,L. & Nomura,M. Mutational analysis of the structure and localization of the nucleolus in the yeast Saccharomyces cerevisiae. *J. Cell Biol.* **143**, 23-34 (1998).

218. Velichutina,I.V., Hong,J.Y., Mesecar,A.D., Chernoff,Y.O. & Liebman,S.W. Genetic interaction between yeast Saccharomyces cerevisiae release factors and the decoding region of 18 S rRNA. *J. Mol. Biol.* **305**, 715-727 (2001).

219. Wai,H.H., Vu,L., Oakes,M. & Nomura,M. Complete deletion of yeast chromosomal rDNA repeats and integration of a new rDNA repeat: use of rDNA deletion strains for functional analysis of rDNA promoter elements in vivo. *Nucleic Acids Res.* **28**, 3524-3534 (2000).

220. Rose,M.D., Winston,F. & Hieter,P. Methods in Yeast Genetics. Cold Spring Harbor Press, Cold Spring Harbor, NY (1990).

221. Sigmund,C.D., Ettayebi,M., Borden,A. & Morgan,E.A. Antibiotic resistance mutations in ribosomal RNA genes of Escherichia coli. *Methods Enzymol.* **164**, 673-690 (1988).

222. Stern,S., Moazed,D. & Noller,H.F. Structural analysis of RNA using chemical and enzymatic probing monitored by primer extension. *Methods Enzymol.* **164**, 481-489 (1988).

223. Altchul,S.F., Gish,W., Miller,E., Myers,E.W. & Lipman,D.J. Basic local alignment search tool. *J. Mol. Biol.* **215**, 403-410 (1990).

224. Thompson,J.D., Higgins,D.G. & Gibson,T.J. CLUSTAL W: improving the sensitivity of progressive multiple sequence alignment through sequence weighting, position-specific gap penalties and weight matrix choice. *Nucleic Acids Res.* **22**, 4673-4680 (1994).

225. Pestka,S., Rosenfeld,H., Harris,R. & Hintikka,H. Studies on transfer ribonucleic acid-ribosome complexes. XXI. Effect of antibiotics on peptidyl-puromycin synthesis by mammalian polyribosomes. *J. Biol. Chem.* **247**, 6895-6900 (1972).

226. Harger,J.W. & Dinman,J.D. An in vivo dual-luciferase assay system for studying translational recoding in the yeast Saccharomyces cerevisiae. *RNA.* **9**, 1019-1024 (2003).

227. Meier,N. & Wagner,R. Binding of tRNA alters the chemical accessibility of nucleotides within the large ribosomal RNAs of E. coli ribosomes. *Nucleic Acids Res.* **12**, 1473-1487 (1984).

228. Litt,M. & Hancock,V. Kethoxal--a potentially useful reagent for the determination of nucleotide sequences in single-stranded regions of transfer ribonucleic acid. *Biochemistry* **6**, 1848-1854 (1967).

229. Noller,H.F. & Chaires,J.B. Functional modification of 16S ribosomal RNA by kethoxal. *Proc. Natl. Acad. Sci. U. S. A.* **69**, 3115-3118 (1972).

230. Dickson,E., Pape,L.K. & Robertson,H.D. Approaches to sequence analysis of 125I-labeled RNA. *Nucleic Acids Res.* **6**, 91-110 (1979).

231. Ford,P.J. & Southern,E.M. Different sequences for 5S RNA in kidney cells and ovaries of Xenopus laevis. *Nat. New Biol.* **241**, 7-12 (1973).

232. Fromont-Racine,M., Senger,B., Saveanu,C. & Fasiolo,F. Ribosome assembly in eukaryotes. *Gene* **313**, 17-42 (2003).

233. Granneman,S. & Baserga,S.J. Ribosome biogenesis: of knobs and RNA processing. *Experimental Cell Research* **296**, 43-50 (2004).

234. Fedoroff,N.V. Deletion Mutants of Xenopus-Laevis 5S Ribosomal Dna. *Cell* **16**, 551-563 (1979).

235. Pieler,T., Appel,B., Oei,S.L., Mentzel,H. & Erdmann,V.A. Point Mutational Analysis of the Xenopus-Laevis 5S Gene Promoter. *EMBO J.* **4**, 1847-1853 (1985).

236. Zeiner,G.M., Hitchcock,R.A., Sturm,N.R. & Campbell,D.A. 3'-End polishing of the kinetoplastid spliced leader RNA is performed by SNIP, a 3'-->5' exonuclease with a Motley assortment of small RNA substrates. *Mol. Cell. Biol.* **24**, 10390-10396 (2004).

237. Pelham,H.R., Wormington,W.M. & Brown,D.D. Related 5S RNA transcription factors in Xenopus oocytes and somatic cells. *Proc. Natl. Acad. Sci. U. S. A.* **78**, 1760-1764 (1981).

238. Pittman,R.H., Andrews,M.T. & Setzer,D.R. A feedback loop coupling 5 S rRNA synthesis to accumulation of a ribosomal protein. *J. Biol. Chem.* **274**, 33198-33201 (1999).

239. Brow,D.A. & Geiduschek,E.P. Modulation of yeast 5 S rRNA synthesis in vitro by ribosomal protein YL3. A possible regulatory loop. *J. Biol. Chem.* **262**, 13953-13958 (1987).

240. Setzer,D.R. & Brown,D.D. Formation and stability of the 5 S RNA transcription complex. *J. Biol. Chem.* **260**, 2483-2492 (1985).

241. Engelke,D.R., Ng,S.Y., Shastry,B.S. & Roeder,R.G. Specific Interaction of A Purified Transcription Factor with An Internal Control Region of 5S Rna Genes. *Cell* **19**, 717-728 (1980).

242. Honda,B.M. & Roeder,R.G. Association of a 5S gene transcription factor with 5S RNA and altered levels of the factor during cell differentiation. *Cell* **22**, 119-126 (1980).

243. Pelham,H.R. & Brown,D.D. A specific transcription factor that can bind either the 5S RNA gene or 5S RNA. *Proc. Natl. Acad. Sci. U. S. A.* **77**, 4170-4174 (1980).

244. Picard,B. & Wegnez,M. Isolation of a 7S particle from Xenopus laevis oocytes: a 5S RNA-protein complex. *Proc. Natl. Acad. Sci. U. S. A.* **76**, 241-245 (1979).

245. Murdoch,K., Loop,S., Rudt,F. & Pieler,T. Nuclear export of 5S rRNA-containing ribonucleoprotein complexes requires CRM1 and the RanGTPase cycle. *Eur. J. Cell. Biol.* **81**, 549-556 (2002).

246. Allison,L.A., Romaniuk,P.J. & Bakken,A.H. RNA-protein interactions of stored 5S RNA with TFIIIA and ribosomal protein L5 during Xenopus oogenesis. *Dev. Biol.* **144**, 129-144 (1991).

247. Claussen,M., Rudt,F. & Pieler,T. Functional modules in ribosomal protein L5 for ribonucleoprotein complex formation and nucleocytoplasmic transport. *J. Biol. Chem.* **274**, 33951-33958 (1999).

248. Rosorius,O., Fries,B., Stauber,R.H., Hirschmann,N., Bevec,D. & Hauber,J. Human ribosomal protein L5 contains defined nuclear localization and export signals. *J. Biol. Chem.* **275**, 12061-12068 (2000).

249. Scripture,J.B. & Huber,P.W. Analysis of the binding of Xenopus ribosomal protein L5 to oocyte 5 S rRNA. The major determinants of recognition are located in helix III-loop C. *J. Biol. Chem.* **270**, 27358-27365 (1995).

250. Wolffe,A.P. & Brown,D.D. Developmental regulation of two 5S ribosomal RNA genes. *Science* **241**, 1626-1632 (1988).

251. Taylor,W., Jackson,I.J., Siegel,N., Kumar,A. & Brown,D.D. The developmental expression of the gene for TFIIIA in Xenopus laevis. *Nucleic Acids Res.* **14**, 6185-6195 (1986).

252. Harris,R. & Pestka,S. Studies on the formation of transfer ribonucleic acid-ribosome complexes. XXIV. Effects of antibiotics on binding of aminoacyl-oligonucleotides to ribosomes. *J. Biol. Chem.* **248**, 1168-1174 (1973).

253. Szymanski,M., Barciszewska,M.Z., Erdmann,V.A. & Barciszewski,J. 5 S rRNA: structure and interactions. *Biochem. J.* **371**, 641-651 (2003).

254. Deshmukh,M., Tsay,Y.F., Paulovich,A.G. & Woolford,J.L., Jr. Yeast ribosomal protein L1 is required for the stability of newly synthesized 5S

rRNA and the assembly of 60S ribosomal subunits. *Mol. Cell. Biol.* **13**, 2835-2845 (1993).

255. Hourdry,J., Brulfert,A., Gusse,M., Schoevaert,D., Taylor,M.V. & Mechali,M. Localization of c-myc expression during oogenesis and embryonic development in Xenopus laevis. *Development* **104**, 631-641 (1988).

256. Richter,J.D. Translational control during early development. *Bioessays* **13**, 179-183 (1991).

257. Tron,T., Yang,M., Dick,F.A., Schmitt,M.E. & Trumpower,B.L. QSR1, an essential yeast gene with a genetic relationship to a subunit of the mitochondrial cytochrome bc1 complex, is homologous to a gene implicated in eukaryotic cell differentiation. *J. Biol. Chem.* **270**, 9961-9970 (1995).

258. Dick,F.A., Karamanou,S. & Trumpower,B.L. QSR1, an essential yeast gene with a genetic relationship to a subunit of the mitochondrial cytochrome bc1 complex, codes for a 60 S ribosomal subunit protein. *J. Biol. Chem.* **272**, 13372-13379 (1997).

259. Dick,F.A. & Trumpower,B.L. Heterologous complementation reveals that mutant alleles of QSR1 render 60S ribosomal subunits unstable and translationally inactive. *Nucleic Acids Res.* **26**, 2442-2448 (1998).

260. Dick,F.A., Eisinger,D.P. & Trumpower,B.L. Exchangeability of Qsr1p, a large ribosomal subunit protein required for subunit joining, suggests a novel translational regulatory mechanism. *FEBS Lett.* **419**, 1-3 (1997).

261. Eisinger,D.P., Dick,F.A. & Trumpower,B.L. Qsr1p, a 60S ribosomal subunit protein, is required for joining of 40S and 60S subunits. *Mol. Cell. Biol.* **17**, 5136-5145 (1997).

262. Bernad,R., Engelsma,D., Sanderson,H., Pickersgill,H. & Fornerod,M. The Nup214/Nup88 nucleoporin subcomplex is required for CRM1 mediated 60S preribosomal nuclear export. *J. Biol. Chem.* (2006).

263. Thomas,F. & Kutay,U. Biogenesis and nuclear export of ribosomal subunits in higher eukaryotes depend on the CRM1 export pathway. *J. Cell. Sci.* **116**, 2409-2419 (2003).

264. Hedges,J., West,M. & Johnson,A.W. Release of the export adapter, Nmd3p, from the 60S ribosomal subunit requires Rpl10p and the cytoplasmic GTPase Lsg1p. *EMBO J.* **24**, 567-579 (2005).

265. Kallstrom,G., Hedges,J. & Johnson,A. The putative GTPases Nog1p and Lsg1p are required for 60S ribosomal subunit biogenesis and are localized to the nucleus and cytoplasm, respectively. *Mol. Cell. Biol.* **23**, 4344-4355 (2003).

266. West,M., Hedges,J.B., Chen,A. & Johnson,A.W. Defining the order in which Nmd3p and Rpl10p load onto nascent 60S ribosomal subunits. *Mol. Cell. Biol.* **25**, 3802-3813 (2005).

267. Eisinger,D.P., Dick,F.A., Denke,E. & Trumpower,B.L. SQT1, which encodes an essential WD domain protein of Saccharomyces cerevisiae, suppresses dominant-negative mutations of the ribosomal protein gene QSR1. *Mol. Cell. Biol.* **17**, 5146-5155 (1997).

268. Wickner,R.B. "Killer character" of Saccharomyces cerevisiae: curing by growth at elevated temperature. *J. Bacteriol.* **117**, 1356-1357 (1974).

269. Muhlrad,D., Hunter,R. & Parker,R. A rapid method for localized mutagenesis of yeast genes. *Yeast* **8**, 79-82 (1992).

270. Lessard,J.L. & Pestka,S. Studies on the formation of transfer ribonucleic acid-ribosome complexes. 23. Chloramphenicol, aminoacyl-oligonucleotides, and Escherichia coli ribosomes. *J. Biol. Chem.* **247**, 6909-6912 (1972).

271. Gnirke,A. & Nierhaus,K.H. tRNA binding sites on the subunits of Escherichia coli ribosomes. *J. Biol. Chem.* **261**, 14506-14514 (1986).

272. Schilling-Bartetzko,S., Bartetzko,A. & Nierhaus,K.H. Kinetic and thermodynamic parameters for tRNA binding to the ribosome and for the translocation reaction. *J. Biol. Chem.* **267**, 4703-4712 (1992).

273. Motulsky H. & Christopoulos A. Fitting Models to Biological Data using Linear and Nonlinear Regression. GraphPad Software Inc., (2003).

274. Petrov,A.N., Roshwalb,S. & Dinman,J.D. Unpublished .

275. Manuvakhova,M., Keeling,K. & Bedwell,D.M. Aminoglycoside antibiotics mediate context-dependent suppression of termination codons in a mammalian translation system. *RNA.* **6**, 1044-1055 (2000).

276. Yoshizawa,S., Fourmy,D. & Puglisi,J.D. Recognition of the codon-anticodon helix by ribosomal RNA. *Science* **285**, 1722-1725 (1999).

277. Noller,H.F. Biochemical characterization of the ribosomal decoding site. *Biochimie* (2006).

278. Hung,N.J. & Johnson,A.W. Nuclear recycling of the pre-60S ribosomal subunit-associated factor Arx1 depends on Rei1 in Saccharomyces cerevisiae. *Mol. Cell. Biol.* **26**, 3718-3727 (2006).

279. Blanchard,S.C., Gonzalez,R.L., Kim,H.D., Chu,S. & Puglisi,J.D. tRNA selection and kinetic proofreading in translation. *Nat. Struct. Mol. Biol.* **11**, 1008-1014 (2004).

280. Rodnina,M.V., Fricke,R. & Wintermeyer,W. Transient conformational states of aminoacyl-tRNA during ribosome binding catalyzed by elongation factor Tu. *Biochemistry* **33**, 12267-12275 (1994).

281. Kothe,U., Wieden,H.J., Mohr,D. & Rodnina,M.V. Interaction of helix D of elongation factor Tu with helices 4 and 5 of protein L7/12 on the ribosome. *J. Mol. Biol.* **336**, 1011-1021 (2004).

282. Christianson,T.W., Sikorski,R.S., Dante,M., Shero,J.H. & Hieter,P. Multifunctional yeast high-copy-number shuttle vectors. *Gene* **110**, 119-122 (1992).

283. Sikorski,R.S. & Hieter,P. A system of shuttle vectors and yeast host strains designed for efficient manipulation of DNA in Saccharomyces cerevisiae. *Genetics* **122**, 19-27 (1989).

284. Grentzmann,G., Ingram,J.A., Kelly,P.J., Gesteland,R.F. & Atkins,J.F. A dual-luciferase reporter system for studying recoding signals. *RNA.* **4**, 479-486 (1998).